RAFAEL HENRIQUE DE OLIVEIRA

Comfort assessment and rail track monitoring based on the collective use of very low-cost inertial sensors aboard in-service trains

São Paulo
2023

RAFAEL HENRIQUE DE OLIVEIRA

Comfort assessment and rail track monitoring based on the collective use of very low-cost inertial sensors aboard in-service trains

Revised version

Thesis presented to the Polytechnic School of the University of São Paulo to obtain the degree of Doctor of Science

Concentration area: Transport Engineering

Supervisor: Prof. Dr. Flávio Guilherme Vaz de Almeida Filho

Co-supervisor: Prof. Dr. Giuseppe Loprencipe

São Paulo
2023

Este exemplar foi revisado e corrigido em relação à versão original, sob responsabilidade única do autor e com a anuência de seu orientador.

São Paulo, 13 de novembro de 2023

Assinatura do autor: 

Assinatura do orientador: 

Catalogação-na-publicação

de Oliveira, Rafael Henrique
Comfort assessment and rail track monitoring based on the collective use of very low-cost inertial sensors aboard in-service trains / R. H. de Oliveira -- versão corr. -- São Paulo, 2023.
261 p.

Tese (Doutorado) - Escola Politécnica da Universidade de São Paulo. Departamento de Engenharia de Transportes.

1.Ferrovias 2.Vias Permanentes 3.Conforto vibracional veicular 4.Sensores inerciais 5.Fusão de sensores I.Universidade de São Paulo. Escola Politécnica. Departamento de Engenharia de Transportes II.t.

de Oliveira, R. H. **Comfort assessment and rail track monitoring based on the collective use of very low-cost inertial sensors aboard in-service trains.** 2023. Tese (Doutorado) - Escola Politécnica da Universidade de São Paulo, São Paulo, 2023.

Aprovado em:

Banca Examinadora

Prof. Dr. _____

Instituição: _____

Decisão: _____

Prof. Dr. _____

Instituição: _____

Decisão: _____

Prof. Dr. _____

Instituição: _____

Decisão: _____

Prof. Dr. _____

Instituição: _____

Decisão: _____

Prof. Dr. _____

Instituição: _____

Decisão: _____

In loving memory of my late father, Cícero, whose unwavering love, support, and guidance always propelled me to pursue my personal fulfilment.

ACKNOWLEDGMENTS

In completing this doctoral thesis, I must owe my gratitude to the individuals and organizations whose support and encouragement have contributed to my academic journey and realization of this doctoral thesis.

First and foremost, I honour the memory of my late father, Cicero Oliveira, whose profound influence and belief in the value of education guided my decision to pursue an academic career. In these five years of his absence, only his example of life gave me the strength to continue to pursue my aspirations while going through the hardest and most painful moment of my life. Though he is no longer with us, his encouragement resonates in every achievement of this thesis.

At this point, I cannot refrain from expressing my heartfelt gratitude to my beloved mother, Lourdes, my always supportive sister, Daniele, my always fun brother-in-law, Gabriel, and my tender niece, Paula. They have been pillars of solid support throughout this endeavour, especially during the most challenging moments.

I extend my most profound appreciation to my outstanding supervisor, Prof. Dr. Flavio Vaz, whose patient guidance and scholarly wisdom have been invaluable throughout this research journey. His belief in my potential, even during moments of self-doubt, has driven me to surpass my expectations and to push the boundaries of knowledge.

Moreover, I cannot express enough gratitude to my co-supervisor, Prof. Dr. Giuseppe Loprencipe, for his contributory role in this thesis. His mentorship has opened doors to opportunities and research improvements that surpassed all my expectations. His encouragement to embrace innovation and pursue unexplored territories has significantly enriched the scope of my research.

Additionally, I extend my sincerest appreciation to the Mobile Diagnostics Department of the Italian Railway Infrastructure Manager (*Rete Ferroviaria Italiana*), in particular Eng. Marco Gallini, Eng. Gennaro Alteriso, and Eng. Giorgio Perrotta for the immeasurable collaboration in enabling the tests to be carried out. Their expertise, cooperation, and support were indispensable in ensuring the success of the experiments conducted for this thesis.

Furthermore, my deepest gratitude goes to the *Companhia Paulista de Trens Metropolitanos* (CPTM), especially the Eng. Sérgio Luís Silva, Fabricio Mattos Souto, Ricardo Penteado Espírito Santo, André Takeshi Kubota, and Cesar Augusto Doratiotto. Their assistance and cooperation in enabling experiments significantly enriched the empirical aspects of this research.

I am also profoundly grateful for the enriching academic and personal conversations I shared with my colleagues throughout this research journey. Among them, I wish to highlight my dear friend Rodrigo Pissardini, whose insightful discussions and support were fundamental in shaping the direction and core concepts of this research. Moreover, his encouragement has played a pivotal role in completing this thesis, especially during challenging times.

This invaluable significance of engaging in conversations and exchanging ideas in the academic construction process was also exemplified by my interactions with my Italian colleagues, Salvatore Bruno, Lorenzo Vita, Giulia Del Serrone, Laura Moretti, Paolo Peluso, and Giacomo Garofalo from the University of Rome. Our academic and personal exchanges made me feel welcome and adapted during my visits to Rome, creating a supportive environment that enriched my research experience.

In navigating the bureaucratic intricacies that accompanied this academic journey, I express my sincere appreciation to the postgraduate program secretary, Luciane Watanabe. Her dedication and guidance eased the administrative processes, ensuring a seamless progression toward the completion of this thesis.

Additionally, I am grateful to the *Coordenação de Aperfeiçoamento de Pessoal de Nível Superior* (CAPES) for the partial funding of this study (Finance Code 001).

In conclusion, the culmination of this doctoral thesis is a testimony to the efforts of public education and research institutions and, above all, their dedicated members, who have played a fundamental role in my journey since primary school. These people and their work, not always recognised as deserved, underscore the value of the collaborative pursuit of knowledge.

ABSTRACT

de Oliveira, R. H. **Comfort assessment and rail track monitoring based on the collective use of very low-cost inertial sensors aboard in-service trains.** 2023. Thesis (Doctorate) - Polytechnic School of the University of São Paulo, São Paulo, 2023.

The periodic rail track quality inspection is mandatory to ensure ride comfort and safety. However, using dedicated track inspection vehicles and systems has drawbacks such as the high acquisition, operation, and maintenance costs, the consequent lower spatiotemporal coverage, and the impact on traffic, which have stimulated research on low-cost, quasi-continuous alternatives. In this context, this research aims to develop a methodology for using very low-cost (consumer-grade) inertial sensors aboard in-service trains for ride comfort and track quality monitoring. The basic hypothesis considers that a collective of low-quality sensors, similar to those embedded in smartphones, can offer robust and accurate performance in this service monitoring by minimizing the variance fluctuation of individual sensors. This concept involves data fusion regarding three critical aspects: a) spatiotemporal data alignment; b) identifying discrepant signals; and c) the integration itself, carried out by simple averaging, a specific case of inverse-variance weighting. Acceleration data was processed in accordance with ISO 2631 to characterize the comfort itself and, indirectly, the track quality. Two types of tests were performed: initial tests using single smartphones and subsequent tests in urban and high-speed railways using multiple devices (up to ten) emulating smartphones (i.e., built using consumer-grade sensors). As a result of the collective approach, the mean (collective) signal of redundant signals yielded a noise reduction consistent with the theoretical noise reduction and improvement of correlation with reference data, either dynamic or geometry reference data for the relevant track parameters. For non-redundant sensors (i.e., in different positions of a train), differences in position and speed variations reduce the similarity between signals and, hence, the mean signal performance. Moreover, the results revealed the reduced impact of the uncertainty in position (apart from the unavailability of satellite positioning systems), attitude and time estimation under the proposed method. The ensemble of conclusions establishes a methodological basis for future applications of these very low-cost sensors, including passengers' smartphones, in monitoring activities as a complement to the ride dynamics assessment and track inspection already performed.

Keywords: Railways. Railway tracks. Vehicle vibration comfort. Inertial sensors. Sensor fusion.

RESUMO

de Oliveira, R. H. **Comfort assessment and rail track monitoring based on the collective use of very low-cost inertial sensors aboard in-service trains.** 2023. Tese (Doutorado) - Escola Politécnica da Universidade de São Paulo, São Paulo, 2023.

A inspeção periódica da via permanente ferroviária é imprescindível para garantir níveis de conforto e segurança. Entretanto, o uso de veículos e sistemas dedicados a essa atividade apresenta inconvenientes como os altos custos de aquisição, operação e manutenção, a consequente menor cobertura espaço-temporal e o considerável impacto no tráfego, fatores que estimulam pesquisa em alternativas de baixo custo e quase contínuas. Nesse contexto, esta pesquisa visa desenvolver uma metodologia para o uso de sensores inerciais de muito baixo custo, semelhante aos existentes em smartphones, a bordo de trens em operação para monitoramento do conforto e da qualidade da via. Parte-se da hipótese de que o uso coletivo destes sensores supera a baixa qualidade individual destes e produz resultados mais acurados e robustos. O conceito considera a fusão de dados em três aspectos críticos: a) alinhamento espaço-temporal dos dados; b) a identificação e exclusão dos sinais discrepantes; e c) a integração em si, realizada por meio de média simples dos sinais, caso especial da média ponderada pelo inverso da variância. As acelerações foram tratadas segundo a ISO 2631 para caracterização do conforto e, indiretamente, da qualidade da via. Foram realizados teste preliminares empregando *smartphones* de forma individual e testes subsequentes em ferrovias urbanas e de alta velocidade usando múltiplos dispositivos (até dez) emulando *smartphones* em nível de qualidade. Como resultado da abordagem coletiva, o sinal médio (coletivo) calculado de sensores redundantes resultaram em em redução de ruído coerente com a teoria e em melhora na correlação com os dados de referência, tando aqueles dinâmicos quanto os associados às geometria da via para os parâmetros relevantes. Para sensores não redundantes (isto é, instalados em diferentes posições do trem), as diferenças em posição e as variações de velocidade reduzem a similaridade entre os sinais e, por conseguinte, o desempenho do sinal médio. Ademais, os resultados evidenciaram o impacto reduzido de incertezas em posição (à parte a indisponibilidade dos sistemas de posicionamento por satélite), atitude e tempo sob o método proposto. As conclusões estabelecem base metodológica para futuras aplicações desses sensores de baixo custo, incluindo *smartphones* de passageiros, em atividades de monitoramento como complemento à inspeção viária já realizada.

Palavras-chave: Ferrovias. Vias permanentes. Conforto vibracional veicular. Sensores inerciais. Fusão de sensores.

LIST OF FIGURES

LIST OF TABLES

LIST OF ABBREVIATIONS, ACRONYMS, AND INITIALISMS

ADAS	Advanced Driver Assistance Systems
AHRS	Attitude and Heading Reference System
CEN	*Comité Européen de Normalisation* (European Committee for Standardization)
CEP	Circular error probable
CLT	Central Limit Theorem
CP	*Comboios de Portugal* (Trains of Portugal)
CPTM	*Companhia Paulista de Trens Metropolitanos* (São Paulo State's Metropolitan Railway Company)
DCM	Direction cosine matrix
DFT	Discrete Fourier transform
DOP	Dilution of Precision
DTFT	Discrete-time Fourier transform
DWT	Discrete wavelet transform
EKF	Extended Kalman Filter
EMU	Electric Multiple Unit
FFT	Fast Fourier transform
FIR	Finite Impulse Response
FT	Fourier transform
GLONASS	*Globalnaya navigatsionnaya sputnikovaya sistema* (Global Navigation Satellite System)
GNSS	Global Navigation Satellite System
GPS	Global Positioning System
GRS-80	Geodetic Reference System 1980
HDOP	Horizontal Dilution of Precision
ICC	Intraclass correlation coefficient

IERS	International Earth Rotation and Reference Systems Service
IIR	Infinite Impulse Response
IMU	Inertial Measurement Unit
INS	Inertial Navigation Systems
IRM	IERS Reference Meridian
IRP	IERS Reference Pole
ISO	International Organization for Standardization
ITRF	International Terrestrial Reference Frame
KF	Kalman Filter
LKF	Linearized Kalman Filter
MEMS	Microelectromechanical system
NMEA	National Marine Electronics Association
PMA	Point Mass Acceleration
PVA	Position, velocity, and time
RMS	Root mean square
SBAS	Satellite-based Augmentation System
SNCF	*Société nationale des chemins de fer français* (National Company of French Railways)
STFT	Short-time Fourier transform
TGMS	Track geometry measurement system
TRT	Track recording train
TRV	Track recording vehicle
UAV	Unmanned Aerial Vehicle
UIC	*Union internationale des chemins de fer* (International Union of Railways)
UGMS	Unattended Geometry Measuring Systems
UKF	Unscented Kalman Filter
WGS-84	World Geodetic System 1984

TABLE OF CONTENTS

1 INTRODUCTION

The ubiquity of mobile devices with built-in sensors, such as smartphones, smartwatches, tablets, and vehicles, has increasingly enabled gathering and analysing data from their surroundings (LEE et al., 2006). In the context of transport services, in-service vehicles and transport users are regarded as roving sensors for a wide range of phenomena, considering the electronic devices they carry during a trip. Consequently, this new opportunistic sensing platform offers greater spatiotemporal coverage at a lower cost than traditional techniques (ABDELHAMID; HASSANEIN; TAKAHARA, 2014; HIGUCHI; YAMAGUCHI; HIGASHINO, 2015; ZHAO; GUO; ZENG, 2016). For transport infrastructure[1] monitoring activities in different transport modes, methods based on in-service vehicles and low-cost sensors may represent a cost-effective alternative or complement to the expensive dedicated vehicles and instruments (GHOSE et al., 2012; DENNIS et al., 2014; ALESSANDRONI et al., 2017; PAIXÃO; FORTUNATO; CALÇADA, 2019; VINKÓ et al., 2023). Moreover, this alternative method represents less impact on traffic since dedicated cars impact road capacity.

Regarding railway infrastructure managing characteristics, periodic track quality inspection is crucial to ensure the proper dynamic behaviour of the train-track system. Irregularities in track geometry and rail surface, variations in track stiffness, and track component failures may increase dynamic loading, decreasing ride comfort and increasing derailment risk, track degradation development, and component failure (ESVELD, 2001). Thus, poor dynamic behaviour resulting from track quality issues increases maintenance needs and costs, and consequently, a timely track inspection can optimise maintenance activities (REAL et al., 2010).

The first dedicated track recording vehicle would have been the French Voiture Mauzin, developed by Andre Mauzin in 1930 as chief engineer at the *Société nationale des chemins de fer français* (SNCF) (PRUD'HOMME, 1997; TERRASSE,

[1] In a broad sense, transport infrastructure is a collective term for fixed elements that are necessary to operate a transport service, such as the track, signals, stations, other buildings, electric wires, etc. (FINGER, 2014)

2008). In the first version of this vehicle, the geometric track auscultation was realised from small wheels dissociated from the main car wheels and rolling on the rails head. However, direct contact sensors, such as the *Mauzin* wheels, have speed limitations that impact train traffic and restrict their use during operating hours. Hence, the current technologies are mainly noncontact of inertial based and employ optical and inertial optical sensors embedded in inspection cars for track and overhead wire conditions (PITA, 2006; MATISA, 2017). The noncontact inertial technique lies in the relation between track quality (IWNICKI, 2006), while the optical methods mainly employ laser triangulation to define the position and condition of the rails (MATISA, 2017).

The technical development suited to high-speed rail networks resulted in multipurpose track recording trains, similar to the passenger-carrying trains with the addition of specialised instruments (WESTON et al., 2015). An example of this diagnostic train concept is the *Treno Diamante* of the Italian Railway Network, which is an eight coaches train equipped with hundreds of sensors of different natures) for track and ride dynamics monitoring natures (including sets of axle box, bogie and car body-mounted accelerometers. The *Diamante* train can perform periodic diagnostics at maximum commercial speeds in the high-speed network of that country (above 300 km/h) (MORETTI, 2017).

More affordable options for track geometry are the Unattended Geometry Measuring Systems (UGMS), modules that can be installed underneath in-service cars. The UGMS stipulated by the Network Rail, the British rail infrastructure manager, comprises inertial sensors combined with laser triangulation surveying equipment mounted on the bogie (NETWORK RAIL, 2007). Compared with dedicated cars or trains, this system generates track quality data at a higher frequency, improves the analysis of degradation trends, and enables predictive maintenance techniques (WESTON et al., 2015).

The main drawbacks of dedicated inspection vehicles are the high acquisition and maintenance costs and the consequent lower spatiotemporal coverage (BRIDGELALL, 2014). Moreover, the operation of these dedicated trains impacts high-traffic lines even when they operate at commercial speeds since they occupy the track. UGMS modules represent a less expensive and in-service-suited

alternative, increasing monitoring data collection with no traffic impact. However, their acquisition and maintenance costs are not negligible, and their use is limited to a certain rolling stock percentage. With the propagation of low-cost microelectromechanical systems (MEMS), inertial sensors have become cheaper, smaller and more energy-efficient (TITTERTON; WESTON, 2004), becoming possible alternatives even less costly and more scalable in railway infrastructure monitoring. However, methods based on inertial sensors have as one of the main problems the high vibration acting on sensors installed on the axle box (WESTON et al., 2015), increasing maintenance needs. Another critical issue identified through the literature review for the present thesis is the proper definition of filters and processing methods to obtain a realistic track geometry in scenarios with speed variation and under the influence of suspension depending on sensor position.

The challenges in using inertial sensors and the need for low-budget, high-scalable monitoring tools created an expanding fruitful research area on the vibration-based track monitoring system. Industrial and navigation-grade[2] inertial sensors, costing hundreds or thousands of dollars, have become more widely employed for such activity. Odashima *et al.* (2017) estimate track vertical geometry irregularities from car body accelerations and applying a Kalman-filter-based technique. Lederman *et al.* (2017a) propose the extraction of signal-energy features from car-body vibration and the use of the unsupervised classifier to detect track changes such as track replacement and ballast tamping. Zoccali, Loprencipe, and Lupascu (2018), proposing an indirect method to assess the track quality, characterise passenger comfort under ISO 2631 standard using an accelerometer installed on the floor of a subway train. These experimental systems used navigation or industrial-grade inertial sensors.

In this context, mobile gadgets with sensing capabilities onboard in-service vehicles

---

[2] Inertial sensors are commercially classified into the following grades (from the lowest to the highest performance level): consumer, automotive, industrial, tactical, navigation, and strategic-grade (GADE, 2005; MURPHY, 2017; VECTORNAV, 2019; SAFRAN COLIBRYS, 2021), as will be described in Section 3.2. The consumer-grade sensors are largely employed in portable electronic devices for less demanding activities such as in motion detection activity, being characterised by their very low-cost, low power consumption, and low-quality. Thus, this work uses the term **consumer-grade** as synonym of **very low-cost** and **smartphone-grade** when describing the sensors.

have been highly studied for road monitoring, using their inertial sensors to monitor passengers' comfort, identify punctual road anomalies, and obtain continuous track quality information. Weston *et al.* (2015a) highlight the noise levels and poor stability of these very low-cost consumer-grade sensors as restrictions for their use in track geometry reconstitution. Seraj, Meratnia, and Havinga (2017) used the inertial sensors of eight smartphones attached to the car body of a track recording coach to characterise track cant, twist, and curvature. Although using more than one inertial sensor, the comparison between sensors placed in different positions was out of the work scope of these authors. Netirail-Infra (2018) developed, tested, and validated a smartphone-based track and ride monitoring application. This system registers the perception of ride comfort in real-time according to ISO 2631 and the peaks in the power spectrum for vibration frequencies related to squats. Paixão, Fortunato, and Calçada (2019) also proposed using a smartphone's acceleration data to characterise structural performance and degradation in geometry, defining the geometry calculation as further work. Thus, the literature review reveals an advancement from low-cost monitoring systems, based on medium-grade sensors, to ultra low-cost alternative methods or complementary monitoring tools, based on consumer-grade sensors similar to those embedded in mobile devices. However, the existing limitations cited by Weston *et al.* (2015a) curb the list of monitored parameters and the scope of the applications.

In order to overcome the individual low-quality of the ultra-low-cost sensors, such as smartphone-grade or consumer-grade inertial sensors, at the cost of a few dollars, this thesis proposes the collective use of these sensors. This concept is based on two main aspects: a) the weighting of each sensor that composes the sensing population, which may be ruled by sensor position and its behaviour when compared with its peers; and b) the integration itself, which can be performed by simple averaging, inverse-variance weighting, or through more sophisticated mathematical tools such as Kalman filter. The thesis identifies the former as an important and understudied issue for proper data fusion.

Moreover, the development of a single-board device dedicated to ride comfort and track monitoring is an essential outcome of this thesis. By developing very low-cost sensor units based on single-board computers that integrate consumer-grade inertial sensors, magnetometers, barometer, and Global Positioning System (GPS) modules,

this research obtains at the same time: a) a more affordable way, when compared with the use of multiple smartphones, to test multiple sensors running at the same trip; b) a more flexible instrument since its elements can be set up and replaced according to our needs; c) a device that can be itself used as an instrument dedicated to road monitoring. The tests performed using multiple sensor sets lay the basis for a collective track monitoring, whether using multiple similar especially constructed devices or obtaining data from smartphones under a crowdsensing[3] concept. Issues on effectively implementing such a crowdsensing system regarding the client application, data storage, and communication are out of the scope of this thesis.

1.1 OBJECTIVES

1.1.1 Main objective

This research aims to define a ride comfort and rail track monitoring methodology based on the collective[4] use of very low-cost sensors installed inside the cabin of in-service trains. The hypothesis is that the low individual quality of the very low-cost sensors, similar to those existing in a smartphone, would be overcome by the concept of collective monitoring, i.e., the weighting and integration of a sensor group operating during the same train ride.

---

[3] The **mobile crowdsensing** concept make use of the sensing, computing, communication, and storage capabilities of mobile devices to enable collective data sharing and, from this, measure and map various phenomena. This concept encompasses a wide sensing spectrum from **participatory** (i.e., with active involvement of individuals) to **opportunistic** sensing (more autonomous, without the explicit action of the individual) (GANTI; YE; LEI, 2011).

[4] The **collective sensing** concept describes “the simultaneous measuring, localization and mapping approaches that incorporate sensor networks” (BLASCHKE et al., 2011),

1.1.2 Specific objectives

- To develop a consumer-grade mini portable track monitoring device. The initial sensor set (also called sensor unit) is composed of a Global Navigation Satellite System (GNSS) receiver and a ten degrees-of-freedom Inertial Measurement Unit (with an accelerometer, a gyroscope, a magnetometer, and a barometer). From that, it would be possible to define which outputs are more relevant (besides the accelerations themselves and considering the vehicles' position and attitude) to describe comfort and track conditions along a line accurately.

- To define the data fusion technique to obtain consolidated vehicle vibration description from the multiple sensors. Initially, this activity would comprise three main steps: data alignment, mathematical weighting (considering data inconsistency, sensor location and orientation influences) and data combination.

- To describe the influence of the sensors' arrangement on the proposed monitoring activity, i.e., the influence of the number of devices and their position on the train vibration characterisation.

- To describe the influence of the inaccuracies inherent to very low-cost sensors and to the assumptions when using these sensors. The thesis focuses on the impact of inaccuracies related to position, time, and attitude estimations.

- To define, from comfort calculation, the track parameters able to be indirectly characterized with the proposed materials and methods, i.e., considering the intrinsic limitation of very low-cost sensors and the sensors placed in the train cabin (under suspensions influence) and defining limits of application.

- To develop, with the fulfilment of the previous objectives, a set of tools for comfort assessment and analysis based on the integration of multiple very low-cost onboard sensors.

1.2 JUSTIFICATION

The main constraints associated with dedicated inspection vehicles and unattended systems are derived from their high acquisition and maintenance costs. Consequently, the track inspection fleet (dedicated vehicles or in-service vehicles with measurement modules) is limited in quantity and inspection activity has reduced spatiotemporal coverage. In other words, the figure of inspection equipment and the network length define a minimum inspection interval, and the traffic level prioritises which lines must be more frequently inspected. Besides these dimensions, special-purpose vehicles may impact commercial and passenger traffic even when operating at maximum line speed. Thus, the search for alternatives with lower cost and greater scalability, resulting in greater spatiotemporal granularity, is stimulated. These requirements would be met by a collective monitoring system based on very low-cost sensors, in which railroad quality data could be generated quasi-continuously, and the infrastructure manager would obtain more detailed information on track degradation development (WESTON et al., 2015; SOLEIMANMEIGOUNI; AHMADI; KUMAR, 2018).

To deal with the known low quality of the very low-cost[5] (smartphone-grade) sensors in this activity, the collective approach considering the fusion of multiple sensors is a possibility scarcely investigated in the literature despite the opportunity represented by the sensor population carried by passengers. The collective approach allows for noise reduction under Central Limit Theorem (CLT) (TITTERTON; WESTON, 2004; GUERRIER, 2008) and robustness improvement through discrepant measurements identification, which is especially important when considering the inhomogeneity of an eventual sensor collectivity in terms of the sensor itself and the influence of its position. Although these new methods may not entirely meet the requirements for railway monitoring and present worse trueness than traditional techniques, they should be precise enough to enable a quasi-continuous comparative analysis and provide intermediate information between two successive track inspections. In such

[5] Very low-cost regarding both the usual cost classification of the inertial sensors and the usual costs (tens of thousands of dollars to millions of dollars) of track monitoring solutions.

an application, the assessment of track degradation progression could be better performed owing to a spatiotemporally fine-grained monitoring. As a result, track maintenance management is enhanced through quicker response to remarkable and unsafe track condition changes.

Regarding enhancing accuracy through integrating multiple sensors, it should be emphasized that the gain does not occur inherently with the increase in the number of identical sensors. As described by Nahin and Pokoski (1980), and discussed by Hall and Mcmullen (2004), combining inaccurate sensors (individual inference probability below 0.5) does not lead to improvement. Concurrently, the combination of highly accurate sensors (individual inference probability above 0.95) also does not yield gains due to their already high individual accuracy. Ultimately, the most significant incremental gain is observed when adding 1 to 7 sensors with reasonable individual inference probabilities. Therefore, it becomes necessary to assess the adherence of the individual consumer-grade sensors to the monitored phenomena (vehicle vibration and, indirectly, track quality) to confirm whether the collective approach results in increased accuracy in these contexts.

Lastly, it is noteworthy that the underlying concept of the proposed technique is the technical viability of a system based on smartphone-gathered data. The very low-cost sensors used in this research are similar to those of a medium-class smartphone. With adaptations, this fact would allow the proposed collective logic to be extrapolated to a collaborative system using vibration data from passengers' smartphones from multiple in-service trains. This crowdsourced data collection concept would be a further step and is initially out of the scope of the present project. However, the intended collective development would lay the foundation for such a system. A hypothetical passenger-based system would effectively enable quasi-continuous (higher spatiotemporal frequency) railroad monitoring, a desirable feature for such a system.

1.3 OVERVIEW OF THE RESEARCH STRUCTURE

Chapter 2 describes the railway track and the activities regarding its inspection. At

the same time, critical aspects of the track-train dynamics are highlighted considering the proposed application.

Chapter 3 presents the most relevant methods for comfort and ride dynamics assessment in railway transportation, emphasising the possibilities and limitations of the discussed data techniques when using consumer-grade sensors.

Chapter 4 presents the results of the literature review on the use of inertial sensors in railroad monitoring. The main findings are discussed according to a proposed taxonomy of the literature in this area. This taxonomy reflects aspects such as the subsystem in a monitoring system, the different techniques, and the instruments used in this research area.

Chapter 5 describes the materials and methods used to accomplish this thesis. Regarding material, the smartphones and the devices developed to emulate smartphones for the present work are detailed. The methods include the data processing techniques and the different test arrangements, the latter being the central aspect of the present thesis.

Chapter 6 present and discuss the preliminary results regarding two datasets: a) data from preliminary tests using medium-grade *smartphones* on a line of the São Paulo Railway Metropolitan Company and a line of the Portuguese Railway Company; and b) preliminary results on the Italian High-speed Railway Network regarding the data description and the identification of discrepant signals.

Chapter 7 presents the validation considering individual and collective results of the tests performed on the Italian High-speed Railway Network and on Line 7 of the São Paulo Railway Metropolitan Company. For the validation, reference data from track recording vehicles encompassing dynamic and track geometry measurements are used. Complementary, the impact on the results of the uncertainties and necessary assumptions arising from using very low-cost sensors is investigated. Lastly, repeatability analysis is presented from multiple traversals on the same track.

The last chapter, Conclusions, discusses how the established objectives were accomplished and how the discussion of the results can define a methodological basis for the collective use of very low-cost sensors. In addition, the chapter enumerates aspects that should be investigated in further works, such as the

improvement of the position solution and the use of sensor devices in free orientation.

2 RAILWAY TRACK AND ITS INSPECTION

This chapter outlines the essential aspects of the railway track and its periodic inspection. Firstly, to provide the conceptual basis for studying the different track measurement systems, the railway track, the main characteristics of its components, its geometric description, and the types of rail track and their variations are defined. At the same time, the influence of these aspects on vibration measurement performance is highlighted. Afterwards, the main aspects of the track inspection and the commercially consolidated measurement tools are presented.

2.1 RAILWAY TRACK AND ITS COMPONENTS

The railway track is an assembly of components designed to perform two main functions efficiently: guiding the railway vehicles and transferring train loads to the formation. In other words, it enables proper train displacement and ensures comfortable and safe ride, economical operation and maintenance, as well as reduced environmental impacts. (ESVELD, 2001; COMITÉ EUROPÉEN DE NORMALISATION, 2017a).

The rail track can be a ballasted or slab track. In a ballasted track (Figure 1), the rails are clipped to the sleepers through the fastening system, and this structure formed by rails and sleepers is supported by a ballast bed (crushed stone or similar granular material). Considering the other sublayers and classifying this structure into two parts (super and substructure), the ballasted track is composed of[6] (SELIG; WATERS, 1995; ESVELD, 2001; DAHLBERG, 2006):

- Track superstructure, which consists of:
    - Steel rails, providing smooth surfaces for the wheels, guide the wheelsets, transfer the forces to the sleepers, and act as electrical

[6] The track elements descriptions are not intended to be complete in terms of their various functions and characteristics. For brevity, this thesis is limited to presenting the most relevant aspects.

conductors for the signalling system.

- Rail pads, elastic elements placed for wear protection in track with concrete sleepers. Additionally, the rail pad stiffness impacts the track stiffness and, thus, the track dynamic behaviour, the bearing capacity, the track geometry quality, and the integrity of track components. From this aspect, the design of the rail pad stiffness is conditioned by the desirable track performance.
- The fastening system, a set of components with the function of fixing the rails to the sleepers
- The sleepers, usually made of timber or prestressed concrete. Their main functions are to support the rails and preserve the track geometry regarding rail position (gauge, level, and alignment).

- Track substructure[7], which consists of:
  - The ballast layers, composed of crushed granular material (usually angular, hard stones and rocks) and comprising the crib (between the sleepers), the top ballast (upper portion disturbed by tamping), the bottom ballast (lower portion not disturbed by tamping), and the shoulder (lateral portion). As main functions, these layers support the track vertically and laterally, provide resilience for the track, and enable drainage.
  - The subbalast, composed of granular material that meets filtering requirements to prevent the interpenetration between the ballast and the subgrade, as well as to curb frost penetration.
  - Geotextiles, permeable geomembranes eventually used to prevent the mutual penetration between two adjacent layers of granular materials and reinforce the soil layer with inadequate mechanical strength.

[7] The distinction between superstructure and substructure may vary by author. In this thesis, the definition presented in Selig e Waters (1995) is used.

- The subgrade, which is the platform that provides stable foundation for the ballast and subbalast layers (track bed) and is levelled out to give it the correct profile. It may comprise two layers: placed soil (fill, to partially replace improper ground or raise the platform to the required elevation) and the formation layer (natural ground).
- The drainage system.

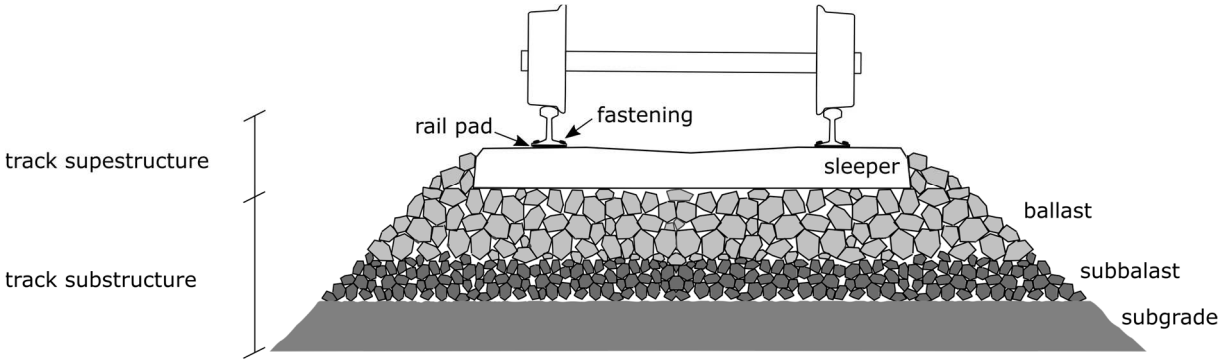

Figure 1 - Track structure main components. Adapted from Selig e Waters (1995) and Dahlberg (2006)

On the other hand, the slab track superstructure has rails usually lying on resilient pads. The rail support can be done according to the following methods:

- Discrete rail support, with sleeper or blocks (embedded or on the top of the roadbed) or without sleepers (monolithic prefabricated or *in-situ* slabs), also considering the appropriate fastening.
- Continuous rail support, with embedded rails or directly fastened and continuously supported rails.

The concrete slab solution requires measures regarding substructure preparation since the slab track is less tolerant to significant settlements. When the track is constructed on embankments and cuttings, this means the need for soil improvements (ESVELD, 2001).

The main advantages of concrete slab tracks over ballasted ones are the higher lateral and longitudinal stability, the higher lateral resistance, the absence of problems due to ballast degradation, the consequent lower maintenance and higher availability, the lower structure height, and the lower weight. These factors make it the primary option for new high-speed lines and subway systems. However, the slab

track has disadvantages that can curb its utilization, such as higher construction and repair costs, higher airborne noise reflection, smaller adaptability to sublayers settlements, and special attention in transition zones.

When comparing ballasted and slab tracks, other relevant aspects are the track resilience and the stiffness of the structure and its components, a key aspect when analysing train excitation. In a ballasted track, the ballast layer provides resilience for low-frequency excitations and the rail pad for high-frequency ones. Moreover, concrete sleepers confer greater stiffness to the track structure than the wooden ones, being crucial the correct rail pad choice to ensure proper dynamic behaviour. In turn, the concrete slab track is a more critical structure since the rail pads give resilience for low and high-frequency excitations.

2.2 RAIL TRACK GEOMETRY

The positions of the rails are defined by the components abovementioned and define the track geometry. The track geometry can be defined as dimensional variation of track position and comprises the track design features (i.e., tangents, curves, and inclinations designed to ensure the desired train displacement under the topographical constraints) and track irregularities (i.e., deviations from the design geometry). From these concepts, the track geometry quality analysis considers track deviations from the mean[8] or the design geometry and considers parameters that describe how rails vary from their expected position (STOW; ANDERSSON, 2006).

Initially, the track reference frame must be defined to enable track geometry and irregularities description (COMITÉ EUROPÉEN DE NORMALISATION, 2019). The term **running table** (part 1) refers to the upper surface of the rail head. Moreover, the **running surface** is formed by the straight lines perpendicular to the track centreline and tangential to the running tables. From these aspects and for the sake of measurement issues, a **track coordinate system** (Figure 2) is defined as a right-

[8] In common practice, the exact design geometry is not known and it is estimated form the mean rail position after short wavelength filtering (JOHNSON, 2006).

handed tri-dimensional cartesian coordinate system centred to the track with the following axes orientation:

- X-axis: running direction.
- Y-axis: parallel to the running surface for a given cross section.
- Z-axis: pointing downwards, perpendicular to the running surface

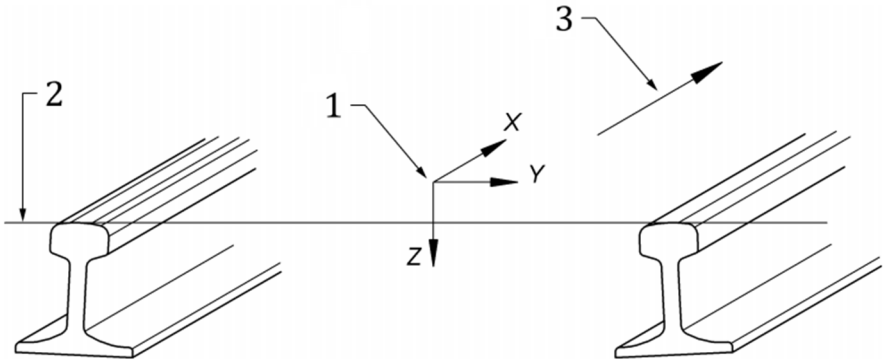

Figure 2 - Track coordinate system illustration, presenting the system axes (1), the intersection between a given cross section and the running surface (2), and the running direction (3) (COMITÉ EUROPÉEN DE NORMALISATION, 2019)

Considering the longitudinal aspect of the design track geometry, the horizontal profile[9] consists of sections classified into tangents (straights), transition curves, or circular curve sections. The basic parameters for horizontal layout description are the **horizontal radius** and its derived parameter, the **horizontal curvature,** which is the inverse of the radius. Regarding the vertical layout, the geometrical elements are the **gradients** and the **vertical curves** for transition between gradients (ESVELD, 2001). These track features are described for the track centre line and are designed considering the compromise between the limit values for the specified operating speeds and the safety, topographical, geological, engineering, historical, and economic constraints (ESVELD, 2001; COMITÉ EUROPÉEN DE NORMALISATION, 2009a).

[9] When discussing track design parameters, the term alignment is also used to refer to the horizontal and vertical track profiles (ESVELD, 2001). However, considering the scope of the present work, the use of the terms profile, layout or macro geometry is preferred in order not to cause misinterpretation with the specific use of alignment when describing track lateral irregularities.

Considering safety and comfort standards, the centrifugal lateral acceleration in a curve is counterbalanced by the **cant** or **superelevation**. This parameter stands for the designed elevation of the outer rail above the inner rail (measured along the vertical of the local horizontal plane). The cant that entirely compensates for the centrifugal force at a given speed is called equilibrium cant. From these definitions, there are derived parameters such as the cant deficient (difference between the applied cant and a higher equilibrium one) or excess (difference between the applied cant and a lower equilibrium one), and the cant gradient (its variation along cant transition[10]) (ESVELD, 2001; COMITÉ EUROPÉEN DE NORMALISATION, 2010a).

Additionally, the vertical profile is described in terms of the vertical radius, the vertical curvature (inverse of the radius), and the track gradient. The friction condition of the metal-to-metal contact on the wheel-rail interface limits the maximum gradient in adhesion railways[11] at values between 30-40 ‰ (ESVELD, 2001).

Another relevant design geometry parameter is the **gauge**, which is the distance (measured along the y-axis in the track coordinate system) between the internal faces of the rails measured at a specific distance below the rail crown. The most common railway gauge, often referred to as standard gauge or UIC gauge, is defined to be 1,435 mm. Moreover, the distance from the top of the rail is typically 14 mm in Europe and 5/8 in. (about 15.8 mm) in North America. Since the gauge determines which vehicles are compatible to run on a considered network and is a crucial aspect concerning railways interoperability, this value is commonly used as a descriptor of a given line or network.

Lastly, the track deviation irregularities (Figure 3) are described by the following parameters (ESVELD, 2001; STOW; ANDERSSON, 2006; COMITÉ EUROPÉEN DE NORMALISATION, 2019):

- **Longitudinal level irregularity** corresponds to the vertical deviation (z-axis in the track coordinate system) of the running table of the rails in relation to the

[10] In common practice, the cant transitions should coincide with the transition curve (COMITÉ EUROPÉEN DE NORMALISATION, 2010a)

[11] This term is used in opposition to the funicular or rack railways to describe the usual railways in which adhesion traction moves the train.

reference position (mean position or the design geometry). The European Committee for Standardization (*Comité Européen de Normalisation,* CEN) defines the following wavelength ranges: D1 (2-25 m], D2 (25-70 m], and D3 (70-150 m], plus optional range D0 (1-5m] to detect short wavelength defects that generate high dynamic forces.

- **Alignment irregularity** is the lateral deviation (y-axis in the track coordinate system) of the running table of the rails in relation to the reference position (mean position or the design geometry). The CEN defines the following wavelength ranges: D1 (2-25 m], D2 (25-70 m], and D3 (70-200 m], plus optional range D0 (1-5m] to detect short wavelength defects that generate high dynamic forces.

- **Cross level or cant irregularity** is the difference in height (vertical in relation to the local horizontal plane) between the left and right rails. When this difference is designed (cant), the deviation from the nominal (or mean) value is considered a cross-level defect. A derived parameter is the **twist**, the cross-level variation over a given length.

- **Gauge irregularity** corresponds to the deviation from the nominal gauge.

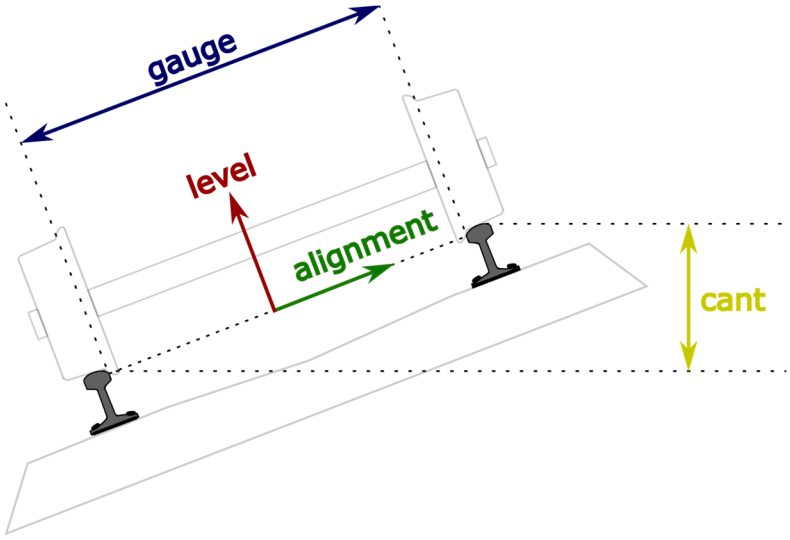

Figure 3 - Illustration of the track irregularities. Adapted from Esveld (2001)

2.3 DYNAMICS OF THE TRAIN-TRACK SYSTEM

Besides providing vehicle guidance through the wheelset guidance, the rails also excite the vehicle components due to the irregularities on the track and the rail surface (ESVELD, 2001). Rail vehicle excitation occurs at the wheel-rail interface, and the associated contact forces are nonlinear functions of variations of lateral and vertical track position and speed (INTERNATIONAL ORGANIZATION FOR STANDARDIZATION, 2003). Besides the track geometry, the irregularities, and speed, other aspects such as track stiffness, vibration isolation given by the suspensions (primary and secondary, Figure 4), vehicle masses, and relative distance to bogie centreline also influence the amplitude of the irregularity-related linear and angular displacements inside the car body (INTERNATIONAL ORGANIZATION FOR STANDARDIZATION, 2003; HUNGRIA, 2017; NETIRAIL-INFRA, 2017). From these aspects, the response-based track inspection principle has been used since the first track recording vehicles (DOW, 2014) and reflects the relationship between vehicle displacements and railroad geometry features and irregularities.

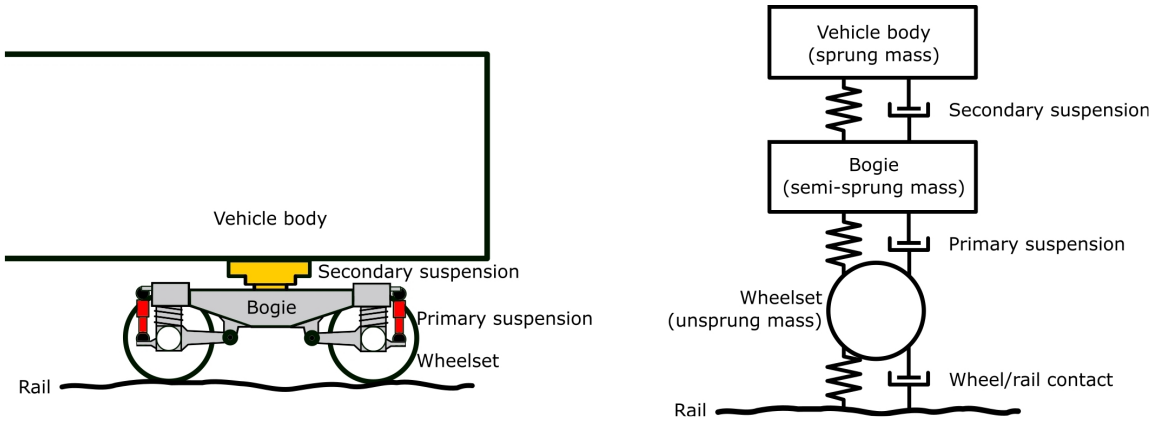

Figure 4 - Schematic representations of the railway vehicle suspensions (left) and the conceptual model of the dynamic interactions between the vehicle masses (right). Adapted from Garg and Dukkipati (1984), Salvador et al. (2016) and RailSystem (2023)

For train dynamics analysis, it is useful to describe the track features that excite the vehicle in terms of their wavelengths. While track designed geometry can be mainly regarded as a set of long-wavelength features, the deviations in geometry (irregularities) and the rail wear are described according to their typical wavelength ranges. Thus, the wheelset will be subjected to an exciting frequency f under the

fundamental relationship $f = \frac{v}{L}$ (HAIGERMOSER et al., 2015; SALVADOR et al., 2016; VINKÓ; BOCZ, 2018), where v is the speed and L is the considered irregularity wavelength modelled as sinusoidal function (COMITÉ EUROPÉEN DE NORMALISATION, 2014) on which the train is running. Typical wavelengths associated with some of the main track aspects can be described as presented in Table 1.

Table 1 - Main track aspects and their corresponding wavelengths (COMITÉ EUROPÉEN DE NORMALISATION, 2017a; ZUCCHI, 2013; HAIGERMOSER et al., 2015; SALVADOR et al., 2016)

Wavelength range [m]	Track aspect
0.03-0.06	Very short wavelength rail corrugation, rail joints, small-size squats
0.06-0.25	Short wavelength rail corrugation, medium-size squats
0.25-0.60	Medium wavelength rail corrugation, large size squats, turnout frog
0.60-0.70	Sleeper spacing
0.60-2	Long-wavelength rail corrugation, Ballast fouling
1-5	CEN optional wavelength range D0 for longitudinal level and alignment (short wavelength defects that generate high dynamic forces)
3-25	CEN wavelength range D1 for longitudinal level and alignment (short wavelength)
25-70	CEN wavelength range D2 for longitudinal level and alignment (medium wavelength)
70-200	CEN wavelength range D3 for longitudinal level (70-150m] and alignment (70- 200 m] (long wavelength, generally considered only for line speed greater than 230 km/h)

Irregularity-related lateral and vertical signals obtained may be simplified by the sum of multiple irregularity-related signatures, each approximated by a sinusoid. This spectral aspect enables Fourier Transform-based analyses of responses to extract track features from vibration signals (GARG; DUKKIPATI, 1984; COLE, 2006). On the other hand, the longitudinal vibration component associated with track irregularities is usually less relevant than its orthogonal counterparts. Regarding longitudinal models (GARG; DUKKIPATI, 1984; COLE, 2006), it can be considered that this component is mainly due to coupler impact transients as an indirect effect of irregularity on adjacent coaches. In addition, this component is marginal when compared to the longitudinal travelling acceleration (HOBEROCK, 1977).

2.3.1 Predominant influence of track quality parameters on vehicle responses

Considering the established knowledge on the railway domain and the theoretical

consideration, the standards and the current practice consider the predominant influence of each track quality parameter on vehicle dynamic responses. Regarding accelerations in train cabin (ZUCCHI, 2013; COMITÉ EUROPÉEN DE NORMALISATION, 2014; WESTON et al., 2015), the predominantly distinguishable vibrations may be due to defects in the following geometry parameters: a) longitudinal level for vertical accelerations; and b) track alignment, twist, and cross level for lateral accelerations. In complement, the European standard regarding geometric quality levels (COMITÉ EUROPÉEN DE NORMALISATION, 2017a) gives a broader portrait of the track parameters' influence on dynamic responses, as presented in Table 2. One must emphasize that the difference between track quality impact on lateral forces and lateral acceleration is due to the primary and secondary suspensions.

Table 2 - Relationship between track parameter and vehicle response (COMITÉ EUROPÉEN DE NORMALISATION, 2017a).

Vehicle response	**Track parameter**			
	Track gauge	**Longitudinal level**	**Twist/cross level**	**Alignment**
Sum of the Lateral forces (ΣY)	x		x	x
Vertical forces (Q)		x	x	x
Lateral acceleration in vehicle body			x	x
Vertical acceleration in vehicle body		x		
Lateral (Y) and vertical (Q) ratio Y/Q	x	x	x	x

Considering the relative motion between the wheelset and the rail, it is also known that the lateral displacement of the wheelset does not fully follow lateral irregularities (WESTON et al., 2007b; ALFI; DE ROSA; BRUNI, 2016) given the wheel/rail clearance. Thus, the correlation between lateral acceleration in the car body and the lateral irregularities is expected to be smaller than that between vertical acceleration and vertical irregularities.

Moreover, the European standard regarding the characterization of track quality (COMITÉ EUROPÉEN DE NORMALISATION, 2014) defines the Point Mass Acceleration (PMA) as an assessment figure for the characterisation of track geometry quality. This figure comprises the combination of various track parameters considering the expected influence of track imperfection on lateral and vertical accelerations, providing noteworthy remarks for the present thesis. The model that

supports the PMA has a mechanical background and considers an unsprung virtual vehicle, which is assumed to be a point mass travelling at a given vertical distance over the track centreline. Moreover, this point mass travels at a constant speed (maximum speed for a given track section). According to the common practice, the lateral and vertical accelerations for the PMA model are given by:

$$a_Y = c \,.\, v^n \,.\, (\overline{AL}'' + z \,.\, (\overline{LL}''' - \psi'')) \quad (1)$$

$$a_Z = c \,.\, v^n \,.\, \overline{LL}'' \quad (2)$$

where:

- v is the maximum line speed.
- $\overline{LL}$ is the longitudinal level for range D1, the average of left and right rails.
- $\overline{AL}$ is the alignment for range D1, average of left and right rails.
- ψ is equal to (*LL* left rail – *LL* right rail)/d, with d being the distance between the centres of the railheads.
- z is the height of the centre of gravity over the track centreline.
- n in the exponent for speed, open for scaling.
- c is the coefficient, open for scaling.
- The derivates are in the space domain.

Under this method, the resultant parameter is the mean or the standard deviation within 100-m length sections of the vectorial sum of vertical and lateral PMAs. It should be emphasized that this method evidences how the pairs LL and vertical acceleration, and AL and lateral acceleration may be correlated. Furthermore, one can infer from the equations that a sinusoidal track feature will result in a sinusoidal (after double derivate) acceleration.

The PMA model is partially compatible with empirical evidence that the acceleration caused by irregularities is approximately proportional to the square of the vehicle speed and proportional to the irregularity amplitude (WESTON et al., 2015), apart

from the nonlinearities due to the suspension systems and the wheel-rail interaction[12] (GARG; DUKKIPATI, 1984).

2.3.2 Vibration modes of the car body

The periodic patterns of track irregularities, the travelling speed, and the result of the combined car body excitation transmitted at the front and rear bogies excite the car body at specific linear and angular vibration frequencies. Concurrently, each vehicle element (1st, 2nd, and 3rd masses) has a natural (or resonant) frequency at each vibration mode depending on the suspension parameters, the masses, and the vehicle components' geometry. These vibration modes, also called eigenmodes, are defined by their modal shape (Figure 5) and self-vibration frequency (eigenfrequency). Thus, the corresponding eigenmode is excited whenever the car body is excited at a frequency close to its natural frequencies (POLACH; BERG; IWNICKI, 2006; HUNGRIA, 2017).

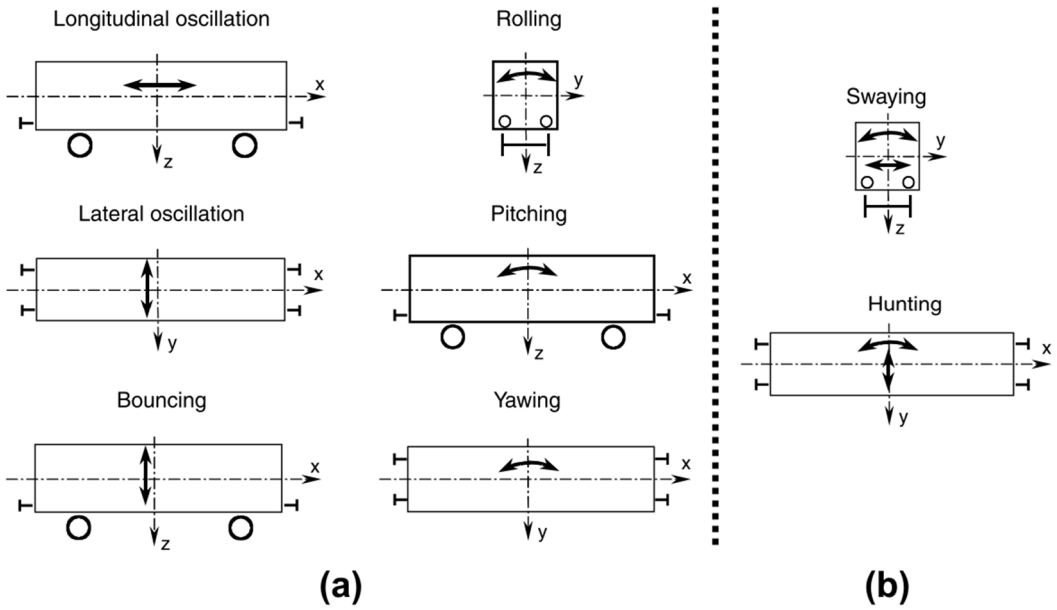

Figure 5 - (a) Basic car body vibration modes and (b) combined car body modes (THOMPSON; JONES, 2006)

[12] Garg and Dukkipati (1984) states that, for simplification, suspensions characteristics are “linearized over certain ranges of suspension travel”. Regarding the wheel-rail interaction, the authors mention that a linear analyses “retains validity for small-amplitude motions”. Thus, these linearities are neglected depending on the required level of complexity of the model.

For the sake of human sensitiveness, passenger coach suspension is usually designed to isolate the cabin for excitation frequencies above about 2 Hz (THOMPSON; JONES, 2006). In this context, the resonance frequency of the sprung mass above the secondary suspension ranges is about 0.5-1 Hz for the main vibration modes (IWNICK, 1998; SALVADOR et al., 2016) and 8-10 Hz for bending (INTERNATIONAL ORGANIZATION FOR STANDARDIZATION, 2003; POLACH; BERG; IWNICKI, 2006). The former frequency range prevails above the bogies, while the latter prevails at the centre of the car body (POLACH; BERG; IWNICKI, 2006).

2.4 TRACK INSPECTION TECHNIQUES

For railway infrastructure management, the periodic inspection of track quality is crucial to ensure proper dynamic behaviour of the train-track system and, thus, a safe operation and a comfortable ride. This activity comprises the inspection of the track elements, track geometry, and track structural conditions.

Regarding the **track elements inspection**, the task is carried out visually or by means of image registration. In the case of the rails, their profiler and the superficial wear can be inspected through laser triangulation or using contact-based profilers, as well as the fatigue cracks can be detected early using ultrasound inspection (ESVELD, 2001; STOW; ANDERSSON, 2006; MERMEC, 2020)

For the **track geometry inspection**, the use of dedicated self-propelled or hauled vehicles, such as the **track recording vehicles** (TRV), is a well-established technique and a more productive alternative to the traditional survey with topographic instruments, the visual inspection, and the manual track geometry trolleys (IWNICKI, 2006; PITA, 2006; NIELSEN et al., 2013; WESTON et al., 2015). The TRVs are cars or trains specifically designed or adapted from existing vehicles, equipped with a **track geometry measurement system** (TGMS), and eventually equipped with other measurement modules regarding rail wear monitoring, **ride dynamics measurements**, communication system diagnostic etc. One of the main attributes when using the recording vehicle is obtaining geometric data in a **loaded state**, containing the desired dynamic responses of the track (NIELSEN et al., 2013;

VINKÓ; BOCZ, 2018).

Since operation fitted to average running speeds is intended, modern track recording techniques mainly employ sensors installed in full-sized rail vehicles that periodically gather loaded track geometry data (IWNICKI, 2006; MATISA, 2017). The technologies employed on these special vehicles can be classified into **versine systems** and **inertial systems**, being also usual a combination of the two concepts (NIELSEN et al., 2013). The versine or chord offset concept obtains the track profile through a transfer function that considers a fixed measurement chord and the offset at the mid-chord position (the versine). In a vehicle-based measurement system, the chord is the vehicle wheelbase. Moreover, the measurement of the chord offset done at the centre of the vehicle can be **contact-based** (using a third wheelset or bogie) or **optical-based** (noncontact measurements with cameras and lasers) (STOW; ANDERSSON, 2006). In turn, the inertial principle considers the vehicle's responses to irregularities.

An example of the **contact-based method** is the use of measuring wheels in contact with the rails in the first version of the French *Voiture Mauzin*, one of the first auscultation vehicles. This version was developed in 1930 by Andre Mauzin, the then-chief engineer at the SNCF (PRUD'HOMME, 1997; TERRASSE, 2008). The subsequent versions of track recording vehicles of SCNF were also named *Mauzin,* although employing different technologies. The first technique employed in such a vehicle was the use of wheels rolling on the rails head and dissociated from the vehicle wheelset. The lateral and vertical displacement of these small wheels with respect to a reference beam depended on track and rail irregularities. Thus, these displacements were converted into electrical signals, sent to the cabin, and registered on paper by a chart recorder. However, the technique has intrinsic limitations associated with high speeds, resulting in substantial stress acting on the contacting instrument and may imply some speed constraints (especially in high-speed lines) and additional instrument maintenance needs (ZEITSCHRIFT et al., 1941).

In order to overcome the problems with traditional contact-based techniques, the technologies mainly employed in track recording cars are based on **inertial sensors** (**response-based**) or optical systems (**noncontact**) (IWNICKI, 2006; MATISA,

2017). The inertial principle was already used on some of the first versions of the recording vehicles and correlates vehicle displacements with railroad irregularities. For all the **response-based** systems mentioned hereafter, tactical, industrial or navigation-grade inertial sensors (medium/high-cost) are preferred to meet the data quality requirements.

Under **dynamic response concept**, direct track geometry and rail corrugation assessment can be performed using accelerometers installed on axle boxes, applying double integration in a simplified approach (NIELSEN et al., 2013; WESTON et al., 2015) or ideally considering the rail-wheel contact modelling in the transfer function (GRASSIE, 1996; QUIRKE et al., 2017; WEI et al., 2018; ZHU; LAW; HUANG, 2018) to estimate irregularities. Accelerometers installed on the bogie and inside the car body are widely used for running behaviour and ride comfort assessment (WICKENS, 2006; NIELSEN et al., 2013; ZUCCHI, 2013); at any rate, they also can be used for geometry analysis if the suspension displacements are known (STOW; ANDERSSON, 2006) or if the train-track dynamic model and its parameters are well known (LI et al., 2017; KRAFT; CAUSSE; COUDERT, 2018). Moreover, inertial platforms (i.e., stabilized platforms) can obtain vehicle inclination in relation to the local horizontal plane and, thus, estimate the track parameters related to these angular parameters, such as the cross level and the twist (ZUCCHI, 2013).

A complementary approach is the analysis of vehicle vibration in terms of its expected spectral response to irregularities. For this, the expected responses considering the vehicle speed and the typical wavelengths for each track feature are established, and the gathered response data is analysed through peak identification in the frequency domain or frequency filtering in specific bands. Additionally, other parameters can be calculated for the frequency-filtered signals, such as the double integration of the signal, the peak (or mean) to peak values, or the standard deviation over a specific length (COMITÉ EUROPÉEN DE NORMALISATION, 2019).

Given the simplicity of installing inertial sensors, the response-based concept has also begun to be widely used in the rolling stock for data collection during commercial operation. As an example of complementary systems to the inspection already performed by the standard track recording cars, Deutsche Bahn employs inertial sensors installed in the restaurant car of high-speed trains to perform track geometry,

running behaviour and ride comfort assessment (NIELSEN et al., 2013).

On the other hand, **optical sensing** is commonly done under a chord/versine concept and through laser triangulation, which consists of scanning the beam along the rail cross-section and recording the light reflected by cameras positioned over each rail. The Plasser & Theurer EM-100 track recording car, used by the São Paulo State's Metropolitan Railway Company (*Companhia Paulista de Trens Metropolitanos*, CPTM), is an example of an optical sensing-based inspection car. In this recording car, track geometry and rail irregularities are surveyed utilising two laser triangulation modules, each of them situated above each rail and combining a laser emitter and a camera for laser reflection detection. Since the relative position between the emitter and the camera is fixed, the time lag between reflection and reception is used to estimate the rail position and the rail surface condition. The rail data from both modules are combined to determine track geometry in relation to the vehicle frame (AUER, 2013). The main disadvantage of this technique is the interference of the ambient light and temperature in measurements. A complementary optical technique is the image and video registration (as performed by the Plasser & Theurer EM-100), allowing human or automated track element inspection.

Examples of the combined use of response-based and noncontact methods are the modern track recording trains (TRT) that are similarly designed or converted from commercial or passenger trains. These special trains carry dozens of inertial (accelerometers and inertial platforms) and optical sensors to perform track inspections and, using complementary sensors, also perform signalling, catenary, and telecommunication inspections. The modern Italian track recording vehicles Aiace and Diamante (ZUCCHI, 2013) and the Japanese *Doctor Yellow* (NAGANUMA; TANAKA; ICHIKAWA, 2000) are examples of this concept. Another example is the British UGMS, a compact module that combines inertial sensors with laser triangulation surveying and can be installed underneath commercial trains (NETWORK RAIL, 2007) and are a more affordable alternative to specialised coaches and vehicles.

In general terms, the georeferencing of track data is usually performed through Global Positioning System (GPS) coordinates (often with differential correction)

integrated with signalling information, odometry and inertial navigation. This aspect is relevant since the sensing platform (i.e., the vehicle that carries the sensors) is mobile, and there is the need for distinction between adjacent tracks (distance between centrelines of about 4 meters) that curbs the use of single-point satellite positioning.

2.4.1 Practical issues regarding response-based methods

One of the main practical issues regarding using inertial sensors is the Nyquist sampling theorem, which states that a signal with a given bandwidth f_0 can only be reconstructed from its sample values if the sampling frequency is over twice its bandwidth f_0. (INGLE; PROAKIS, 2000). From this theorem, the sample rate must be greater than the Nyquist sample rate $f_N = 2f_0$ for a proper signal characterisation without aliasing. Moreover, the f_0 frequency defines the low-pass filter's minimum cut-off frequency applied as an antialiasing filter when sampling (MANOLAKIS; INGLE; KOGON, 2005). Adopting a reverse calculation, the minimum monitorable track irregularity λ for a fixed sample rate depends on the running speed v and is given by $\frac{2.v}{f_S}$.

Moreover, another practical issue regarding sensors positioned in the cabin is the influence of sensor position on signals. If a sensor is placed right over one of the sides of a given bogie, it is expected to follow more closely the track irregularities of this side. When displaced away from this bogie, the influence of the other bogies increases, and the signal presents a distinct form due to phase shift and differences in magnitude. For example, considering an accelerometer over the rear bogie and another one over the front bogie on the same side, they will be in phase for bounce mode responses and out of phase for pitch mode responses (STOW; ANDERSSON, 2006). Regarding magnitude, acceleration at coach extremities is expected to be more significant than at the body centre (TANIFUJI, 1988; POLACH; BERG; IWNICKI, 2006). On the other hand, tendencies of vibration variation from the front to the rear coach of the train set are intricate and depend on factors such as the suspension parameters (mean value and variation between coaches), the equivalent

conicity[13], the stiffness and damping coefficients of coaches coupling, the speed, the train length and the mass variation between coaches (TANIFUJI, 1988; POLACH; BERG; IWNICKI, 2006; KANG, 2014).

Lastly, the inertial principle has intrinsic limitations and requirements. Regarding the influence of measurement speed on signal, the systems have their efficiency undermined at very low speeds. Weston et al. (2007a), for instance, states that axlebox-mounted accelerometers are able to monitor short wavelength rail geometry only at a speed higher than 15 m/s. Regarding inertial sensors installed in the carboy instead of bogie the axlebox-mounted sensors, it is also known that suspensions substantially attenuate vibration levels and act as a low pass filter (THOMPSON; JONES, 2006), curbing the proper description of shorter wavelength irregularities from the car body vibration.

2.5 CHAPTER FINAL CONSIDERATIONS

The track description identified critical concepts for the proposed response-based monitoring system, such as the track coordinate system and the description of track parameters according to this coordinate system and the local navigation system (local horizontal plane). Furthermore, regarding the material of track components, the possible track stiffness variation was also identified depending on the material variation (i.e., timber or concrete sleepers, ballasted or slab tracks) and the consequent influence on vehicle excitation.

Moreover, from the established train-track dynamics knowledge, the dominant influence of specific track features was identified, namely the influence of the longitudinal level on the vertical vibration and the alignment on the lateral vibration.

---

[13] The equivalent conicity is a wheel-rail contact geometry parameter for straight track and very large radius curve defined as the “tangent of the cone angle of a wheelset with coned wheels whose kinematic movement has the same wavelength as the given wheelset for a certain amplitude of the lateral wheelset movement” (COMITÉ EUROPÉEN DE NORMALISATION, 2021). Thus, it considers the appropriate wheel and rail profiles assessment.

Lastly, the issues related to the current response-based monitoring techniques evidence some possible limitations of the proposed technique. These limitations arise from the following aspects: a) use of very low-cost, low-quality inertial sensor that does not meet the requirements for the current systems and techniques; b) use of strap-down inertial sensors aboard train cabin, gathering vibration data under the influence of both suspension and without information about relative displacement between the wheelset and the body. At the same time, the techniques for spectral analysis and filtering of the obtained acceleration may indicate a set of mathematical techniques that could be used. These will be detailed in the next chapter and contextualized for the proposed application.

3 COMFORT AND RIDE DYNAMICS MONITORING

This chapter presents the main methods for comfort and ride dynamics assessment in railway transportation, highlighting their possible use as an indirect track quality index. Firstly, the standard regarding comfort (ISO 2631 and EN 12299) are presented and discussed regarding the constraints when using consumer-grade sensors for the stipulated measurements. Moreover, regarding both comfort and stability issues, ride dynamic parameters are discussed considering the usual measurement system and the predefined limit values for specific cases. For instance, the particular values are presented for trains running on the Italian and São Paulo's railway network.

3.1 ISO 2631

The ISO 2631-1 - *Mechanical vibration and shock - Evaluation of human exposure to whole-body vibration - Part 1: General requirements* - aims to define methods for whole-body vibration quantification concerning the "human health and comfort, the probability of vibration perception, and the incidence of motion sickness". (INTERNATIONAL ORGANIZATION FOR STANDARDIZATION, 1997). This standard considers two frequency ranges: from 0.5 to 80 Hz for health, comfort, and perception; and from 0.1 to 0.5 Hz for motion sickness. Moreover, this part of ISO 2631 considers vibration transmitted through different supporting surfaces: the feet of a standing person, the seat surface, the back, and the feet of a seated person, or the supporting area of a recumbent person. These areas define the interface between the human body and the source of the vibrations.

Regarding the vibration measurement, the standard describes the acceleration as the primary quantity with the alignment of the transducers with the preferred axes (longitudinal, lateral, and lateral). Moreover, direct measurement is recommended with the measurement location corresponding to the considered interfaces previously described for standing, seated, or recumbent body.

The considered ISO standard defines that vibration frequencies should be weighted according to human sensitivity for each frequency. Therefore, the acceleration signal is analysed through frequency-weighting of acceleration spectra, considering the frequency range of interest for the human response to vibrations (from 0.5 to 80 Hz) and its respective 23 one-third octave bands, each with a specific weighting factor. Thus, the resultant frequency-weighted root-mean-square acceleration a_w for a given axis is given by Eq. 3:

$$a_w = \sqrt{\sum_{i=1}^{23} (W_i \cdot a_i)^2} \tag{3}$$

where Wi is the recommended weighting factor for the i_{th} one-third octaves band, and ai is the RMS acceleration for the i_{th} one-third octaves band for the given axis. There are different frequency weighting curves depending on the application, position, and axis, reflecting the different ways vibration affects humans. W_k is the recommended curve for the z-direction and W_d for the x and y-directions for the usual comfort analysis. However, part 4 of this standard recommends the curve Wb for the z-direction for rail vehicles. Figure 6 depicts these weighting curves, being remarkable the slight difference between W_k and W_b.

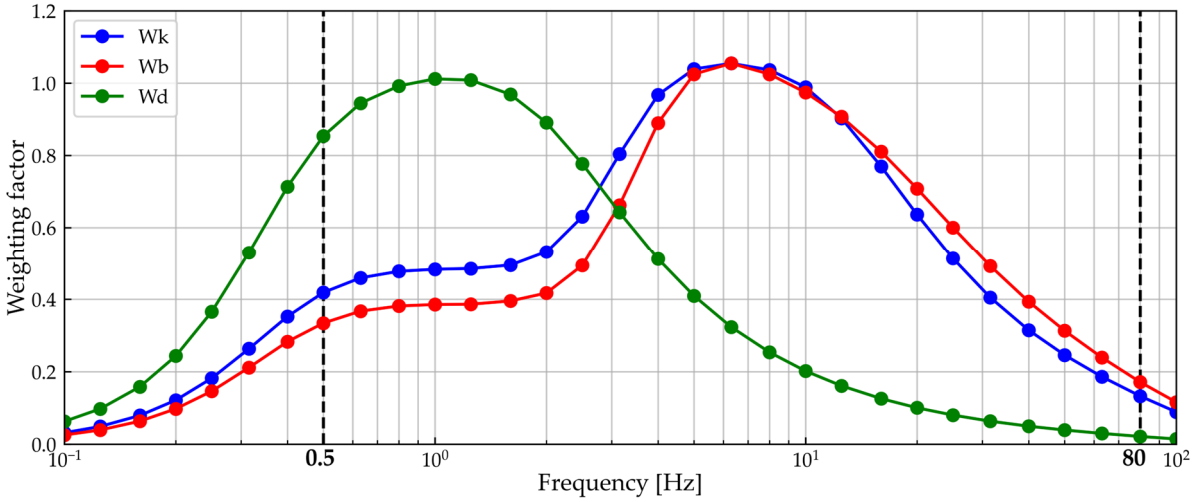

Figure 6 - Weighting factors versus central frequency of each one-third octave band

The continuous comfort assessment considers levels of ISO frequency weighted acceleration evaluated as a sequence of RMS values over a short period, typically 5 seconds. The vibration total value a_v can be calculated from the orthogonal

components as:

$$a_v = \sqrt{(k_x \cdot a_{wx})^2 + \left(k_y \cdot a_{wy}\right)^2 + (k_z \cdot a_{wz})^2} \quad (4)$$

where a_{wx}, a_{wy}, and a_{wz} are the RMS frequency-weighted accelerations for, respectively, the axes x, y and z, and k_x, k_y, and k_z are the multiplying factor. The total value is recommended for comfort analyses with multiplying factor equal to 1 for seated, standing, and recumbent passengers. For the present work, since the central aspect is the relationship between track quality and comfort, the analysis will be decomposed in terms of the lateral and vertical components as they are those effectively associated with the track quality.

Furthermore, the calculated values can be compared with those indicated by ISO 2631 concerning the expected reaction to vibration in public transportation (Table 3). This standard emphasises that these values are not limits for accelerations but only approximations since other relevant factors need to be considered, such as exposure time, the activity performed when exposed to the vibration, acoustic noise, and temperature. This fact explains the superposition of the value ranges presented in Table 3.

Table 3 - Likely reactions regarding comfort in public transportation (INTERNATIONAL ORGANIZATION FOR STANDARDIZATION, 1997)

a values (m/s^2)	**Likely reaction**
less than 0.315	Not uncomfortable
0.315-0.63	Little uncomfortable
0.5-1.0	Fairly uncomfortable
0.8-1.6	Uncomfortable
1.25-2.5	Very uncomfortable
more than 2	Extremely uncomfortable

3.2 EN 12299

The scope of EN 12299 is the comfort assessment associated with low levels of acceleration and roll velocity in rail vehicles considering the effects of vibration exposure measured on the floor of the vehicle body (COMITÉ EUROPÉEN DE

NORMALISATION, 2009b). The standard does not include higher acceleration levels, such as those related to health deterioration effects. Specifically, the following items are considered by the EN 12299 standard:

- Theoretical aspects of the effects of vibration exposure on ride comfort and vehicle assessment with respect to ride comfort.
- Vibration transfer on whole body through interfaces or through floor interface. The standard considers passengers standing or seated.
- Test procedures, regarding definitions, reference systems, requirements, measurement and evaluation rules, and report guidance. The standard considers indirect measurements[14].
- This standard defines no limiting values related to service quality.

The standard identifies typical characteristics of railway vehicle motions and their measurements and evaluation. Firstly, regarding the type of evaluation, it can be performed in quasi-stationary (mean comfort, evaluated on a long-time basis of at least some minutes) or non-stationary (specific procedure for quasi-static lateral acceleration due to curving, with particular consideration in curve transitions; and instantaneous sensation at discrete events, on a short-time basis of typically 5 seconds).

Regarding the frequency range of motions, the expected values are:

- Values up to 15 Hz in the lateral direction due to track characteristics, vehicle body swing-roll and way vibration modes at lower frequencies, suspensions characteristics and other vehicle body motions at higher frequencies.
- Values up to 40 Hz in the vertical direction due to track characteristics, suspensions characteristics, wheel defects, and vehicle body modes.
- Values from 0 Hz to 2 Hz for comfort on curve transitions and for discrete

[14] Indirect measurement considers the measurement of motion quantities such as accelerations or roll velocity. Direct measurement considers the measurement of actual passengers' reactions, e.g., by means of a questionnaire to be filled by passengers.

events.

The EN define specific procedures for quantifying comfort indexes starting from ISO-based frequency-weighted acceleration concerning different methods, as summarized in Table 4.

Table 4 - Comfort assessment methods, their quantities, specifications, and applications. Adapted from (COMITÉ EUROPÉEN DE NORMALISATION, 2009b).

	Mean comfort standard method	**Mean comfort complete method**	**Continuous comfort**	**Comfort on curve transition**	**Comfort on discrete events**
Comfort indexes	N_{MV} (mean value)	N_{VA} (seated passenger, in French: *voyager assis* - VA) N_{VD} (standing passenger, in French: *voyager debout* - VD)	C_{CX} (continuous on x-axis) C_{CY} (continuous on y-axis) C_{CZ} (continuous on z-axis)	P_{CT}	P_{DE}
Motion quantities	Accelerations in three directions	Accelerations in three directions	Accelerations in three directions	Lateral accelerations, lateral jerk, roll velocity	Lateral acceleration
Measuring position	Floor	VA: floor and interfaces VD: floor	Floor	Floor	Floor
Application on passenger comfort assessment	Yes	Yes	Yes	Yes	Yes
Application on vehicle assessment	Yes	No	Yes	Yes, for tilting vehicles	No
Application on track design geometry assessment	No	No	No	Yes	No
Application on track maintenance	Yes	No	Yes	No	Yes
Application on vehicle maintenance	Yes	No	Yes	No	No

The evaluation of Continuous Comfort in accordance with EN 12299 considers a 5-seconds time basis and is carried out through:

- Measurement of the accelerations on the floor (and the seat interface for the Mean Comfort complete method). Since the accelerations are closely dependent upon the location, the measurements shall be carried out at the centre and at both ends of the passenger compartment. Additional

measurements above the pivot of the bogie may be carried out considering specific test purposes.

- Digitization with appropriate anti-aliasing filter.
- Frequency weighting of the signal in accordance with ISO 2631, obtaining the frequency-weighted accelerations $\ddot{x}_{W_d}$, $\ddot{y}_{W_d}$, and $\ddot{z}_{W_b}$. For these frequency weighting, the W_d curve is applied for the x and y-axes, while the W_b curve is used for the z-axis.
- calculation of RMS values over 5-seconds periods, resulting in the frequency weight RMS accelerations $a_x^{W_d}$, $a_y^{W_d}$, and $a_z^{W_b}$. These values are also, respectively, the Continuous Comfort indexes C_{CX}, C_{CY}, and C_{CZ}. These measures are functions of time for each axis.

Conversely, the evaluation of Mean Comfort (both standard and complete methods) considers 5-minutes test zones with constant speed, with test speed depending on the test purposes. The correspondent index is obtained by following the aforementioned steps for Continuous assessment plus the following steps:

- For the Standard Method: calculation of the 95th percentile over 5-minutes periods (test zones) measured at the floor interface (subscript P): $a_{x,P95}^{W_d}$, $a_{y,P95}^{W_d}$, and $a_{z.P95}^{W_b}$. The Mean Comfort Standard index is obtained as follows:

$$N_{MV} = 6 \cdot \sqrt{\left(a_{x,P95}^{W_d}\right)^2 + \left(a_{y,P95}^{W_d}\right)^2 + \left(a_{z,P95}^{W_b}\right)^2} \tag{5}$$

  Depending on the application, the partial comfort indexes for the x, y, and z axes (using the respective percentiles) can be considered.

- For the Complete Method: additional calculation of the 50th percentiles (i.e., median) measured at the floor (subscript P), the seat pan (A), and the seatback interfaced (D): $a_{x,P50}^{W_d}$, $a_{y,P50}^{W_d}$, and $a_{z,P50}^{W_b}$ for measurements at the floor interface and analogous for A and D interfaces. The Comfort index for seated passengers is obtained as follows:

$$N_{VA} = 4 \cdot \left(a_{z,P95}^{W_b}\right) + 2 \cdot \sqrt{+\left(a_{y,A95}^{W_d}\right)^2 + \left(a_{z,A95}^{W_b}\right)^2} + 4 \cdot \left(a_{x,D95}^{W_d}\right) \quad (6)$$

The Comfort index for standing passengers is obtained as follows:

$$N_{VD} = 3 \cdot \sqrt{16 \cdot \left(a_{x,P50}^{W_d}\right)^2 + 4 \cdot \left(a_{y,P50}^{W_d}\right)^2 + \left(a_{z,P50}^{W_b}\right)^2} + 5 \cdot \left(a_{y,P95}^{W_d}\right) \quad (7)$$

3.3 RIDE DYNAMIC BEHAVIOUR

Besides the comfort assessment in accordance with the aforementioned standards, railway practitioners may also adopt admissible values for dynamic quantities regarding the running behaviour as a whole. For these analyses, the usual data source are the **vehicle dynamics measurement systems** installed aboard in-service trains or diagnostic vehicles. These measurement units may encompass inertial sensors distributed over the different vehicle frames (wheelset, bogie, and car body) and placed at different positions. As the running behaviour depends on both track and vehicle characteristics, the dynamic parameters measured aboard a reference (diagnostic) train at a stipulated speed may be used to describe track condition degradation, and the non-compliance with the specified limits may result in operational restrictions (e.g., speed limitation or interdiction).

Regarding these aspects, the European standard EN 14363 - *Railway Applications - testing for the acceptance of running characteristics of railway vehicles - test of running behaviour and stationary tests* - defines measurement settings, data processing and analyses methods for testing the running characteristics[15] and the consequent homologation of railway vehicles in Europe (COMITÉ EUROPÉEN DE

[15] This standard characterizes running behaviour as the characteristic of a running vehicle regarding its interaction with the track, covering specific terms such as running safety, track loading, and ride characteristics. The parameters used for the running behaviour assessment are: a) forces between wheel and rail; or b) lateral forces between wheelset and axle box, and/or c) accelerations. (COMITÉ EUROPÉEN DE NORMALISATION, 2022).

NORMALISATION, 2022). Additionally, this standard is generally applied for other technical tasks such as track or vehicle monitoring in operational use. Thus, the Italian railway infrastructure manager (*Rete Ferroviaria Italiana*, RFI) adopts this standard as basis for its document stipulating requirements for ride dynamics on high-speed, high-capacity lines, which is entitled *Standard di Qualità Geometrica del Binario e Parametri di dinamica di Marcia per Velocità fino a 300 km/h (*Standard for Geometric Track Quality and Running Behaviour Parameters for Speeds up to 300 km/h). This Italian document establishes admissible peak values considered (in relation to the zero level) for the following parameters:

- Vertical and lateral acceleration measured in the car body ($\ddot{z}$ and $\ddot{y}$, respectively). For vertical, the accelerometer is placed over the bogie centre pin, while for lateral (transversal), the measurement axis should be aligned with the track transversal direction. The Italian standard is not explicit regarding the data processing, but EN 14363 defines the acceleration in the vehicle body should be filtered with a low-pass (at 10 Hz) filter for lateral and with a pass-band (0.4 Hz to 4 Hz) filter for vertical acceleration[16].

- Vertical and lateral acceleration measured on the bogie.

As described by EN 14363, the limit values for dynamic parameters depend on the vehicle characteristics. Thus, the RFI standard stipulates this measurement must be carried out aboard an ETR500Y[17] high-speed train and at line maximum speed or below it up to a maximum of 10 km/h. Moreover, the maximum interval between successive inspections is of four months. The limit values of these parameters for the ETR500Y high-speed trains class regarding speeds up to 300 km/h are presented in Table 5.

[16] With a focus on geometry data collection for vehicle simulation and homologation, EN 13848 (Railway applications - Track - Track geometry quality - Part 1: Characterization of track geometry) (COMITÉ EUROPÉEN DE NORMALISATION, 2019) establishes a frequency range between 0.4 and 20 Hz for vehicle dynamics assessment at different speeds.

[17] ETR stands for *Elettro Treno Rapido,* Rapid Electric Train

Table 5 - Limit values for the car body accelerations for the ETR500Y

	Vertical [m/s²]	**Lateral (transversal) [m/s²]**
First quality level	≤ 1.0	≤ 1.0
Second quality level	$1.0 < \ddot{z} \leq 1.5$	$1.0 < \ddot{y} \leq 1.5$
Third quality level (immediate intervention)[18]	$1.5 < \ddot{z} \leq 3.0$	$1.5 < \ddot{y} \leq 2.0$

This standard also defined that maintenance work from car body acceleration evidence should consider the long wavelength irregularities (D2 and D3) and analysed together with the geometry measurement “on absolute basis” regarding geometric correction. Regarding bogie lateral accelerations, limit values are conditioned by ride stability and must be analysed with the D1 irregularities measured by track recording vehicles.

The São Paulo Metropolitan Trains Company (*Companhia Paulista de Trens Metropolitanos* - CPTM) establishes maximum accelerations to which the train elements must tolerate (Table for the CPTM TUE[19] 9500 train) in accordance with the EN 61373 (*Railway applications - Rolling stock equipment - Shock and vibration tests*, with the aim of standardising vibration and impact tests for equipment used in railway vehicles).

Table 6 - Limit accelerations regarding structural resistance to vibration for the CPTM TUE 9500, vibration frequency up to 100 Hz on the three orthogonal directions (COMPANHIA PAULISTA DE TRENS METROPOLITANOS, 2013).

Component place	**Maximum acceleration, vibration up to 10 Hz**	**Maximum impact load, up to 300 times a day**
Car body	0.2 g	2 g (any direction)
Bogie	4 g	12 g (vertical); 6 g (horizontal)
Wheelset	6 g	12 g

Regarding passengers’ comfort, CPTM’s specifications define ISO 2631 as the reference. Moreover, the CPTM specifications for the Electric Multiple Unit (EMU) acquisition (COMPANHIA PAULISTA DE TRENS METROPOLITANOS, 2013) stipulate a **derailment detection system** that monitors accelerations of wheel-rail

[18] For acceleration above the third quality level, the RFI standard establishes a speed limitation as a protective restriction (up to 250 km for high-speed lines with maximum speed between 250 km/h and 300 km/h; up to 200 km/h for high-speed lines with maximum speed equal to 250 km/h.

[19] TUE stands for *Trem Unidade Elétrico,* Electric Multiple Unit.

contact for travel speeds above 10 km/h. The system must detect repetitive pulses of vertical or lateral acceleration above pre-set values.

Regarding sensors' requirements, similar to that discussed in section 2.4.1 (*Practical issues regarding response-based methods*), the target frequencies and the maximum acceleration expected in each vehicle mass condition features such as maximum range, sensitivity, resolution, precision, sample rate, and antialiasing filter parameters. For instance, Table 7 presents the accelerometers' requirements for ride dynamic monitoring in the Italian Railway Network and illustrates the smaller acceleration magnitude in the car body in relation to the other installation places as a natural result of vibration attenuation performed by the suspensions.

Table 7 - Requirements for accelerometers used in the ride dynamic monitoring systems of the Italian Railway Network (RETE FERROVIARIA ITALIANA, 2018a)

Parameter	Range [g]	Sensitivity [mV/g]	Resolution [mg]	Precision [mg]	Sample rate [kHz]
Z acceleration wheelset	100	20	25	500	1
Z acceleration bogie	20	100	4	100	1
Z acceleration car body	2	1000	0.65	10	1

3.4 CHAPTER FINAL CONSIDERATIONS

The standards concerning vibration tests and vibration data analysis, whether for comfort analysis or the running behaviour characterisation as a whole, provide support for a complete understanding of the railway vehicle dynamics and the influence of track geometry quality on car vibrations. Furthermore, they provide insights into the impact of the sensors' position, orientation, and specifications on the results of these monitoring activities. From this, the thesis aims to quantify the influence on results quality due to the intrinsic limitations of very low-cost sensors and the use of vibration sensors attached to the car body.

The present thesis performs comfort analyses in accordance with ISO 2631 with adaption due to test limitations (described in Chapter 5 - *Material and methods*) because of its greater simplicity compared to the European indexes, which is compatible with the proposed method and with an eventual application on

passengers' smartphones. In the scope of the thesis to correlate the results with the track parameters, it is more appropriate to analyse them in terms of the weighted accelerations in their lateral and vertical components without calculating the total acceleration (ISO standard) or total indexes considering quantiles (EN standard), enabling separate correlation analyses with lateral and vertical irregularities. Moreover, in contrast to a simple threshold analysis using raw accelerations, the frequency-weighted accelerations according to the comfort standard provide meaningful and useful values in the context of a railway ride and the eventual user applications.

4 LITERATURE SURVEY ON THE USE OF INERTIAL-BASED TECHNIQUES FOR RAILWAY MONITORING ACTIVITIES

This chapter presents the results of the literature review on the use of inertial sensors in railway monitoring. Initially, the general aspects of this subject that permeate the selected literature will be presented with a basis on the consolidated background literature in each subarea. The features covered are the typology and sub-services of the vehicle-based monitoring systems, the main characteristics and classification of the inertial sensors, and the reference frames for measurements.

Afterwards, the main specific findings of the related works are presented according to a proposed classification of the techniques. This classification considers the grade of the inertial sensor, the number of installation points, the concept, the data processing techniques, and the data fusion techniques. The data fusion issues are detached from the general data processing discussion despite eventual superposition given their importance and specificity for the present thesis.

4.1 REFERENCE FRAMES

Since the monitoring concepts addressed in this thesis consider vehicles and passengers as moving sensing platforms, the correct description of the measurement referred to the proper reference frame is crucial to enable alignment among measurements and between results and track reality, ensuring system quality. Thus, prior to discussing the monitoring activities, this section establishes essential aspects regarding the reference frames used to describe vehicles and sensors' states.

4.1.1 Geodetic reference frame

A geodetic reference frame[20] (or geodetic datum[21]) is the spatial reference for representing the position of locations and objects on Earth and similarly on other planetary bodies. It is defined by a set of parameters encompassing an abstract coordinate system, its realization and, often, a reference surface (PETIT; LUZUM, 2010; NATIONAL GEODETIC SURVEY, 2021). The coordinate system is defined in terms of origin, orientation, and scale, while the realization considers accessible reference points (i.e., with known coordinates) on the Earth's surface. In complement, the reference surface can be horizontal (e.g., an ellipsoidal model of the Earth as the horizontal reference surface for geographic coordinates measurements) or vertical (e.g., the mean sea level as the equipotential surface for orthometric height measurements).

In the International Terrestrial Reference Frame (ITRF) defined by the International Earth Rotation and Reference Systems Service (IERS), the Cartesian Coordinates System presents the following description: geocentric system with metric scale, Z-axis defined by the IERS Reference Pole (IRP), X-axis defined by the IERS Reference Meridian (IRM), and Y-axis completes a right-handed system (HOFMANN-WELLENHOF; LICHTENEGGER; WASLE, 2008). Thus, this system co-rotates with the Earth in its diurnal movement and may be defined as an Earth-centred, Earth-fixed (ECEF) frame in the navigation context.

The ITRF is realized by terrestrial control stations (reference points) with precisely determined coordinates. Moreover, this frame is regularly updated to consider temporal effects, and its realizations are named after the ITRF acronym plus the

---

[20] While the term **system** refers to the set of conventions for coordinate axes, the term **frame** is applied to the physical realisation of a given system by means of accessible points whit precise known coordinates. A frame is not necessarily linked to a reference surface since its solutions can be specified using a Cartesian Coordinate System. (PETIT; LUZUM, 2010; JEKELI, 2012). However, if needed, the Cartesian coordinates can be transformed to geographic coordinates (latitude, longitude, and ellipsoidal height) referred to an ellipsoid as a reference surface.

[21] The concept of geodetic **datum** is inconsistent in the literature (JEKELI, 2012) and can also refer only to the horizontal and the vertical reference surfaces themselves. However, the most consolidated definitions establish datum as synonym of geodetic reference frame or, more precisely, as the set of parameters that define a frame and, often, a reference surface for the Geographic Coordinate System (PETIT; LUZUM, 2010).

epoch of formation of this frame. Its solutions do not directly use a reference surface (ellipsoid) because they are specified by their Cartesian coordinates. However, the Geodetic Reference System 1980 (GRS-80) ellipsoid is recommended when the Cartesian coordinates need to be transformed into geographic coordinates.

The geodetic datum used as the reference by GPS is the World Geodetic System 1984 (WGS-84), based initially on the GRS-80 with subsequent refinements. Since the 2005 ITRF realization, the WGS-84 is closely aligned (discrepancies of the order of centimetres at the origin) with the ITRF. The WGS-84 frame considers the realization through about 1500 terrestrial sites from Transit satellite system observations, the precursor of the GPS. Table 8 presents the parameters that define the geocentric ellipsoid used by WGS-84 (HOFMANN-WELLENHOF; LICHTENEGGER; WASLE, 2008).

Table 8 - WGS-84 ellipsoid (G1150) parameters (HOFMANN-WELLENHOF; LICHTENEGGER; WASLE, 2008).

Parameter	**Value**
Ellipsoid's semimajor axis	6 378 137.0 m
Ellipsoid's flattening	1/298.257 223 563
Earth's angular velocity	$7\ 292\ 115 \cdot 10^{-11}$ rad/s
Earth's gravitational constant	$3\ 986\ 004.418 \cdot 10^{8}$ m^3/s^2

Under these concepts, an International Terrestrial Reference Frame provides globally consistent, Earth-centred spatial reference. In complement, local horizontal datums can be developed for local applications through the alignment of an ellipsoid aiming for the best fit with the topographic surface in the area of interest. The characterization of these systems considers the definition of the datum origin point (i.e., the point on the ellipsoid that was chosen to match the topographic surface) and the ellipsoid orientation. (HOFMANN-WELLENHOF; LICHTENEGGER; WASLE, 2008; JEKELI, 2012). Thus, the system is not necessarily geocentric. This difference is crucial when merging data from different sources (e.g., data gathered by GPS receiver *versus* the railway track reference mapping) and, when necessary, coordinate transformations.

4.1.2 Local tangent plane frame

Besides the geodetic reference frames, a local tangent plane frame can be defined to describe position and displacements within a localized area (GROVES, 2008). This frame is Earth-fixed, i.e., the origin is a fixed point relative to the Earth around which positioning activities are to be carried out. From this, the horizontal reference plane is defined by the tangent to the parallel and the tangent to the meridian at the origin. The coordinates system can be defined with the z-axis pointing down along the normal direction (ellipsoid normal), the x-axis pointing North, and the y-axis pointing East, in a right-handed arrangement called North, East, Down. An alternative right-handed arrangement may consider East, North, Up orientation.

4.1.3 Navigation frame

The local navigation frame, also named navigation frame, has as its origin the point at which a navigation solution is sought (e.g., the vehicle's centre of mass or the user’s position) (TITTERTON; WESTON, 2004; GROVES, 2008). The conventions for the horizontal reference plane and the axes orientation is equal to that adopted for the local tangent plane, resulting in a frame fixed in relation to the cardinal directions. Thus, it can adopt the North, East, Down or the East, North, Up fixed orientations.

Since the origin is at the vehicle position, this frame is suitable for attitude description in relation to the cardinal directions and the local horizontal plane, while the position is described in relation to an Earth-fixed frame (global or local-level) in terms of geodetic, projected, or local tangent plane coordinates.

As discussed in Groves (2008) and observed in several studies in this research area, some authors name this frame as geodetic or local geographic frame. However, regarding the use of similar names for Earth-fixed frames, this thesis will adopt only the term **navigation frame** as described in this section and defined by Titterton and Weston (2004) and Groves (2008).

4.1.4 Track frame

As described in Section 2.1, the track coordinate system is defined as a right-handed tri-dimensional cartesian coordinate system centred on the track centre line. The axes orientation considers the z-axis along the running direction, the y-axis parallel to the running surface for a given cross section, and the z-axis pointing downwards, perpendicular to the running surface. From this description, the track frame is defined at each track cross section.

4.1.5 Vehicle body frame

The vehicle (or body) frame is fixed to the vehicle's position and orientation. Thus, the origin is fixed in its centre of mass, the x-axis points forward, the y-axis points to the right (starboard), and the z-axis points downward in an orthogonal coordinates system. This orientation is also called **Front, Right, Down,** and the x, y, and z axes are also known as, respectively, roll, pitch, and yaw axes (GROVES, 2008).

Regarding the proposed monitoring and the sensor placement, it should be noted that there will be a slight rotation between the wheelset frame (which will more closely follow the track frame) and the vehicle body frame, a difference due to the suspension stiffness in roll, pitch, and yaw.

Regarding roll angle, this influence and the difference between the car body roll angle and the track cant is well defined in the railway standards and is described by the roll coefficient (COMITÉ EUROPÉEN DE NORMALISATION, 2010b). To better understand this vehicle’s parameter, it is necessary to introduce aspects related to the non-compensation of lateral accelerations. Whenever the train travels at a speed different from the design (equilibrium) speed on a curve, the centrifugal acceleration experienced by the passengers is not totally compensated (cant deficiency if the speed is above the equilibrium speed), or the lateral component of vehicle weight is greater than the centrifugal force (cant excess if the speed is below the equilibrium speed) (ESVELD, 2001; ROCHAT, 2007; ZUCCHI, 2013). As a result, in both cases,

the lateral component of the resulting force causes the car body (sprung mass) to roll in the same direction of this component. Thus, there is a difference between the wheelset roll angle, which approximately follows the track cant, and the car body roll angle under the effect of lateral non-compensated acceleration (COMITÉ EUROPÉEN DE NORMALISATION, 2017b), as illustrated in Figure 7 for both cant excess and cant deficiency for non-tilting trains

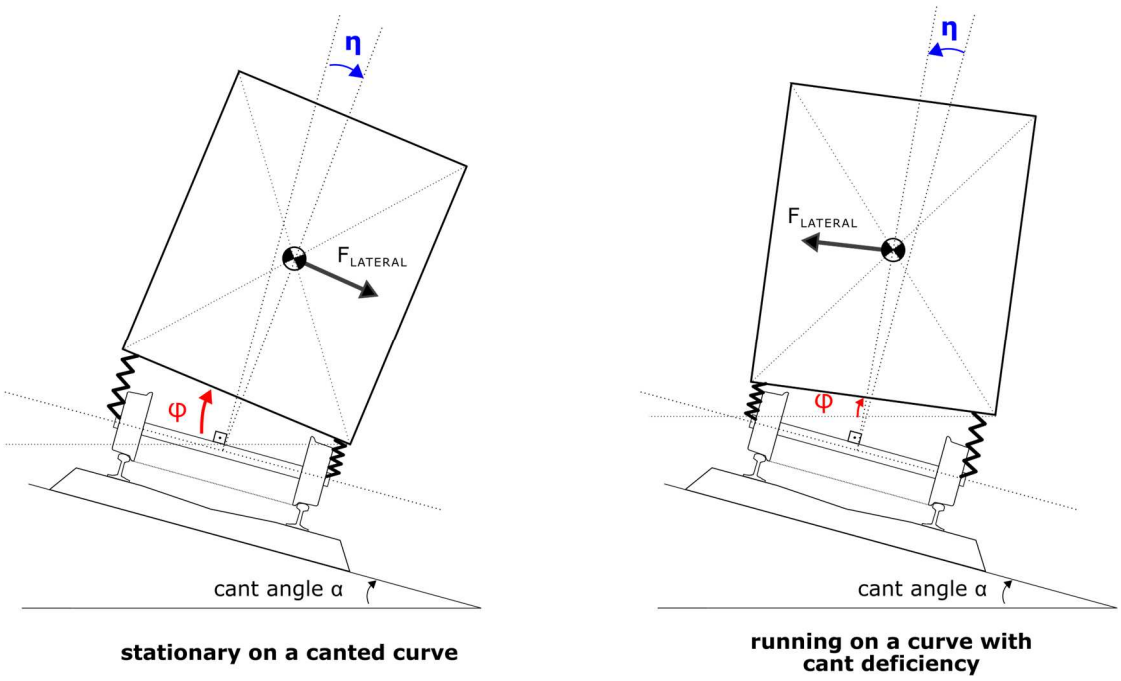

Figure 7 - Lateral components of the resulting force and its influence on the roll of the sprung mass. Illustration for non-tilting trains. Adapted from Comité Européen de Normalisation (2009b), Hungria (2017), and Talgo (2020).

For non-tilting trains, case of ERT500 trains, the roll coefficient correlates with the acceleration in the vehicle plane and the resulting lateral acceleration is given by:

$$a_i = (1 + s_r) \cdot a_q \tag{8}$$

where a_i is the lateral non-compensated acceleration in the vehicle floor plane, a_q is the lateral non-compensated acceleration in the track plane, and s_r is the roll flexibility coefficient (usually 0.4 for modern rolling stock). For non-tilting trains, the roll flexibility coefficient is always positive and the a_i is always greater than the lateral non-compensated acceleration in the track plane.

Regardless of eventual dissymmetry[22] of the vehicle, the vehicle roll angle φ due to the flexibility of the suspension is the composition of the cant angle α with the vehicle roll angle relative to the axis of the wheelset η as presented in Figure 6. From the roll flexibility coefficient definition given in EN 15273 (COMITÉ EUROPÉEN DE NORMALISATION, 2017b), it follows that the value of the coefficient s_r is the ratio of the angle η to the cant angle α for a stationary vehicle on a canted track. For the present case, a linear behaviour (as in most analyses presented in the aforementioned ISO standard) is considered as the non-linearities and the hysteresis of the roll angles caused by the fiction in the suspension are not relevant.

4.1.6 Sensor frame

The sensor frame is fixed to the measurement unit and has the sensor centre of mass as origin. In a strap-down system, the axes are usually **aligned to the vehicle frame** axes, but not necessarily the origins coincide.

The main aspect regarding sensing activity is that the raw measurements are referred to this frame. Each sensor (e.g., accelerometer, gyroscope, magnetometer, and barometer) has its coordinate frame in an IMU chipset. The coordinate systems are orthogonal, and possible misalignments between axes in each frame are handled through a calibration procedure. Moreover, differences between gyroscope and accelerometer frames in terms of origin are negligible for the present application. Regarding orientation, it is necessary to identify the eventual deviations for each sensor on the chip dataset and perform the necessary corrections.

4.2 MONITORING ACTIVITIES BASED ON IN-SERVICE VEHICLES

In-service vehicles have become a relevant data source either through dedicated

[22] Dissymmetry “may be due to a structural imperfection, to poor adjustment of the suspension […] and to an offset of the load” (COMITÉ EUROPÉEN DE NORMALISATION, 2017b)

onboard sensors or even taking advantage of the sensing capabilities ported by the passengers (i.e., smartphones, smartwatches, tablets etc.). Under a wide range of concepts such as **probe vehicles, vehicles and passengers as mobile sensors**, and **mobile crowdsensing,** these alternative sensing systems have been developed for a wide application range, comprising, for example, traffic monitoring, air quality monitoring and track quality characterization.

The systems can be described in their four subsystems or sub-activities (OLIVEIRA, 2017): sensing, positioning, communication, and processing and visualizing systems. The following subsections describe the main aspects regarding these subsystems and are detailed according to their pertinence to the scope of the thesis.

4.2.1 Sensing subsystem

The sensing subsystem comprises the set of sensors applied on the acquisition and register of the data related to the phenomenon to be monitored. One considers one of the following options or combinations among them:

- Sensors already installed in-vehicle sensors. These sensors aim to enhance the driving experience regarding convenience, safety, and comfort, but their data may be applied to services unrelated to the vehicle operation. Examples are those used by the Advanced Driver Assistance Systems (ADAS) in road transportation, namely radar, infrared, and ultrasonic distance sensors, video cameras, as well as other vehicle diagnostic sensors such as fuel sensors, exhaust sensors etc. (ABDELHAMID; HASSANEIN; TAKAHARA, 2014; GUERRERO-IBÁÑEZ; ZEADALLY; CONTRERAS-CASTILLO, 2018). As examples, the data gathered by these sensors could also be employed for estimating traffic flows animation or temperature/air quality monitoring through the road network. In rail transportation, the active suspension systems are equipped with accelerometers (GOODALL, 2003) and can eventually enable data recording for further track quality assessment.

- Sensors specially installed in an in-service vehicle for specific monitoring activity. An example is the adaptation of train coaches through the installation

of accelerometers to monitor comfort and running behaviour (NIELSEN et al., 2013)

- The use of sensing technology carried by the transport users, such as crowd sensing systems that consider data gathered by passenger's smartphones, smartwatches, and tablets in public transport (HIGUCHI; YAMAGUCHI; HIGASHINO, 2015; ZHAO; GUO; ZENG, 2016; AZZOUG; KAEWUNRUEN, 2017; SERAJ; MERATNIA; HAVINGA, 2017). It uses the remarkable sensing and processing capabilities of electronic gadgets, which may comprise accelerometer, gyroscope, barometer, thermometer, GNSS module etc.

4.2.2 Positioning subsystem

In a broad sense, the positioning[23] system situates in space and time the sensing platform and, thus, the gathered data. Therefore, it comprises the vehicle description in terms of geographic coordinates, speed, time, and attitude, enabling data georeferencing, spatial orientation and synchronization.

Regarding vehicle-based systems, the quality (accuracy and completeness) of this system is pivotal given the inherent mobility of the sensing platform and the different quality requirements depending on the monitored variable. Thus, the requirements are ruled by the intrinsic characteristics of the monitored phenomenon. For track quality monitoring, horizontal accuracy in position must allow differentiation of two adjacent tracks or lines. Moreover, sensor attitude and travelling speed are relevant for the correct association between the measured acceleration and the track quality,

[23] In the strict sense, positioning is the activity that describes an object through coordinates (its position) referred to a fixed reference system (GROVES, 2008; HOFMANN-WELLENHOF et al., 2013). In a broad sense, positioning can also refer to the position and attitude (angular position) determination. On the other hand, navigation is an active process that comprises the determination of current state (position, velocity, and attitude) and the definition of the course corrections to attain a desired position. In other words, involves trajectory determination and guidance (BLITZKOW, 2004; HOFMANN-WELLENHOF et al., 2013). Although used for the Inertial Navigation Systems (INS) and the Global Satellite Navigation Systems (GNSS), systems that only provides position, velocity and eventual attitude solution (GROVES, 2008), the use of the term in the present work could imply a full navigation activity or the use of situational data to perform it, activities that are entirely out of scope.

as well as for the eventual description of angular vibration modes. Regarding rail-guided vehicles, the attitude may be especially important since bank and slope track angles mainly rule it and can be used in a map-matching algorithm to improve position quality.

In contrast, the quality requirement may be less demanding for applications such as air quality or temperature mapping. The differentiation between tracks or lines is not critical for these phenomena, and horizontal accuracy is demanded depending on the desired resolution. In complement, this subsystem can be limited to data georeferencing and synchronization activity, with attitude information being of minor importance.

The leading technology for this activity is the ensemble of worldwide satellite-based navigation systems known as Global Navigation Satellite Systems[24] (GNSS). Currently, the fully operational GNSS are the American Global Positioning System (GPS), the Russian *Globalnaya navigatsionnaya sputnikovaya sistema* (GLONASS, meaning exactly Global Navigation Satellite System), the Chinese BeiDou Navigation Satellite System (BDS) and the European Galileo. Each GNSS is composed of three segments:

- The space segment, comprising the constellation with a sufficient number of satellites to ensure simultaneous visibility of at least four satellites.
- The control (or ground) segment, with the control stations and antennas that perform system maintenance, track the satellites, monitor atmospheric data, and upload messages to the satellites.
- The user segment, comprising the receivers and the associated information services. Receivers can be classified according to the type of observable (pseudorange, carrier phase, and Doppler shift), the number of tracked

[24] In fact, GNSS is also used for some authors (UNITED NATIONS, 1998; INTERNATIONAL CIVIL AVIATION ORGANIZATION, 1999; HOFMANN-WELLENHOF; LICHTENEGGER; WASLE, 2008) to define the satellite-based "radio positioning system that includes one or more satellite constellations (...) that provides 24-hour three-dimensional position, velocity, and time (...) anywhere on, or near, the surface of the Earth". Under this definition, GNSS is a singular worldwide system that considers the sum of the different existing systems (GPS, GLONASS, GALILEO etc.). However, GNSS is also employed as a plural concept (systems) to individualise the multiple satellite-based systems. The latter definition is useful to emphasize that these systems can work independently.

frequencies, and the number of tracked constellations. The possible positioning techniques for a given receiver depend on these features.

Using the signals broadcasted by the satellites, a GNSS receiver solves the positioning equations to estimate the user position, velocity, and time (PVT). Regarding single-point positioning, the most basic technique, the position is estimated through trilateration-based pseudorange positioning. Moreover, velocity determination is achieved using the Doppler shift of the received frequencies. For both calculations, at least four observables (i.e., four satellites) simultaneously measured are needed (GROVES, 2008; HOFMANN-WELLENHOF; LICHTENEGGER; WASLE, 2008a).

Using single L1 frequency and civilian code, the single-point positioning technique presents a typical horizontal position error of 13 m at the probability level of 95% under standard scenarios. On the other hand, messages from satellite-based augmentation systems (SBAS) can correct satellite-related and ionospheric-related errors and increase the integrity, availability, and continuity of the position solutions. However, GPS accuracy is tightly associated with the receiver environment, and factors such as signal multipath, signal blockage, and atmospheric interference may reduce position accuracy (HOFMANN-WELLENHOF; LICHTENEGGER; WASLE, 2008; DIGGLEN, 2009).

Integration with an Inertial Navigation System (INS) provides position estimates by means of the estimated displacement and the relative positioning from a known point. A strap-down INS aligned to the vehicle frame comprises accelerometers providing linear accelerations and gyroscopes providing angular rates, enabling the reconstitution of angular motions through numerical integration. These displacement estimates are applied in a dead reckoning algorithm, i.e., starting from a known position and adding the subsequent motions, obtaining the estimated vehicle trajectory. While the errors of an INS usually increase with the square of the time due to the integration drift, the GNSS errors have long-term stability. Moreover, inertial navigation does not suffer from signal visibility problems. From these factors, GNSS and INS are regarded as complementary systems in high-performance navigation systems (HOFMANN-WELLENHOF et al., 2013).

4.2.2.1 Attitude estimation

In navigation activity, attitude is the vehicle orientation with respect to a reference frame and can be mathematically described in terms of a set of Euler angles (roll, pitch, and yaw), a rotation matrix (Direction Cosine Matrix - DCM), or a quaternion. Considering one of the possible representations, this activity involves the determination of the rotation matrix between a fixed frame (e.g., the local tangent plane or the navigation frame) and the body frame in Euclidean space (ROGERS, 2003; GROVES, 2008). Regarding the scope of this thesis, this is a relevant activity regarding pitch and roll estimation for gravity compensation.

In an approach considering magnetometer, accelerometer, and GPS data, the obtention of the rotation matrix needs the knowledge of at least two vectors (acceleration $\boldsymbol{f}$ and magnetic field $\boldsymbol{m}$) in both the frame in which information is sensed (i.e., the body frame for a strap-down configuration) and the frame in which the information may be inferred from the models (i.e., the navigation or the local frame). The cross product of the vectors $\boldsymbol{f}$ and $\boldsymbol{m}$ may be used as additional vector in order to enable the solving of the matrix. The relationship between the rotation matrix $\boldsymbol{C}_b^n$ (from the body frame to the navigation frame) and the vectors are described as follows, with the index *b* standing for the body frame and *n* for the navigation frame (ROGERS, 2003).

$$\boldsymbol{f}^n = \boldsymbol{C}_b^n \cdot \boldsymbol{f}^b \tag{9}$$

$$\boldsymbol{m}^n = \boldsymbol{C}_b^n \cdot \boldsymbol{m}^b \tag{10}$$

$$\boldsymbol{f}^n \times \boldsymbol{m}^n = \boldsymbol{C}_b^n \cdot (\boldsymbol{f}^b \times \boldsymbol{m}^b) \tag{11}$$

Assuming a strapdown configuration, the sensor axes can be considered aligned to the body exes and, thus, the vectors $\boldsymbol{f}^b$ e $\boldsymbol{m}^b$ are respectively the accelerations and the magnetic field sensed by the measurement unit. Regarding the vector $\boldsymbol{f}^n$, the accelerations are inferred from the known gravity (using Earth's gravity model) and the vehicle motion (e.g., using GPS velocity data when available). On the other hand, the vector $\boldsymbol{m}^n$ is inferred from the Earth's magnetic field model. In turn, the matrix $\boldsymbol{C}_b^n$

depends on the rotation sequence and, for instance, is presented for the XYZ sequence:

$$\boldsymbol{C}_b^n = \begin{bmatrix} cos\,\theta\,cos\,\psi & -cos\,\varphi\,sin\,\psi + sin\,\varphi\,sin\,\theta\,cos\,\psi & sin\,\varphi\,sin\,\psi + cos\,\varphi\,sin\,\theta\,cos\,\psi \\ cos\,\theta\,sin\,\psi & cos\,\varphi\,cos\,\psi + sin\,\varphi\,sin\,\theta\,sin\,\psi & -sin\,\varphi\,cos\,\psi + cos\,\varphi\,sin\,\theta\,sin\,\psi \\ -sin\,\theta & sin\,\varphi\,cos\,\theta & cos\,\varphi\,cos\,\theta \end{bmatrix} \quad (12)$$

where ψ, θ, and φ are, respectively, the roll, pitch, and yaw attitude angles.

When available, a gyroscope outputs angular speed around the sensor frame axes, which can be used to estimate variations of attitude through integration if the angular propagation[25] is correctly addressed. However, the gyroscope bias result in drift over time of the integrated angular estimates and curbs its use alone in long-term direct use. Thus, usual solutions are fusion algorithms in which the gyroscope-based estimates provide short-term information, and accelerometer-magnetometer-based estimates give long-term attitude changes. For these algorithms, techniques such as the complementary filter (fixed-gain or adaptative), the Kalman Filter and variations are consolidated and widely employed (ROGERS, 2003; GROVES, 2013).

Another relevant issue regarding IMU attitude estimation accuracy is the influence of disturbances on magnetometer and accelerometer-based attitudes. In absence of vehicle motion information (e.g., form GPS), vehicle accelerations in high-dynamics applications, as well as sustained acceleration during long interval, disturb acceleration-derived pitch and roll estimates (GROVES, 2008; MICHEL et al., 2018). Smoothing or integration with gyroscope as short-term information are strategies to deal with the errors induced by the high dynamics. On the other hand, the local magnetic disturbances generated by objects such as vehicles, buildings, bridges, and power lines produce heading (yaw) errors and are also handled through smoothing, adoption of magnitude thresholds or integration with short-term information if the anomalies are considered. Regarding the disturbance generated by the vehicle itself and its systems and equipment, a calibration procedure considering vehicle-derived magnetism can be carried out (GROVES, 2008).

---

[25] The angular propagation reflects the difference between the angular rates in the sensor frame and the rates in the navigation frame, in which numerical integration must be carried out.

Most IMU-based algorithms, such as those used in the smartphones[26], consider the external acceleration and the magnetic perturbations negligible (GROVES, 2008; MICHEL et al., 2018) or are already handled through integration with a gyroscope. The use of external data is possible to obtain external accelerations; however, when considering consumer-grade applications and low-cost GPS receivers, inadequacy regarding GPS data aspects (sample rate, accuracy, availability) may curb its use to correctly describe vehicle accelerations for such applications. In this context, as described in Groves (2008), adopting a common simplification from the algorithm presented at the beginning of the section, the attitude computation from gyroscope, accelerometer, and magnetometer measurements is performed through the following steps:

a) Roll and pitch initial estimation by levelling, the process of initializing the roll and pitch attitude components from accelerometer measurements. From Eq. (9), the roll θ and pitch angles φ are solved as follows:

$$\tan \varphi = \frac{f_y}{f_z} \tag{13}$$

$$\tan \theta = -\frac{f_x}{\sqrt{f_y^2 + f_z^2}} \tag{14}$$

b) Fusion of the accelerometer-based pitch and roll estimates with gyro-based estimates obtained through numerical integration, with the latter smoothing out the accelerometer-based short-term errors due to vehicle manoeuvres.

c) The corrected roll and pitch estimates are used with the three-axis magnetometer measurements to obtain the magnetic heading (yaw angle) from Eq. (10).

d) The magnetic and gyro-derived headings are integrated, with the former contributing to the long-term changes and the latter to the short-term ones, similarly to step b.

[26] The Android documentation (GOOGLE, 2017), e.g., does not explicit the orientation algorithm. However, preliminary tests performed yielded attitude values compatible with those obtained from a complementary filter.

4.2.3 Communication subsystem

The communication subsystem comprises the tools for data transmission, which can be performed concomitantly with the sensing activity, at a predefined rate or at the end of a test period. Regarding onboard sensors and depending on the monitoring exigences, this communication can be performed between sensors (sensor-to-sensor), between vehicles (vehicle-to-vehicle), between sensor or vehicles and the roadside infrastructure (sensor or vehicle-to-infrastructure), or between sensors or vehicles and the third-party communication network (sensor or vehicle-to-network)

4.2.4 Processing and visualizing subsystem

The communication subsystem comprises the tools and processes that extract information from data and enable decision-making through visualization (charts, static or dynamic maps etc.) and resulting reports. Depending on the application, this activity can be performed online, partially online, or offline, as well as focused on the passenger or the transport infrastructure manager.

4.2.5 System quality parameters

For the aforementioned subsystems, it is crucial to define the parameters that describe the system performance and the conformity with the requirements (i.e., its quality). Aiming at the accurate definition of these parameters for further discussion in this thesis, this section defines the parameters that may describe the position, the sensing techniques, and their results. Since considerations about the communication system of the proposed application are out of the scope of the thesis, the specific quality parameters of such a system (latency, download/upload ratio, download rate etc.) will not be addressed. Regarding the positioning and the sensing subsystems, as well as the system's performance as a whole, the more are listed in the following. Since the exact definitions may vary in the literature, this thesis adopts the definitions

provided by the *Systems and Software Engineering Vocabulary* of the concerning international organisations (INTERNATIONAL ORGANIZATION FOR STANDARDIZATION; INTERNATIONAL ELECTROTECHNICAL COMISSION; INSTITUTE OF ELECTRICAL AND ELECTRONICS ENGINEERS, 2017):

- Accuracy: qualitative concept that stands for the conformity between the measurement and the true value of the measurand. Regarding a positioning system, it is also possible to define the following accuracies (HOFMANN-WELLENHOF; LICHTENEGGER; WASLE, 2008):
    - Absolute accuracy: degree of conformity between the position solution given by the system and the true position.
    - Relative accuracy: concerning the accuracy with which the relative position between users of the same system that the same epoch is determined.
    - Repeatable accuracy (precision): the accuracy with which the user can return to a previously determined position with the same positioning system.
- Sample rate: number of samples in a given time unit (usually seconds).
- Availability: the degree to which the system is operational and available to use, usually expressed in terms of percentage of time.
- Integrity: the degree to which the system prevents unauthorized access or modification.
- Reliability: the degree to which the system performs the required functionality (i.e., meeting the requirements) under stated conditions for a specified period.
- Robustness: the degree to which the system is able to function correctly in the presence of invalid inputs or stressful context.
- Repeatability: the closeness of the agreement of successive results of measurements of the same measurand under the same measurement conditions.

- Reproducibility: the closeness of the agreement between measurements of the same measurand under changed[27] measurement conditions.

4.3 INERTIAL SENSORS

Inertial sensors are devices that respond to the rotational and translational motions with respect to an inertial (free-float) reference frame, i.e., gyroscopes and accelerometers (TITTERTON; WESTON, 2004). In more practical terms, an accelerometer is a sensor that measures the proper acceleration[28] along an axis, with the assemblage of three orthogonal accelerometers to build a triaxial device (i.e., with 3 degrees of freedom) being usual. In turn, the gyroscope measures the angular rate around an axis and is also usually assembled in a triaxial unit. Moreover, an Inertial Measurement Unit (IMU) usually integrates one or more accelerometers with one or more gyroscopes to measure the movements experienced by the unit. Some IMUs also contain a magnetometer for heading reference, although it is not an inertial sensor by definition.

One of the main classifications of the IMUs is the distinction between inertial platforms and strep-down units. The platform technology has been applied since the first inertial devices and considers the inertial sensors mounted on a stable platform that provides mechanical isolation from the rotational motion of the vehicle. Given its accuracy, this technique is still used for more demanding applications given its accuracy, including track monitoring. However, it is also demanding in terms of cost, maintenance, and necessary space. On the other hand, the strap-down technology has a more straightforward mechanical concept and considers the firm attachment of

---

[27] The changed condition include: “the principles of measurement; method of measurement; observer; measuring instrument; reference standard; location; conditions of use; time” (INTERNATIONAL ORGANIZATION FOR STANDARDIZATION; INTERNATIONAL ELECTROTECHNICAL COMISSION; INSTITUTE OF ELECTRICAL AND ELECTRONICS ENGINEERS, 2017)

[28] Proper acceleration is the “physical acceleration experienced by an object relative to the locally co-moving free-float frame” and “felt through points of action” (FRAUNDORF, 2010). Gravity and centrifugal accelerations are not proper accelerations. From this fact, an accelerometer at rest in the ground frame sense approximately a 1g upwards acceleration (normal force acting on the sensor) or, in other words, a minus g-vector. In a curve, the accelerometer senses the centripetal acceleration instead of the centrifugal one.

the inertial sensors to the monitored object. The main drawbacks are associated with a more demanding signal processing regarding coordinates rotation.

In terms of measurement principles, the inertial sensors can be characterized as follows:

- Accelerometers (TITTERTON; WESTON, 2004):
    - Mechanical: mass-spring devices.
    - Solid-state, exploiting diverse physical phenomena and comprising vibratory devices, surface acoustic wave accelerometers, silicon sensors, fibre optic accelerometers, and optical accelerometers.
- Gyroscopes (TITTERTON; WESTON, 2004; GADE, 2005; PASSARO et al., 2017):
    - Mechanical gyros: spinning mass devices.
    - Optical gyros (Sagnac effect): fiber optic gyros, ring laser gyros.
    - Coriolis effect: micro-electromechanical system (MEMS) gyroscopes.

Compared with traditional mechanical, optical, and solid-state inertial sensors, the main advantages of the MEMS-based inertial sensors are the size and weight reduction, the low power consumption and the low production cost (TITTERTON; WESTON, 2004). The high-performance MEMS inertial sensors cost hundreds or thousands of dollars and mainly focus on automotive, industrial, tactical, and navigation applications (MURPHY, 2017). However, the recent technology progress focused on mobile gadgets is noteworthy, yielding very low-cost and small smartphone-grade IMU units at the cost of about cents and a size of about square centimetres.

In this context, it should be noted that a MEMS sensor is not a synonym for a very low-cost sensor. In other words, not all sensors based on this technology are of the same grade or cost level: high-performance MEMS sensors for demanding applications are cheaper than their equivalents with classic technologies, but they are expensive compared to sensors of less demanding applications. Thus, a more relevant classification is regarding the sensor grade, i.e., considering its main

features and the suitable applications. Although this is a commercial classification used by manufacturers, it offers a basis for comparison and specification. Thus, the inertial sensors can be classified into (GADE, 2005; MURPHY, 2017; VECTORNAV, 2019; SAFRAN COLIBRYS, 2021):

- Strategic-grade as a non-commercially available grade consisting of critical military applications. For this grade, a very high in-run bias stability (less than 30 μg for accelerometers and 0.005°/hour for gyroscopes) and a correspondent very high positioning performance (minimum circular error probable[29] (CEP) of 1 nautical mile per 24 hours) are required.

- Navigation-grade as the highest-grade commercially available. It presents a high performance in position and orientation definition with high in-run bias stability (about 50-100 μg for accelerometers and 0.01°/h for gyroscopes) yielded by high-performance MEMS and mechanical inertial sensors. These features consider the capability to reach a CEP of 1 nautical per hour (SHKEL, 2013). The cost of these sensors is hundreds of thousands of dollars.

- Tactical-grade as a high grade for autonomous navigation during short GNSS outages (less than 10 minutes), encompassing activities such as assisted vehicular navigation, smart munitions etc., reaching a positioning performance given by a CEP of about 10 nautical miles per hour. The in-run bias stability is about 1-10 mg for accelerometers and less than 1°/h for gyroscopes. The cost ranges from thousands to dozens of thousands of dollars.

- Industrial-grade as a wide range of applications covering activities such as high-performance control (10-100 mg bias for accelerometer), Unmanned Aerial Vehicle (UAV) navigation (10°/h bias), impact/shock identification, stabilization etc. Given the range of applications, it is not necessarily characterized by a positioning performance, and specific sensor features are more or less relevant according to each application (e.g., higher impact resistance). The price also varies according to these specifications, ranging from hundreds to thousands of dollars.

---

[29] Errors in positioning and navigation are historically defined by the CEP (SHKEL, 2013).

- Automotive-grade, encompassing activities such as stability control, collision detection, and other non-critical motion-activated functions. Its price ranges from dozens to hundreds of dollars. In recent years, the emergence of highly automated driving has raised the level of sensors classified as automotive, with in-run bias stability ranging from 2 to 8°/h (BERMAN, 2019) for gyroscopes.

- Consumer-grade, comprising very low-cost (ranging from a few cents to a few dollars), low-quality, low power consumption sensors suitable for smartphones, smartwatches, and tablets in motion detection activity. Some authors considered the automotive and the consumer-grade in the same group, but automotive applications and components have specific requirements that are more strict than those for general purpose/consumer-grade sensors (MURPHY, 2017).

It is noteworthy that the abovementioned values give only the order of magnitude of the sensors parameters since the literature does not present consistent values in such aspects. Moreover, each specific application will demand other important features such as low noise, low power consumption, short/long-term stability, repeatability, range, bandwidth, shock and vibration sensitivity etc. However, the distinction between the consumer-grade and the other grades should remain clear regarding its very low-cost, low-quality, low power consumption for less demanding activities such as motion detection in electronic gadgets.

Finally, the main terms related to units and systems built on inertial sensors are clarified as follows.

- As previously mentioned, the Inertial Measurement Units integrate gyroscopes, accelerometers and, eventually, magnetometers. Moreover, they output only their raw measurements (angular rate, linear acceleration, and magnetic field).

- An Inertial Navigation System integrates the same sensors of an IMU, but outputs estimated navigation data (position, velocity, attitude) using external data regarding initial absolute positions in dead reckoning algorithms.

- As from its name, an Attitude and Heading Reference System (AHRS) yields

the attitude, with the heading information coming from a magnetometer. Thus, it should contain a magnetometer besides the inertial sensors.

4.4 INERTIAL TRACK MONITORING BASED ON IN-SERVICE VEHICLES

In the following subsections, the literature on the inertial track monitoring systems based on in-service vehicles is described in its core elements, the components and techniques related to the sensing and processing subsystems. This section aims not to offer an exhaustive literature review but to obtain a large sample of articles that effectively contribute to a comprehensive overview of the state of the art in this research area. Therefore, the search protocol for the core set of papers encompasses the following:

- Database: *Web of Science Core Collection*, a bibliographic database with items from the highest impact scientific journals and conference proceedings. *Web of Science* offers also advanced tools for research and citation context (CLARIVATE, 2021).
- Search strings: 1) (accelerometer* OR gyroscope* OR inertial) AND rail*; and 2) smartphone AND rail*.
- Temporal scope: up to February 2023.

Thus, the research papers identified with the adoption of this protocol were scrutinized in terms of their relevance to the scope of the present thesis in a broad sense, including initiatives with medium and high-cost (industrial or navigation-grade) inertial sensors, as well as sensors installed on the wheelset or the bogie. Therefore, The survey scope is broader than that of this thesis since the similarities and distinctions contribute to a better comprehension of the proposed sensing activity and the definition of the materials and methods to be employed. Another criterion for selection, more subjective, is the paper's effective contribution to the state of the art on the use of inertial sensors aboard railway vehicles for dynamic monitoring. In consequence, initiatives such as the use of inertial sensors at fixed points of the railway infrastructure and the use of smartphone data to calculate travel times, and

the use of smartphones to calculate travel times or mapping passenger movements were excluded.

The several initiatives carried out in previous studies can be classified under different aspects: the monitoring concept, the grade of the inertial sensors, their location on the vehicle, the number of measurement points, the monitored track parameters, the data processing techniques (which materialize the concept) and the fusion techniques (for works that consider this possibility).

4.4.1 Monitoring concept

According to the techniques used to extract information from inertial data, two main concepts can be identified within this research area: explicit or implicit approaches. In the explicit approach, the track profile is explicitly estimated from the linear and angular displacements data. For this, detailed knowledge of the vehicle dynamic model and its parameters is mandatory. In turn, the implicit approach considers signal-derived features in the time or frequency domain correlated with track characteristics. Alternatively, this approach can consider indexes related to comfort and safety as indirect track quality figures.

It should be noted that some of the works described below are focused on rail surface monitoring (e.g., corrugation and squats) instead of track geometry or stiffness characterization. Although this differs from this thesis's scope, these research works offer relevant insights regarding vehicle dynamics and signal acceleration processing. Moreover, this section describes a relevant sample of works in the field and not its totality.

4.4.1.1 Explicit approach

Weston *et al.* (2007a) proposed measuring the vertical track irregularities from an in-service vehicle. For this, the authors considered a bogie-mounted gyroscope for long-wavelength features (above 8 m) and an axle-box mounted accelerometer for

short-wavelength features (below 8 m, which are filtered by the primary suspension and the bogie wheelbase). Instead of the simple double integration in the time domain, the authors considered the curvature of the longitudinal profile in the space domain and its relationship with the pitch rate (from gyroscope) and the vertical acceleration. Thus, the vertical displacement was given by the double integration of this curvature in the space domain plus filtering for long wavelengths. At speeds below about 8 m/s, the estimates from the axle box accelerometer data become noisy and useless. In this scenario, the estimates from the gyroscope can be used alone, although with loss of short wavelength information. Moreover, it can still work correctly at speeds down to about 1 m/s. In a correlated work, the same authors (WESTON et al., 2007b) applied the same concept to lateral irregularities using the yaw rate.

Real *et al.* (2011) determined the vertical rail profile from acceleration measured at both ends of a wheelset axle. From a simplified two masses, one degree-of-freedom, the authors used the Fourier transform to establish the transfer functions relating the vertical displacements on axle boxes with the vertical rail profile and the vertical displacements in the bogie frame. Ultimately, a profile obtained from the inertial method is explicitly obtained through the inverse Fourier transform.

Lee *et al.* (2012a) described a method for track irregularities monitoring from accelerometers (lateral and vertical) installed on the bogie and the axle box of high-speed trains. The approach used the Kalman filter to estimate, from the vehicle model, the vertical and lateral displacements associated with the measured accelerations. Afterwards, third-order Butterworth bandpass filters were employed to separate the wavelengths associated with dynamic stability and ride comfort (from range D1 to D3 for longitudinal level and alignment). Finally, a compensation filter (finite impulse response) was used to remove discrepancies caused by the relative movement between the vehicle and the track, obtaining estimates for the track irregularities. The results were promising even for the short wavelength irregularities, an important fact since the usual methods do not provide good results. Another pertinent issue this work addresses is using a distance-wavelength representation instead of a time, a frequency, or a space representation. For this, the authors used a Fourier Transform similar to the Short Time Fourier Transform (i.e., convolution with

window function) but considering irregularities in the time domain and their transform to the wavelength domain.

Li *et al.* (2015) also discussed the use of axle box vertical and longitudinal accelerations but for rail squats identification. The authors proposed three innovations concerning the implementations already established. The first recommendation is to use the longitudinal acceleration to improve squat detection since they present lower background noise from track elements' vibration and are more sensitive to impact-related vibration from squats. The second innovation is a set of signal processing solutions regarding the disturbance of wheel defects. In turn, the third improvement considers the use of multiple traverses and multiple instrumented axle boxes, reducing the noise and the effect of vehicle hunting (which reduces the detection rate due to the absence of contact). Another relevant aspect is that the peak identification is performed in the wavelet power spectrum, a suitable frequency-time representation for nonstationary phenomena.

Odashima *et al.* (2017) applied the Kalman Filter to estimate track irregularities from noisy acceleration measurements. For this, the authors started from the railway vehicle model contemplating only vertical and pitch motions. The model considered the following parameters: the stiffness and damping of the suspensions, the mass, moment of inertia and base of the car body, the mass and moment of inertia of the bogie, and the base of the wheels. From this information, they obtained an equation of motion for a vehicle on a straight track and considered its discretization in a Kalman Filter algorithm.

Obrien *et al.* (2018) had as scope the determination of the track longitudinal profile from the inertial response of in-service vehicles, more precisely from a tri-axial accelerometer and a tri-axial gyroscope installed in a non-powered bogie. The authors started from a two-dimensional car model and the train’s dynamic parameters obtained in a field calibration exercise. Thus, a cross-entropy optimisation was applied, comprising the Monte Carlo simulation to create trial solutions (which are statistically adherent to the measured signal) and the definition of the track longitudinal profile that generates the model responses that best match the measured vertical acceleration and pitch angular rate obtained.

Zhu, Law and Huang (2018) conceptualized and performed numerical simulations over a system to characterize the track structural parameters from the dynamic response of in-service trains. The bases were the vehicle-track interaction and track system (on a Winkler elastic foundation) models. From the accelerations measured on the bogie and the axle box, the track-vehicle contact forces are estimated, and changes in this force are obtained from comparison with the modelled one with a given stiffness variation. Thus, the estimation of the track stiffness variation is performed through an optimization problem. In the end, the authors aimed to explicitly obtain the track damage, i.e., the track stiffness reduction due to mechanisms such as fasteners looseness foundation settlement, rail fastener loosening, and lack of ballast compaction.

Vinkó et al. (2023) evaluate the feasibility of onboard measurements using smartphones for rail track geometry estimation. Two Galaxy S series (high-end[30]) smartphones (S6 and S10 gathering data at, respectively, 200 and 500 Hz) were attached to the window of a TRV with geometry and dynamic measurement units operating synchronously. The tests were performed on a track stretch of about 50 km (information obtained in an approximate way through Google Maps) in Budapest, Hungary. Firstly, the raw acceleration data was compared with the reference vibration data from the TRV and was identified as highly correlated (Person's coefficient correlations above 0.81) in signal magnitude and waveform. From the heading and pitch angles calculated from gyroscope data (deviation in the range of 0.2-0.6º), the curvature and the radius of the horizontal curves (relative errors up to 1.1%) were also acceptably estimated.

Moreover, these authors performed further analysis from gyroscope data filtered by an elliptic bandpass filter to mitigate gyro drift and noise. Firstly, the heading angle is obtained by the simple integration in time of the filtered gyroscope yaw rate (gyroscope reading around the vertical axis), and the curvature is calculated as the yaw rate divided by the vehicle speed. Owing to the inaccuracy of the speed estimates from the smartphone GNSS receiver, the authors used the speed values

[30] According to the Samsung, "the Galaxy S series is Samsung's high-end range of flagship smartphones" (SAMSUNG, 2023).

from the TRV. Secondly, the quasi-static value of track cant is obtained from two mains considerations:

- The formulation of the non-compensated lateral acceleration with the gravity-related component and the centripetal component (which depends on the curvature previously calculated). For this, the authors considered the lateral acceleration smoothed with 5 Hz low-pass filter.

- The consideration of the roll coefficient that relates the tilting angle of the car body and the track cant angle. The authors obtained this constant value for the specific vehicle from the coefficient formulation and iteration using known cant data on the track tests.

From these aspects, the authors obtained an expression for the quasi-static track cant depending on fixed values (gravity acceleration, distance between the points of contact of the wheels, and the roll coefficient), on values obtained from the smartphone (yaw-angle rate and lateral acceleration), and on values obtained from the TRV (vehicle speed). As a result, relative errors up to 5.6% were obtained. Finally, the estimation of track twins from the values of track cant is performed through two different developed methods:

- Taking the derivative by convolution of the previously estimated cant, being the convolution kernel obtained in order to represent the twist base length considering the vehicle speed and the phone sample rate.

- Direct calculation as a product of the distance between the points of contact of the wheels, the twist base length, and the roll-rate gyro data, divided by the vehicle speed.

For twist validation, the authors considered only values that exceeded the established limit value (10 mm) and identified that only severe twist irregularities were consistently detected. Moreover, the positional errors of the detected irregularities ranged from 2 to 10.4 m in absolute values. As a limitation to be further investigated, the authors highlight the improvement of GNSS position and speed estimations. However, in general conclusion, they empathize that using these very low-cost sensors is a technological opportunity to be explored in rail track management.

Choi (2023) describes parametric models[31] to estimate track irregularities in high-speed lines using measurements from lateral and vertical accelerometers installed on the axle box and the bogie. Initially, lateral and vertical displacements are estimated considering a discrete state-space model for displacement estimation from noisy accelerations and a Kalman Filter algorithm. Subsequently, instead of the challenging and complex use of the physical models, the author proposed a hybrid parametric model between the finite impulse response (FIR) and the infinite impulse response (IIR) models. Hence, an adaptative Kalman Filter is applied to obtain the unknown parameters of track irregularities from the estimated displacements. The estimated irregularities presented a good agreement with the reference geometry data in spatial and wavelength domains.

4.4.1.2 Implicit approach

The track quality can be implicitly evaluated based on direct vibration evaluation in light of the influence of track irregularities or stiffness variation on vehicle vibrations. For this, signal-derived features and statistical measures in the time, space and frequency domains are considered.

Regarding track geometry and rail corrugation characterization, Mori *et al.* (2010) presented a system of probe vehicles for real-time track monitoring. For this, a portable probe system (the size of an executive suitcase) was developed, comprising a noise meter, a triaxial accelerometer, a gyroscope for roll angle, and a GPS receiver. The technique employed microphonics to detect rail corrugation from cabin noise, partially resulting from wheel-rail contact. The energy peaks on the sound spectrum were proven to be associated with rail wear magnitude. In parallel, irregularities in the track geometry were detected by accelerometers and the roll gyroscope. As expected from the vehicle model, peaks in vertical and lateral

[31] As stated by Hoelzl et al. (2022) in the context of on-board railway infrastructure monitoring, the parametric models “feature parameters that define the dynamics of the time series and determine the relationship between the potentially unknown excitation source and the observed response”. On the other hand, the nonparametric methods are less strict about the fit to a specific model structure, comprising time-frequency representations, numerical integration, and statistical measures.

accelerations (root mean square - RMS - values) were associated with, respectively, peaks in vertical and lateral irregularities. Mover, peaks in roll angle (RMS values) were related to cross level defects.

Although focusing on velocity and location information, as well as on wheel monitoring, Heirich *et al.* (2013) studied the use of the vibration signature in the spatial domain as a key for vehicle location and provided relevant insights for track monitoring systems. First, the authors considered a simple vehicle model with the main sources of vibration, i.e., the high-frequency components due to wheel imperfections, track irregularities, and background noise (such as from the engine). Then, from the consequent deductions, the signal was filtered to remove the slow train motion effect (high-pass filter) and background noise (notch filters at engine harmonics) and obtain the vibration components related to wheel-track interaction that authors classified as the speed-dependent ones. Thus, a cross-correlation analysis and a consequent shift correction are performed using a prior vibration signal attached to a track map as reference data. Among the possible improvements in the proposed system, the authors highlight the importance of the optimized sensor installation, placing it the nearest possible to the bogie.

Dealing with the low quality of the consumer-grade sensors and the suspension influence, Hong, Hussin and Saman (2014) presented a track monitoring solution based on an Arduino microcontroller and a consumer-grade IMU composed of a triaxial accelerometer and a triaxial gyroscope installed in the train cabin. The acceleration measurement and inclination estimates were used on track misalignment identification through acceleration peaks and frequency spectrum over time analysis.

Salvador *et al.* (2016) identified track defects, track singularities, and vibration modes (including the vibration included by the motors at their harmonics) from axle box accelerations. For this, the Short Time Fourier Transform was applied, and the resulting track spectrograms were analysed in terms of energy variation in specific frequency ranges. A relevant discussion in this work is the description of the excitation frequencies of the different track defects and features wavelengths (function of the speed) and their coupling with natural frequencies of the different track and train elements. The sprung masses, for example, have natural frequencies

ranging approximately from 0.7 to 3 Hz, and these frequencies are resonant with the excitation frequencies of track features over 25 m for speeds over 50 km/h.

Lederman *et al.* (2017a) propose a data-driven track monitoring from the dynamic responses of trains in revenue service. Given the challenges posed by speed variation and positional inaccuracy, the possible features extracted from acceleration signals (in the spatial or the frequency domain) were explored, and their sensibility to modifications in the track (track replacement or tamping) was evaluated through a support vector machine used as supervised classification. The authors concluded the superiority of the signal energy features in this identification. Additionally, they tested unsupervised track change detection filters and verified the superiority of the Haar wavelet filter for this activity. In subsequent work (LEDERMAN et al., 2017b), the authors proposed data fusion for features extracted from multiple sensors aboard multiple vehicles and their multiple passages on the same track. The main challenges on fusing this data are presented: lack of synchrony, spatial misalignment, and noisy or malfunctioning behaviour of individual sensors. The proposed algorithm started from data alignment through cross-correlation analysis and shift correction to deal with positioning imprecisions. Thus, an adaptative Kalman Filter is applied in the data combination, in which the sensor variance in relation to the previous estimate is used as reliability measure and conditions the sensor's weight. For validation on operational data, two regional passenger trains were each of them instrumented with two industrial-grade uniaxial accelerometers (at 2kHz) and a low-cost GPS receiver. As a result, the fusion approach improved the track change identification accuracy and robustness regarding positional uncertainties. In contrast to this thesis, fusion at level 0 (raw data level) is not proposed and industrial-grade accelerometers were employed.

Seraj, Meratnia, and Havinga (2017) employed inertial sensors (accelerometer, gyroscope, and magnetometer) of eight smartphones attached to the car body of a track recording car to characterise track cant, curvature, and twist. These authors applied discrete wavelet transform and sub-band coding algorithms to extract long and short wavelength features and yield results compatible with measurements of the state-of-the-art technique. Although using multiple sensors, data fusion and the comparison among the installation points were out of the scope.

Paixão, Fortunato, and Calçada (2019) make use of a smartphone installed on the cabin floor and close to the bogie centreline to gather vibration data and compare it with track quality. The authors obtained a good correlation between the standard deviation of vibration and the standard deviation of track longitudinal level in ranges D1 and D2. From these promising results, the creation of a structured approach for the characterisation of structural performance and degradation in geometry is defined as a further step.

De Rosa et al. (2021) present machine learning-based classifiers to characterize lateral and cross level irregularities from lateral and roll bogie accelerations, dealing with the well-known problem of inertial methods in the lateral direction. Three different classifier algorithms are used: decision tree, support vector machine, and Gaussian support vector machine, which were trained using simulation data considering Italian high-speed operational features. In the testing phase, the classifier's performance using data gathered by the inspection train only on straight sections was promising (accuracy > 87%, kappa coefficient ≥ 0.58), with the study of curved sections and replication for vertical accelerations and irregularities being topics of further research.

Balouchi, Bevan, and Formston (2021) propose a car body-based track monitoring system with the addition of a low-cost MEMS triaxial accelerometer (not detailed in terms of its specifications). A continuous wavelet transform was applied as a bandpass filtering of the input signal and representation in time domain, in a multiresolution analysis in terms of six frequency bands. The band-pass filtering at different frequency ranges would allow the differentiation between, e.g., lower frequency responses due to voided sleepers and higher frequency vibration due to corrugation. A complementary contribution is the proposed compensation factors for speed variations, using the approximately quadratic relationship between speed and acceleration for a given level of irregularity observed in simulations. In practice, a factor ruled by the derived inverse exponential proportionality is proposed to normalise accelerations to that experienced at the maximum track speed (for the tests reported by the authors, approximately 23 m/s). Good agreement was observed between compensated accelerations and the discrete faults detected from reference data (inspection train), particularly in the vertical direction, with possible statistical

improvement considering multiple instrumented trains, multiple passages, and the use of machine learning methods.

Tsunashima and Hirose (2022) propose a track fault detection through a time-frequency analysis comprising two steps: a) empirical mode decomposition, which decomposes the time series into intrinsic oscillatory modes; and b) the Hilbert transform for time-frequency representation of each component. The method was tested on simulation data and on data from field tests. Regarding the latter, vertical car-body acceleration data was gathered at 82 Hz aboard an in-service vehicle on a regional line, with a number of passages (not specified) over a three-year interval. The analysis procedure began by calculating the RMS for vertical accelerations at short (not specified) intervals to identify critical sections, i.e., those whose values exceeded 1 m/s² at high frequency in the total number of trips. Then, the time-frequency plane resulting from the Hilbert transform is assessed for a detailed analysis of the critical sections. The method identified large defects that generate large vertical acceleration, while minor defects and the identification of lateral irregularities should be discussed in future work.

Gonzalo *et al.* (2022), on the other hand, focus on a new method for location estimation from onboard inertial measurement. In the context of track and ride quality monitoring activities, the aim is to improve the spatial alignment between data from successive passages when using in-cab IMU-based systems. The first aspect addressed by this method is the speed estimation through the identification of the harmonic content in the spectrogram of the accelerations (three axes) and the angular rates (three axes), whose behaviour approximately follows the speed profile due to the relationship between excitation and speed. Thus, speeds from the spectrogram and from GNSS are combined through a Kalman Filter. In the second step, the distances estimated from the speeds are adapted using the cross level as a reference, i.e., using the gyroscope-estimated cross level for spatial alignment with respect to the reference cross level. To deal with the drift in the numerical integration of the angular rates, the authors propose the section division into constant cross level and transition subsections, removing the linear drift for each of them. In field tests

employing the IMU-based device[32] developed by the authors (sample rate of 1 Hz for the GNSS and 256 Hz for the IMU), the resulting errors were usually below 20 m.

Focusing also on train location and using the potential repeatability of indirect measurements of track irregularity, (CHEN et al., 2022) identify the possibility of matching between vehicle's attitude responses to a reference map of irregularities in a feature matching strategy. In practice, the proposed procedure comprises the following steps: a) the subsequence of the measured vehicle's attitude responses is obtained; b) the initial subsequence is initially positioned using the GNSS coordinates; and c) within a search window (40 m due to GNSS expected inaccuracy), the subsequence is displaced in order to find the shift in space that maximises the correlation with the reference map. For 50-m subsequences, the value found as the minimum to ensure accuracy convergence, the method reached an error of 0.4 m (RMS) in longitudinal position when using roll and pitch estimates from body-mounted low-cost (industrial-grade) IMU.

An alternative implicit approach is the consideration of **comfort indexes** as indirect track quality figures. This concept has been used in rail transportation since track features and irregularities substantially influence ride comfort. For this evaluation, the standard established by the International Organization for Standardization (ISO 2631-1:1997) (INTERNATIONAL ORGANIZATION FOR STANDARDIZATION, 1997) is the most used alternative. This standard provides methods for whole-body vibration assessment regarding human health and comfort, vibration perception, and incidence of motion sickness, and comprises guidance on vibration measurement and evaluation using frequency-weighted root-mean-square accelerations.

Zoccali, Loprencipe, and Lupascu (2018), proposing an indirect method to analyse the track quality, characterise the passenger comfort in accordance with ISO 2631 standard using an accelerometer installed on the floor of a subway train. With this approach and its geovisualization, multiple transversals exhibited a consistent correlation between high frequency-weighted vertical accelerations and the presence of track switches. In turn, Azzoug and Kaewunruen (2017) created a smartphone

[32] The sensor grade is between tactical and industrial, as can be deduced from the sensor description presented in a previous paper (ENTEZAMI et al., 2016).

application for comfort analysis and tested it on two devices. The authors applied an artificial neural network using data gathered by a more accurate piezoelectric accelerometer for training, and a comparison between this technique output and track geometry parameters was recommended as further work.

NETIRAIL-INFRA (2018) presents the development of a smartphone-based track and ride monitoring application that registers the perception of ride comfort in the cabin according to ISO 2631 and its relation with track features such as switches, crossings, track stiffness variations, and deteriorated turnouts. Do *et al.* (2020) performed a similar ISO-based analysis employing smartphones and identifying the association between discomfort peaks and track stiffness transition zones.

Rodríguez et al. (2021) present a methodology to monitor ride quality and, indirectly, track quality by gathering acceleration data from smartphones and tablets aboard in-service trains. In general terms, the proposed methodology for continuous monitoring considers a cycle with two stages. In the first stage, initial measurement is performed, and results are compared with the current standard guidelines regarding track quality and ride comfort to determine the need for corrections. If the track condition is still adequate, the second stage starts with a new measurement campaign and the comparison of results with both the standard guidelines and the previous measurement. In case of acceptable condition, subsequent measurement campaigns are performed until the need for correction is detected. The track renewal begins a new measurement cycle. From this cycle, the track acceptability is detected, and the variation over consecutive campaigns characterizes the evolution of track condition, contributing to predictive maintenance.

These authors performed tests in a 645-m section in a transition zone (from a ballasted to a slab structure in a tunnel) of an urban railway line. The recording devices were attached directly to the floor at three different measurement points as required by the standard: the front bogie, the rear bogie, and the middle of the car. Regarding comfort analysis, acceleration data was processed in accordance with EN 12299 (Mean and Continuous Comfort, with adaption due to the short section under analysis) and, additionally, by applying a proposed simplified method as the sum of the maximum and the minimum obtained values divided by the average value for a given interval. Regarding track quality, punctual structures such as bridges, tunnels,

switches, and track transitions were visualized in the vertical acceleration signal. For the effective use of acceleration in track characterization, the authors propose the simple use of threshold taking into account a record of measurements on the same track. The simplified approach, thus, is not reciprocal to the standardized indexes and would be more suitable for relative analyses. As other limitations, the authors list the need for a constant position (given the vibration magnitude difference between the vehicle's centre and extremities) and orientation during the measurement and for the successive campaigns, the influence of variations on the suspension system, and the impossibility of detailed monitoring (such as fastening loosing and sleeper cracking). More detailed aspects regarding the track geometry parameters and the influence of the speed variation are not addressed.

Another alternative for an implicit characterization approach is considering a **safety index** since track features and irregularities condition derailment risk. In this regard, it is crucial to establish the distinction between comfort and safety assessments. The current practice shows that vibration components lower than about 2 Hz have a more significant influence on ride quality, while vibration components from 2 to 10 Hz are more related to dynamic stability (LEE et al., 2012). The description in terms of wavelength depends on the speed, but it is possible to state that stability is mainly associated with short wavelengths. From the abovementioned distinction between ride quality and derailment risk, it is concluded that the results of each of these methods will be more correlated to the corresponding wavelength than to a complete characterization of the spectrum.

Through stability assessment, Barbosa (2016, 2017) employs inertial measurements from low-cost sensors in a new indirect method for railway track quality characterization. The author started from an extended Kalman filter-based inertial navigation algorithm to estimate vehicle attitude from measured acceleration and angular speeds. Afterwards, the inverse vehicle dynamic problem is considered to estimate lateral (L) and vertical (V) forces on the wheels from the inertial measurements and the attitude. In the end, these forces are used to calculate a dimensionless safety index equal to the difference between the L/V limit for stability and the measured L/V. Thus, this index is used to evaluate track quality and identify sections with harmful irregularities. The results showed good relationship with twist and longitudinal level defects. However, addressing further work, the author indicates

limitations on the use of very low-cost IMUs due to their noise magnitude.

4.4.2 Sensor grade

The sensor grade considers its typical application and reflects its quality and cost. Regarding the proposed approach (use of consumer-grade sensors), identifying the used sensor grade in the surveyed papers is pivotal. However, most literature is scarce when describing the apparatus used in the tests and contrary to the scientific principle of reproducibility.

Weston *et al.* (2015a) highlighted the noise levels and poor stability of consumer-grade sensors, similar to those proposed in the present paper, as restrictions for their use in track profile direct reconstitution. Moreover, the installation on the axle box and the bogie subjects the sensors to high accelerations. Thus, a substantial number of the works employ sensors that range from automotive to tactical grade, yielding more accurate measurement and greater resistance to harsh environments. However, recent research has shown the growing interest in using consumer-grade sensors, especially regarding eventual smartphone-based collaborative systems or the provision of information to the transport user.

4.4.3 Sensor location

According to the sensor location, the classification considers whether the sensor is installed: a) in the axle box; b) in the bogie; or c) in the car body. This characterization is relevant given the influence of the suspensions on measurements. In practice, this influence works as a lowpass filter since the suspensions' primary function is to isolate high-frequency vibrations. Moreover, discussing the optimum placements or the proximity to the bogie could also be considered a subclassification of the c) case.

Regarding the suspension influence, the direct approach is facilitated when sensors are installed on the axle box (BOCCIOLONE et al., 2007; BONGINI; GRASSIE;

SAXON, 2011; REAL et al., 2012; DU et al., 2013; LI et al., 2015; WANG et al., 2017) or on the bogie (WESTON et al., 2007b; IONTCHEV; KENOV; MILETIEV, 2013; ABUHAMDIA et al., 2014; QUIRKE et al., 2017). However, the use of sensors installed in the car body (LEDERMAN et al., 2017a; SERAJ; MERATNIA; HAVINGA, 2017; ZOCCALI; LOPRENCIPE; LUPASCU, 2018; PAIXÃO; FORTUNATO; CALÇADA, 2019) indicates a greater propensity to the implicit methods given the filtering influence of the suspensions.

4.4.4 Number of installation points

Most of the works consider the installation of the sensors at a single point (e.g., the axle box or the bogie centre mass) or different points in different frames (e.g., an accelerometer in the train cabin and another one in the bogie). Regarding the axle box and bogie-based systems, some works consider installation at both extremities to depict each rail profile.

For cabin-based approaches, the proposed systems usually consider a single installation point at a near-optimal point. As one of the exceptions, (SERAJ; MERATNIA; HAVINGA, 2017) installed four pairs of smartphones distributed along the track recording coach used in their tests. However, the comparison between the signal was out of the scope of their work. In turn, Barbosa (BARBOSA, 2016, 2017) suggested as a further step for his work the use of multiple devices (4 units using sensors better than the consumer-grade ones), each of them placed in each train cabin extremity for a better vehicle displacement description. Finally, Vinkó et al. (2023) tested a pair of smartphones in the same transversal section of the TRV, with one installed on the right and the other on the left.

4.4.5 Data processing tools

This subsection describes the data processing tools used to enable the abovementioned approaches. These tools are not mutually exclusive and can be

combined when necessary, as well as can also be used for fusion purposes. However, data fusion will be discussed only in the following subsection given its importance for the proposed thesis.

Regarding digital signal processing and extracting information from data, the main tasks are signal filtering and signal analysis (INGLE; PROAKIS, 2000). The main objectives for filtering, a signal-in signal-out operation, are noise removal and the separation of frequency bands regarding different track wavelength ranges. For the considered application, spectrum analysis considering the frequency content related to the track feature wavelength is a typical activity. The time domain alternative for this task are the measures of central tendency and dispersion (mean, variance, standard variation, root mean square) within track sections. The main mathematical tools for these processes are described as follows.

4.4.5.1 Fourier transform and variations

Frequency analysis is the process of decomposing a signal into its frequency components, i.e., sinusoidal or complex exponential signals (MANOLAKIS; INGLE; KOGON, 2005). The Fourier transform (FT) is the mathematical transform for this task, changing the representation of a function from the time (or space) domain to the time (or spatial) frequency domain.

The Fourier Transform for frequency analysis of a generic continuous-time (or space) signal $x_c(t)$ is given by:

$$X_C(F) = \int_{-\infty}^{\infty} x_c(t) e^{-j2\pi Ft} dt \tag{15}$$

where $X_C(F)$ is the signal spectrum (as a function of the frequency *F*) and $e^{-j2\pi Ft}$ is the complex exponential signal representation. In complement, a discrete-time signal $x(n)$ is absolutely summable (sum of its absolute values is less than infinity) is described by the discrete-time Fourier transform (DTFT) given by:

$$X\left(e^{-j\omega}\right) = \sum_{n=-\infty}^{\infty} x(n) e^{-j\omega n} \tag{16}$$

where $\omega = 2\pi f$ is the frequency in radians per sample and f is the frequency in cycles per sample. As stated by Eq. (16), the DTFT is calculated over an infinite summation and yields a continuous function for frequency. A computable alternative is the discrete Fourier transform (DFT), which is calculated over an equally-spaced finite sequence of values into a same-length sequence of equally-spaced samples of the DFTF. Evaluating the DTFT $X(e^{-j\omega n})$ at N equidistant frequencies from an N-point original sequence $x(n)$ (i.e., $\omega_k = (2\pi/N)k, 0 \leq k \leq N-1$), the DFT $X(k)$ is given as follows:

$$X(e^{-j\omega}) = X\left(e^{-j\left(\frac{2\pi}{N}\right)k}\right) = \sum_{n=0}^{N-1} x(n)e^{-j\left(\frac{2\pi}{N}\right)kn} = X(k) \tag{17}$$

The DFT is efficiently computed by a family of fast algorithms called fast Fourier transform (FFT) algorithms, which are implemented in the data analysis libraries for programming languages or platforms.

The energy computed from the FFT is the power spectrum or power spectral density (PSD), which yields the signal power distribution as a frequency function. The PSD is computed as the modulus squared of the FFT for each frequency component, and it is equivalent to multiplying each frequency bin of an FFT by its complex conjugate.

A limitation of FT derived methods is the loss of time information, making these techniques unsuitable for time-variant, nonstationary signals such as the train vibrations. A solution for this problem is the short-time Fourier transform (STFT) or windowed FT (MERTINS, 1999), an algorithm that segments the signal into narrow intervals (narrow enough to ensure the stationarity) and applies the Fourier Transform for each segment. Its usual output is the spectrogram (or spectrograph) as a time-frequency representation. In the segmentation step, the spectral leakage is prevented using an appropriate window function (i.e., not the rectangular one).

Regarding the suitability to time-variant signals, the STFT is widely used in vibration-based track monitoring (HEIRICH et al., 2011; SALVADOR et al., 2016; VINKÓ; BOCZ, 2018).

4.4.5.2 Wavelets

Regarding time-frequency representations, the main problem with STFT is its fixed time resolution for all frequencies. This fact results in a trade-off between time and frequency accuracies when choosing the window function.

The wavelet transform is a solution for the FT limitations, considering the projection of the signal into functions known as wavelets (MERTINS, 1999). These functions are similar to the windows in the STFT but can be scaled to depict the signal components with different frequencies better. The wavelet transform $W_X(t)(b,a)$ of the signal $\psi(t)$ is defined by:

$$W_X(t)(b,a) = |a|^{\frac{1}{2}} \int_{-\infty}^{\infty} x(t)\, \psi^* \left(\frac{t-b}{a}\right) dt \tag{18}$$

in which ψ is the wavelet (which can be regarded as a bandpass impulse response), the parameter a is associated with the centre frequency and the bandwidth of this bandpass, and the parameter b is a translation in time. Its computable version, the discrete wavelet transform (DWT), performs a multiresolution analysis considering two basic functions: the scaling and the wavelet functions.

Seraj, Meratnia, and Havinga (2017) applied the wavelet transform to the track monitoring problem given its suitability to transient signals. For the vehicle-based methods, track wavelengths are fixed, and the frequencies are proportional to the velocity, resulting in a non-constant resolution throughout the analysis, which is unsuitable to the constant resolution yielded by the FT. Thus, the wavelet transform can resolve this FT limitation by adapting the window size to the frequency.

4.4.5.3 Filtering techniques

Filtering is a critical activity in the considered research area since it has two primary uses: noise removal, especially important for low-quality sensors, and signal separation considering the different frequency bands associated with the different track wavelength ranges. The main feature of a linear filter in time or frequency

domains is its impulse response, i.e., the output when the input is a normalized impulse. Regarding this feature, the filters can be classified into (SMITH, 1999):

- **Finite Impulse Response** (FIR), in which impulse response is of finite duration (or finite length). In this context, the impulse response is also named filter kernel. Using convolution, it is the most straightforward way to implement a filter.

- **Infinite Impulse Response** (IIR) filters, in which impulse response exponentially decays in amplitude and is consequently infinitely long. It is implemented through the recursion technique.

Besides the impulse response, a linear filter has two other relevant characteristics: its step response and frequency response. The step response stands for the output when the input is a step function, and it is an essential feature regarding the preservation of step responses of the original signal (e.g., the track curvature variation). The frequency response, also called transfer function, is the signal magnitude and phase changes (as frequency functions) when passing through the filter. Regarding this latter specification, a filter can be classified as low-pass, high-pass, band-pass, band-stop etc.

Besides the implementation classification described above, the filter can be classified according to its use: in the time domain (e.g., for smoothing), frequency domain (e.g., for separating frequencies), or custom (e.g., for deconvolution).

The moving average is the most basic FIR, time-domain filter on digital signal processing. Despite its simplicity, this filter is optimal in reducing random white noise and maintaining step response (SMITH, 1999). From this, it can be regarded as a good filter for preliminary data analysis. In practice, it comprises a signal convolution using a very simple kernel, i.e., a rectangular pulse.

Alternatively, the Butterworth filter (IIR filter) is widely applied on spectral decomposition for direct band evaluation in track characterisation (WESTON et al., 2007b; LEE et al., 2012; REAL et al., 2014; OBRIEN et al., 2018) or the calculation of frequency weighted accelerations for comfort analysis (ISO, 1997). The main characteristic of this filter is that its frequency response is as flat as possible when separating frequencies.

4.4.5.4 Kalman filter

R. E. Kalman (KALMAN, 1960) proposed a new approach for state estimation problems regarding linear dynamic systems perturbed by noise and measurements (for state estimation) linearly related to the state but also disturbed by noise (GREWAL; ANDREWS, 2008). In such problems, the main issues to deal with are the prediction of random signals, the separation of random signals from random noise, and the detection of signals with a well-known form in the presence of random noise. Kalman's formulation for this estimation problem, the **Kalman Filter**, is a discrete-time, recursive, linear minimum mean square error method.

The Kalman Filter algorithm has two main steps. Firstly, in the **prediction phase**, the filter estimates the current state variables and their uncertainties based on prior knowledge of the considered phenomenon (physical model). Subsequently, in the **update phase**, the estimates are updated considering the new measurements (and their uncertainty) and the measurement model through a weighted average using the certainty as weight. This formulation can also be regarded as a subsequent product of Gauss' work in estimation techniques resulted in the introduction of the following modern estimation concepts (HALL; MCMULLEN, 2004):

- Observability, referring to the number and type of observations that are necessary to estimate the state vector.
- Dynamic modelling, considering the development of a system dynamic model (in other words, the knowledge of the physical phenomena), which is necessary to describe the evaluation of the state vector in time.
- A priori estimate, i.e., an initial value for the state vector from which the solutions are obtained.
- Observation noise, considering its probabilistic interpretation from the observations.

From these aspects, the Kalman Filter has as core elements (GREWAL; ANDREWS, 2008; GROVES, 2008):

- The **state vector**. The state of the dynamic system is characterized by the values of its attributes of interest (state variables) at a given epoch. Thus, the state vector has these state variables as its components.

- The **error covariance matrix** associated with the state vector. This matrix represents the uncertainties and the degree of correlation between the errors in the state estimates. Since the Kalman Filter is an iterative process, initial values for the state vector and the covariance matrix must be set at the beginning.

- The **system model**, which describes the dynamic behaviour of each state variable based on the known deterministic properties of the system. In other words, it describes how state and covariance matrix. There is also the **system noise**, which can be defined as the random dynamic disturbances on the system with given statistical properties.

- The **measurement vector** is the set of properties of the system that can be directly measured by the considered sensors and are a function of the state vector. This information is used to obtention all the state estimates after initialization. Moreover, the **measurement noise covariance matrix** describes the statistics of the **measurement noise**.

- The **measurement model** based on the known deterministic properties of the system regarding the expected measurement vector behaviour as a function of the true state vector.

- The **Kalman Filter algorithm** itself, which uses the measurement vector, the measurement model, and system models to obtain optimum[33] estimates. As previously explained, it comprises two main phases: the prediction (or system propagation, or time update) phase and the measurement update phase**,** and they are described here in terms of vectors and matrices involved in each of them. The first phase comprises predicting the state vector estimate and error

[33] The state estimation is better than the estimate obtained by using only one measurement alone and it is optimal if process and measurement noises are assumed to be normally distributed (HUMPHERYS; REDD; WEST, 2012).

covariance matrix using the currently valid initial measurements and system model-related information. The second phase starts from this prediction and calculates the new state and error covariance estimate incorporating information from the new measurements and using measurement model-related information.

There are algorithm variations that consider approximations for nonlinear problems, such as the Linearized Kalman Filter (LKF), the Extended Kalman Filter (EKF), and the Unscented Kalman Filter (UKF). While the LKF considers the linearization of the models about a fixed nominal trajectory, the EKF performs this linearization about the estimated trajectory at every time step. On the other hand, the UKF applies the so-called unscented transform, i.e., transforms that use some sampling and weighting implementation (GREWAL; ANDREWS, 2008).

A basic example is the use of Kalman Filter on GPS receivers for navigation purposes. The raw position estimation from the GPS signals can reach an accuracy of a few meters, but it is noisy. Thus, it can present unreal variations in the position considering the receiver's expected displacement (i.e., the motions of the host vehicle). In this context, this Kalman Filter algorithm uses the dynamic model of the vehicle as one of its main components (besides GNSS measurements modelling) (GREWAL; ANDREWS, 2008).

The Kalman Filter is suitable when solving an inverse problem, i.e., when trying to obtain track geometry as an unknown state to be estimated from noisy acceleration measurements (LEE et al., 2011; ODASHIMA et al., 2017).

4.4.6 Data fusion

Data fusion can be defined as combining data from multiple sensors to provide more accurate or specific inferences than using a single sensor (HALL; LLINAS, 2008). It comprises activities such as data alignment, association, and estimation (i.e., combined estimation from multiple inputs). The monitoring concept addressed in this research can encompass three main modes of data fusion:

- Sensors of different nature (e.g., accelerometer and gyroscope fusion to provide inclination estimation).
- Similar sensors (e.g., multiples accelerometers to provide a smaller signal to noise ratio).
- Different traverses on the same road stretch (e.g., vibration signal from successive vehicles travelling on the same road).

For the materialization of these concepts, the fusion techniques can be classified regarding aspects such as fusion level and mathematical technique, as explained in the following sections.

Data fusion can be classified according to its position or level in the data-to-information flow. Regarding these aspects, fusion approaches usually contemplate three levels of abstractions (CASTANEDO, 2013):

- Low-level or measurement-level fusion. At this level, the raw signals are the input of the fusion algorithm. The output is a combined signal with greater accuracy due to the lower signal-to-noise ratio (reduction by $1/\sqrt{N}$ regarding multiple similar sensors).
- Medium-level or feature-level fusion. The features extracted from the raw signal (e.g., RMS acceleration within given sections) are fused to obtain a combined feature.
- High-level or decision-level fusion. This level considers symbolical representations of the considered problem (e.g., a preliminary decision) as sources and combines them to obtain a more accurate decision.

The mathematical techniques for data combination depend on the fusion level. Classic estimation methods are used for low or medium level fusion considering data from the same phenomenon. Examples are the use of the complementary filter for attitude estimation (XING et al., 2016) and the Kalman Filter for the integration of features extracted from different passages (LEDERMAN et al., 2017b). Another possibility is calculating the mean signal or feature under Central Limit Theorem (CLT) as in calculating the average roughness of a given section as the average

index from N passages (BHARDWAJ et al., 2020). On the other hand, decision-level fusion may consider weighted decision methods (voting techniques), classical inference, and Bayesian inference.

4.5 CHAPTER FINAL CONSIDERATIONS

The literature review established the conceptual basis for the proposed thesis, from general aspects of monitoring activities based on vehicles to the data processing techniques effectively used in the related works. Moreover, it demonstrated the growing interest in the development of alternative methods for railway monitoring, providing cost-effective tools, i.e., systems with lower implementation and maintenance costs, and lower impact on traffic. To this end, the use of sensors already on the transport network, such as passengers' smartphones, emerges as an opportunity.

Regarding the thesis concepts, the first challenge identified in the literature is related to the quality limitation of consumer-grade sensors. This limitation arises not only regarding noise levels but also the reliability of the measurements. The second challenge is linked to the sensor installed in the train cabin. The lowpass filter represented by the suspensions (especially the secondary) curbs short-wavelength features characterisation such as the rail corrugation. From these limitations, the implicit approaches seem more appropriate for this thesis.

Moreover, the comparison between indirect methods reveals the advantage, under the proposed very low-cost, cabin-based approach, of a comfort-based assessment according to ISO 2631. The first advantage is the possibility of comfort description for each linear and angular axis, facilitating the correlation with each track irregularity parameter. The second advantage is the output with intrinsic meaning, i.e., frequency-weighted RMS values that can be evaluated on a comfort scale and compared with other results. Finally, another advantage is the set of signal processing tools the standard provides, focused on railway issues (part four of the standard) and the frequencies monitorable in the cabin.

Regarding data fusion techniques, the research on the fusion of multiple traverses

provided relevant tools such as the cross-correlation analysis for data alignment and using the weighted average to integrate multiple similar features. However, some of the main aspects of the collective concept are research gaps. In this context, the central aspects related to the intended weighted data fusion need to be developed, namely the description of the influence of the sensor position (distance from the bogie centreline) and the best approach to deal with temporary malfunctioning sensors and eventual inhomogeneous sensor population. Thus, further development on these issues will compose the central contribution of this thesis.

5 MATERIALS AND METHODS

This chapter describes the materials and methods adopted for the proposed very-low costs collective monitoring of comfort and track quality. Initially, the equipment used for vibration sensing is described, comprising the smartphones used in the individual preliminary test and during certain intervals in the other tests, as well as the consumer-grade devices specially developed for the collective tests aboard in-service vehicles.

Subsequently, data processing and analyses methods comprising the measurement model for accelerometers, gyroscopes, the algorithms for time-shift correction and fusion among the multiple sensors, the algorithm for pitch and roll estimations, and the description of ISO 2631 algorithm employed for the comfort assessment. Finally, the preliminary individual tests and the collective tests performed aboard trains are described.

5.1 HARDWARE SETUP

5.1.1 Smartphones used in the preliminary tests

Preliminary tests were performed using two Android-based mid-range smartphones, namely the *Lenovo Vibe K5* and the *Samsung Galaxy A30*. Both feature a triaxial accelerometer, a triaxial gyroscope (description in Table 9 and 10), a triaxial magnetometer, and a GPS receiver.

Table 9 - Accelerometer, gyroscope, and magnetometer main features for the *Lenovo Vibe K5* smartphone (INVENSENSE, 2012; SENODIA, 2014)

	Accelerometer	**Gyroscope**	**Magnetometer**
Sensor name	MPU-6050, InvenSense		ST480, Senodia
Full-scale range	+- 16 g	2000 °/s	+- 4800 µT
Noise spectral density	400 µg/√Hz	0.005 °/s/√Hz	-
Sensitivity scale factor	2048 LBS/g	16.4 LBS/(°/s))	0.15 µT/LSB (X, Y) 0.25 µT/LSB (Z)

Table 10 - Accelerometer, gyroscope, and magnetometer main features for the *Galaxy A30* smartphone (YAMAHA CORPRATION, 2011; ST MICROELECTRONICS, 2017)

	Accelerometer	**Gyroscope**	**Magnetometer**
Sensor name	LSM6DSL iNEMO inertial module, ST Microelectronics		YAS539, Yamaha Corporation
Full-scale range	+- 4 g	1000 °/s	+- 1200 µT
Noise spectral density	80 µg/√Hz	0.01 °/s/√Hz	-
Sensitivity scale factor	8196 LBS/g	32.8 LBS/(°/s))	0.15 µT/LSB (X, Y) 0.25 µT/LSB (Z)

The AndroSensor application (FIVASIM, 2017) was used for data recording. Moreover, the sample rates of 100 Hz for the accelerometer and 1 Hz for GPS were adopted since they proved to be the maximum stable rates for both during previous tests. Tests using more than 100 Hz as the sample rate resulted in an unstable performance of the aforementioned gadgets, with recurrence of intervals of a few seconds in which new acceleration readings are not recorded. For the sake of comparison, in recent work (VINKÓ et al., 2023), high-end smartphones (Galaxy S-series) were used at have been successfully used at sample rates of 200 Hz (Galaxy S6) and 500 Hz (Galaxy S10). In any case, the filtering effect by the suspensions for high frequencies renders the discussion about high frequencies for the proposed applications innocuous.

5.1.2 Development of a consumer-grade monitoring device

The concept of a low-cost collective monitoring system is attached to the idea of crowdsensing and the use of sensors from smartphones to describe vehicle vibrations and, consequently, enable track quality estimation. Therefore, viability tests of this monitoring concept should consider the use of multiple sensors operating in parallel during the same train trip. Since the acquisition and use of smartphones present drawbacks such as cost of acquisition and power limitations, this research created sensor nodes using smartphone-grade sensors to emulate these gadgets affordably.

Nine sensor sets were built for the tests performed on the Italian railway network. Each apparatus comprises a Raspberry single-board microcomputer, an IMU (accelerometer, gyroscope, magnetometer, and barometer), and a mini GPS module.

This section describes each item and situates them according to the most used techniques in these applications.

5.1.2.1 Raspberry Pi Zero W microcomputer

The Raspberry Pi Zero W is a low-cost single-board microcomputer with a 1 GHz single-core microprocessor, 512 RAM, and a 40-pin general-purpose input/output (GPIO) (RASPBERRY PI FOUNDATION, 2020). This Raspberry model measures 6.5 x 3.0 cm and has 802.11 wireless LAN (Wi-Fi) and Bluetooth connectivity, facilitating the parallel control of the nine sensors during the experimental tests. Another relevant feature of a Wi-Fi enabled single board is the possibility of data transmission concomitant to the system operation without needing physical uninstallation and reinstallation. The Raspberries used in this research run the official Linux-based Raspbian operating system.

5.1.2.2 Inertial measurement unit

A MEMS-based IMU is a single-chip multi-axis sensor that estimates at least linear accelerations and angular velocities and, thus, integrates an accelerometer and a gyroscope. For this research, the InvenSense MPU-9250 inertial module was used, a 10 degrees-of-freedom module that incorporates the three-axis MEMS inertial sensors (accelerometer and gyroscope) to a magnetometer and a pressure module BMP280 (a barometer plus a thermometer) (BOSCH, 2015; INVENSENSE, 2019). It is connected to the Raspberry through an inter-integrated circuit (I2C). This smartphone-grade module measures 1,4 x 1,4 cm and features a digital motion processor that provides fused output for gesture recognition applications. Table 11 presents the main features of the MPU-9250 accelerometer, gyroscope, and magnetometer.

Table 11 - MPU-9250 accelerometer, gyroscope, and magnetometer main features (INVENSENSE, 2019).

	Accelerometer	Gyroscope	Magnetometer
Full-scale range	User-programmable: +- 2, 4, 8 or 16 g	User-programmable: 250, 500, 1000 or 2000 °/s	+- 4800 µT
Noise spectral density	300 µg/√Hz	0.01 °/s/√Hz	-
Sensitivity scale factor	User programmable: 16384, 8192, 4096 or 2048 LBS/g	User-programmable: 131, 65.5, 32.8 or 16.4 LBS/(°/s))	0.6 µT/LSB
Output data rate	up to 4000 Hz	up to 8000	-

The C++/Python library named RTIMULib was used for sensors setup, conversion of voltage outputs and initial calibration on Raspbian. This library enables the acquisition of the following MPU-9250 outputs:

- Three-axial linear proper accelerations in the sensor frame, in g.
- Three-axial angular rates in the sensor frame, in rad/s.
- Three-axial magnetic field in the sensor frame, in µT.
- Temperature, in °C.
- Pressure, in hPa.
- Attitude (roll, pitch, and yaw, in degrees) calculated by RTIMULib through Extended Kalman Filter (EKF) using the inertial data plus magnetic data. The RTIMULib attitude estimation considers an Extended Kalman filter algorithm, which always includes acceleration in its estimations. Nevertheless, whenever the vehicle is under sustained accelerations (e.g., the centrifugal acceleration when in a curve at constant speed), the attitude angles estimation based on accelerometers is disturbed and curbs the use of usual fusion algorithms (XING et al., 2016).

The output data rate of 100 Hz was defined considering processing and storage performance on preliminary tests, the aimed data analyses (initially focused on medium/large wavelength geometric characteristics), and the usual sample rate for medium-grade smartphones. Although maintaining 100 Hz during the first minutes, the mean sample rate effectively obtained during the tests was 83 Hz. Furthermore, a full-scale range of ± 2g was adopted for the accelerometer considering the typical

values for smartphones, suitability to expected maximum accelerations in train cabin (less than 1g disregarding gravity) (INTERNATIONAL ORGANIZATION FOR STANDARDIZATION, 1997; WESTON et al., 2015), the trade-off between range and sensitivity, and the exposure to significant non-linearity errors when operating near the limits of the range.

5.1.2.3 Mini Global Positioning System module

A U-blox mini GPS module, NEO-6M model (U-BLOX, 2011), was used in each sensor set. This receiver performs single-point positioning using only GPS constellation and satellite-augmented GPS positioning. NEO-6M main characteristics are presented in Table 12.

Table 12 - U-blox NEO-6M mini GPS module main characteristics (U-BLOX, 2011).

Receiver type	50 channels, GPS L1 frequency, C/A Code
Satellite-based Augmentation Systems (SBAS)	Wide Area Augmentation System (WAAS), European Geostationary Navigation Overlay Service (EGNOS), and Multi-functional Satellite Augmentation System (MSAS)
Maximum update rate	5 Hz
Time-To-First-Fix[1]	Cold or warm start: 27 s Hot start: 2 s Aided start: < 3 s
Horizontal position error[2]	GPS: 2.5 m SBAS: 2.0 m
Velocity error[2]	0.1 m/s
Bearing error[2]	0.5 degree

[1] Satellites at -130 dBm. The signal strength depends on the physical characteristics along the signal transmission path.

[2] CEP 50%, satellites at -130 dBm, obtained from 24-hour static position solution

The performance in preliminary tests and the usual sample rate for medium-grade smartphones lead to an output data rate of 1 Hz for the GPS module, which requires interpolation to assign GPS positions with IMU readings at 100 Hz (interpolation within a one-second interval). Furthermore, GPS and IMU data are recorded in separate files since this configuration performed more consistently during preliminary tests. The timestamp from the Raspberry operational system is recorded in each file to enable matching and interpolation.

Using the Python library called GPSD, position, velocity, and time (PVT) data are obtained in accordance with the National Marine Electronics Association (NMEA)

protocol. In more detail, the following data is obtained for the considered tests: geographic coordinates of the acquisition point (latitude and longitude), time (UTC) of the acquisition point, velocity, height, and the number of visible satellites.

Figure 8 presents the developed device in its mais items and depicts the axes orientation adopted for the test results description, compatible with the track frame described in the EN standards.

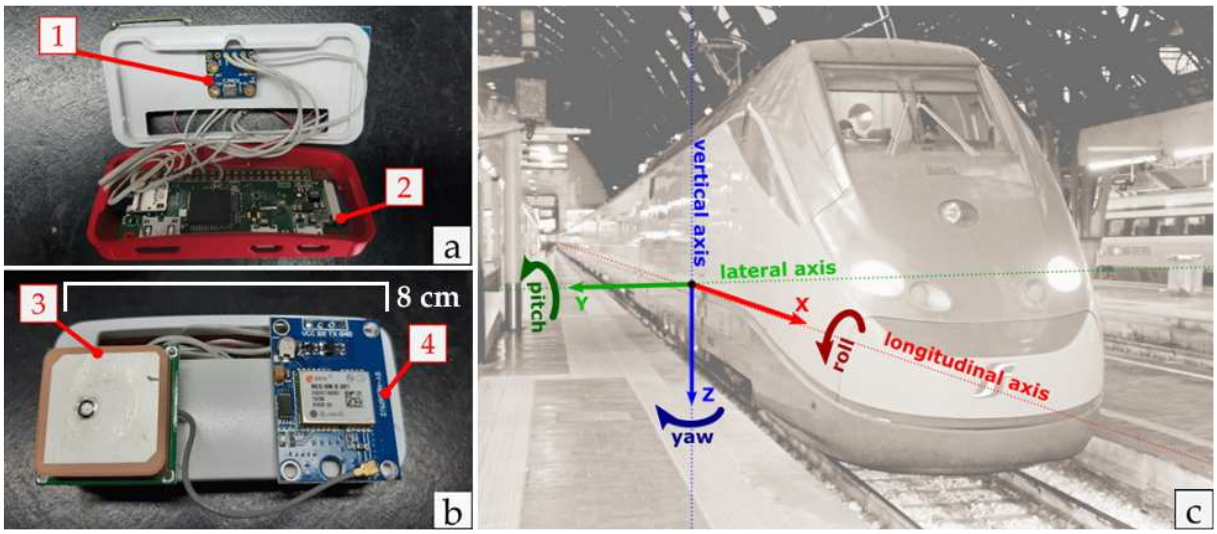

Figure 8 - The developed device and the axes orientation used in the tests: (a) device's internal view showing the IMU module (1) bonded to the case and the Raspberry Pi Zero W (2); (b) external view with the GPS antenna (3) and the u-Blox GPS module (4) bonded to the case; (c) the axes orientation for describing test results (DE OLIVEIRA et al., 2022)

5.2 MEASUREMENT MODEL

To characterise the quantities that the considered sensor set can measure aboard a vehicle in terms of their relationship with track features, basic models of the inertial measurements and the pressure module are built in this thesis based on vehicle dynamics and the constraints of the proposed monitoring method. The components of this model are presented in the following subsections.

5.2.1 Accelerometer model

Based on elements presented in previous works (cited as follows) and considering the vehicle-track behaviour discussed in Chapter 2, the simplified acceleration vector $\boldsymbol{a}$ perceived in the sensor frame s aligned to the body frame is obtained as:

$$\boldsymbol{a^s} = \boldsymbol{g^s} + \boldsymbol{c^s} + \boldsymbol{t^s} + \boldsymbol{n^s} + \boldsymbol{b^s} + \mu^s =$$

$$\begin{bmatrix} -g\ sin\ \theta \\ -g\ cos\ \theta\ sin\ \varphi \\ -g\ cos\ \theta\ cos\ \varphi \end{bmatrix}^s + \begin{bmatrix} \dot{v} \\ c_H\ v^2\ cos\ \varphi - c_V\ v^2\ sin\ \theta \\ c_H\ v^2\ sin\ \varphi - c_V\ v^2\ cos\ \theta \end{bmatrix}^s + \begin{bmatrix} i_X \\ i_Y \\ i_Z \end{bmatrix}^s + \boldsymbol{n^s} + \boldsymbol{b^s} + \mu^s \quad (19)$$

The vectors in Eq. 19 are described in the following subsections. Moreover, the following convention is adopted to describe the accelerometer model:

- Linear x, y, and z: x is the longitudinal axis (positive sense is oriented with the train displacement sense), y is the lateral axis (rightwards considering the train displacement sense), and z is the vertical axis pointed downwards.
- Rotations: right-hand orientation. The track angles and curvatures follow the same orientation (e.g., positive cant angle to the right).

These conventions result in an accelerometer model presentation slightly different from the presented in previous works (HEIRICH et al., 2011; DE OLIVEIRA et al., 2022) but without impact on results if the gravity compensation is performed using coherent signals.

In order to correctly interpret the accelerometer outputs and better understand the relationship between the forces acting on the vehicle and the sensed accelerations, it is essential to emphasize that the accelerometer, as an inertial sensor, will sense only the proper accelerations. In the case of a vehicle on a curve, a strapdown accelerometer will sense the centripetal acceleration and the inverse vector for the gravity (upwards acceleration[34]), as illustrated in Figure 9 for both cant excess and

[34] Since this acceleration is generated as a reaction to the gravity, it will be treated as a “gravity-related component” in this thesis.

deficiency.

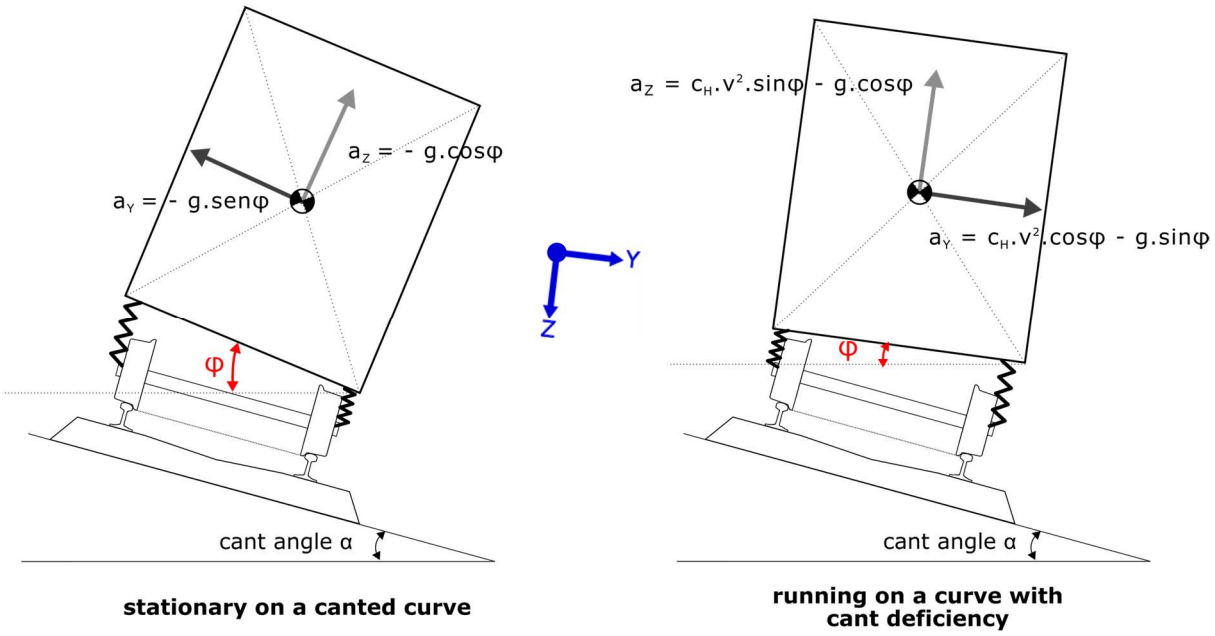

Figure 9 - Accelerations (only the components due to gravity and centripetal force) as sensed by the accelerometers for two situations: standing vehicle (on the left) and vehicle at speed higher than the equilibrium speed for a given curve (on the right).

5.2.2 Gravity-related component

The vector $\boldsymbol{g^s}$ is the gravity-related component in the sensor frame. This component is obtained from the minus gravity vector in the navigation frame (equivalent to the vector identified in a situation of zero pitch and roll angles) rotated to the sensor frame by the use of a direction cosine matrix (DCM) (TITTERTON; WESTON, 2004; HEIRICH et al., 2011). In Eq. (20), the first element is the DCM from the navigation to the sensor frame, for the XYZ rotation sequence. The matrix describes the rotation to be performed in Euclidean space in terms of the Euler angles yaw (ψ), pitch (θ), and roll (φ), i.e., the orientation of the sensor frame with respect to the navigation frame. The second element in Eq. (20), multiplying the DCM, is the minus gravity vector in the navigation frame (n index). Hence, the resulting vector in Eq. (20) is the rotated minus gravity vector in the sensor frame (s index).

$$\begin{bmatrix} cos\,\theta\,cos\,\psi & cos\,\theta\,sin\,\psi & -sin\,\theta \\ -cos\,\varphi\,sin\,\psi + sin\,\varphi\,sin\,\theta\,cos\,\psi & cos\,\varphi\,cos\,\psi + sin\,\varphi\,sin\,\theta\,sin\,\psi & sin\,\varphi\,cos\,\theta \\ sin\,\varphi\,sin\,\psi + cos\,\varphi\,sin\,\theta\,cos\,\psi & -sin\,\varphi\,cos\,\psi + cos\,\varphi\,sin\,\theta\,sin\,\psi & cos\,\varphi\,cos\,\theta \end{bmatrix}_n^s . \begin{bmatrix} 0 \\ 0 \\ -g \end{bmatrix}^n = \begin{bmatrix} g\,sin\,\theta \\ -g\,cos\,\theta\,sin\,\varphi \\ -g\,cos\,\theta\,cos\,\varphi \end{bmatrix}^s \quad (20)$$

The roll and pith angles are mainly associated, respectively, with the track slope and cant plus the influence of the suspensions' stiffnesses on these angles. Complementary, high-frequency variations in these angles also depend on the body vibration modes due to track irregularities. Thus, it is possible to identify a **very long wavelength component** related to track macrogeometry (cant and slope designed variations) and **wavelength components shorter than 200 m** (range D3 and below) ruled by the geometry irregularities.

In this thesis, this component is named gravity-related component to ensure simplicity without undermining conceptual accuracy. As discussed in section 4.3, the component effectively sensed is the reaction to the gravity.

5.2.3 Kinematic component

The vector $\boldsymbol{c^s}$ is the kinematic component, i.e., associated with vehicle displacement on the road regardless of dynamic response to geometry irregularities. Whenever the vehicle is moving, the speed variation $\dot{v}$ is perceived in the x-direction.

Concurrently, the horizontal (c_H) and the vertical (c_V) curvatures produce a centripetal acceleration in the vehicle frame given as being equal to $c \cdot v^2$, where v is the vehicle speed. For both, analogous rotation to that performed for gravity-related component is also performed for centrifugal acceleration values arising from horizontal and vertical curvatures (HEIRICH et al., 2011). Similar to the considerations made for the gravitational component, it is also possible to identify a **very long wavelength component** associated with the track macrogeometry (cant, slope, and curvatures designed variations) and **shorter wavelength components** shaped by the track irregularities.

5.2.4 Track irregularity component

In turn, the vector $\boldsymbol{t^s}$ is the linear track irregularity component. Regarding the y and z axes, components can be regarded as the sums i_y and i_z of multiples **irregularity-related sinusoidal signatures** as concluded from the **models** presented in Section 2.2. The component i_x is different in form and associated with second-order effects of track irregularities on the vehicle dynamics, considerably less significant than their orthogonal counterparts. In this vector, only the displacements directly resulting from geometry irregularities are considered, and not indirect influence of the irregularities on vehicle attitude and on the decomposition of the other acting forces (already regarded in previous vectors).

A generic vertical irregularity with L wavelength excites the vehicle running at a speed v with an excitation frequency f given by:

$$f = \frac{v}{L} \tag{21}$$

In a simplified way and neglecting aspects of a more complete wheel-rail contact model, the **vertical displacement** y by the wheel perceived due to a specific vertical irregularity with wavelength L can be approximated by (MUKHERJEE; MAJHI, 2016; HUNGRIA, 2017; OLIVEIRA et al., 2017; SERAJ; MERATNIA; HAVINGA, 2017):

$$y = e.\sin\left(\frac{2\pi}{L}.v.t\right) \tag{22}$$

where v is the running speed, t is the time and e is the irregularity amplitude. Similar relation can be developed for the lateral displacement considering the lateral irregularities, even though it is known that the lateral displacement of the wheelset does not fully follow lateral irregularities (WESTON et al., 2007b; ALFI; DE ROSA; BRUNI, 2016) given the wheel/rail clearance, as presented in section 2.3.1.

The vertical and lateral displacement effectively perceived by the vehicle body (sprung mass) depends on the irregularity severity variation, the suspension and other train dynamic properties, and the track stiffness. However, this displacement

and its derived acceleration will follow a sinusoidal form, enabling frequency-domain methods for tracking irregularity description from the vehicle's vibration frequencies.

When varying the sensor position along a given coach, this vector changes according to its proximity to the bogie centreline. When placed right over a bogie centreline, the sensor experiences only the car body linear excitation at this section. However, when the sensor is displaced from this bogie section, the influence of this bogie is reduced and that of the other bogie increases. Adopting the extreme case, sensors placed in opposite bogies will experience similar signal but with a shift in time, with time lag equal to the distance divided by the speed. Eventual variations among the dynamic parameters of the coaches (suspension parameters and masses) along a train may also modify the signal amplitude when displacing a sensor from one coach to another.

5.2.5 Other components

Moreover, the vector $\boldsymbol{n}^{s}$ is the background vibration due to the traction motor vibration, the auxiliary power system and the heating, ventilation, and air conditioning (HVAC) system (MUTTER et al., 1981; STOW; ANDERSSON, 2006). For trailer coaches, there is no component due to the traction motor. Furthermore, for the considered tests, the preliminary analysis of the signals for intervals with stationary train demonstrated the absence of relevant vibration components due to the other subsystems. Thus, this component will be ignored in further consideration.

Lastly, the vector $\boldsymbol{b}^{s}$ is the slowly time-varying sensor bias, and the vector μ^{s} is the sensor noise (EUSTON et al., 2008; HEIRICH et al., 2011).

5.2.6 Gyroscope model

Angular speed measured in the sensor frame is mainly affected by variations of track features (namely the cant, the slope, and the bearing variations) but also by angular vibration modes and the influence of suspension on these angles. Considering the

propagation of Euler angles over time (TITTERTON; WESTON, 2004), the relationship between gyroscope measurements in the sensor frame $[\omega_X, \omega_Y, \omega_Z]^s$ and the vehicle body angular rates referred to the navigation frame n is also obtained from rotation matrices and is given by (disregarding the noise and the bias for the moment):

$$\begin{bmatrix} \dot{\varphi} \\ \dot{\theta} \\ \dot{\psi} \end{bmatrix}^n = \begin{bmatrix} \omega_X + \omega_Y \sin\varphi \tan\theta + \omega_Z \cos\varphi \tan\theta \\ \omega_Y cos\varphi + \omega_Z \sin\varphi \\ \omega_Y \sin\varphi sec\theta + \omega_Z \cos\varphi sec\theta \end{bmatrix}^n \quad (23)$$

in which θ is the vehicle pitch, φ is the vehicle roll, and ψ is the vehicle yaw angle. Roll and pitch angles are of small magnitude for the considered application[35]. The result is reduced sinus and cosine values, and some components in the matrix described above can be disregarded without detriment to the desired application. Thus, adapting from Heirich *et al.* (2011) and considering noise and bias, a good approximation for the relationship between angular speed measured in the sensor frame and the vehicle attitude rate is:

$$\begin{bmatrix} \omega_X \\ \omega_Y \\ \omega_Z \end{bmatrix}^s = \begin{bmatrix} \dot{\varphi} \\ \dot{\theta} \\ \dot{\psi} \end{bmatrix}^n + \boldsymbol{b}^s + \mu^s \quad (24)$$

Since the goal is to use this model only to calculate vehicle attitude and gravity compensation, the division into components of vehicle attitude linked to macro (design) and micro geometry (irregularities) will not be discussed.

5.2.7 Pressure module model

The orthometric height Hb is calculated from barometric measurements according to the following hypsometric formula derived from the standard atmospheric model and

[35] For instance, track slope and cant are limited to about, respectively, 1 and 4.2° for the Italian high-speed lines considering its maximum admissible slope (18‰) and superelevation (105 mm) (ZUCCHI, 2013)

considering a linear variation of the temperature with the geopotential altitude (INTERNATIONAL CIVIL AVIATION ORGANIZATION, 1993; GROVES, 2008; RICHARDS TECH, 2018):

$$Hb = \frac{T_S}{k_T} \cdot \left[\left(\frac{p_b}{p_s} \right)^{-\frac{R.k_T}{g_0}} - 1 \right] \quad (25)$$

In Eq. (25), k_T is the atmospheric temperature gradient (-6.5 x 10^{-3} K/m) for orthometric height up to 11 km, p_b is the local pressure obtained by the barometer (with its imprecision), p_s is the sea-level (0 m) pressure (101.325 kPa), T_S is the standard sea-level temperature of 288.15 K, R is a constant derived from the universal gas constant divided by the molecular air mass (287.1 J/kg.K), and g_0 (9.80665 m/s²) is the average sea-level gravity acceleration. This technique presents a good relative performance and can be satisfactorily used for slope detection (BOSCH, 2015) despite eventual systematic errors associated with the atmospheric model and errors associated with atmospheric variations (LI; HARVEY; GALLAGHER, 2013). Using these values and the abovementioned formula, the RTIMULib library employs the following formula to estimate height:

$$H = 44330.8 \cdot \left[1 - \left(\frac{p_b}{101.325} \right)^{0.190294} \right] \quad (26)$$

From these estimates, directly given in the RTMULib output, and adding GPS information[36] about horizontal displacement, the longitudinal slope can be estimated. However, since it is not an inclination or a rotation sensor in the strict sense, it is necessary to emphasize that this slope is not precisely equal to the vehicle pitch or the track slope.

In fact, the obtained inclination is the slope of the longitudinal trajectory of the sensor, which does not match the track slope or the car body pitch due to the relative longitudinal rotation between track and train cabin (suspensions effect). Although

[36] The noisy behaviour of GPS geometric height does not allow its use for this purpose, being used only the horizontal information. The smaller accuracy in altimetry than in horizontal coordinates from single-point positioning is expected for GPS and it was identified for the considered tests.

these differences due to the slight relative rotation, this sensor trajectory is mainly ruled by the track and allows for a better long-wavelength pitch estimation than that from the accelerometer, which is highly affected by vehicle accelerations. However, the main contribution of barometric altimetry is the description of the track profile, enabling map and feature matching and positioning improvement.

5.3 TESTS DESCRIPTION

The central aspect of the collective concept is the use of in-service vehicles. This conditions how the test should be carried out, preferentially using in-service trains or diagnostic trains that are physically similar to commercial trains regarding the number of coaches and yield dynamic and geometric data as ground truth for further analyses.

Considering these aspects, the following tests were carried out:

- Preliminary tests using smartphones on the Jade line of São Paulo's metropolitan railway network and the Figueira da Foz-Coimbra line of the Portuguese Railway Company.
- Two weeks of tests throughout the Italian high-speed network aboard two different RFI's track recording trains.
- Two round trips on Line C of the Rome Metro.
- A round trip aboard the CPTM's track recording vehicle on the CPTM's Line 7 (Jade, from Jundiaí to Luz Station)
- Three round trips on the CPTM's Line 7 (Jade, from Francisco Morato to Luz Station)

5.3.1 Preliminary tests

For a preliminary valuation of the limits of the individual use of accelerometer-grade

sensors, tests were performed on lines where variations in stiffness generate a perceptible difference in vibration in the train cabin. Unfortunately, it was not possible to obtain reference data on the track quality and perform analyses beyond the one related to this rail track parameter.

Therefore, the test was performed in the urban lines described as follows.

- Jade (13) line of São Paulo's metropolitan railway network (*Companhia Paulista de Trens Metropolitanos*, CPTM). The analysis focuses on the vibration distinction between the stretch in ballast (first 2.6 km from the *Engenheiro Goulart* initial station) and the track slab stretch, which is slightly perceptible by the passengers. The tests were performed on 14th April 2018 few days after its inauguration, considering six successive trips aboard the Electric Multiple Unit (EMU) 9000 series with eight coaches. For data collection, the *Lenovo* smartphone was positioned over the last bogie of the last car.

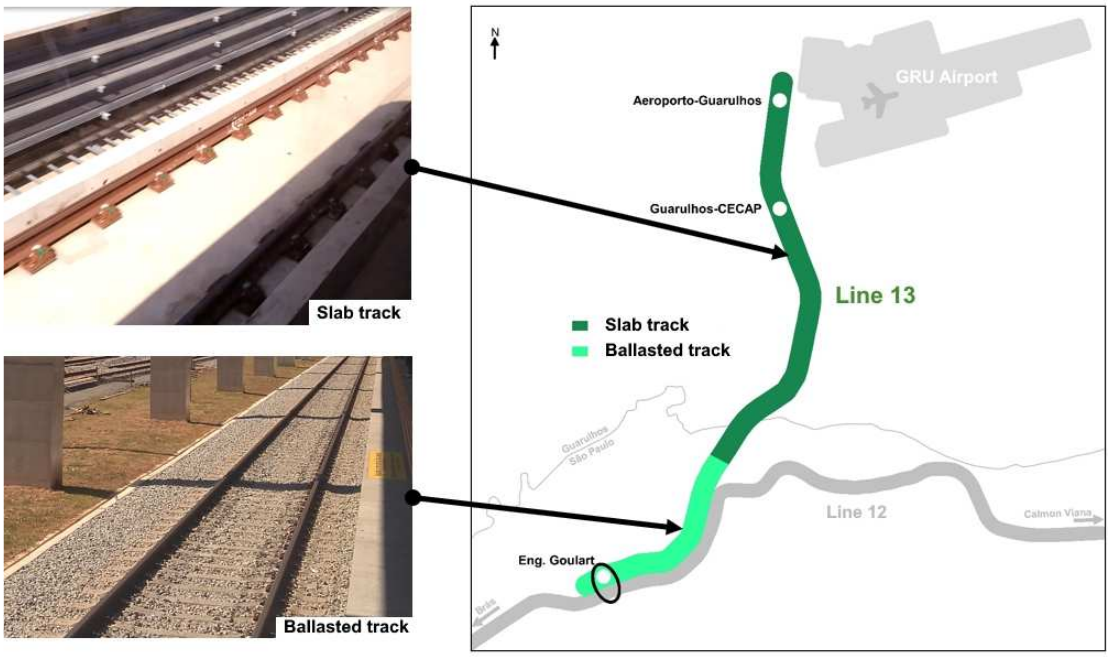

Figure 10 - Line 13 non-scale map (at right) and representation of its slab track (at left, top) and ballasted track (at left, bottom) sections

- Figueira da Foz-Coimbra line of the *Comboios de Portugal* (CP, literally Trains of Portugal), where a 550-metres length steel truss bridge (close to *Lares* bifurcation) yields a strongly perceptible vibration in relation to the rest of the line. The test was performed aboard the EMU 2240 series with three

coaches, and due to logistic restrictions, only one test trip was carried out. For data collection, the *Samsung* smartphone was positioned over the last bogie of the last car.

For vibration evaluation, the spectrogram analysis (by Short Term Fourier transform) of vertical acceleration as described in Section 4.2.6 is performed. Given the exploratory purpose of these trips and the fact that data gathering took place in a non-ideal situation, with the smartphone not attached to the vehicle body, the analysis will be limited to this basic evaluation of vibration level variation during the trips.

5.3.2 Tests on the high-speed lines of the *Rete Ferroviaria Italiana* (RFI)

Experimental tests for the collective use of the inertial sensors were performed during an inspection week onboard the diagnostic train ETR500Y2 (*Diamante*, Figure 11), owned by the Italian railway infrastructure manager (*Rete Ferroviaria Italiana, RFI*) and similar to the *Frecciarossa* trains (ETR500 model, second generation) used exclusively on the high-speed network. The subsequent sections describe this diagnostic train and the sensor distribution adopted for each test day.

5.3.2.1 The diagnostic trains *Diamante*

The *Diamante* train (an acronym for *Diagnostica e Manutenzione Tecnologica*) is composed of eight coaches, each with two bogies, and one locomotive at each extremity, carrying more than 200 onboard sensors for the inspection of track, energy system, signalling, telecommunication and ride dynamics) (ZUCCHI, 2013; MORETTI, 2017; MERMEC, 2020). The coach dedicated to the running dynamic characterisation has high-grade MEMS accelerometers on the axle box and the vehicle body to measure vertical and transversal dynamic quantities at 1 kHz. Moreover, laser-based systems are installed in another coach for track geometry recording. The *Diamante* train performs a 5-days inspection throughout the Italian

high-speed/high-capacity network every two weeks and can operate on the high-speed lines at speed up to 330 km/h (compatible with maximum commercial speeds). Position data is obtained from a Differential GPS receiver and an odometer. Regarding the *Diamante* trains, the odometer has spatial resolution of 0.5 m and measurement uncertainty (2 σ) of ± 2 m/km.

Figure 11 - External and internal view of the Diamante train.

Table 13 - ETR500 (second generation) main features (VANNI, 2011; MANJU, 2019)

Car body material	Aluminium alloy
Coach length	26,100 mm
Coach width	2,845 mm
Coach height	3,800 mm
Distance between bogies centres	19,000 mm
Maximum homologated speed	360 km/h (second generation)
Axle load	17 ton
Track gauge	1,435 mm (standard)

The track irregularity parameters surveyed by the inspection trains each 0.25 m are described in Table 14.

Table 14 - Track irregularity parameters surveyed by the inspection train ETR500Y2 and their features (ZUCCHI, 2013)

Parameter	Measurement technology	Chord length	Measurement resolution	Measurement uncertainty (2 σ)
Longitudinal level - right/left (range D1: 3-25 m)	Optical laser	23.220 m	0.5 mm	± 1 mm
Longitudinal level - right/left (range D2: 25-70 m)	Optical laser	23.220 m	0.5 mm	± 3 mm
Longitudinal level - right/left (range D3: 70-150 m)	Optical laser	23.220 m	0.5 mm	± 5 mm
Alignment - right/left (range D1: 25-70 m)	Optical laser	23.220 m	0.5 mm	± 1.5 mm
Alignment - right/left (range D2: 25-70 m)	Optical laser	23.220 m	0.5 mm	± 4 mm
Alignment - right/left (range D3: 70-200 m)	Optical laser	23.220 m	0.5 mm	± 10 mm
Twist	Optical laser + inertial platform	3.000 m and 9.000 m	0.5 mm	± 1.5 mm
Cross level	Inertial platform	-	1 mm	± 5 mm
Gauge	Optical laser	-	0.5 mm	± 1 mm

The track recording system also outputs the longitudinal level (LL) and alignment (A) on a 10-metres chord. Moreover, combinations and derived parameters are also calculated on board or offline and delivered by the RFI system, namely:

- LL and A standard deviations for D1 (combining right and left) within 200 metres sections.
- From raw cross level, the system also outputs the cross-level deviation within a 10-m window and the superelevation deviation (difference between design superelevation and cross level).

Moreover, the vehicle dynamic measurement unit aboard the *Treno Diamante* (at 1 khZ) obtains vertical and lateral accelerations on the bogie and in the car body for ride dynamics assessment and complementary analyses of long-wavelength track features (ZUCCHI, 2013). Table 15 presents the requirements for the accelerometers used in ride quality and stability monitoring by the Italian Railway Network manager. The accelerometers' position and identification are presented in Figure 12. In the identification code used in Figure 12, CR stands for *carrello* (Italian for bogie) and CS for *cassa* (Italian for car body). The position predicted by the RFI standard for the accelerometer installed in the car body is exactly over the bogie pivot.

Table 15 - Requirements for accelerometers used in the ride dynamic monitoring systems of the Italian Railway Network (RETE FERROVIARIA ITALIANA, 2018a)

Parameter	Range [g]	Sensitivity [mV/g]	Resolution [mg]	Precision [mg]	Sample rate [kHz]
Z acceleration wheelset	100	20	25	500	1
Z acceleration bogie	20	100	4	100	1
Z acceleration car body	2	1000	0.65	10	1

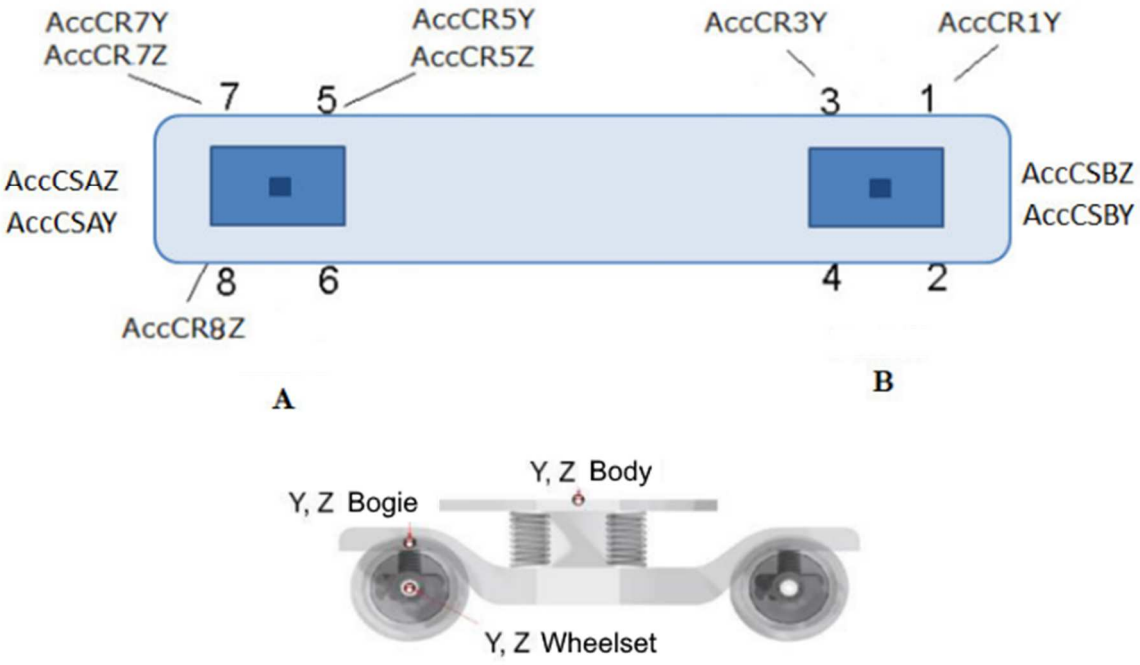

Figure 12 - Sensors' position in the dynamic monitoring coach (RETE FERROVIARIA ITALIANA, 2018b)

5.3.2.2 Test description

The tests throughout the Italian high-speed, high-capacity rail network (Figure 13) were performed from 14 to 17 January 2020 aboard the *Diamante* train. The tracks have international gauge (1435 mm) and are mainly designed (with exceptions) under international guidelines for high-speed lines: a minimum curve radius of 4000 m and a maximum slope of 1.25%. Owing to logistic restrictions, the tests were performed during the last four days of a 5-days inspection, which itineraries are presented in Table 16.

Figure 13 - Italian high-speed, high-capacity rail network, base map from OpenStreetMap (2023)

Table 16 - Itinerary of the experimental tests performed within the Diamante train through the Italian high-speed rail network

Test day	Origin	Intermediary stops	Destination	Approx. length (km)
#1	Naples	Rome > Florence > Bologna	Milan	800
#2	Milan	Turin > Brescia > Milan > Brescia	Vicenza	640
#3	Vicenza	Venice > Padua > Venice	Milan	410
#4	Milan	Bologna > Florence > Rome	Naples	800

The sensors were directly attached to the train floor with double-sided adhesive tape. The IMU x-axis was aligned to the vehicle's longitudinal axis, while the y-axis was aligned to the lateral axis and the z-axis to the vertical axis in the vehicle frame. Moreover, we adopted a different sensor distribution inside the train for each test day to enable analyses regarding the influence of the sensors' positions on measurements. These distributions (Figures 14 and 15) are described as follows:

- **Day #1.** The nine sensor sets were installed at the same approximate point. The sensors were attached to the car floor under the ninth right window in the eighth coach (right over the bogie), made available by RFI for our tests.

- **Day #2**. The nine sensors were distributed along the eighth coach under each of the ninth window. The distance between two consecutive sensors is about 2,1 m.

- **Day #3.** We installed a sensor in each coach at the same position: under the ninth right window in the given coach (right over the bogie). The distance between two consecutive sensors is equal to the coach length: 26,1 m.

- **Day #4.** The nine sensors were distributed along the same transversal section aligned with the ninth right window of the eighth coach. Since we needed to maintain a free corridor for the RFI staff, eight sensors were equally spaced along the right half of the transversal section, while the ninth sensor was installed at the left extremity of this section.

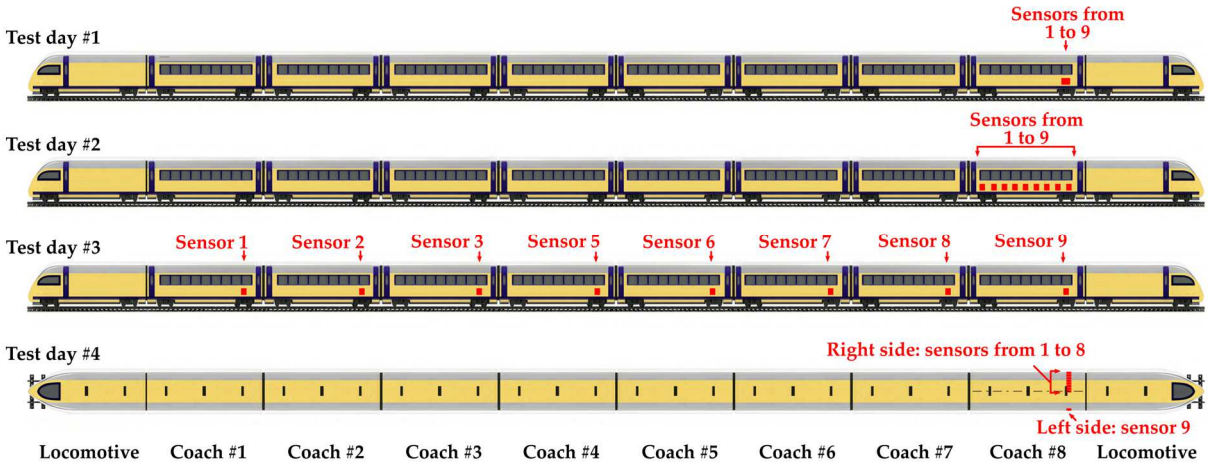

Figure 14 - Sensor distributions inside the *Diamante* train for the four test days.

Figure 15 - Sensor distributions inside the *Diamante* train for: (a) the first day; (b) the second day, and (c) the fourth day

Under the aforementioned acceleration model, the different arrangements adopted in the tests can be interpreted according to the following aspect:

Day #1: sensors yield similar data in terms of **g**, **c**, and **t** since they are approximately in the same position. There are differences among them in terms of **b** even after the calibration (eventual thermal, mechanical, and electrical variations among the sensors) and **μ** (stochastic nature of noise) (VECTORNAV, 2021).

Day #2: sensors yield similar data in terms of **g** and **c** (coach as a whole perceiving approximately the same pitch and roll angles and the same curvatures) and different data in terms of **b**, **μ**, and **t** (phase shifts and differences in amplitude due to distance to bogies centrelines). Differences also arise from speed variations, which results in bogies riding at different speeds over the same irregularity.

Day #3: At constant speed, sensors yield signals with similar shape in terms of **t**, with expected magnitude variations due to suspension parameters variation from one car to another and expected train set dynamics (higher vibration in the last cars). At varying speed, there are differences resulting from the difference in speed at which each coach travels over a given irregularity. The signals are similar in terms of **g** and **c**, with discrepancies in magnitude due to possible differences in roll and pitch coefficients. For these three components, there is a phase shift proportional to the

distance among sensors. Moreover, they produce different data in terms of **b** and **μ**.

Day #4: sensors yield similar data in terms of **g** and **c**, and different data in terms of **b** and **μ**. Regarding **t**, variation in transversal position results in major or minor influence of a specific track side.

Notably, bias can be reasonably handled as a constant within the eight selected intervals with slow variation during the trips. Thus, offset error can be estimated and corrected considering accelerometer readings during trip intervals in which the sensor is motionless and horizontal. Moreover, the offset is not critical for frequency-weighted accelerations since it is perceived as a long-wavelength feature outside the comfort frequency boundaries. Another negligible aspect is the sensor lateral distance to track centreline on curves, resulting in slight centrifugal accelerations discrepancy.

The results obtained using the consumer-grade sensors will be compared to reference data regarding dynamic and geometry measurements by *Treno Diamante* using reference position data (including time) for data matching, preferably using data collected concomitantly with the tests. The reference data availability is described in Table 17, considering the partial or total unavailability of concurrent data due to problems in the systems of the inspection train. Regarding the geometry parameters, the discrete standard deviation calculation (i.e., within fixed segments of equal length) of the track parameters is used in Italia, United Kingdom, Australia, and China (ZUCCHI, 2013; LIU et al., 2015; OFFENBACHER et al., 2020) as a track quality index.

Table 17 - Reference data availability for the Italian tests

Test day	Reference data		
	Geometry	Train position	Ride dynamics
#1	No, provided data is from another inspection week	No, provided data is from another inspection week	No, provided data is from another inspection week
#2	Yes	Yes	Yes, partially
#3	Yes	Yes	Yes, partially
#4	Yes	Yes	Yes, partially

A preliminary trip was carried out aboard the Aiace train, which is similar to Diamante in its track inspection features, from 17 to 20 December 2019 in order to understand the inspection routine and test data collection strategies. Due to issues with GPS

positioning for this dataset and a lack of concurrently collected reference data, the data collected on this preliminary trip will not be addressed.

5.3.3 Tests on Rome Metro Line C

Additionally, tests during two round trips on Rome Metro Line C (Figure 16) were performed using two pairs of sensors, each pair placed together on the train's floor (without adhesive) at each end of the train and on the same side. These trips were performed on 31 January 2020, between the *Giardinetti* and *Pantano* stations (surface stretch). This line has a driverless Automatic Train Control (ATC) system, which yields more consistent speed profiles between different traversals (a desired feature for repeatability analysis). The EMUs operating on this line have six cars with gangway connections, resulting in a total length of 109.4 m. The line has a gauge of 1435 mm and a maximum speed of 90 km/h. Table 18 presents the stations on the Line C surface stretch (ballasted stretch and partially underground between *Torre Angela* and *Torre Gaia* and between *Finocchio* and *Graniti*) and the approximate distance between them obtained from OSM data.

Figure 16 - Rome Metro Line C, base map from OpenStreetMap (2023)

Table 18 - Line C stations (surface stretch)

Station	Distance to next station (m)
Giardinetti	556
Torrenova	748
Torre Angela	815
Torre Gaia	959
Grotte Celoni	1089
Fontana Candida	706
Borghesiana	1186
Bolognetta	609
Finocchio	842
Graniti	742
Pantano	- (final station)

5.3.4 Tests on Line 7 of the CPTM network

Test abroad the CPTM's track recording vehicle and aboard an in-service train were performed on Line 7 (from Jundiaí to Luz Station, Figure 17) of the CPTM network, a 61 km double track railway line with 18 stations serving municipalities in the North-western of the Metropolitan Region of São Paulo Urban and the Jundiaí Urban Agglomeration. This line is a sub-service of the 7-10 Service, incorporating line 7 and line 10 (from Luz Station to Rio Grande da Serra Station). The following subsections describe the two tests carried out on this line: the first on board the track recording vehicle in a single round trip and the second on board a train in service.

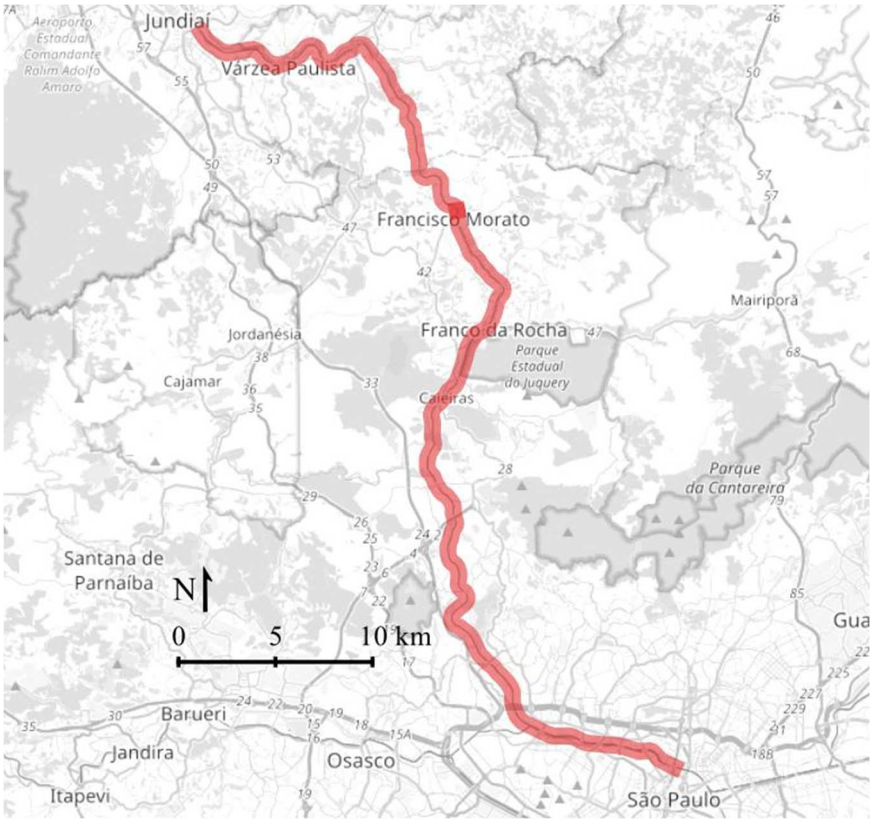

Figure 17 - CPTM Line 7, basemap from OpenStreetMap (2023)

5.3.4.1 Test aboard the track recording vehicle

The first test on CPTM's Line 7 was carried out aboard the track recording car EM100 Plasser & Theurer (Figure 18), in a complete round trip on 6 April 2022. This vehicle performs the track geometry and rail inspection by means of laser triangulation and gathers the following data each 0.25 m:

- Track geometry: longitudinal level (left and right, 10-m and 20-m chord), alignment (left and right, 10-m and 20-m chord), warp (20-m chord), twist (10-m chord), cross level, and gauge.
- Rail profile in accordance with UIC classification and rail wear.
- Position data: chainage, geographic coordinates, and line and track identification. The data is georeferenced through odometry and the manual identification of key milestones along the trip.

- Additional context data: speed, date, trip direction, TRV identification. The time at which each sample was taken is not recorded.

The inspection is performed concomitantly with video recording by a front camera. Another laser triangulation module is dedicated to catenary inspection but operates only at night due to solar radiation interference. The TRC also has an ultrasound measurement module for rail testing, which operates separately due to speed restrictions for the operation of this subsystem. The technical description of the EM100 is presented in Table 19.

Figure 18 - EM100U Plasser & Theurer (OLIVEIRA et al., 2022)

Table 19 - Plasser & Theurer EM100U technical characteristics (MONGIÒ, 2014)

Length	18,90 m
Width	4,13 m
Distance between bogies centres	12,00 m
Motor power	320 kW
Tare weight	58 t
Operation speed (laser triangulation for track geometry and rail wear inspection, video inspection, catenary inspection)	100 km/h
Operation speed (ultrasonic rail testing)	60 km/h

Ten sensor units were installed aboard the EM100U and distributed to enable the description of the difference between car centre and car extremities, as well as to offer redundancy at each of the three monitored sections (front, middle, and rear sections). The adopted orientation (left, right, front, rear) considers the train orientation, i.e., the main driver's cab being the front one. The distribution is depicted in Figure 19 and is described as follows:

- Sensors #1, #2, and #3 were installed in the rear driver’s cab (rear section), with #1 at the dashboard's centre and the other sensors at the extremities of

the dashboard.

- Sensors #6, #7, #8, and #9 were installed on a section near the car's central section (1.7 m from the actual centre owing to space unavailability inside the EM100U. Sensors #6 and #7 were installed on the right, while sensors #8 and #9 were installed on the left.

- Sensors #10, #11, and #13 were installed in the rear driver's cab (rear section), with #1 at the dashboard's centre and the other sensors at the extremities of the dashboard.

In all cases, the sensors were fixed to the car body (dashboard or floor) using double-sided tape.

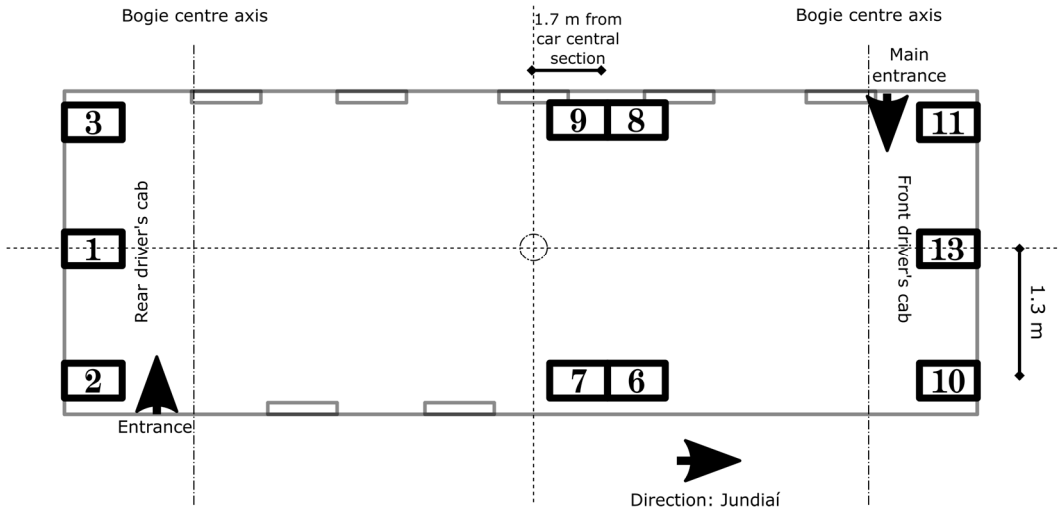

Figure 19 - Sensor distribution aboard the EM100U

5.3.4.2 Test aboard an in-service train

In addition, a complete operation day on 4 May 2022 was monitored by 10 sensor sets aboard an in-service TUE9500 passenger train (Figure 20) on the 7-10 CPTM service (from Jundiaí to Rio Grande da Serra, via Luz Station). Table 20 presents the itinerary of the considered day, which resulted in 3 complete traversals on Line 7. The repeated traversal enabled repeatability analysis and comparison with data gathered by the track recording vehicle. Additionally, the technical features of the TUE9500 train are presented in Table 21.

.

Figure 20 - Hyundai Rotem TUE9500 at left (BISSACOT, 2018) and sensors' installation at right (the author)

Table 20 - Itinerary during the test day aboard the CPTM TUE9500

Time	Station
04:30 (departure)	Lapa (yard)
04:40	Pirituba
From 05:10 to 07:50	Ipiranga
08:20	Mauá
From 09:10 to 10:20	Lapa (station)
10:57	Mauá
11:20	Rio Grande da Serra
11:50	Mauá
12:30	Lapa (station)
13:50	Jundiaí
15:00	Lapa (station)
15:50	Mauá
16:30	Lapa (station)
17:30	Francisco Morato
18:20	Lapa (station)
19:00	Mauá
19:40	Lapa (station)
21:00	Jundiaí
22:20 (arrival)	Lapa (yard)

Table 21 - CPTM TUE9500 main features (COMPANHIA PAULISTA DE TRENS METROPOLITANOS, 2013, 2016)

EMU length (8 coaches with gangway)	170 m
Coaches' length	21,700 mm (motor) 19,850 mm (trailer)
Width	3,050 mm
Height	4,545 mm
Maximum design speed	100 km/h
Acceleration	0.9 m/s²
Deceleration	1.1 m/s² (operational) 1.2 m/s² (emergency)
Track gauge	1,600 mm

The following sensors' arrangement (Figure 21) was implemented for the test aboard the in-service passenger train:

- Sensor #1 was installed in the front driver's cab (considering the Jundiaí direction as the main direction) at the dashboard centre.
- Each of sensors #2 and #3 was installed inside each of the rear electrical enclosures of coach #2, respectively, on the left enclosure and the right one.
- Each of sensors #6 and #7 was installed inside each of the rear electrical enclosures of coach #4, respectively, on the left enclosure and the right one).

The remaining sensors were installed to mirror the installation of the previous ones. Therefore, they were arranged as follows:

- Each of sensors #8 and #9 was installed inside each of the front electrical enclosures of coach #5, respectively, on the left enclosure and the right one).
- Each of sensors #10 and #11 was installed inside each of the front electrical enclosures of coach #7, respectively on the left enclosure and the right one).
- Sensor #13 was installed in the rear driver's cab at the dashboard centre.

Similar to the previous tests, the sensors were attached to the vehicle body using double-sided tape.

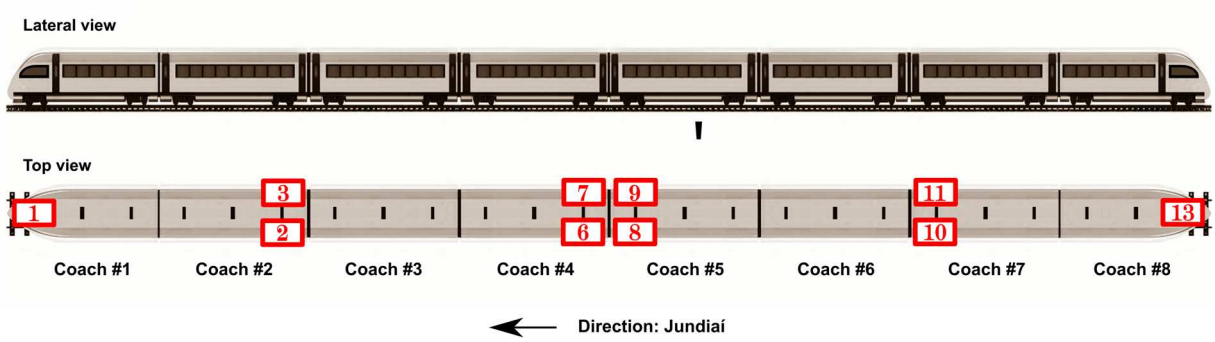

Figure 21 - Sensors' installation arrangement in the CPTM TUE9500

5.4 DATA PROCESSING AND ANALYSIS TECHNIQUES

The following sections describe the techniques used to extract comfort information from inertial data collected during the tests, as well as to assess the results in terms of conformity with reference data and repeatability.

5.4.1 Data pre-treatment

Firstly, for each sensor, GPS data (position, velocity, and time) were linearly interpolated at IMU update intervals (83^{-1} second) between two consecutive GPS updates (1 s interval), referencing data in time and space. The use of linear interpolation may introduce a position error when georeferencing IMU data since it considers constant speed between two GPS samples. For the worst case (i.e., maximum speed and maximum speed variation for the Italian High-speed train within the 1-second interval), the maximum error due to the interpolation is about 0.42 m, an order of magnitude below typical errors for GPS positioning. However, when available, the thesis will privilege the use of reference GPS data (from the inspection trains) and the correspondence with the IMU data through the GPS time.

Moreover, for a proper calculation of distances between sensors and between sensors' positions and the reference map (for map matching), the geographic coordinates from GPS solutions (latitude and longitude, WGS84 datum) were

transformed to Universal Transverse Mercator (UTM) projected coordinates (East and North coordinates, in metres).

5.4.2 Similarity metrics

The collective method imposes the need for carrying out similarity assessment in the following stages:

- Initial stage: identification of discrepant sensors. The acceleration signals will be compared in their longitudinal, lateral, and vertical components. Considering the particularities of rail transport, it will be determined which similarity metric and which axis are most suitable for the identification of the malfunctioning sensor.
- Intermediate stage: synchronization through the remotion of the time lag between signals (or space alignment removing the space shift), a critical aspect when calculating the mean signal from the individual signals (as described in section 5.4.3)
- Final stage: comparison between sensors' results, results validation (comparison with more accurate data and track quality features) and repeatability analyses (comparison between successive passages).

The following subsections describe the similarity metrics selected due to their prevalence of use in the literature and suitability for the proposed method.

5.4.2.1 Time-lagged cross-correlation

The time-shift correction and the similarity between two signals can be measured through time-lagged cross-correlation (FLINTSCH et al., 2012), also named cross-correlation in the context of signal processing (PENNY, 2000). The linear cross-correlation coefficient r between two signals x_i and y_i with N samples is a generalization of the Pearson's correlation coefficient considering lag between the

series and is defined as (KOHN, 2006):

$$r = \frac{\sum_1^N (x_i - \bar{x}).(y_{i+L} - \bar{y})}{\sqrt{\left[\sum_1^N (x_i - \bar{x})^2\right]\left[\sum_1^N (y_i - \bar{y})^2\right]}} \quad (27)$$

where $\bar{x}$ and $\bar{y}$ are the mean values of x and y, respectively, and L is the lag between the signals. The numerator is the cross-correlation function, while the denominator performs its normalisation by the standard deviation of both series. The Correlation coefficient is invariant to variables scaling and shifting.

Stationarity[37] and normality are conditions for the proper interpretation of the resulting correlation coefficient. However, moderate violations of such assumptions do not significantly affect the correlation coefficient. Besides this fact, the violations are less critical when the goal is to obtain a metric to describe the relationship between two variables (or, as in the present case, to describe the similarity between signals) instead of making statements regarding the statistical significance of the result (i.e., when statistically testing whether a particular correlation is non-zero) (HAVLICEK; PETERSON, 1976; HUNDLEBY; NUNNALLY, 1994).

The time-lagged cross-correlation is performed between pairs of individuals of the sensor population to enable two main activities: a) quantify the similarity between two signals and allow the exclusion of discrepant signals, and b) data alignment as a step for data fusion (analogue for spatial shift and alignment).

[37] A process is stationary “if the density functions describing the process are invariant under a translation of time” (BROWN; HWANG, 2012). In practical terms, a stationary process “has the property that the mean, variance and autocorrelation structure do not change over time” (NATIONAL INSTITUTE OF STANDARDS AND TECHNOLOGY, 2022).

5.4.2.2 Signal coherence

The signal coherence is a statistic that describes the relationship between two signals in the frequency domain (PENNY, 2000). The coherence between the signals x_i and y_i is a function of the frequency defined as:

$$C_{xy}(f) = \frac{\left|P_{xy}(f)\right|^2}{P_{xx}(f) \cdot P_{yy}(f)} \tag{28}$$

where $P_{xx}(f)$ and $P_{yy}(f)$ are the Power Spectral Density (Fourier transform of the auto-covariance function) for, respectively, the signals x and y, and $P_{xy}(f)$ is the Cross Spectral Density (Fourier transform of the cross-covariance function) between x and y. The coherence measures the linear correlation between the signals at each frequency and also requires normality and stationarity.

An important aspect regarding the collective approach is that the coherence is invariant to a constant time lag between the signals. Given these characteristics and the expected inertial sensor signals behaviour for the collective monitoring, the signal coherence is suitable for the identification of discrepant signals together with the coefficient correlation.

5.4.2.3 Consistency and total agreement coefficients

The previous similarity metrics are invariant to scale and systematic (bias) errors While the bias does not impact the results in terms of comfort analyses since the frequency-weighting eliminates the constant component of the signal, the scale problem may be relevant depending on calibration issues, sensor degradation, or differences in vibration magnitude between sensors.

Besides dimensional metrics such as the root-mean-square deviation, the mean squared deviation or the mean absolute error, there are also dimensionless metrics (similar to Pearson's coefficient) that describe the degree of conformity or complete agreement between two series of measurements. The intra-class correlation

coefficients (ICC) are descriptive statistics to measure the consistency or agreement between observers or measurements of the same quantity, being widely employed as a parameter to describe repeatability and reproducibility (HUNDLEBY; NUNNALLY, 1994; MCGRAW; WONG, 1996; WOLAK; FAIRBAIRN; PAULSEN, 2012). The ICCs can be interpreted as the proportion of the total variance attributable to the objects being measured in opposition to the variation among measurements. Unlike the Pearson coefficient, it ranges from 0 to 1. Different ICC estimators have been proposed within the analysis of variance (ANOVA) and random-effects model frameworks considering aspects such as the sources of variances, the use of single or average measurements, and whether the aim is to evaluate consistency or total agreement. For the present thesis, noninterchangeable measurements and two sources of systematic variance (two-way model) assumptions are adopted as suitable for assessing the reproducibility of measurements (NICKERSON, 1997).

In the ICC and ANOVA context, it is useful to interpret the measurements that will be compared in terms of rows and columns. Each column represents one of the series of measurements (two for the envisaged comparisons between signals or results), and each row represents an object of measurement (a time instant or a given track section). Thus, the metrics to evaluate consistency (i.e., agreement regardless of systematic error) and total agreement can be described in the two-way ANOVA framework as, respectively (MCGRAW; WONG, 1996; NICKERSON, 1997):

$$r_C = \frac{MSr - MSe}{MSr + (k+1)MSe} \tag{29}$$

$$r_A = \frac{MSr - MSe}{MSr + (k+1)MSe + \frac{k}{n}(MSc - MSe)} \tag{30}$$

where MSr is the mean square between rows (representing the variance of the row means around the total mean), MSc is the mean square between columns (representing the variance of the column means around the total mean), MSe is the mean square error (residual variance not attributable to row or columns effects), k is the number of columns, and n is the number of rows. While the consistency coefficient is sensitive to scale difference and insensitive to systematic errors, the total agreement coefficient is sensitive to both.

The comparison between Pearson's correlation coefficient and the ICCs can be summarised as follows[38]:

- Pearson's correlation coefficient describes the linear relationship between two variables x and y under the model $x = a + b \cdot y$. Therefore, it tolerates differences in mean (a) and scale (multiplicative factor b), being recommended when the variables do not have the same unit of measurement. Moreover, it is widely employed to describe similarity between signals regardless of bias (easily eliminated as a constant component) and scale issues (negligible for redundant sensors without calibration and degradation problems).

- The ICC for consistency describes the linear relationship between two variables x and y under the model $x = a + b$. Thus, it allows for differences in mean but not in scale. Therefore, it is a relevant indicator to verify possible differences in signal magnitude and the shape of the resulting RMS curves regardless of vertical shifts due to different noise levels.

- The ICC for total agreement describes the linear relationship between two variables x and y under the model $x = y$. Thus, it does not tolerate differences in mean and scale, being a more appropriate indicator for repeatability and reproducibility.

5.4.3 Data fusion algorithm

Data fusion is performed for the collective test to obtain a unique signal describing the vibration condition along a trip. Firstly, it is essential to emphasise that data fusion is preferentially performed within a homogeneous group of sensors, i.e., sensors under similar vibration patterns. Sensors installed in different longitudinal positions of a train may present differences in signal form (depending on the relative position to the bogie centre) and magnitude (mainly depending on the speed and the

[38] As can be inferred from the relative discussions of Lin's concordance coefficient (LIN, 1989), which is considered equivalent to the total agreement coefficient under the assumptions necessary for evaluating repeatability and reproducibility (NICKERSON, 1997).

suspensions' conditions), resulting in an inappropriate fused signal. Another issue is that these different sensors' composition should be performed in the space domain, which introduces the imprecision of the GPS position into the calculations.

Regarding the data fusion algorithm itself and considering multiple sensors operating simultaneously, the first data fusion algorithm step is the signals **resampling** to a common and equally spaced time vector. The second algorithm step is the **temporal alignment** of the signals, as described in the previous section. Both procedures can be performed in the spatial domain when considering sensors in different positions but under similar conditions in terms of speed, vehicle characteristics and position in relation to the bogie.

Finally, the last algorithm step is the **combination of the signals** by using the mean calculation. Since the N different signals were resampled and aligned to a common time vector, the mean signal is directly obtained by calculating the mean of the samples at each instant. This application is a specific case of **inverse-variance weighting** (AITKEN, 1935; DELLAERT, 2013)**,** i.e., the linear weighted average of multiple signals using the inverse of the variance as the weight. In other terms, the weights are proportional to the precision of each observation. This linear combination of observations is widely used in meta-analysis[39] and sensor fusion (DELLAERT, 2013). When fusing two Gaussian measurements, the inverse-variance weighting minimizes the variance of the resulting average, being an optimal estimator.

The multiple observation y_i are combined to give a combined estimate x through a weighted average with weights w_i (DEEKS; ALTMAN; BRADBURN, 2001):

$$x = \frac{\sum y_i . w_i}{\sum w_i} \tag{31}$$

In the case of combining multiple signals, y_i are the observation at the same time instant and x is the combined estimate for this time instant. In order to minimize the variance of the linearly combined estimate x, the weights w_i are the inverse of the squared standard errors (i.e., the inverse of the variances):

[39] Meta-analysis is a statistical process that involve the calculation of summary statistic for multiple studies (DEEKS; ALTMAN; BRADBURN, 2001)

$$w_i = \frac{1}{\sigma_i^2} \tag{32}$$

As the sensors are the same, with variations only depending on possible mismanufacturing and occasional problems in operation, a simplified and suitable approach is the use of the same weight ($w_i = 1$) when sensors operate as expected and a null weight (exclusion) in case of bad operation. Hence, for this thesis, simple average in used. However, it is important to know the algorithm in its generic and complete form since integration among different sensors (e.g., among different smartphones and among sensors of different quality grades) can be envisaged.

The resulting variance for the combined estimate is given in the Eq. (33) and is always smaller than the variance of any individual measurement[40]. In the case of measurement of equal standard deviation, it can be demonstrated from Eq. (33) that the resulting standard error is equal to the individual standard error (presumed equal for the N sensors) multiplied by $1/\sqrt{N}$, as also demonstrated by the Central Limit Theorem (CLT) regarding the theoretical decrease of noise (or variability of the mean) when averaging N independent measurements by a $1/\sqrt{N}$ factor (TITTERTON; WESTON, 2004; GUERRIER, 2008).

$$\sigma_{Total}^2 = \frac{1}{\sum \frac{1}{\sigma_i^2}} \tag{33}$$

5.4.4 Pitch and roll estimation for gravity compensation

In order to **compensate accelerations for gravity-related components**, roll and pitch estimates are required. The definition of these angles is a subproblem of the attitude determination (roll, pitch, and yaw) described in section 4.2.2.1. For this task, this thesis will consider two algorithms: a) the RTIMULib EKF native algorithm,

[40] In a Bayesian standpoint, the weight as the inverse of variance indicates the **information** a measurement carries. Thus, the information is additive since the resulting variance it the inverse of the sum of the weights (DELLAERT, 2013).

conceptually similar to those used on smartphones in terms of the use of accelerometer data; and b) a proposed gyroscope-based algorithm, which is free of the error introduced by the vehicle's longitudinal accelerations and the sustained (centripetal) lateral and vertical accelerations in curves. The main goal is to identify the actual impact on comfort assessments of the inaccuracy of vehicle inclination estimation when considering acceleration distortions. The hypothesis is that the imprecision due to these distortions does not substantially affect results regarding comfort and track irregularities characterization, enabling the use of the usual attitude algorithms.

5.4.4.1 RTIMULib EKF algorithm

The RTIMULib EKF algorithm is able to fuse data from a sensor set composed of triaxial inertial sensors (accelerometer and gyroscope) and triaxial magnetometer in order to describe the attitude in terms of quaternions. In this section, the most relevant aspects of the considered algorithm considered are presented (RICHARDS TECH, 2018):

- State initialization. The state vector, which includes the quaternions and the gyro bias (angular rate) estimates, is initialized considering prior knowledge. For the considered algorithm, it is set to null values.

- Prediction step: the gyro readings are integrated over time to compute the state transition matrix. A new state prediction is obtained using this matrix and the process noise covariance matrix, which express how accurate the model is.

- Update step: at this stage, measurements are obtained from accelerometers and magnetometers, and the measurement residual between the measured and the predicted state (previous step) is calculated. From this, the measurement noise covariance matrix and the Kalman gain for the measurement update, related to its uncertainty, are obtained. Finally, the state vector is updated using the Kalman gain and the measurement residual.

Regarding filter design, the values that initialize the covariance matrices for the process (Q matrix) and for the measurements (R matrix) control the influence, respectively, of the model (in this context, of

the gyroscope response) and of the measurements (estimations given by the accelerometer and magnetometer). For the RTIMULib, the Q initialization value is set to 0.001, while the R initialization value is 0.0005. These values implicitly define the contribution range of the gyroscope and the accelerometer-magnetometer set in attitude estimations. Using reverse calculation, it was estimated that the described configuration results in a higher contribution of the accelerometer-gyroscope set for information below about 0.2 Hz (long-term), while the gyroscope would mainly condition information above this threshold (short-term). This aspect is relevant to the proposed application since comfort and track irregularities are features analysed at frequencies near or above this threshold.

5.4.4.2 Proposed pitch and roll estimation algorithm

Even if the sensor fusion presented in the previous item results in smoothing of vehicle manoeuvring accelerations, the error introduced by sustained accelerations remains. In the railway domain this aspect is more critical considering lateral accelerations in curves. This work, then, proposes an alternative algorithm in order to deal with the sustained acceleration issue.

Since the present approach considers the collective use of sensors, this thesis proposes a simplified way to estimate angles considering the fused response of the sensor population. For roll angle, the first step is the numerical integration of the angular speed combination (mean signal) around the x-axis. This integration can be done for small inclination angles since the angular speed ω in the sensor frame is approximately equal to the angular speed in the navigation frame. The second step is the random-walk effect correction regarding track constraints: when travelling on a tangent, the roll angle must be about 0°. Under this concept, integration drift is estimated through the best-fitting line for considering only tangent sections and the

remotion of this value, enforcing an angle of about 0° on these sections. Thus, the i_{th} roll value (φ_i) at the instant t_i is given by:

$$\varphi_i = \varphi_{i-1} + \int_{t_{i-1}}^{t_i} \omega_X\,(t)dt\; - y(t_i) \tag{34}$$

where $\omega_X(\mathrm{t})$ is the angular speed around the x-axis and $y(\mathrm{t})$ is the best fitting linear function for tangent sections.

The proposed gyroscope-based calculation has limitations since modelling the random-walk by a best-fitting line is only feasible for short trip stretches. However, the strategy proved to be appropriate in providing reasonable values for the intervals in which the validation was carried out (up to about 80 km).

In turn, the slope pattern along a rail track does not allow the logic applied to the roll angle since there are no sections in which the slope angle is known to be constantly null. However, the barometer yields heights that can be used to estimate trajectory inclination, being necessary complementary information about travelled distance. Thus, pitch estimation is done through a complementary filter (alpha = 0.98) combining angular speed signals for high-frequency variations and inclination from combined barometer heights for low-frequency variations, once again using the mean signal from the sensor population. Barometric height is obtained from RTIMULib height output, which approximately follows the datasheet relationship of ± 0.12 hPa for ± 1 m and the conventional barometric formula considering a constant temperature. Variations in temperature impact absolute values but do not affect the height variations approximation. In the end, an additional correction step is necessary to identify and eliminate data linked to pressure transient (i.e., when crossing a tunnel), once again using track constraint: inclination derived from the barometer should not be greater than the maximum slope angle (about 1.1°). Thus, i_{th} pitch value (θ_i) is given by:

$$\theta_i = (1\; -\; 0.98).(gyr_i) + 0.98.\,(bar_i) =$$

$$(1\; -\; 0.98).\left(\theta_{i-1} + \int_{t_{i-1}}^{t_i} \omega_Y\,(t)dt\;\right) + 0.98.\left(atan\;\frac{h_i - h_{i-1}}{d_H}\right) \tag{35}$$

where gyr_i is the pitch estimation from angular speed $\omega_Y(\mathrm{t})$ and bar_i is the pitch estimation from barometric height variation $(h_i - h_{i-1})$ and horizontal distance d_H (the former obtained from GPS data). Thus, GPS influence is reduced to the travelled distance estimation. Moreover, it should be noted that unavailability intervals coincide with pressure transients intervals, in which barometric estimation is disregarded.

Alternatively, some algorithms aim to identify high dynamic intervals from accelerometer data in order to compensate for external acceleration (SABATINI, 2006; SUH et al., 2006; LEE; PARK; ROBINOVITCH, 2012; WIDODO; WADA, 2016; XING et al., 2016; JUSTA; ŠMÍDL; HAMÁČEK, 2020), usually defining thresholds for the exclusion of the accelerometer from estimations. However, as described in Xing et al. (2016), the threshold definition is problematic when using accelerometers with large random noise. Another possibility is using speed and bearing data from GPS to estimate and compensate for centripetal acceleration under an acceleration model-based approach (EUSTON et al., 2008; ROBERTS; TAYEBI, 2011; DE CELIS; CADARSO, 2018). At any rate, the influence of GNSS quality (sample rate, accuracy, and availability) on estimation is relevant, especially considering single point positioning. Considering the specificities of these alternatives and the limitation of the very low-cost sensors, the proposed accelerometer-free approach has proved to be sufficient for the proposed comparison.

5.4.5 Data analysis based on Short Term Fourier Transform (STFT)

The preliminary tests aimed only to assess the capability of mid-range smartphones in detecting variation in vibration patterns during a trip that is sensible by passengers. For the sake of simplicity for an initial data exploration and adequacy to evaluate a transient phenomenon in the frequency domain, the most suitable tool is the short-term Fourier transform.

For the preliminary tests, the spectrogram was yielded as the output of the STFT using a Tukey window (alpha = 0.5) and window length of 250 samples (about 2.5 seconds for a sample rate of about 100 Hz). This configuration yielded the best visual results and is coherent with those used in similar works. At any rate, slight parameter

variations are not critical since the goal is only a visual comparison between track stretches.

5.4.6 Data analysis based on ride comfort analyses in accordance with ISO 2631

ISO 2631 is used to analyse only the dataset gathered in the tests within the Italian Railway Manager, which has reference data for validation. Comfort indexes were already successfully used as indirect track quality figures in literature. Moreover, this analysis yields results with intrinsic meaning. In other words, an RMS acceleration does not have an intrinsic meaning, while a frequency-weighted RMS acceleration in accordance with ISO 2631 can be analysed in terms of expected comfort reactions.

Besides variations such as the British Standard 6841 (1984), which differs from ISO in the weighting curves, there are other methods for assessment of vibration comfort, such as those based on acceleration percentiles prescribed by the *Union internationale des chemins de fer* (UIC) and by the CEN (UIC 513 and EN 12299), as well as the Sperling's method (POLACH; BERG; IWNICKI, 2006; THOMPSON; JONES, 2006). ISO 2631 was chosen because it is the most widely accepted (especially ISO 2631-4 for the railway industry) and the most used in related works, allowing methodological comparisons.

This thesis analyses the comfort according to ISO 2631 using the weighting factors for **standing passengers** since the measurements were performed by attaching the sensors directly to the train floor. For eventual correlation with the comfort of seated passengers, corrections were to be made regarding the transmissibility of the material between the passenger and the rigid part of the vehicle (e.g., the cushioning material for seats).

For the present work, as an algorithm mathematically equivalent to recommended by ISO 2631 (as presented in section 3.1), the frequency weighting of acceleration spectra was performed through signal decomposing into each one-third octave band and the subsequent weighted sum of data of these bands, resulting in a weighted signal in the time domain (IRVINE, 2021; INTERNATIONAL ORGANIZATION FOR

STANDARDIZATION, 2005). Butterworth 6th order passband digital filters were applied under ISO 2631 specifications for signal decomposing with a forward and a backward pass to curb phase shift. In the end, the root-mean-square of the weighted accelerations is calculated within 200-m segments as the unit of analysis recommended by the European Standard and the Italian manuals (COMITÉ EUROPÉEN DE NORMALISATION, 2010a; ZUCCHI, 2013) regarding track quality description.

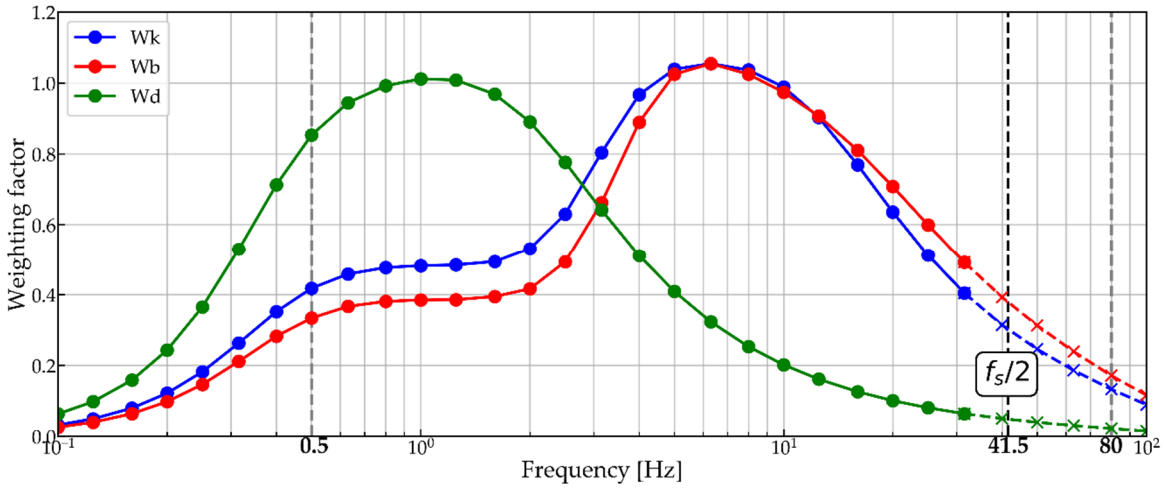

Figure 22 - Weighting factors versus central frequency of each one-third octave band

Given the sample rate during tests (around 83 Hz), close to the usual maximum frequency sampling for average smartphones, only 19 of the 23 one-third octave bands of interest (from 0.5 Hz to 80 Hz) can be analysed in light of the Nyquist theorem. However, the resulting inaccuracy is of a small magnitude. Figure 22 depicts the weighting curves and highlights the non-analysable bands with cross markers and dashed lines, which shows that humans are less sensitive to vibrations over 10 Hz. Moreover, the more remarkable frequencies for high-speed lines are usually under 20 Hz (KIM et al., 2009), related to the fact that passenger coach suspension aims to isolate the car body from frequencies above about 2 Hz (THOMPSON; JONES, 2006).

5.5 DATA PROCESSING TOOLS

The codes for all data processing were implemented on Jupyter Notebook, an

interactive interface for the composition, execution and dissimination of Python codes. In particular, the following Python libraries were used:

- Pandas: data manipulation and analysis, allowing importing data from formats such as comma-separated values and Microsoft Excel.
- Geopandas: geoprocessing capabilities to Pandas objects.
- SciPy: interpolation tools, Discrete Fourier Transform algorithms, signal processing tools, statistical functions.
- NumPy: arrays and matrices operations.
- Matplotlib: data plotting.
- Pingouin: statistical library specifically used for the ICC coefficients calculation.

5.6 CHAPTER FINAL CONSIDERATIONS

The aforementioned techniques and tools are organised in a collective monitoring method of ride comfort and, indirectly, railway track quality. The goal is to use data extracted from combinations of sensors to obtain more robust results than using individual sensors. Following the procedures summarised in Figure 23, the following groups of collective results will be obtained:

- Individual results for the N sensors. The contribution of the collective approach is the exclusion of discrepant signals at the initial stages.
- Result from the mean signal when sensors are redundant. This product of the collective concept can theoretically reduce noise without loss of information.
- Mean results from the N results. No noise reduction exists since noise is internalised in the RMS results as approximately a constant value (assuming that its spectral behaviour varies little over time). However, the mean result approximates that of an average sensor and its noise.

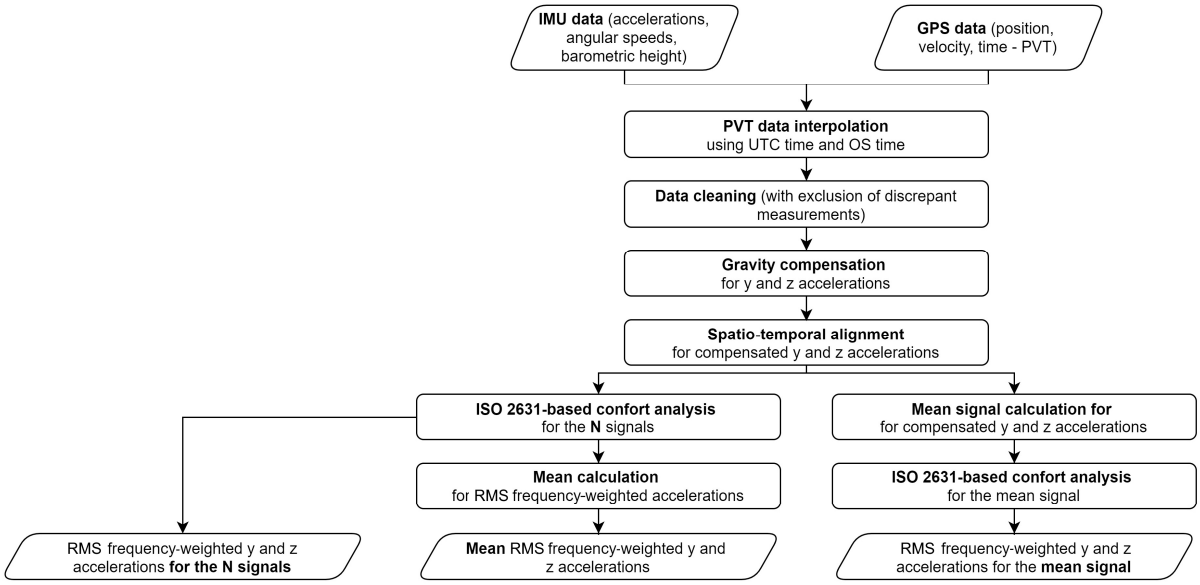

Figure 23 - Schematic flowchart of the procedure for the collective comfort monitoring

6 PRELIMINARY ANALYSES

This chapter describes the initial analyses seeking to establish basic concepts of the inertial sensors' behaviour and their relationship with the characterization of the vehicle's vibration and displacements. Firstly, the preliminary tests performed using medium-grade smartphones were described. Secondly, preliminary results of the collective tests are presented considering the description of raw accelerations, the similarity between acceleration signals, the identification of discrepant sensors, and the corrections for synchronisation errors.

6.1 PRELIMINARY TESTS USING SINGLE SMARTPHONE (CPTM AND CP)

The first dataset to be analysed is from the trip on the CPTM 13 Line. Six round trips were performed at a cruising speed of about 50 km/h during revenue operation. Since the main goal was solely the comparison in terms of vibration energy, no noise filter was applied before STFT calculations.

Figure 9 presents one of the spectrograms obtained for the transition zone, from ballasted track (left in the spectrogram) to slab track. During the trip, a passenger could sense a very slight difference in terms of vibration between both stretches. It should be emphasized that the difference is minor given that the track was newly opened, and the differential dynamic response mitigation is usually addressed in track design.

Although this vibration pattern, the spectrograms (Figure 24 being a representative example) did not reflect the slightly perceptible vibration variation. At the same time, a specially intense vibration for the instant 72 s was observed. However, this is not an observed tendency for the slab stretch for these tests.

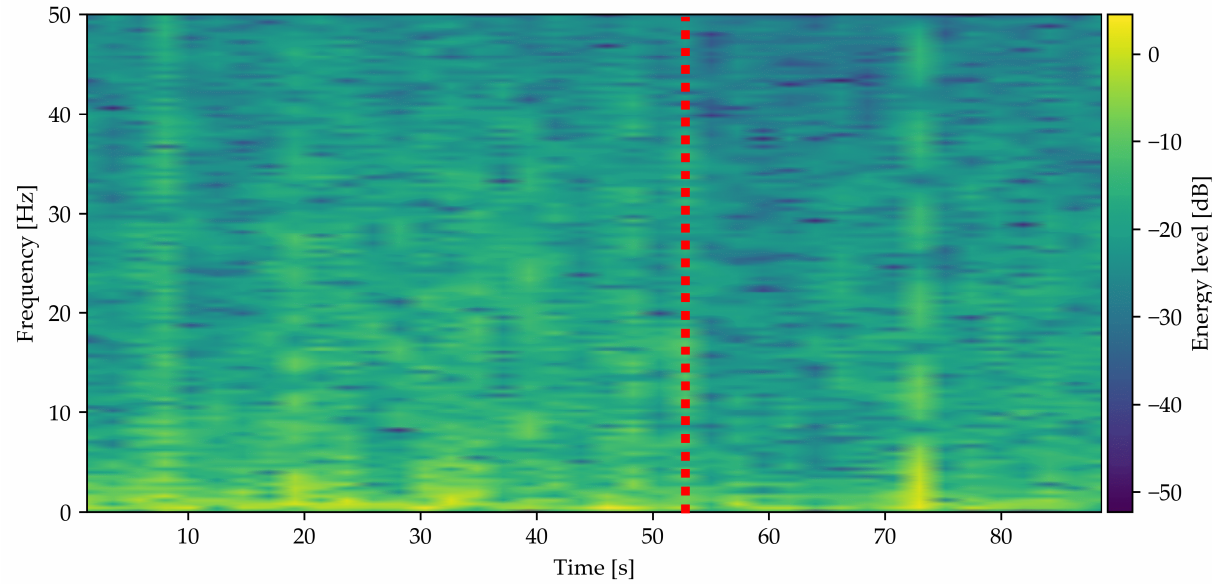

Figure 24 - Spectrogram for the test on Jade line of São Paulo's metropolitan railway network, raw vertical acceleration

For the test performed on the Figueira da Foz-Coimbra line at a cruising speed of about 34 km/h, the more significant difference in vibration resulted in a more clearly perceptible result in the spectrogram, as depicted in Figure 24. It is also remarkable that this variation (i.e., higher energy represented by the yellow tone) occurs mainly at frequencies below 10 Hz, expected for monitoring in the vehicle cabin.

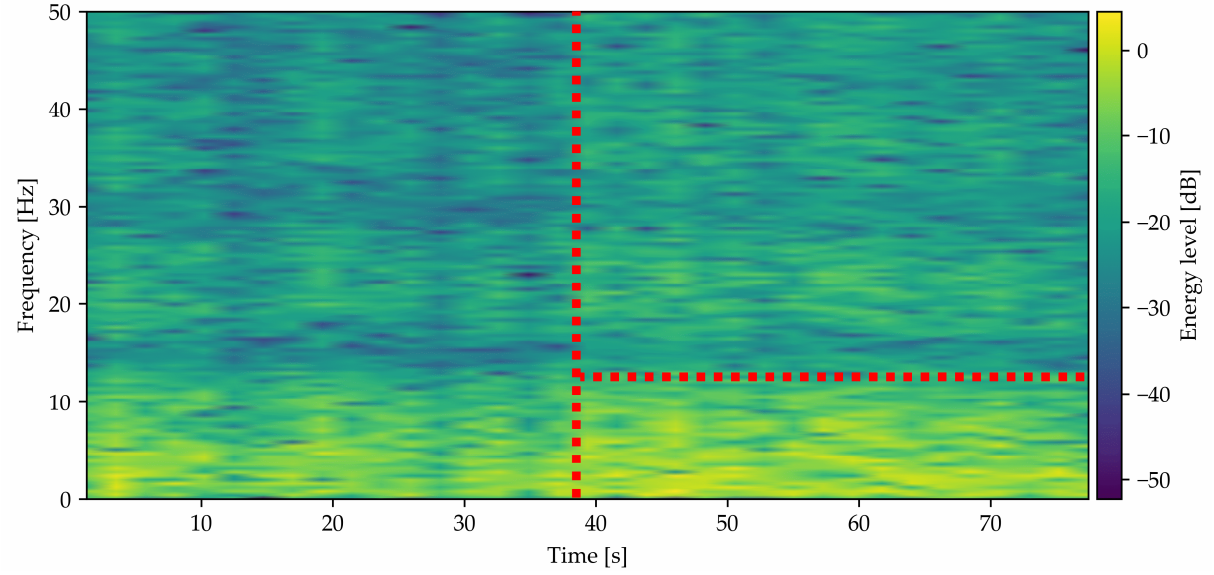

Figure 25 - Spectrogram for the test on Figueira da Foz-Coimbra line of the Portuguese Railway Company, raw vertical acceleration

The preliminary tests revealed the sensitivity of the very low-cost sensors installed in the train cabin for characterising prominent variations in the vibration pattern due to stiffness variations. Other relevant contribution is the identification of instabilities in

data recording when using data sampling greater than 100 Hz.

6.2 PRELIMINARY RESULTS OF ITALIAN TESTS

For the analyses, when necessary for reasons of efficiency of data handling and to attempt to eliminate the influence of speed variation on measurements, only trip intervals in which the trains travelled at a quasi-constant[41] speed are considered. Moreover, considering the problems with the GPS data for the first test week and the unavailability of GPS reference data gathered during these trips, only data gathered during the test week will be analysed. Table 22 shows the selected intervals for statistical comparison, also regarded as road sections in the space domain. In the *Train direction* column, F stands for *forwards*, while B stands for *backwards*. The speed values (average and standard deviation) consider the mean values for the sensor group in order to reduce noise influence.

Table 22 - Trip intervals/road stretches with quasi-constant speed for the Italian tests

Test day	Stretch ID[42]	Start time (s)	End time (s)	Length (m)	Average speed (m/s)	Std. deviation speed (m/s)	Approximate location	Train direction
#1	A	8400	8600	13260	66.3	0.7	Montepulciano	F
#1	B	13200	13500	20090	67.0	1.6	Modena	F
#2	A	4600	5250	53940	83.0	0.7	Novara	F
#2	B	18100	18380	15180	54.2	1.4	Milano	F
#3	A	6710	6940	13961	60.7	1.6	Padova	B
#3	B	23200	23430	10189	44.3	0.7	Soave	F
#4	A	9850	10050	10080	50.4	1.0	Parma	B
#4	B	23200	25300	139399	66.4	0.8	Arezzo	B

6.2.1 Description of the raw accelerations

Initially, Tables 23 to 25 present the descriptive statistics for the entire first test day (considering speed variations) as representative of the accelerometer population behaviour during the other tests. Complementary, Figure 26 presents the histogram

[41] The constant (or, being strict, quasi-constant) speed stretches defined in section 7.3.5 as those with a standard deviation in speed of less than approximately 1.6 m/s².

[42] Due to the availability of additional reference data, the constant speed stretches differ from that adopted in the paper presenting the thesis' preliminary results (DE OLIVEIRA et al., 2022).

of accelerations gathered by sensor 1 for the same test day as a representative of the sensor populations. To avoid distorting the parameters, only the intervals of trains in motion or in short stops were considered, excluding the interval for waiting to start work at the beginning of each day and the midday break. Additionally, the Augmented Dickey-Fuller test (ADF) (DICKEY, 2005) was applied for these trip intervals, and the hypothesis of non-stationary was rejected at a significance level of 0.1%, except for sensor 3 regarding vertical acceleration.

For the lateral and the vertical accelerations, the proximity between mean and median, the skewness close to zero and the kurtosis close to 3 are indications of distribution close to normal. On the other hand, the greater deviation from a normal distribution regarding longitudinal accelerations is an expected result given the predominant influence of train accelerations and the fact that they are concentrated in short intervals. In the other directions, macrogeometry (centripetal accelerations) and geometry irregularities prevail.

Table 23 - Descriptive statistics and test for stationarity for longitudinal accelerations, the first day of the test week on the Italian railway

Sensor	Mean [m/s²]	Median [m/s²]	Range [m/s²]	Standard deviation [m/s²]	Skewness	Kurtosis	Augmented Dickey-Fuller test for stationarity (statistic, p-value)
1	0.40	0.38	2.15	0.22	1.61	6.40	-18.1, p < .001
2	-0.12	-0.14	2.32	0.21	1.67	7.14	-6.7, p < .001
3	-0.03	-0.02	152.10	3.45	0.46	182.94	-23.4, p < .001
4	-29.12	-28.15	156.19	24.5	0.42	0.04	-66.6, p < .001
5	0.27	0.25	2.66	0.24	1.25	4.35	-15.7, p < .001
6	-0.02	-0.04	2.80	0.22	1.50	5.93	-10.7, p < .001
7	0.47	0.45	2.47	0.22	1.62	6.78	-6.7, p < .001
8	0.42	0.40	2.41	0.22	1.62	6.63	-8.0, p < .001
9	0.31	0.29	2.12	0.21	1.66	6.85	-8.0, p < .001

Table 24 - Descriptive statistics and test for stationarity for lateral accelerations, the first day of the test week on the Italian railway

Sensor	Mean [m/s²]	Median [m/s²]	Range [m/s²]	Standard deviation [m/s²]	Skewness	Kurtosis	Augmented Dickey-Fuller test for stationarity (statistic, p-value)
1	0.15	0.14	3.64	0.32	0.11	2.12	-11.5, p < .001
2	-0.22	-0.21	3.67	0.31	0.14	2.30	-14.8, p < .001
3	-1.11	0.81	156.42	23.94	-0.26	2.99	-7.6, p < .001
4	-22.24	-27.65	156.69	31.24	0.61	0.18	-17.1, p < .001
5	1.58	1.56	4.05	0.31	0.17	2.29	-16.4, p < .001
6	0.47	0.47	3.84	0.33	0.11	1.97	-15.2, p < .001
7	0.38	0.37	3.78	0.32	0.14	2.10	-15.8, p < .001
8	0.06	0.04	3.51	0.31	0.11	2.30	-19.6, p < .001
9	0.86	0.85	3.67	0.32	0.11	2.03	-13.1, p < .001

Table 25 - Descriptive statistics and test for stationarity for vertical accelerations, the first day of the test week on the Italian railway

Sensor	Mean [m/s²]	Median [m/s²]	Range [m/s²]	Standard deviation [m/s²]	Skewness	Kurtosis	Augmented Dickey-Fuller test for stationarity (statistic, p-value)
1	-9.58	-9.58	6.05	0.37	-0.05	2.40	-30.3, p < .001
2	-9.70	-9.69	4.55	0.28	-0.09	1.82	-31.7, p < .001
3	-2.55	-0.73	156.8	22.63	0.3	2.19	-2.7, p =.06
4	-18.84	-16.07	156.77	30.72	0.46	-0.03	-16.1, p < .001
5	-9.35	-9.35	4.45	0.26	-0.13	1.98	-24.6, p < .001
6	-9.78	-9.78	5.83	0.4	-0.04	1.26	-33.0, p < .001
7	-9.33	-9.33	9.22	0.41	-0.07	2.44	-30.6, p < .001
8	-9.57	-9.57	7.23	0.39	-0.03	2.07	-35.3, p < .001
9	-9.64	-9.64	5.99	0.33	-0.09	2.35	-32.7, p < .001

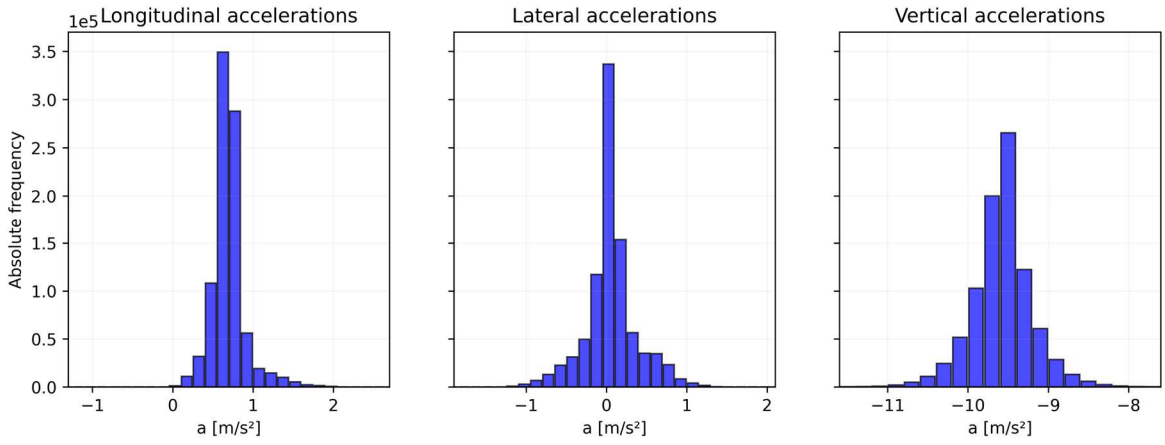

Figure 26 - Histograms of accelerations for sensor 1, first day of the test week

Figures 27 and 28 depict, respectively, time and frequency domain representations of the raw signals and the mean signal for the first day, stretch A. These graphs present

similar y-scale in time representation and FFT results to compare the magnitudes observed on the three axes. The first day was selected for this initial analysis because the sensors are theoretically redundant (under a similar solicitation), and the differences are due to noise and offset. For graphic clarity, offset elimination was done by forcing the response for each axis to be null (x and y axes) or equal to g (z-axis). However, offset is not critical for frequency-weighted accelerations since it is perceived as a long-wavelength feature outside the comfort frequency boundaries.

This example represents the raw output obtained in other stretches and its relationship with the mean signal, which presents a notably smaller variance in amplitude that is convergent with the expected noise reduction. For this stretch, variance in the z-axis ranges from 0.06 to 0.14 m/s² and has a mean equal to 0.11, while the mean signal variance is equal to 0.04 m/s² (reduction factor of about $1/\sqrt{N}$ with N = 7 sensors although not weighting the signals). The same reduction factor is identified for the x-axis, while for the y-axis, a smaller reduction factor is obtained due to the major influence on variance of the high magnitude accelerations in a curve.

The z-direction vibration is considerably more relevant than its orthogonal counterparts. Regarding y-direction acceleration, it is noteworthy that despite the long-wavelength behaviour that appears to follow the cant angle, the curves are not directly distinguishable owing to the speed influence on the magnitude of the non-compensated lateral acceleration. If the vehicle speed is close to the balance speed (i.e., the speed at which the lateral component of gravity exactly compensates the lateral component of centrifugal acceleration) on a given horizontal curve, the residual lateral acceleration will be close to zero and unusable for curve identification.

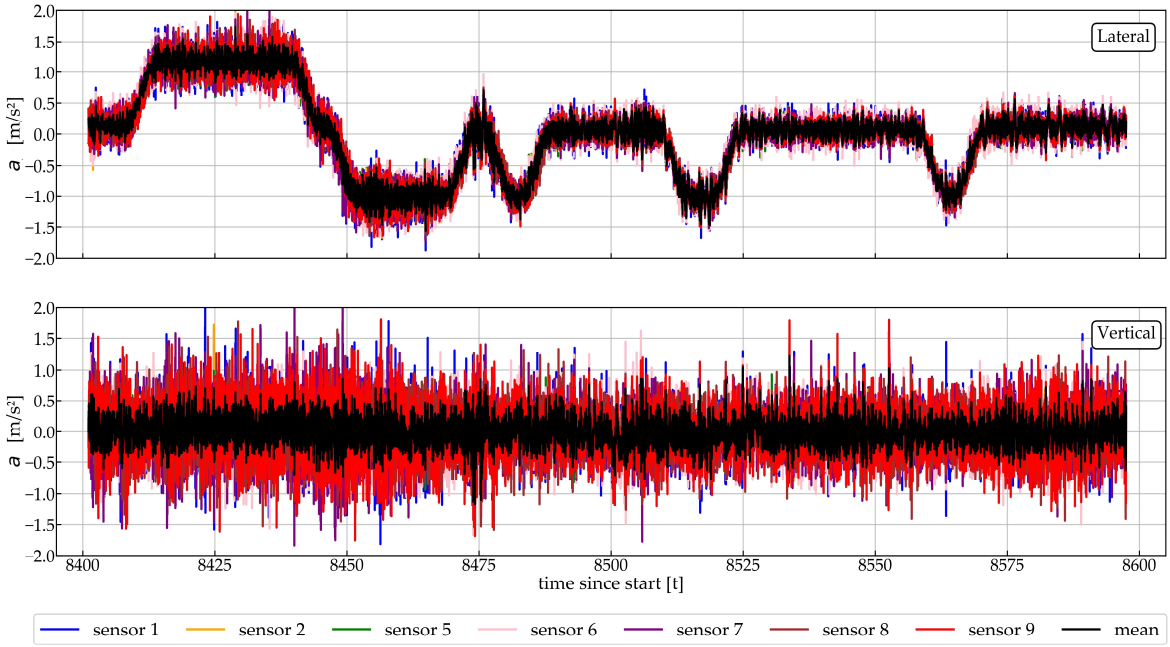

Figure 27 - Raw accelerations and mean accelerations for the Italian test week, the first day, stretch A

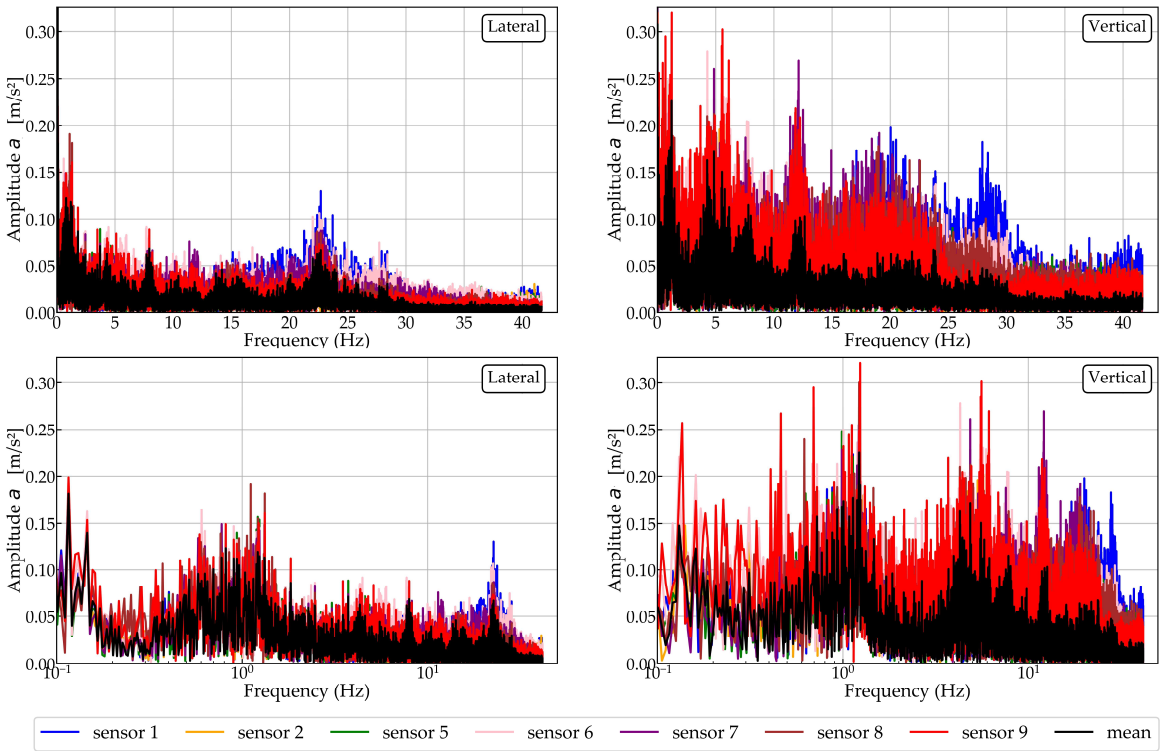

Figure 28 - Frequency content (FFT) of raw accelerations and mean accelerations for the Italian test week, first day, stretch A (linear scale at top, log scale at bottom)

6.2.2 Description and identification of discrepant measurements

The initial comparison (visual and using descriptive statistics) among responses for all test days of the test week showed an unexpected behaviour of sensors 3 and 4 for all days (sensor 4 was not installed for the third day) and sensor 1 for the second test day. This behaviour is not explicable by scale, offset, calibration issues, or installation errors since sensors were tested and calibrated immediately before the tests. Thus, the malfunctioning of the sensors has the following possible explanations:

- Hardware-related issues: failure due to mechanical shock, vibration, humidity and radiation effects, temperature changes, and electrostatic dischargers, added to possible failure tendency due to manufacturing problems (STARK, 1999).

- Software-related problems: stochastic problems in initialization or processing limitation issues, which result in temporary (changing during a test day or from a test day to another) malfunctioning.

Regarding these possible causes, the following discrepant behaviours are identified and classified by this thesis considering the preliminary analysis of data gathered during the Italian tests:

- **Sensor failure**: discrepant behaviour probably due to hardware-related issues resulting in eventual permanent sensor damage. The discrepant behaviour is usually characterized by almost always null outputs with occasional peaks regarding one or more inertial quantities, and unstable sample rate (rate of half or less of that selected, as verified for sensor 3 on day 3 of week 2). Correlation coefficients are close to zero.

- **Sensor medium-term discrepant behaviour** probably due to software-related issues such as sensor's initialization stochastic problems. It is characterized by the sensor malfunctioning (behaviour similar to sensor failure) from one test to another but returning to its expected state on the subsequent test. This behaviour was presented by sensor 1, which worked properly on all the test days on the Italian railway except on day 2 of week 2.

Also in this category are the variations in noise level from one test day to another, although with a reduced impact on the quality of the information gathered (e.g., sensor 9 on day 4 of week 2, with a noisier signal but still highly correlated with the other sensors)

- **Sensor short-term discrepant behaviour**, with temporary (intervals of seconds) malfunctioning characterised by abnormal peaks or, more frequently, null outputs. These momentary disturbances have a little or moderate impact on the correlation with the sensor population. For instance, the graph in Figure 29 shows sensor 8 malfunctioning during the 4th day of the test week on the Italian network, during the intervals delimited le black dashed vertical lines, in which the signal from sensor 8 is almost null, and it is not adherent to the other ones.

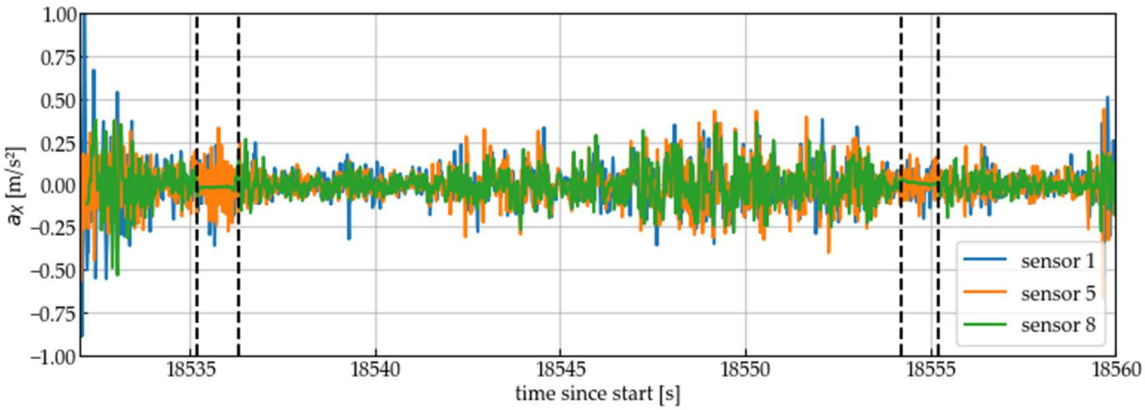

Figure 29 - Vertical acceleration during a sample interval of the 4th day of the test week on the Italian network as an example of temporary sensor malfunctioning

Besides the qualitative description of sensor discrepant behaviour, the proposed collective system requires the establishment of a procedure for sensor exclusion. Thus, similarity and agreement parameters were calculated for the raw accelerations and are presented in Tables 26 to 37. For the comparative parameters, each of the N sensors was compared to its N-1 peers, and the table shows only the extreme values (maximum or minimum depending on the parameter) and the median. Moreover, for the root-mean-square deviation (RMSD), Pearson's correlation coefficient and the total agreement coefficient, time lag was corrected using a window search of about 10 seconds. For the signal coherence, since each pair of signals results in a vector of correlations in function of frequency, the highest coefficient in the spectrum was selected.

Table 26 - Similarity analysis between sensors for longitudinal acceleration, the first day of the test week on the Italian railway

Sensor	Standard deviation [m/s²]	RMSD [m/s²] (min / median)	Pearson coefficient (max / median)	Consistency (max / median)	Total agreement (max / median)	Coherence (max / median)
1	0.20	0.18 / 0.4	0.82 / 0.7	0.82 / 0.7	0.66 / 0.27	0.52 / 0.42
2	0.19	0.13 / 0.54	0.89 / 0.8	0.89 / 0.8	0.78 / 0.18	0.84 / 0.66
3	18.77	18.79 / 18.82	0.06 / 0.06	0.0 / 0.0	0.0 / 0.0	0.0 / 0.0
4	22.91	23.09 / 23.26	0.02 / 0.01	0.0 / 0.0	0.0 / 0.0	0.0 / 0.0
5	0.21	0.22 / 0.3	0.83 / 0.72	0.82 / 0.72	0.57 / 0.42	0.69 / 0.49
6	0.19	0.13 / 0.44	0.89 / 0.78	0.89 / 0.78	0.79 / 0.24	0.77 / 0.54
7	0.21	0.18 / 0.35	0.81 / 0.7	0.8 / 0.7	0.66 / 0.36	0.83 / 0.64
8	0.31	0.35 / 0.53	0.56 / 0.5	0.5 / 0.47	0.36 / 0.19	0.65 / 0.49
9	0.29	0.26 / 0.42	0.58 / 0.52	0.53 / 0.49	0.48 / 0.27	0.45 / 0.41

Table 27 - Similarity analysis between sensors for lateral acceleration, the first day of the test week on the Italian railway

Sensor	Standard deviation [m/s²]	RMSD [m/s²] (min / median)	Pearson coefficient (max / median)	Consistency (max / median)	Total agreement (max / median)	Coherence (max / median)
1	0.31	0.22 / 0.61	0.83 / 0.74	0.83 / 0.74	0.75 / 0.29	0.44 / 0.34
2	0.3	0.18 / 0.56	0.85 / 0.83	0.85 / 0.83	0.83 / 0.33	0.77 / 0.55
3	21.81	21.83 / 21.86	0.0 / 0.0	0.0 / 0.0	0.0 / 0.0	0.0 / 0.0
4	32.07	37.56 / 38.02	0.04 / -0.02	0.0 / 0.0	0.0 / 0.0	0.0 / 0.0
5	0.29	0.63 / 1.14	0.86 / 0.75	0.86 / 0.75	0.27 / 0.11	0.69 / 0.44
6	0.31	0.18 / 0.56	0.86 / 0.74	0.86 / 0.74	0.83 / 0.32	0.67 / 0.42
7	0.31	0.22 / 0.6	0.85 / 0.76	0.85 / 0.76	0.75 / 0.3	0.77 / 0.5
8	0.51	0.55 / 0.98	0.51 / 0.49	0.44 / 0.42	0.33 / 0.13	0.64 / 0.4
9	0.35	0.28 / 0.63	0.72 / 0.70	0.71 / 0.70	0.66 / 0.28	0.45 / 0.35

Table 28 - Similarity analysis between sensors for vertical acceleration, the first day of the test week on the Italian railway

Sensor	Standard deviation [m/s²]	RMSD [m/s²] (min / median)	Pearson coefficient (max / median)	Consistency (max / median)	Total agreement (max / median)	Coherence (max / median)
1	0.31	0.44 / 0.79	0.25 / 0.16	0.24 / 0.16	0.14 / 0.05	0.4 / 0.28
2	0.23	0.34 / 0.64	0.50 / 0.25	0.5 / 0.24	0.34 / 0.12	0.74 / 0.51
3	18.17	18.73 / 18.89	0.06 / 0.0	0.0 / 0.0	0.04 / 0.0	0.0 / 0.0
4	31.22	32.75 / 32.98	0.06 / 0.02	0.0 / 0.0	0.04 / 0.0	0.0 / 0.0
5	0.22	0.41 / 0.56	0.50 / 0.25	0.5 / 0.22	0.23 / 0.09	0.7 / 0.44
6	0.33	0.34 / 0.66	0.38 / 0.17	0.35 / 0.17	0.34 / 0.12	0.66 / 0.42
7	0.36	0.69 / 1.01	0.35 / 0.18	0.32 / 0.18	0.12 / 0.05	0.74 / 0.49
8	0.54	0.56 / 0.7	0.21 / 0.15	0.16 / 0.13	0.15 / 0.08	0.61 / 0.39
9	0.39	0.41 / 0.69	0.25 / 0.17	0.22 / 0.17	0.21 / 0.08	0.4 / 0.32

Table 29 - Similarity analysis between sensors for longitudinal acceleration, the second day of the test week on the Italian railway

Sensor	Standard deviation [m/s²]	RMSD [m/s²] (min / median)	Pearson coefficient (max / median)	Consistency (max / median)	Total agreement (max / median)	Coherence (max / median)
1	8.61	9.43 / 9.68	0.12 / -0.01	0.12 / 0.0	0.11 / 0.0	0.07 / 0.03
2	0.24	0.24 / 0.67	0.71 / 0.49	0.69 / 0.48	0.55 / 0.1	0.55 / 0.36
3	8.59	11.7 / 12.1	0.12 / -0.01	0.12 / 0.0	0.11 / 0.0	0.0 / 0.0
4	32.84	34.66 / 36.02	0.02 / 0.01	0.0 / 0.0	0.0 / 0.0	0.0 / 0.0
5	0.22	0.24 / 0.45	0.77 / 0.53	0.77 / 0.51	0.53 / 0.16	0.58 / 0.23
6	0.21	0.24 / 0.52	0.85 / 0.59	0.85 / 0.56	0.55 / 0.15	0.58 / 0.31
7	0.28	0.25 / 0.52	0.61 / 0.49	0.58 / 0.48	0.51 / 0.13	0.47 / 0.35
8	0.20	0.25 / 0.63	0.85 / 0.61	0.85 / 0.58	0.53 / 0.1	0.42 / 0.23
9	0.11	0.24 / 0.45	0.65 / 0.62	0.63 / 0.59	0.1 / 0.03	0.22 / 0.13

Table 30 - Similarity analysis between sensors for lateral acceleration, the second day of the test week on the Italian railway

Sensor	Standard deviation [m/s²]	RMSD [m/s²] (min / median)	Pearson coefficient (max / median)	Consistency (max / median)	Total agreement (max / median)	Coherence (max / median)
1	3.29	4.76 / 5.78	0.11 / 0.03	0.02 / 0.01	0.01 / 0.0	0.19 / 0.06
2	0.25	0.2 / 1.34	0.83 / 0.67	0.83 / 0.66	0.72 / 0.05	0.59 / 0.29
3	5.75	5.76 / 5.95	0.02 / -0.02	0.02 / 0.0	0.01 / 0.0	0.0 / 0.0
4	33.79	36.0 / 36.44	0.13 / 0.02	NaN	0.0 / 0.0	0.0 / 0.0
5	0.3	0.26 / 1.5	0.74 / 0.62	0.72 / 0.62	0.6 / 0.04	0.71 / 0.18
6	0.24	0.2 / 1.21	0.86 / 0.74	0.85 / 0.72	0.72 / 0.07	0.72 / 0.42
7	0.67	0.67 / 1.34	0.36 / 0.31	0.22 / 0.21	0.2 / 0.06	0.48 / 0.32
8	0.27	0.27 / 1.54	0.79 / 0.62	0.79 / 0.62	0.57 / 0.04	0.56 / 0.32
9	0.25	0.25 / 1.38	0.86 / 0.68	0.85 / 0.67	0.62 / 0.05	0.57 / 0.27

Table 31 - Similarity analysis between sensors for vertical acceleration, the second day of the test week on the Italian railway

Sensor	Standard deviation [m/s²]	RMSD [m/s²] (min / median)	Pearson coefficient (max / median)	Consistency (max / median)	Total agreement (max / median)	Coherence (max / median)
1	8.4	11.11 / 13.56	0.02 / 0.01	0.0 / 0.0	0.01 / 0.0	0.12 / 0.02
2	0.26	0.34 / 0.61	0.17 / 0.05	0.16 / 0.05	0.04 / 0.01	0.16 / 0.06
3	6.69	9.94 / 10.19	0.0 / 0.0	0.0 / 0.0	0.01 / 0.0	0.0 / 0.0
4	33.79	33.81 / 33.86	0.0 / 0.0	0.0 / 0.0	0.0 / 0.0	0.0 / 0.0
5	0.29	0.38 / 0.78	0.32 / 0.17	0.3 / 0.16	0.09 / 0.0	0.33 / 0.0
6	0.27	0.37 / 0.6	0.32 / 0.08	0.3 / 0.08	0.1 / 0.01	0.37 / 0.09
7	0.36	0.65 / 0.9	0.35 / 0.07	0.35 / 0.07	0.03 / 0.01	0.29 / 0.16
8	0.26	0.3 / 0.62	0.31 / 0.05	0.31 / 0.05	0.15 / 0.03	0.6 / 0.17
9	0.20	0.3 / 0.59	0.30 / 0.07	0.30 / 0.07	0.15 / 0.02	0.59 / 0.16

Table 32 - Similarity analysis between sensors for longitudinal acceleration, the third day of the test week on the Italian railway

Sensor	Standard deviation [m/s²]	RMSD [m/s²] (max / median)	Pearson coefficient (max / median)	Consistency (max / median)	Total agreement (max / median)	Coherence (max / median)
1	0.18	0.07 / 0.42	0.95 / 0.93	0.95 / 0.93	0.93 / 0.26	0.66 / 0.35
2	0.18	0.11 / 0.51	0.93 / 0.93	0.93 / 0.93	0.83 / 0.19	0.66 / 0.48
3	25.78	25.94 / 26.0	0.04 / 0.03	0.0 / 0.0	0.0 / 0.0	0.0 / 0.0
4	-	-	-	-	-	-
5	0.18	0.07 / 0.42	0.96 / 0.93	0.96 / 0.93	0.93 / 0.27	0.79 / 0.56
6	0.18	0.11 / 0.42	0.96 / 0.94	0.96 / 0.94	0.83 / 0.26	0.82 / 0.62
7	0.18	0.19 / 0.26	0.96 / 0.93	0.96 / 0.93	0.65 / 0.47	0.82 / 0.68
8	0.17	0.42 / 0.67	0.95 / 0.94	0.95 / 0.94	0.25 / 0.12	0.82 / 0.62
9	0.18	0.1 / 0.42	0.95 / 0.92	0.95 / 0.92	0.85 / 0.25	0.81 / 0.48

Table 33 - Similarity analysis between sensors for lateral acceleration, the third day of the test week on the Italian railway

Sensor	Standard deviation [m/s²]	RMSD [m/s²] (max / median)	Pearson coefficient (max / median)	Consistency (max / median)	Total agreement (max / median)	Coherence (max / median)
1	0.18	0.18 / 0.69	0.87 / 0.69	0.87 / 0.66	0.59 / 0.11	0.28 / 0.07
2	0.18	0.14 / 0.69	0.87 / 0.72	0.87 / 0.7	0.73 / 0.11	0.28 / 0.08
3	24.27	26.14 / 26.36	0.01 / 0.00	0.0 / 0.0	0.0 / 0.0	0.0 / 0.0
4	-	-	-	-	-	-
5	0.18	0.42 / 1.08	0.87 / 0.80	0.87 / 0.79	0.23 / 0.04	0.24 / 0.12
6	0.19	0.11 / 0.75	0.87 / 0.77	0.87 / 0.77	0.84 / 0.09	0.24 / 0.1
7	0.2	0.21 / 0.57	0.85 / 0.75	0.85 / 0.75	0.58 / 0.15	0.2 / 0.14
8	0.19	0.11 / 0.76	0.85 / 0.80	0.85 / 0.8	0.84 / 0.11	0.2 / 0.12
9	0.21	0.18 / 0.7	0.85 / 0.70	0.85 / 0.69	0.61 / 0.11	0.18 / 0.06

Table 34 - Similarity analysis between sensors for vertical acceleration, the third day of the test week on the Italian railway

Sensor	Standard deviation [m/s²]	RMSD [m/s²] (max / median)	Pearson coefficient (max / median)	Consistency (max / median)	Total agreement (max / median)	Coherence (max / median)
1	0.16	0.3 / 0.48	0.34 / 0.13	0.32 / 0.11	0.15 / 0.01	0.31 / 0.06
2	0.17	0.22 / 0.35	0.02 / -0.03	0.0 / 0.0	0.0 / 0.02	0.32 / 0.03
3	25.7	26.78 / 26.99	0.02 / -0.01	0.0 / 0.0	0.0 / 0.0	0.0 / 0.0
4	-	-	-	-	-	-
5	0.15	0.2 / 0.3	0.34 / 0.11	0.31 / 0.11	0.15 / 0.02	0.17 / 0.03
6	0.15	0.3 / 0.46	0.15 / 0.06	0.11 / 0.08	0.03 / 0.01	0.15 / 0.08
7	0.19	0.56 / 0.86	0.11 / 0.07	0.08 / 0.06	0.01 / 0.01	0.11 / 0.06
8	0.13	0.2 / 0.37	0.19 / 0.09	0.18 / 0.09	0.15 / 0.03	0.13 / 0.08
9	0.14	0.2 / 0.3	0.20 / 0.08	0.20 / 0.08	0.11 / 0.03	0.13 / 0.05

Table 35 - Similarity analysis between sensors for longitudinal acceleration, the fourth day of the test week on the Italian railway

Sensor	Standard deviation [m/s²]	RMSD [m/s²] (min / median)	Pearson coefficient (max / median)	Consistency (max / median)	Total agreement (max / median)	Coherence (max / median)
1	0.18	0.1 / 0.42	0.93 / 0.87	0.93 / 0.86	0.86 / 0.27	0.89 / 0.56
2	0.19	0.07 / 0.53	0.94 / 0.91	0.94 / 0.91	0.93 / 0.2	0.89 / 0.63
3	8.46	8.46 / 8.47	0.02 / 0.01	0.0 / 0.0	0.0 / 0.0	0.0 / 0.0
4	12.65	12.86 / 12.94	0.03 / 0.01	0.0 / 0.0	0.0 / 0.0	0.0 / 0.0
5	0.22	0.13 / 0.5	0.92 / 0.85	0.92 / 0.85	0.83 / 0.24	0.65 / 0.55
6	0.20	0.07 / 0.5	0.94 / 0.88	0.94 / 0.88	0.93 / 0.24	0.89 / 0.6
7	0.21	0.1 / 0.4	0.94 / 0.87	0.94 / 0.87	0.86 / 0.32	0.83 / 0.56
8	0.19	0.42 / 0.59	0.91 / 0.87	0.91 / 0.87	0.28 / 0.15	0.43 / 0.27
9	0.21	0.14 / 0.42	0.88 / 0.85	0.87 / 0.85	0.79 / 0.28	0.34 / 0.31

Table 36 - Similarity analysis between sensors for lateral acceleration, the fourth day of the test week on the Italian railway

Sensor	Standard deviation [m/s²]	RMSD [m/s²] (min / median)	Pearson coefficient (max / median)	Consistency (max / median)	Total agreement (max / median)	Coherence (max / median)
1	0.25	0.12 / 0.5	0.92 / 0.90	0.92 / 0.91	0.9 / 0.32	0.84 / 0.64
2	0.25	0.08 / 0.5	0.95 / 0.90	0.95 / 0.90	0.95 / 0.34	0.93 / 0.7
3	7.46	7.46 / 7.47	0.02 / 0.01	0.0 / 0.0	0.01 / 0.0	0.0 / 0.0
4	11.24	11.35 / 11.47	0.02 / 0.01	0.0 / 0.0	0.01 / 0.0	0.0 / 0.0
5	0.25	0.5 / 0.79	0.95 / 0.89	0.95 / 0.89	0.33 / 0.18	0.88 / 0.7
6	0.25	0.3 / 0.5	0.95 / 0.91	0.95 / 0.91	0.56 / 0.33	0.93 / 0.73
7	0.26	0.08 / 0.5	0.95 / 0.90	0.95 / 0.90	0.95 / 0.33	0.82 / 0.68
8	0.26	0.3 / 0.77	0.89 / 0.89	0.89 / 0.89	0.56 / 0.16	0.62 / 0.49
9	0.28	0.16 / 0.51	0.87 / 0.84	0.87 / 0.84	0.81 / 0.32	0.66 / 0.57

Table 37 - Similarity analysis between sensors for vertical acceleration, the fourth day of the test week on the Italian railway

Sensor	Standard deviation [m/s²]	RMSD [m/s²] (min / median)	Pearson coefficient (max / median)	Consistency (max / median)	Total agreement (max / median)	Coherence (max / median)
1	0.25	0.32 / 0.63	0.46 / 0.35	0.45 / 0.34	0.34 / 0.1	0.79 / 0.57
2	0.18	0.22 / 0.42	0.52 / 0.32	0.52 / 0.32	0.3 / 0.16	0.87 / 0.63
3	10.55	13.06 / 13.34	0.2 / 0.09	0.01 / 0.0	0.01 / 0.0	0.0 / 0.0
4	11.76	13.96 / 14.18	0.0 / -0.01	0.01 / 0.0	0.0 / -0.0	0.0 / 0.0
5	0.24	0.3 / 0.46	0.57 / 0.44	0.56 / 0.42	0.34 / 0.18	0.9 / 0.57
6	0.19	0.37 / 0.55	0.57 / 0.46	0.56 / 0.45	0.21 / 0.12	0.9 / 0.71
7	0.2	0.55 / 0.98	0.53 / 0.44	0.53 / 0.43	0.12 / 0.03	0.8 / 0.67
8	0.19	0.22 / 0.43	0.36 / 0.31	0.35 / 0.31	0.3 / 0.14	0.55 / 0.5
9	0.26	0.27 / 0.46	0.35 / 0.30	0.34 / 0.30	0.28 / 0.15	0.66 / 0.52

Compared to the RMSD, the Pearson coefficient has the advantage of being dimensionless, allowing the definition of a common limit value for both longitudinal and lateral. Regarding the total agreement, it is noted that the penalisation for small variations in scale and bias is high and inhibits its use in axes whose vibration magnitude of vibrations is low (e.g., longitudinal axis, sensor 8 on day 4). The signal coherence, in turn, penalises considerably small variations in the noise level, which is not the case with the Pearson coefficient (e.g., longitudinal axis, sensors 8 and 9 on day 4). These penalised sensors have a very similar shape to the others, as demonstrated by the elevated Pearson coefficient and, as will be seen in the following chapter, by results that adhere to the reference data. From this finding, it can be concluded that Pearson's correlation coefficient is the most appropriate option for discrepancies identification.

Comparing the orthogonal axes, the predominance of the non-compensated accelerations on the lateral axis and the prevalence of the vehicle accelerations on the longitudinal one results in elevated Pearson’s correlation coefficient even when the sensors are in different positions. On the other hand, the vertical axis accelerations are predominantly due to track irregularities, and the magnitude variation due to speed variation drastically decreases the correlation between sensors placed in different positions. Thus, the correlation analysis should preferably be carried out on the lateral and longitudinal axes according to the following procedure for sensor exclusion:

1. Data cleaning and preparation for **longitudinal or lateral raw accelerations**: a) exclusion of initial and final intervals; and b) resampling to a common frequency.

2. Pearson correlation coefficient is calculated for each pair of signals for longitudinal and lateral, and the median correlation coefficient of each sensor is obtained. Those with a low median correlation value (< 0.45 for the present dataset) are excluded from further calculations.

This thesis will compare two approaches for identification and exclusion of discrepant sensors: a) **total exclusion** for a given trip, adopting the aforementioned procedure for the whole trip; and b) **windowed exclusion**, in which the aforementioned identification is carried out within a 5-second window (length conditioned by the

typical intervals of temporary sensor malfunctioning for the considered dataset) and the discrepant sensors are excluded only for this 5-seconds interval.

Regarding the identification of redundant sensors, Pearson's correlation coefficients are strongly affected in the arrangements for days 2 and 3 concerning vertical accelerations, where the sensors are not in the same section of the train and, thus, are not redundant. This is an expected result of the difference in the shape of the signals, and not just the magnitude, when distributed over the train. Further analysis of this aspect will be carried out in the following chapter.

Finally, it is emphasised that the described behaviour for the raw acceleration is similar for analysing the angular rates. Moreover, although the identification of discrepant sensors occurs regarding the accelerations, the other outputs of the IMU (angular rate, temperature, and pressure) also presented discrepant values and the acceleration values are used in this process as they have a clearer interpretation in the light of the models used in this thesis.

6.2.3 Synchronization correction

Initially, Figure 30 presents graphically the impact of time lag on the cross-correlation algorithm when analysing two raw signals of an entire trip (results from the previous section) or only constant speed stretches (stretch A for each day) considering a given pair of sensors. When the sensors are in the same position, time shifts between signals have a similar value due to non-synchronisation during the entire trip and impact the correlation coefficients (reduction from 0.5 to 0 for vertical acceleration with a 0.4 s shift) greatly, emphasizing the relevance of the synchronization correction through this method.

For the other arrangements, as the speed variations affect both the time-lag and the signal form, the calculated for an entire journey has an average meaning as the influence of velocity (speed and direction) variations and synchronization error. As the signal shape is also greatly impacted by the speed variation, the resulting correlation coefficient is almost the same low value regardless of time shift. However, when considering constant speeds, signals are more similar to each other, and the

time shift correction due to both synchronization error and difference in position increases the coefficient.

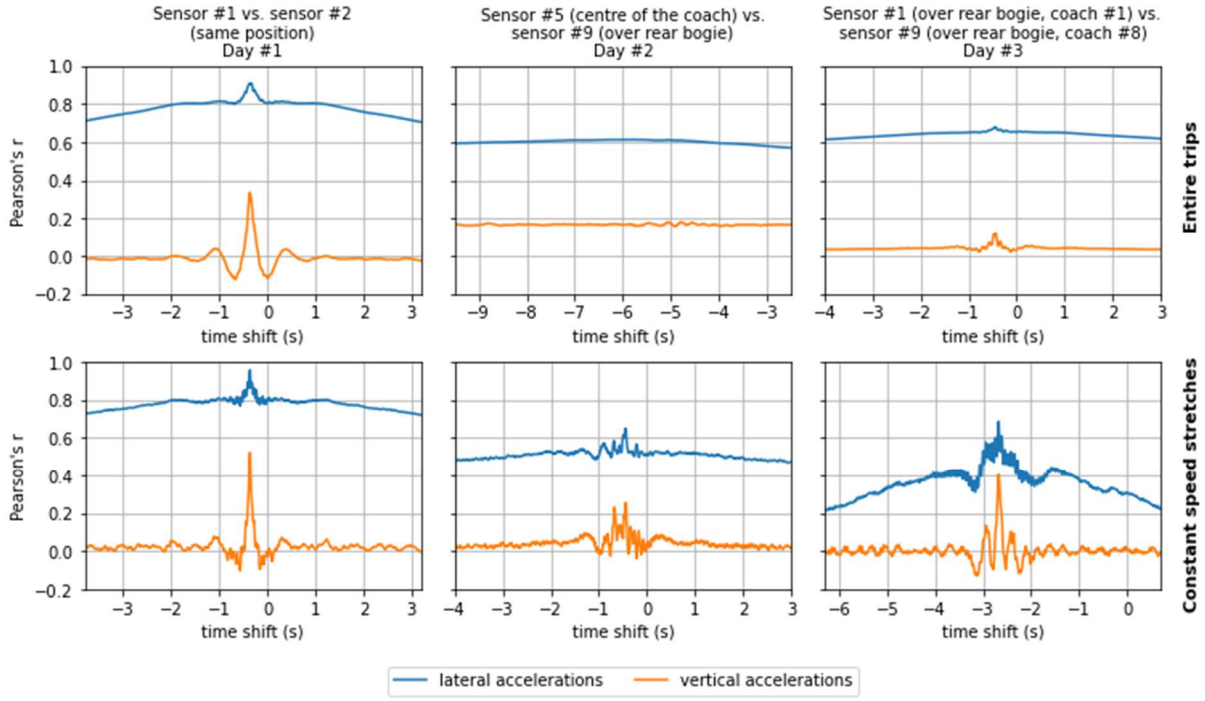

Figure 30 - Impact of the time-lag on the Pearson's r for entire trips (top) and constant speed stretches (bottom)

For the statistical analysis of the synchronisation errors calculated for all sensors in all arrangements, the present section will consider only the stretches of constant speed presented in Table 22. Initially, Figures 31 to 33 present the comparative graphs for longitudinal, lateral, and vertical accelerations for the eight selected stretches to illustrate the time shift between signals before time correction. The same scale in both axes is used for the twenty-four graphs to enable magnitude comparison. To reduce noise[43] and facilitate visual comparisons, the graphs consider accelerations after moving average filtering with 140 samples window.

[43] The noise would not affect the time lag (BROOKS, 2015).

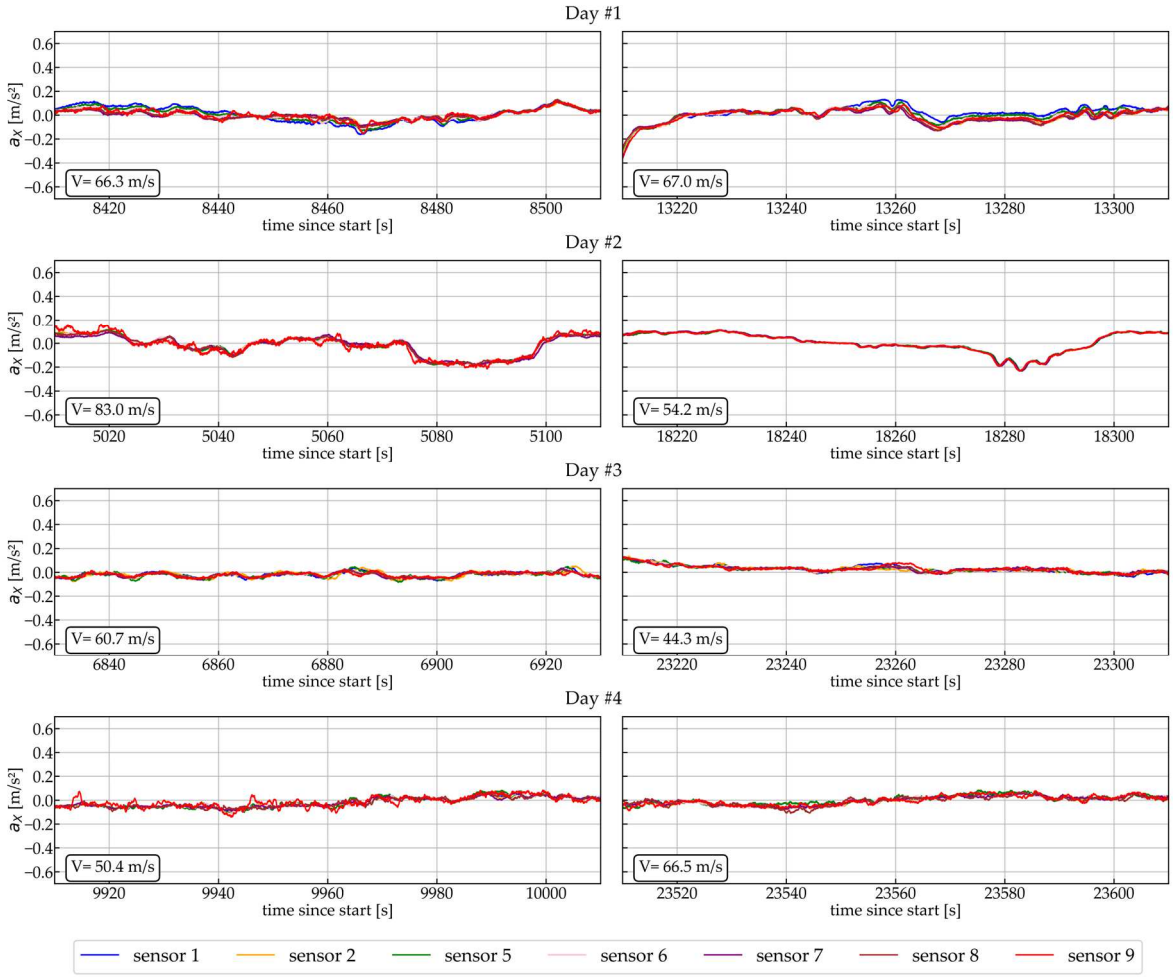

Figure 31 - Moving average filtered longitudinal acceleration comparison, excerpts from the eight constant speed stretches

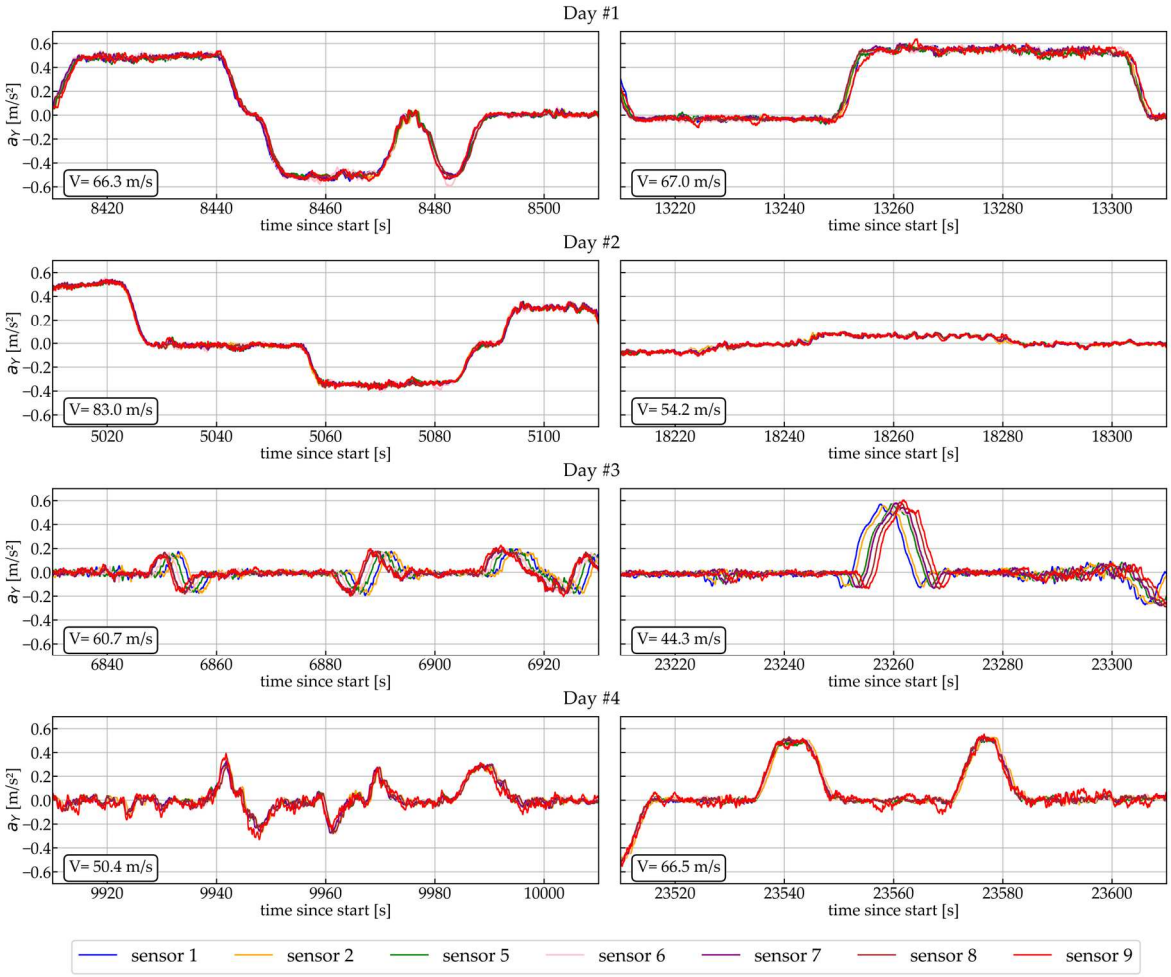

Figure 32 - Moving average filtered lateral acceleration comparison, excerpts from the eight constant speed stretches

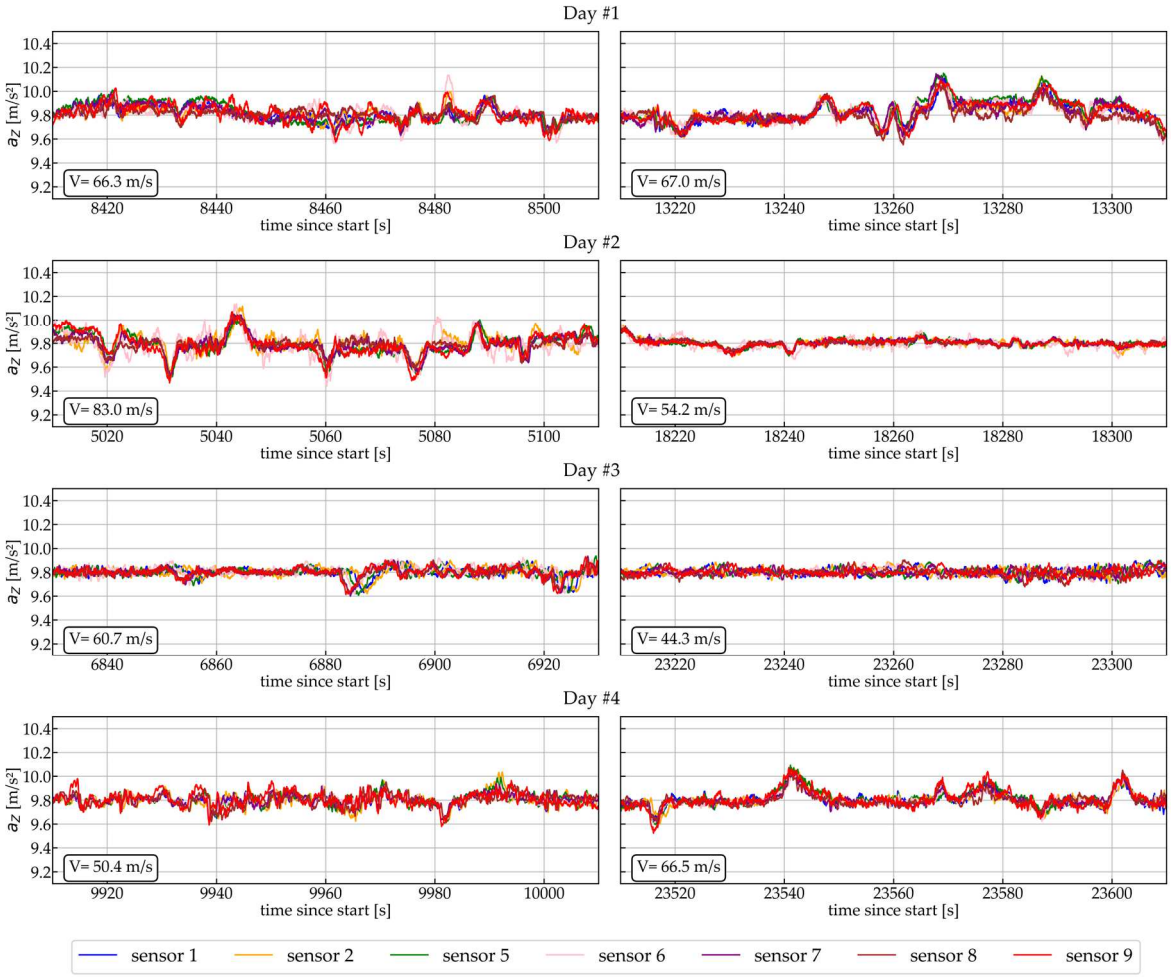

Figure 33 - Moving average filtered vertical acceleration comparison, excerpts for the eight constant speed stretches

For the sake of brevity, the statistical summary for the time shifts obtained from the time-lagged cross-correlation algorithm is presented in Tables 38 to 40 as a product of the synchronisation error and the phase difference between the sensors due to the possible time-differential response to a specific track feature. This result enables comparisons of lag distribution between axes, between days, and between stretches of the same day.

Table 38 - Statistical summary of the time lags for the longitudinal direction

Day	Stretch	Maximum	Minimum	Median	Mean	Std. Dev.
Day 1	A	0.649	-1.092	0.420	0.425	0.490
	B	0.733	-0.912	0.516	0.473	0.471
Day 2	A	0.432	-0.144	0.348	0.449	0.165
	B	0.384	-0.072	0.168	0.204	0.132
Day 3	A	1.477	-1.163	0.372	0.368	0.718
	B	0.637	-1.116	0.168	0.186	0.482
Day 4	A	0.948	-0.984	0.552	0.548	0.577
	B	1.129	-0.624	0.444	0.566	0.524

Table 39 - Statistical summary of the time lags for the lateral direction

Day	Stretch	Maximum	Minimum	Median	Mean	Std. Dev.
Day 1	A	0.817	-0.900	0.348	0.421	0.483
	B	0.841	-0.924	0.516	0.481	0.491
Day 2	A	0.252	-0.072	0.384	0.425	0.089
	B	0.288	-0.108	0.120	0.121	0.127
Day 3	A	3.216	-0.588	1.898	1.932	1.157
	B	-0.132	-4.706	0.108	0.126	1.208
Day 4	A	0.960	-0.972	0.624	0.598	0.565
	B	1.381	-0.624	1.525	1.543	0.572

Table 40 - Statistical summary of the time lags for the vertical direction

Day	Stretch	Maximum	Minimum	Median	Mean	Std. Dev.
Day 1	A	0.829	-0.900	0.312	0.420	0.486
	B	0.853	-0.948	0.516	0.472	0.499
Day 2	A	0.312	-0.108	0.372	0.424	0.107
	B	0.384	-0.084	0.156	0.154	0.140
Day 3	A	3.204	-0.600	1.874	1.936	1.151
	B	-0.132	-4.706	0.144	0.145	1.202
Day 4	A	0.948	-0.984	0.600	0.582	0.566
	B	1.297	-0.600	1.525	1.535	0.558

For the first and fourth days, time lags for x, y and z directions are entirely due to synchronisation errors. Differences between axes are reduced and probably due to variations internal to the devices derived from possible latency between IMU and GPS ruled by the Raspberry processing limitations, other IMU-related latencies, or eventual delay in IMU response depending on the axis. At the same time, differences

between stretches of the same day are due to time deviations of each sensor during the operation. Therefore, it is recommended to apply the correction for sub-stretches of well-defined dynamic contours (e.g. between stops at stations) rather than performing a single correction for the entire trip. Regardless of the magnitude of these differences in time shift, it must be emphasised that the proposed correction process through time-lagged cross-correlation is applied precisely to eliminate them, using the signal set itself and the features it represents as inertial markers of synchronization.

The time shift behaviour for the days with sensor distribution along the train (days 2 and 3) requires closer scrutiny with regard to the acceleration model. For the second day (sensors distributed in the same coach), the time lag for the x-axis is also ruled for synchronisation errors. However, the time shift for the y-axis combines the effects of lateral irregularity (with phase shift due to distance to one of the bogies) and the track curvature (with no phase shift).

For the third day, x-axis time lag, there is the additional small influence of gravity-related components due to pitch angle, as well as the slight influence of force transmission along the train set from one coach to another (compression and traction forces), factors that may explain a greater variance for time lags on the stretch A, the third day. For y and z axes, the synchronisation errors are summed with the phase shifts in macrogeometry response and vertical irregularity responses, with theoretical time lags calculated from the space s (about 26.3 m, coach length) between the sensors and the trains speed v (lags $t = s/v$). For stretch A in the z-axis, theoretical lag ranges from 0.430 (sensor 1 *versus* sensor 2) to 3.010 s (sensor 1 *versus* sensor 9), while measured lag ranges from 0.563 to 3.420 s. For stretch A on the same axis, theoretical lag ranges from -0.589 (sensor 1 *versus* sensor 2) to -4.124 s (sensor 1 *versus* sensor 9), while measured lag ranges from -0.600 to -4.334 s.

Considering the differences between time lags of the same sensor for different axes, synchronisation strategies are adopted depending on the context. It is recommended to initially correct only for the time shift calculated for longitudinal acceleration, which is even desirable in the context of a complete journey and the greater influence of vehicle accelerations (which serve as inertial markers for synchronisation). For high-speed analyses, variations between axes of the order of 0.1s can represent

inaccuracies of the order of 8 metres in space, and a second correction per axis, in time or space depending on the context, is recommended.

Through time-lag cross-correlation correction, the systematic component of the synchronization error is eliminated. However, the short-term (random) error between successive IMU samples remains due to the Raspberry clock's short-time deviations. The magnitude of these deviations can be estimated by using GPS time as a reference and analysing the random component (standard deviation) of the difference between GPS time and IMU time. For the datasets analysed (Italian and Brazilian tests), this component (standard deviation) has a mean value of 3.75 milliseconds. For a speed of 83 m/s, maximum for the dataset, this constitutes a component of the order of 0.31 m in the space domain, almost an order of magnitude below the shortest irregularity wavelength under analysis.

6.2.4 Comparison with smartphone outputs

Figure 34 depicts the graphical comparison between the outputs of the developed devices (represented by sensor 1) and those of a mid-range smartphone (Lenovo). It should be stated that the roll and pitch angles for sensor 1 are those given by the RTIMULib EKF algorithm. The smartphone recording interval lasted about 1 hour with the smartphone positioned on the train floor next to the other sensors on day 1 of the Italian test week. However, the smartphone presented unstable behaviour regarding values and sample rate most of the time, inhibiting proper data handling. Therefore, a 200-seconds sample of stable recording was selected.

There is a high noise level for smartphone accelerations (e.g., a standard deviation of about 1.0 m/s, while sensor 1 has a standard deviation of 0.4 for the same axis). Hence, the correlation coefficients between the raw acceleration signals are equal to or less than 0.1. Exceptions are made for the roll and pitch data, with correlation coefficients of, respectively, 0.92 and 0.90 for the raw outputs. When a moving average filter for noise attenuation is applied to the smartphone outputs (25-sample window to result in standard deviation equivalent to that of the developed devices), the correlation coefficients increase substantially (0.73 for x, 0.45 for y, and 0.33 for

z), indicating similarities between responses and differences due to noise.

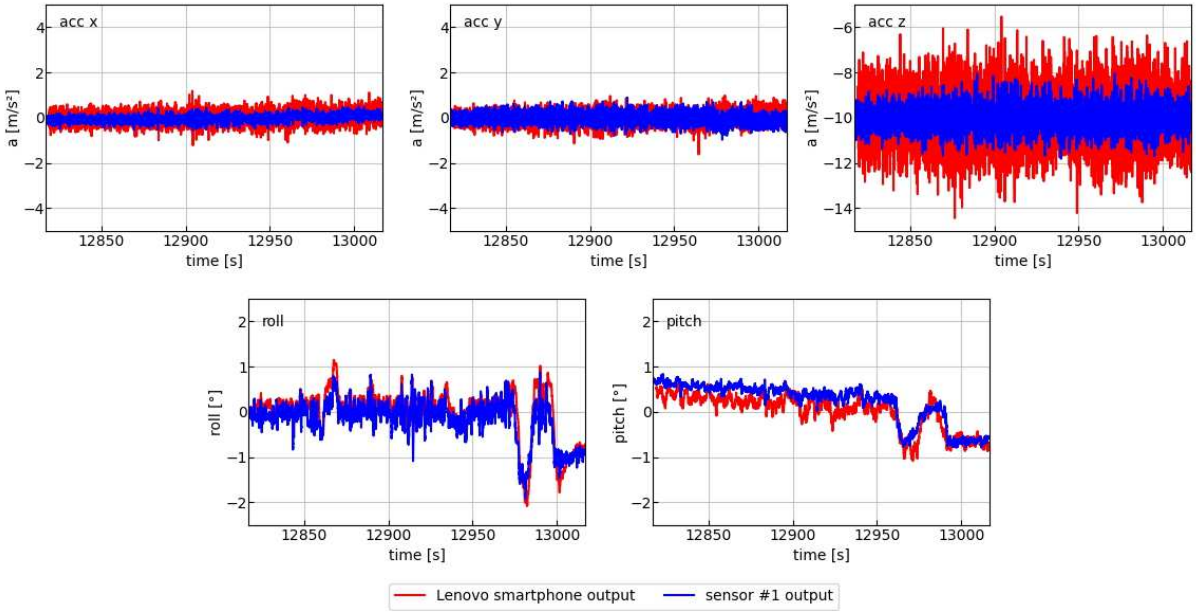

Figure 34 - Comparison between a mid-range smartphone and the developed devices in terms of acceleration and inclination outputs

The yaw angle, dependent on the magnetometer data, is not discussed because of the instability of results presented by both sensors, a behaviour verified for all sensors in all test scenarios due to probable magnetic interference from the test environment.

6.3 CHAPTER FINAL CONSIDERATIONS

The adequate characterisation of behaviour failures of the consumer-grade sensor provided by the tests using mid-range smartphones and the sensor group highlights the potential in the general characterisation of the condition of the railway track, such as stiffness variations and geometry elements. On the other hand, the limitations inherent to the very low-cost devices regarding temporary malfunctioning or synchronisation error demand strategies for the appropriate combined use of data from this sensor population.

As main outcomes, this chapter outlines two of the core strategies of the collective approach: identification of discrepant sensors and correction of sensor synchronisation. For the former, the similarity analyses allowed the identification of

the Pearson coefficient and comparisons in terms of longitudinal and lateral raw accelerations as the most appropriate for the different possible spatial configurations of the sensor population. In addition, the analysis of synchronisation errors highlighted possible deviations between axes of the same sensor set and the impact of the difference in position, indicating that an initial correction using longitudinal data and subsequent additional correction by axis, either in time (if sensors are redundant, i.e., installed on the same section) or in space (sensors distributed along the train) is more appropriate.

7 RESULTS AND DISCUSSION

In this chapter, the comfort in terms of lateral and vertical frequency-weighted accelerations is calculated using the inertial and position data gathered by the proposed consumer-grade devices. The individual and collective results are, thus, discussed in terms of the influence of intrinsic limitation and simplifications of the proposed technique and confronted with the reference data. In this regard, the chapter comprises three main parts:

- Initial validation through comparison with **reference acceleration data** obtained from the TRV. This validation is carried out only for the Italian tests for the days with synchronous dynamic data made available. It aims to establish the coherence between the vibration characterized by the collectivity of very low-cost sensors and the vibration characterized by a more accurate sensor.
- Quantification of the impact of the methods employed and the restrictions associated with the use of consumer-grade sensors on the quality of results. Specifically, the following aspects are addressed:
    - Sensor distribution
    - Number of sensors and sensor weighting
    - Position accuracy
    - Pitch and roll accuracy
    - Speed variation
- Repeatability analysis considering **multiple passages along the same track stretch**. This analysis considers data gathered on Rome Metro Line C and São Paulo CPTM Line 7.

When reference data is available, the aforementioned discussion considers also comparison with **reference geometry data** obtained from the TRV. From the previously discussed models, lateral and vertical accelerations are more correlated

with specific track features. Thus, the demonstration of at least a moderate correlation with certain parameters is expected to be an indicator of the reasonableness of the vibration results. Moreover, this comparison makes it possible to highlight potentials and limitations for indirect use as an indicator of track irregularities. In this regard, the analyses developed in the following subsections will focus on **lateral and vertical accelerations**.

All these analyses will consider the acceleration processed according to the comfort ISO standard for fixed 200-m track sections (RMS frequency-weighted acceleration within these track sections), as well as will consider the sensors individually and the resulting mean signal after the exclusion of the anomalous sensors. Moreover, the results for the Italian tests consider only data gathered during the test week due to problems with GPS receivers during the first test week that hinder the straightforward use of the respective data.

For comparison between sensors or between the population of sensors, it may be necessary in some cases to isolate the influence of speed variation. For these analyses, the test week on the Italian railway will be considered only for the sections of quasi-constant speed stretches already presented.

7.1 VALIDATION THROUGH COMPARISON WITH REFERENCE DATA

As presented in section 5.3.2.1, the Italian diagnostic trains have a dynamic measurement module that gathers lateral and vertical acceleration[44] data on the bogie and the car body using high-grade accelerometers whose description is presented in the mentioned section. Thus, the adherence of the vibrations reported by the low-cost sensors to the experienced vibration can be performed by comparison with the results offered by these higher-quality sensors, named in this work as reference inertial sensors. In other words, it is carried out an accuracy analysis by calculating the correlation and the agreement between the results from

[44] The acceleration data is filtered for gravity effects, but the description of the algorithm used in this process has not been made available by the RFI.

the very low-cost sensors and the results given by a more accurate inertial sensor. As previously stated, all comparisons are made considering the RMS frequency-weighed acceleration within 200-meters sections. Lastly, the values calculated for the validation section will be confronted with the geometry irregularity data also obtained by the inspection train, identifying whether the reference accelerometers and the low-cost accelerometers present the same sensitivity to vibrations due to certain parameters at certain ranges.

These analyses are considered only for the stretch of constant speed B on day 4 of the test week on the Italian railway. The selection is because it is the only stretch of constant speed in the whole data set (Brazilian and Italian tests) with redundant sensors and complete reference data (geometry, inertial, and position data). Thus, individual sensors will be analysed, but also the average signal. Furthermore, since the reference sensors were installed in the first car and the sensors under test were on the eighth car, the influence of speed variation should be eliminated at this validation stage. Ideally, validation should be performed for the first day, in which the sensors are installed at approximately the same point on the right of the vehicle and under the same vibration. However, due to data recording problems in the inspection trains, full reference data is only available for the other three days of the test week.

7.1.1 Comparison with reference inertial data

For this validation, the following approach for position, time and attitude was assumed:

- Attitude estimation derived from the accelerometer-gyroscope-magnetometer fusion (RTIMULib).
- Initial synchronization correction among the sensors is carried out. Thus, synchronization correction between the sensor group and the reference data is performed through cross-correlation between the speed profile gathered by the reference sensors and the mean speed profile gathered by the consumer-grade sensor group. In the next step, track chainage is attributed to the sensor group by using the correspondence in time with reference position data and by

adding the known distance between the sensor group and the reference sensors (of about 183 m). Finally, a fine adjustment in data alignment is performed in the space domain using the cross-correlation between reference inertial data and the group of signals.

This procedure uses the reference position data to minimize the influence of errors in time and space between the sensor group and the track reality. However, in a generalized approach, position on track would be obtained through map matching of the mean GPS solution among the sensors, with position deviations being in the order of magnitude of the GPS errors. Variations regarding these aspects and their influence on results are to be discussed in the following section.

Considering the influence of the speed variation, the following validation steps will consider only the constant speed section for which there is reference data (section B) for the test week, as previously presented. Tables 41 to 48 summarize the obtained coefficients between each of the very low-cost sensor devices and each of the reference accelerometers (A and B). The tested sensors are identified from 1 to 9. The malfunctioning sensors 3 and 4 (both outputting null values during most of the stretch with occasional peaks) were included in some of the calculation of mean signal calculations to illustrate the influence of a malfunctioning sensor on the performance of the mean signal. Regarding the relationship between the two reference sensors, it is emphasised for proper interpretation of the tables that the vertical reference accelerometer B presented a result considerably lower than that of A (total agreement of 0.64 despite of correlation coefficient of 0.93). This discrepancy is not observed for lateral reference sensors (correlation coefficient of 0.904 and total agreement of 0.897).

Table 41 - Pearson correlation coefficient between the very low-cost accelerometers and the reference accelerometers, second stretch with constant speed of day four, Y axis

	1	2	3	4	5	6	7	8	9	Mean signal	Mean signal w/o 4, 3	Mean signal w/o 4, 3, 9	Mean signal with windowed exclusion	Mean response w/o 4, 3	Mean response w/o 4, 3, 9
A	.81	.81	.05	.00	.79	.82	.80	.81	.49	.23	.76	.76	.77	.79	.80
B	.76	.76	.07	.00	.75	.76	.75	.76	.49	.24	.72	.72	.72	.75	.76

Table 42 - Pearson correlation coefficient between the very low-cost accelerometers and the reference accelerometers, second stretch with constant speed of day four, Z axis

	1	2	3	4	5	6	7	8	9	Mean signal	Mean signal w/o 4, 3	Mean signal w/o 4, 3, 9	Mean signal with windowed exclusion	Mean response w/o 4, 3	Mean response w/o 4, 3, 9
A	.55	.73	.12	.00	.59	.74	.73	.72	.38	.40	.79	.77	.78	.70	.72
B	.56	.71	.18	.00	.58	.72	.72	.71	.37	.44	.76	.75	.76	.69	.71

Table 43 - Consistency coefficient between the very low-cost accelerometers and the reference accelerometers, second stretch with constant speed of day four, Y axis

	1	2	3	4	5	6	7	8	9	Mean signal	Mean signal w/o 4, 3	Mean signal w/o 4, 3, 9	Mean signal with windowed exclusion	Mean response w/o 4, 3	Mean response w/o 4, 3, 9
A	.79	.79	.00	.00	.78	.80	.79	.80	.49	.15	.74	.74	.74	.79	.79
B	.73	.74	.01	.00	.73	.74	.73	.74	.49	.16	.69	.68	.68	.73	.74

Table 44 - Consistency coefficient between the very low-cost accelerometers and the reference accelerometers, second stretch with constant speed of day four, Z axis

	1	2	3	4	5	6	7	8	9	Mean signal	Mean signal w/o 4, 3	Mean signal w/o 4, 3, 9	Mean signal with windowed exclusion	Mean response w/o 4, 3	Mean response w/o 4, 3, 9
A	.54	.71	.01	.00	.57	.72	.72	.69	.33	.26	.78	.75	.78	.54	.71
B	.49	.60	.01	.00	.51	.64	.64	.60	.27	.23	.68	.65	.67	.49	.60

Table 45 - Total agreement coefficient between the very low-cost accelerometers and the reference accelerometers, second stretch with constant speed of day four, Y axis

	1	2	3	4	5	6	7	8	9	Mean signal	Mean signal w/o 4, 3	Mean signal w/o 4, 3, 9	Mean signal with windowed exclusion	Mean response w/o 4, 3	Mean response w/o 4, 3, 9
A	.76	.77	.00	.00	.76	.77	.76	.76	.36	.16	.72	.70	.73	.77	.77
B	.73	.73	.01	.00	.72	.74	.72	.73	.34	.17	.71	.69	.70	.70	.74

Table 46 - Total agreement coefficient between the very low-cost accelerometers and the reference accelerometers, second stretch with constant speed of day four, Z axis

	1	2	3	4	5	6	7	8	9	Mean signal	Mean signal w/o 4, 3	Mean signal w/o 4, 3, 9	Mean signal with windowed exclusion	Mean response w/o 4, 3	Mean response w/o 4, 3, 9
A	.07	.19	.01	.00	.06	.19	.2	.18	.04	.27	.44	.40	.42	.11	.13
B	.06	.15	.01	.00	.04	.16	.17	.11	.03	.19	.40	.36	.37	.09	.10

Table 47 - Root-mean squared deviation (m/s²) between the very low-cost accelerometers and the reference accelerometers, second stretch with constant speed of day four, Y axis

	1	2	3	4	5	6	7	8	9	Mean signal	Mean signal w/o 4, 3	Mean signal w/o 4, 3, 9	Mean signal with windowed exclusion	Mean response w/o 4, 3	Mean response w/o 4, 3, 9
A	0.025	0.024	0.877	0.110	0.025	0.025	0.026	0.026	0.052	0.096	0.029	0.030	0.027	0.024	0.025
B	0.027	0.027	0.877	0.107	0.028	0.027	0.028	0.027	0.056	0.096	0.030	0.031	0.028	0.027	0.027

Table 48 - Root-mean squared deviation (m/s²) between the very low-cost accelerometers and the reference accelerometers, second stretch with constant speed of day four, Z axis

	1	2	3	4	5	6	7	8	9	Mean signal	Mean signal w/o 4, 3	Mean signal w/o 4, 3, 9	Mean signal with windowed exclusion	Mean response w/o 4, 3	Mean response w/o 4, 3, 9
A	0.178	0.117	0.934	0.124	0.194	0.114	0.111	0.123	0.223	0.094	0.064	0.072	0.067	0.149	0.138
B	0.209	0.148	0.935	0.090	0.225	0.145	0.142	0.154	0.253	0.107	0.094	0.103	0.097	0.161	0.150

The mean signals have equivalent or slightly worse performance than the best sensor for the y-axis. For the z-axis, the performant of the mean signal is considerably better than the best individual sensor, with significant improvement in terms of agreement to reference values (0.19 to 0.44 for total agreement coefficient, 0.111 to 0.064 m/s² for RMSD) reflects the contribution of noise reduction in the collective approach. The performance regarding the mean result, which does not deal with noise reduction, is better than the mean signal for the y-axis and similar or worse for the z-axis. The minor magnitude and less strict cause-effect relationship between lateral acceleration and lateral irregularities, combined, may result in a less predictable contribution of the mean approach when evaluating its adherence to the reference data. Thus, variations between sensors, averages and references regarding the lateral axis would have a higher stochastic component.

The improvement when removing the sensors classified as malfunctioning (3 and 4) according to the process described in the previous chapter highlights the importance

of correlation-based criteria regarding the collective behaviour of the sensors. At the same time, the non-improvement when removing sensor 9 (which was not identified as malfunctioning but showed a correlation with the reference below the others) demonstrates the robustness of the mean results and the suitability of the threshold defined for correlation-based criteria. In complement, the contribution of the windowed exclusion of the discrepant sensors was not proven, as a further indicator of the robustness of the mean to deviant sensors. Thus, for simplicity, the total exclusion of discrepant sensors is adopted for further calculations.

Regarding the variation between coefficients, the slight difference between correlation and consistency indicates the reduced influence of signal scale deviations on the comparisons. On the other hand, the higher difference between correlation and total agreement is explained by the high penalization when there is an offset between results, even though the graphs have the same shape and allow similar identification of discomfort peaks.

The offset aspect is better described in Figures 35 and 36, which depict the RMS frequency-weighted values for lateral and vertical accelerations, respectively. In both figures, the top graph reproduces the individual responses and that of the mean signal, while the bottom graph depicts the mean signal, the mean response, and the reference results. Moreover, the graphs present the same scale to enable vibration magnitude comparisons. The noisier signal of the consumer-grade sensors results, regarding the RMS calculation, in an error component to be added to the RMS values and produces a positive offset of the curve, which varies from sensor to sensor. Considering the vertical axis, the noise reduction of the mean signal, thus, maintains approximately the shape of the curves of the individual sensors (correlation and consistency values close to the individual ones), but consistently reduces the error due to noise and produces negative offset with respect to the average of the individual sensors and approximation to the results of the reference sensors (improvement of the total agreement value). Regarding the lateral component compared to the vertical one, the proximity between responses and the smaller magnitude allows us to understand how stochastic variations in acceleration responses impact the relationships between outcomes less predictably.

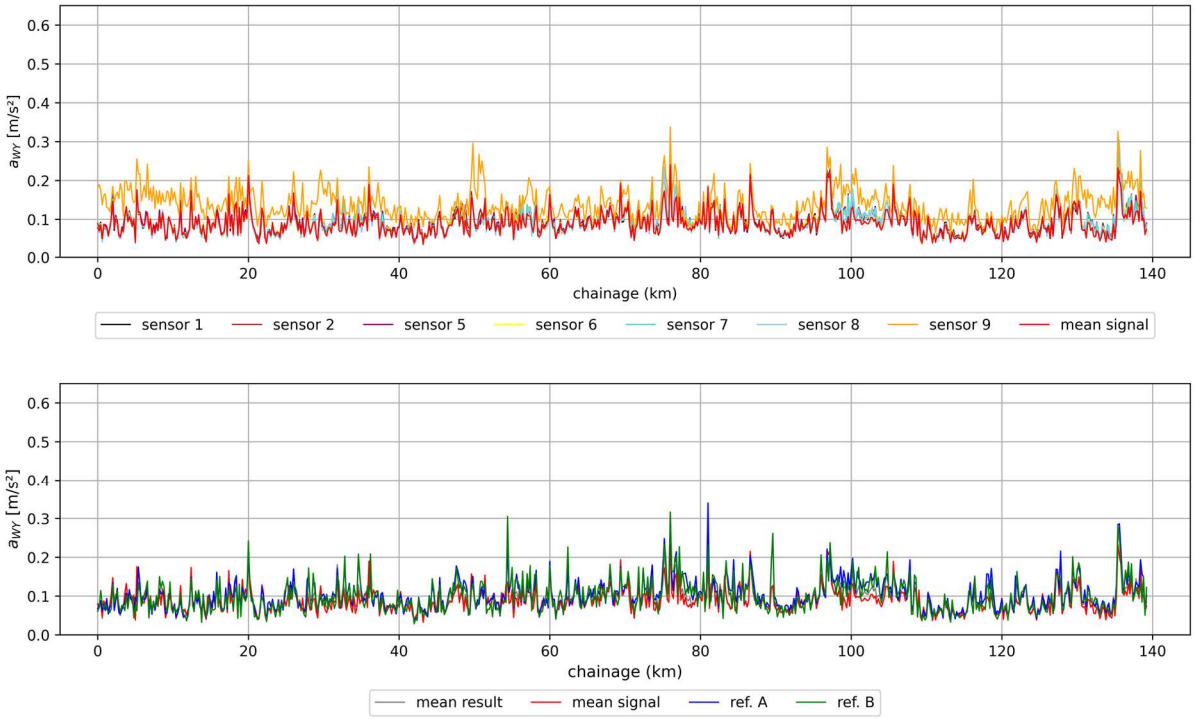

Figure 35 - RMS frequency-weighted lateral accelerations for the consumer-grade devices and the reference inertial sensors, stretch B, fourth day of the test week on the Italian railway

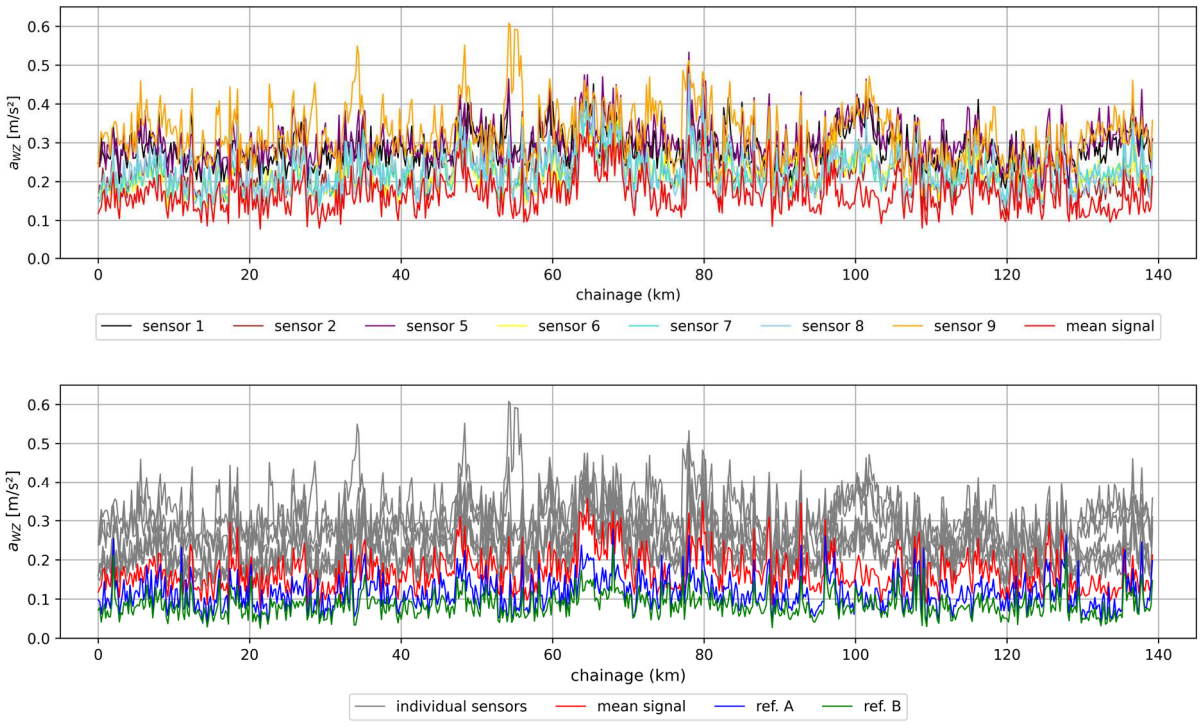

Figure 36 - RMS frequency-weighted vertical accelerations for the consumer-grade devices and the reference inertial sensors, stretch B, fourth day of the test week on the Italian railway

7.2 COMPARISON WITH REFERENCE GEOMETRY DATA

To provide an overview of the track quality on the validation stretch, the longitudinal level and alignment data (each 0.25 m) for ranges D1 and D2 gathered by the inspection train are presented in Figure 37. The graphs also present the alert limits for speeds between 230 and 300 km/h in accordance with EN 13848-5 (COMITÉ EUROPÉEN DE NORMALISATION, 2017a).

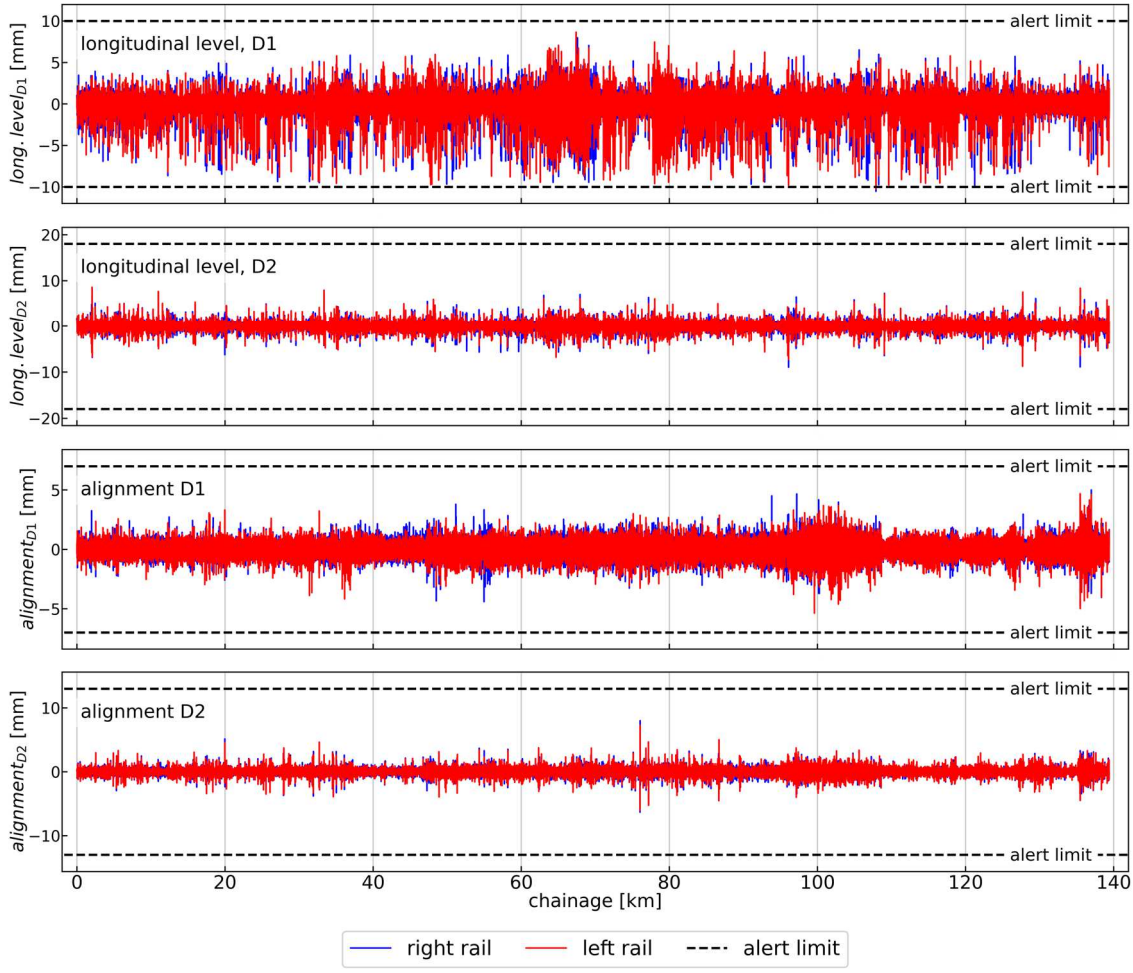

Figure 37 - Track longitudinal level and alignment (ranges D1 and D2) for the fourth day, stretch B.

Additionally, it is noteworthy that some of the correlation between track features and vibration may be due not to a direct relationship but due to an indirect one given by the intrinsic correlation between track parameters since irregularities can develop from common local-dependent causes such as ballast and subgrade conditions or are geometrically dependent. Table 49 presents the correlations between track parameters (standard deviation within 200-m sections) for this stretch as

complementary information. As expected, left and right measurements of the same parameter are highly correlated. Nevertheless, controlling for spurious associations is not in the present scope since the aim is merely to verify whether comfort results adhere to track quality.

Table 49 - Correlation between track parameters for the fourth day, stretch B

	Gauge (deviation)	Cross level	Twist, 3m	Twist, 9m	Longitudinal level, left, D1	Longitudinal level, right, D1	Alignment, left, D1	Alignment, right, D1	Longitudinal level, left, 10m	Longitudinal level, right, 10m	Alignment, left, 10m	Alignment, right, 10m	Alignment,	Longitudinal level,	Longitudinal level, left, D2	Longitudinal level, right, D2	Alignment, left, D2	Alignment, right, D2	Longitudinal level, left, D3	Longitudinal level, right, D3	Alignment, left, D3	Alignment, right, D3
Gauge (deviation)	1	.37	.35	.26	.29	.32	.48	.39	.29	.32	.48	.41	.15	.17	.09	.13	.26	.21	.23	.24	.28	.28
Cross level	.37	1	.93	.62	.67	.62	.38	.44	.66	.62	.38	.44	.18	.19	.36	.33	.3	.31	.29	.29	.23	.23
Twist, 3m	.35	.93	1	.81	.67	.62	.31	.36	.67	.61	.31	.36	.17	.23	.38	.36	.33	.33	.32	.31	.37	.37
Twist, 9m	.26	.62	.81	1	.43	.4	.24	.28	.42	.39	.23	.27	.17	.18	.31	.31	.36	.36	.3	.29	.59	.59
Longitudinal level, left, D1	.29	.67	.67	.43	1	.84	.16	.27	.99	.84	.17	.26	.08	.38	.5	.41	.18	.19	.29	.27	.13	.12
Longitudinal level, right, D1	.32	.62	.62	.4	.84	1	.26	.22	.84	.99	.26	.21	.1	.38	.43	.46	.2	.2	.28	.28	.12	.12
Alignment, left, D1	.48	.38	.31	.24	.16	.26	1	.76	.16	.25	.98	.75	.42	.02	.1	.16	.53	.47	.18	.2	.21	.22
Alignment, right, D1	.39	.44	.36	.28	.27	.22	.76	1	.26	.21	.75	.98	.43	.03	.2	.19	.51	.56	.24	.24	.25	.24
Longitudinal level, left, 10m	.29	.66	.67	.42	.99	.84	.16	.26	1	.85	.16	.25	.06	.38	.49	.4	.16	.18	.28	.26	.13	.12
Longitudinal level, right, 10m	.32	.62	.61	.39	.84	.99	.25	.21	.85	1	.25	.2	.08	.38	.42	.45	.18	.18	.27	.27	.11	.11
Alignment, left, 10m	.48	.38	.31	.23	.17	.26	.98	.75	.16	.25	1	.76	.39	.02	.08	.14	.47	.42	.17	.19	.2	.21
Alignment, right, 10m	.41	.44	.36	.27	.26	.21	.75	.98	.25	.2	.76	1	.4	.02	.19	.17	.48	.51	.24	.23	.24	.24
Alignment,	.15	.18	.17	.17	.08	.1	.42	.43	.06	.08	.39	.4	1	.19	.16	.19	.42	.43	.19	.19	.24	.24
Longitudinal level,	.17	.19	.23	.18	.38	.38	.02	.03	.38	.38	.02	.02	.19	1	.2	.2	.05	.06	.13	.14	.08	.08
Longitudinal level, left, D2	.09	.36	.38	.31	.5	.43	.1	.2	.49	.42	.08	.19	.16	.2	1	.9	.27	.29	.62	.6	.18	.18
Longitudinal level, right, D2	.13	.33	.36	.31	.41	.46	.16	.19	.4	.45	.14	.17	.19	.2	.9	1	.3	.31	.62	.63	.2	.2
Alignment, left, D2	.26	.3	.33	.36	.18	.2	.53	.51	.16	.18	.47	.48	.42	.05	.27	.3	1	.93	.35	.36	.5	.5
Alignment, right, D2	.21	.31	.33	.36	.19	.2	.47	.56	.18	.18	.42	.51	.43	.06	.29	.31	.93	1	.35	.35	.5	.5
Longitudinal level, left, D3	.23	.29	.32	.3	.29	.28	.18	.24	.28	.27	.17	.24	.19	.13	.62	.62	.35	.35	1	.97	.28	.27
Longitudinal level, right, D3	.24	.29	.31	.29	.27	.28	.2	.24	.26	.27	.19	.23	.19	.14	.6	.63	.36	.35	.97	1	.28	.27
Alignment, left, D3	.28	.23	.37	.59	.13	.12	.21	.25	.13	.11	.2	.24	.24	.08	.18	.2	.5	.5	.28	.28	1	1
Alignment, right, D3	.28	.23	.37	.59	.12	.12	.22	.24	.12	.11	.21	.24	.24	.08	.18	.2	.5	.5	.27	.27	1	1

As previously emphasized, the mean signal is more appropriately interpreted when considering redundant signals (i.e., sensors subjected to almost the same vibration). Although the redundancy is not entirely true for day 4, it was found that the integration of sensor 9 into the mean set did not degrade the results, expected due to the high correlation between left and right for alignment and longitudinal levels, the track parameters that most influence vehicle vibration. Thus, comparisons with track parameters will be performed for two mean signals, always without discrepant sensors: respecting the redundant sensor concept (without sensor 9, named **mean signal**)**,** and integrating sensor 9 (identified as **mean signal w 9**), in order to measure the influence of this difference in position. Analogous treatment is reserved for the mean result, with and without the result of sensor 9.

The correlations between track parameters (standard deviation within 200-m sections) and vibrations (RMS values within 200-m sections) are presented in Tables 50 and 51 for, respectively, the lateral and vertical directions. These tables present only significant correlation (p-value > 0.05) greater than 0.4 for the mean signal or the reference accelerometers. The lateral and vertical accelerations gathered by the consumer-grade sensors are significantly correlated with, respectively, alignment and longitudinal level (range D1 and 10-m). Regarding the reference accelerometers' performance, correlation coefficients close to or greater than 0.5 are also found for the longer wavelengths (range D3) of lateral and vertical irregularities. Hence the lower performance for the D3 range highlights that these very low-cost sensors are less sensitive to long-wavelength irregularities (namely low-amplitude and low-frequency displacement). Another result from individual analysis is the discrepant behaviour of sensor 9, with smaller correlation coefficients not due to sensor malfunctioning but rather to a more irregular track on the right side.

Table 50 - Correlation between sensors responses and track parameters, lateral acceleration

	1	2	5	6	7	8	9	Mean signal	Mean signal w 9	Mean result	Mean result w 9	A	B
Alignment, left, D2	0.72	0.73	0.71	0.73	0.72	0.70	0.48	0.70	0.70	0.73	0.71	0.80	0.81
Alignment, right, D2	0.73	0.73	0.71	0.74	0.73	0.70	0.49	0.70	0.70	0.73	0.72	0.81	0.82
Alignment, total, D1	0.57	0.57	0.56	0.59	0.58	0.59	0.42	0.48	0.49	0.59	0.58	0.63	0.55
Alignment, left, D1	0.55	0.55	0.55	0.57	0.56	0.57	0.45	0.48	0.49	0.57	0.57	0.58	0.51
Superelevation deviation	0.47	0.46	0.46	0.46	0.46	0.45	0.21	0.47	0.46	0.47	0.44	0.50	0.46
Alignment, right, D1	0.53	0.53	0.52	0.54	0.53	0.54	0.35	0.44	0.44	0.54	0.55	0.64	0.55
Alignment, left, 10m	0.51	0.51	0.5	0.53	0.52	0.53	0.42	0.43	0.44	0.53	0.53	0.53	0.47
Alignment, right, D3	0.40	0.4	0.38	0.41	0.39	0.38	0.21	0.40	0.40	0.40	0.38	0.46	0.50
Cross level	0.39	0.39	0.39	0.39	0.39	0.39	0.14	0.40	0.39	0.40	0.37	0.43	0.39

Table 51 - Correlation between sensors responses and track parameters, vertical acceleration

	1	2	5	6	7	8	9	Mean signal	Mean signal w 9	Mean result	Mean result w 9	A	B
Longitudinal level, left, D1	0.61	0.85	0.65	0.86	0.81	0.83	0.44	0.91	0.91	0.82	0.80	0.73	0.71
Longitudinal level, total, D1	0.61	0.84	0.64	0.83	0.8	0.82	0.36	0.91	0.90	0.81	0.77	0.74	0.72
Longitudinal level, left, 10m	0.6	0.83	0.64	0.85	0.8	0.82	0.43	0.90	0.90	0.81	0.79	0.71	0.70
Longitudinal level, right, D1	0.61	0.78	0.62	0.77	0.76	0.75	0.29	0.85	0.83	0.77	0.72	0.71	0.71
Longitudinal level, right, 10m	0.6	0.77	0.61	0.77	0.75	0.74	0.29	0.84	0.83	0.76	0.71	0.69	0.70
Cross level	0.54	0.65	0.53	0.64	0.62	0.61	0.42	0.61	0.61	0.64	0.64	0.52	0.52
Superelevation deviation	0.55	0.64	0.52	0.63	0.61	0.59	0.42	0.60	0.60	0.63	0.63	0.55	0.55
Longitudinal level, left, D2	0.33	0.5	0.36	0.52	0.5	0.46	0.30	0.55	0.57	0.48	0.47	0.83	0.82
Longitudinal level, right, D2	0.32	0.44	0.34	0.46	0.46	0.39	0.21	0.49	0.51	0.43	0.41	0.8	0.79
Twist, 3 m	0.33	0.47	0.29	0.45	0.41	0.4	0.24	0.48	0.47	0.42	0.41	0.42	0.42
Longitudinal level, left, D3	0.23	0.31	0.21	0.30	0.31	0.3	0.24	0.32	0.33	0.30	0.30	0.51	0.56
Longitudinal level, right, D3	0.23	0.3	0.21	0.29	0.30	0.29	0.23	0.30	0.32	0.29	0.30	0.50	0.55

Another relevant aspect is that, for the vertical direction, the mean signal yields a result almost as good as the best sensor (for lateral) and considerably better than the best sensor (for vertical) in terms of correlation with track parameters, which indicates the suitability of measuring strategies based on the mean signal. In addition, the distinctly better performance of the mean signal in relation to the mean result in the vertical reflects the gain from the noise reduction, a behaviour not observed for lateral acceleration possibly due to the lower coupling to track quality. Considering the comparison with the reference accelerometers' performance, the mean signal yields significantly worse results for the most correlated lateral irregularities but

significantly better results for the vertical ones. The lack of sensitivity for the longer wavelength irregularities (below about 0.9 Hz for the speed in the given stretch), though, is not corrected by the mean approach.

For visual characterisation of the described results, Figures 38 and 39 compare the lateral and vertical results for the mean signal with the most correlated track parameters, enabling visual confirmation of the concordance between results and reference data.

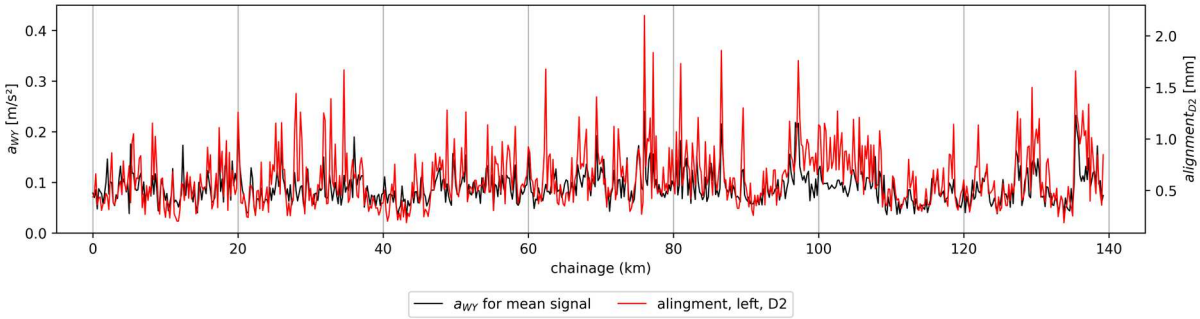

Figure 38 - Root-mean-square frequency-weighted lateral acceleration (mean signal) *versus* alignment (left, range D2)

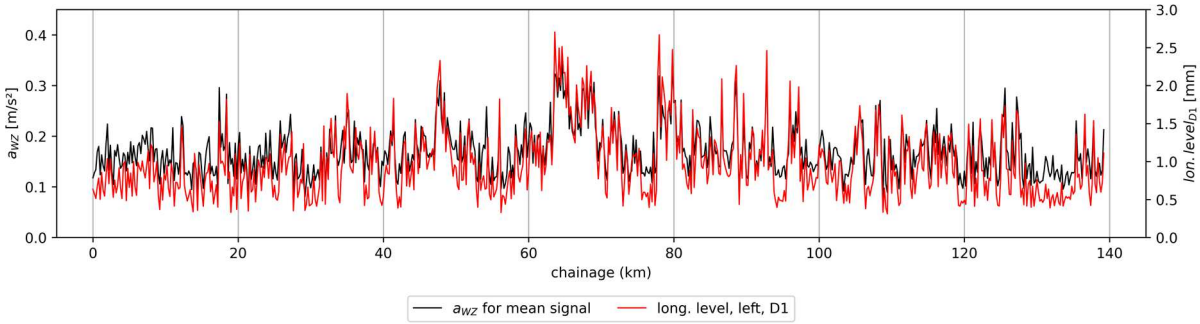

Figure 39 - Root-mean-square frequency-weighted vertical acceleration (mean signal) *versus* longitudinal level (left, range D1)

7.3 INFLUENCE OF THE METHOD'S SETTINGS AND CONSTRAINTS ON RESULTS

7.3.1 Position and distribution of the sensors

From the results presented in section 6.2, it is possible to infer that the distribution of the sensors along the trains results in sensors reacting differently to the same track

apart from the variation expected from the quality of the sensors. This difference in response is ruled by two aspects: a) the difference in position by itself resulting in signal shape and magnitude differences (i.e., due to variations from one suspension to another, as well as to the proximity to the bogie pivot), and b) the speed at which each sensor travels over a given section.

7.3.1.1 Tests on the Italian railway

7.3.1.1.1 Raw data comparison

Initially, the raw signals are compared to characterize the influence of sensor position on the shape and magnitude of acceleration signals. Considering the effect of macrogeometry on lateral acceleration values and the resulting higher correlation in this direction even for sensors in different positions, this analysis of raw signals is carried on only for vertical accelerations. Moreover, the comparison is performed for the constant speed stretches and also stretches with speed variations (Table 52, same convention as for Table 22), representative subsamples of the complete trips in terms of the proportion of stretches without and with significant speed variation. The resulting Pearson correlation coefficients for the six sections are presented in the boxplot of Figure 1, in order to graphically illustrate the behaviour of the sensor population and enable direct comparison. In addition, the statistical summary for the coefficients is presented in Table 53. For stretches with varying speed and sensors in different positions, the correlation is calculated in the space domain.

Table 52 - Selected trip intervals/road stretches with speed variation for the Italian tests

Test day	Start time (s)	End time (s)	Aprox. length (m)	Average speed (m/s)	Std. deviation speed (m/s)	Percentage constant speed	Approximate location	Train direction
#1	14300	16000	50,400	56.8	25.3	30%	Fidenza to Milano	F
#2	4600	5250	124,100	64.5	22.3	41%	Torino to Milano	B
#3	22534	30511	183,200	23.5	15.6	47%	Vicenza to Milano	F
#4	21799	23117	49,500	37.9	18.6	52%	Firenze to Arezzo	B

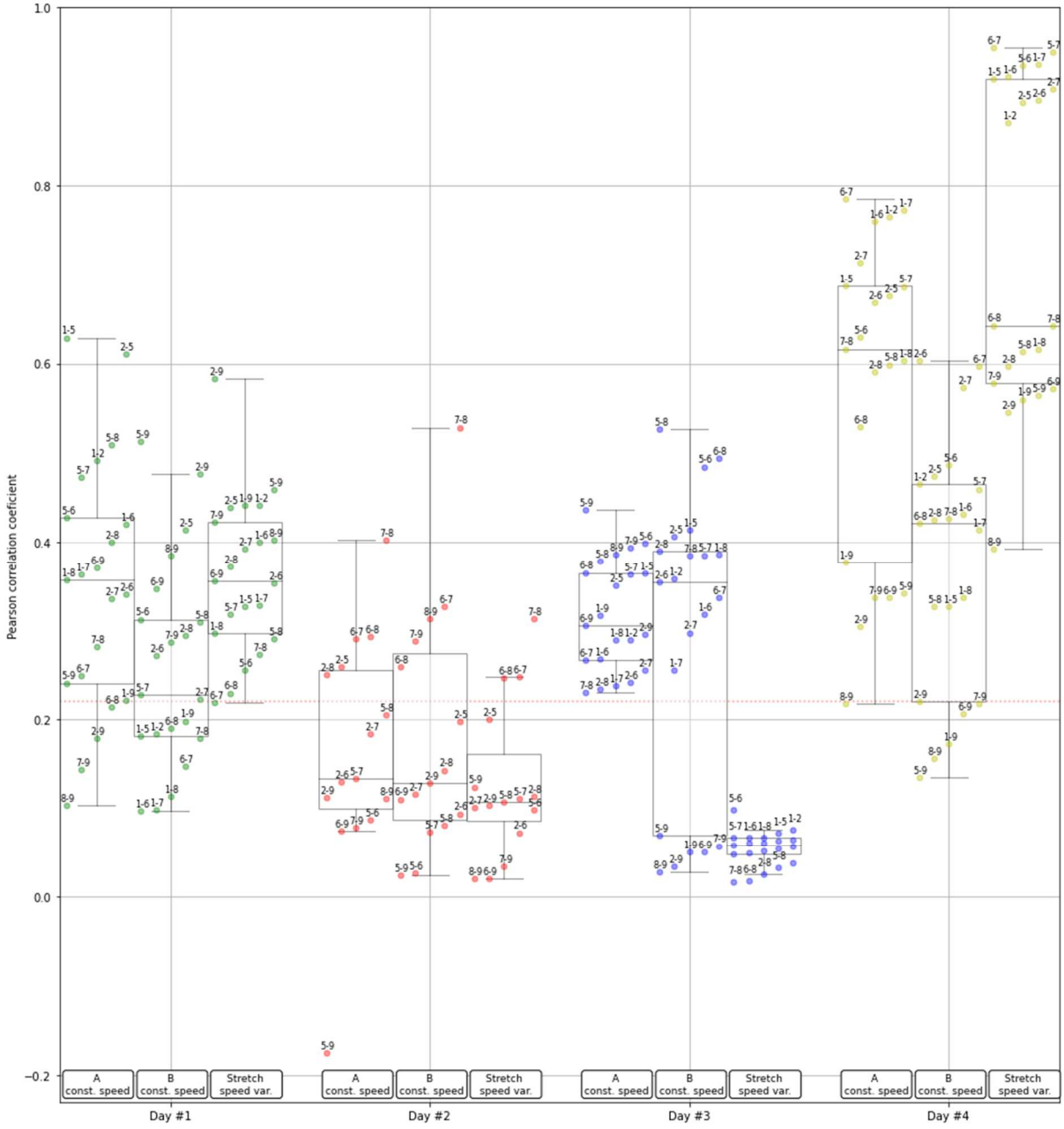

Figure 40 - Boxplot of the correlation coefficients for the raw vertical acceleration

Table 53 - Statistical summary of the Pearson correlation coefficients for raw vertical acceleration, Italian tests

Day	Mean / Standard deviation Pearson's r		
	Quasi-constant speed A	Quasi-constant speed B	Entire trip
#1	0.35 / 0.14	0.26 / 0.12	0.36 / 0.09
#2	0.16 / 0.13	0.18 / 0.13	0.13 / 0.08
#3	0.32 / 0.06	0.31 / 0.06	0.05 / 0.02
#4	0.58 / 0.17	0.37 / 0.14	0.74 / 0.18

The first general conclusion is that the distribution of the sensors affects the

correlation of the raw signals as a clear result of the differences in shape between the signals, with even clearer distinction speed variations. For constant and non-constant speed stretches, the mean similarity for day 2 (sensors distributed along a coach) is lower than for the other days (except for day 3, varying speed), behaviour expected given the difference in signal shape due to the distance to the bogie. Moreover, the relationship between proximity and signal similarity on day 2 is moderate to weak. For instance, sensors 7 and 8, which are adjacent, are the most similar for this day in all sections. Sensors 5 (in the centre) and 9 (at the far end) show the greatest dissimilarity for the constant speed stretches, but intermediate similarity for the stretch with variation. Sensor 2 (near the extremity) and sensor 5, against the expected behaviour, show similarity always above the group average. In conclusion, sensor-to-sensor variation appears to have a relevant contribution to this sensor-to-sensor relationship.

On day 3, at constant speed, the signals are expected to be more similar since they are at homologous positions, over the rear bogie on each of the coaches. Under speed variations, however, the greater distances between the sensors on day 3 result in a considerable decrease in similarity. On the other hand, there is no clear relationship between proximity and signal similarity, indicating that the influence of an eventual tendency to greater or smaller vibrations at the extremities of the is not verified.

For this dataset and considering only the stretches with speed variation, in which the distinction between arrangements is more evident, a threshold of 0.22 (red line in Figure 40) could be used as a minimum Pearson's coefficient for the redundant sensors' identification. The exceptions, pairs 7-8, 6-7, and 6-8 on the second day, are relatively close and could indicate a tolerance for the distance between sensors to be considered redundant in the same coach. However, the small correlation even for other pairs of neighbouring sensors (5-6 and 8-9 on day 2) highlights the role of the sensor-to-sensor variation in curbing the redundancy identification solely from signal analysis.

7.3.1.1.2 RMS frequency-weighted results

Initially, Figures 41 and 42 compare lateral and vertical RMS frequency weighted accelerations for extracts of the eight stretches with the same x and y scales for all

graphs to enable magnitude comparisons. As already verified in other situations, the resulting vibrations in the lateral direction are of smaller magnitude compared to the vertical, and consequently, there is greater agreement between sensors. Additionally, Figures 43 and 44 present the mean RMS frequency-weighted lateral acceleration by sensor to enable comparison between sensors and between arrangements in terms of vibration magnitude. In these boxplots, *mean sig.* stands for the mean signal.

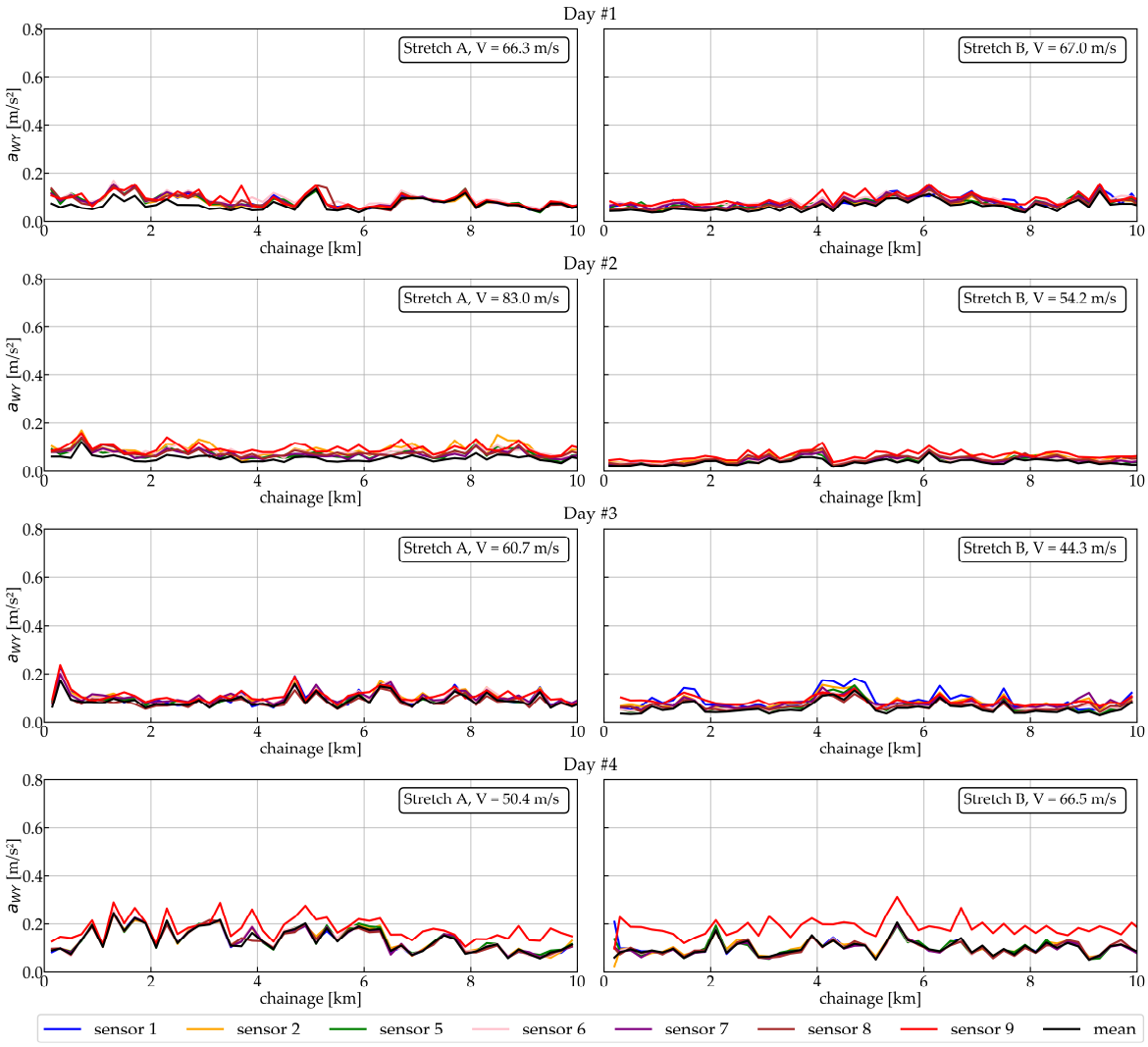

Figure 41 - Root-mean-square frequency weighted lateral acceleration comparison, excerpts for the eight constant speed stretches of the Italian tests

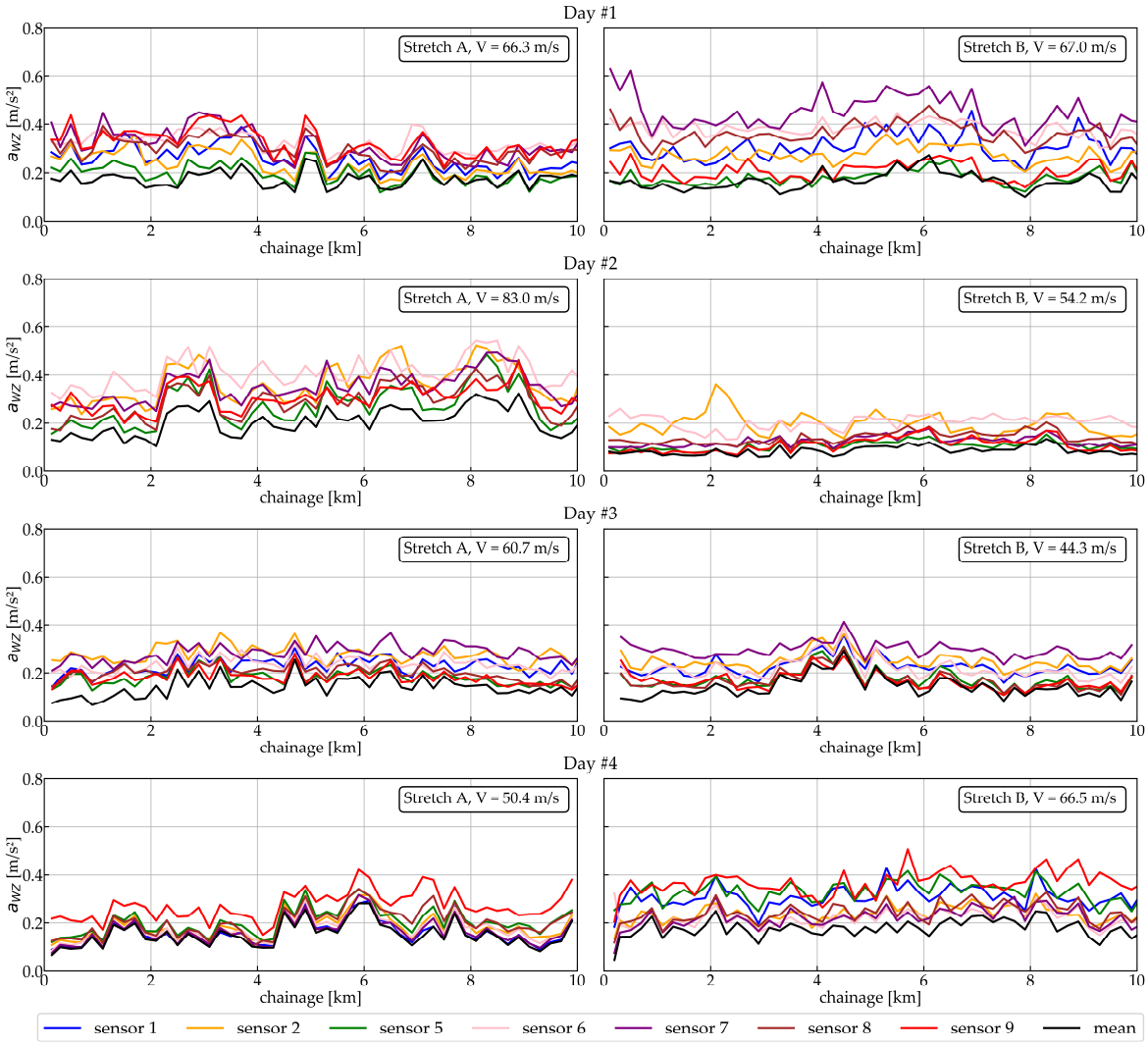

Figure 42 - Root-mean-square frequency weighted vertical acceleration comparison, excerpts for the eight constant speed stretches of the Italian tests

In parallel, paired t-test was conducted to statistically evaluate the difference between the mean RMS vibration responses. As a result of the influence of the sensor-to-sensor variation, there was a statistically significant difference (0.05 as the level of significance) between the mean RMS results for most situations and even for the redundant sensor arrangements. In complement, equality cannot be statistically rejected even in the situation of sensors installed in different coaches and under speed variation, in which a greater difference between the results would be expected. Thus, the major influence of sensor-to-sensor variance on the differences between results is identified. The exceptions for which the null hypothesis of equality between means cannot be rejected are listed as follows (about 6% of the situations):

- Day 1: pair 6-9 for stretch A (constant speed).

- Day 2: pair 2-7 for stretch A (constant speed); pair 2-6 for stretch B (constant speed); pair 8-9 for the stretch with speed variation.
- Day 3: pairs 1-6, 2-7 and 5-9 for stretch A (constant speed); pairs 5-9, and 8-9 for stretch B (constant speed); pairs 5-8, 1-9, and 6-9 for the stretch with speed variation.
- Day 4: pairs 1-7 and 5-8 for stretch A (constant speed).

For lateral acceleration, the lower magnitude of vibrations decreases the difference between them, with equality in about 17% of the situations and no apparent influence of the differences in sensor arrangement.

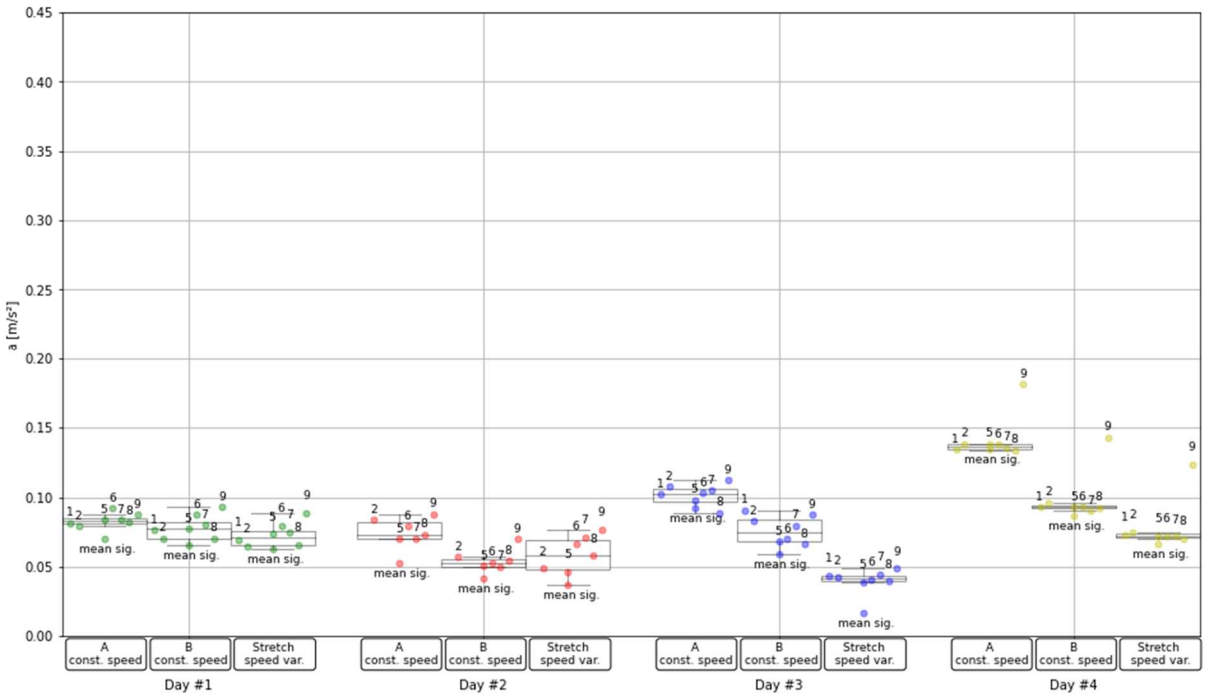

Figure 43 - Boxplot of the mean RMS frequency-weighted lateral accelerations

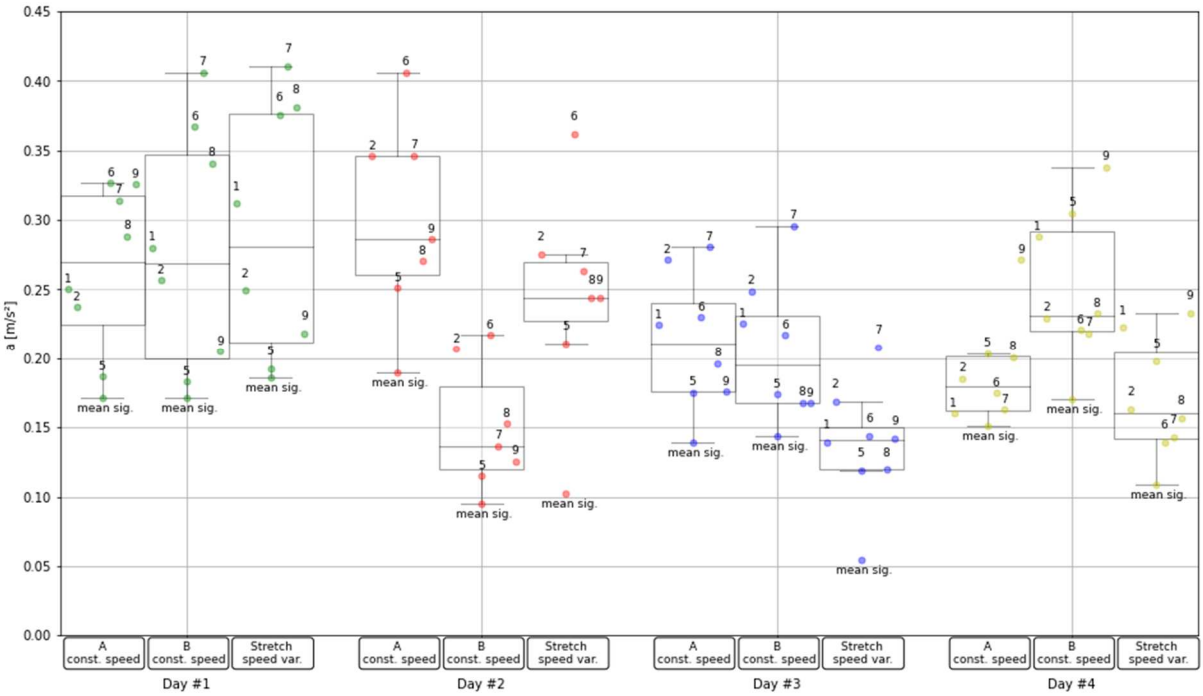

Figure 44 - Boxplot of the mean RMS frequency-weighted vertical accelerations

From the dispersions of the mean vibration values given in Figures 43 and 44 and regarding sensors placed in different positions, it is not possible to identify a clear correlation between sensor position and a higher/smaller vibration magnitude for day 2 since the magnitude of variation among the sensors is similar to those presented for the first day and, thus, may be mainly due to the variance between sensors. For instance, sensor 5 yields the smallest magnitude among individual sensors for both stretches on the second day, the expected behaviour for a sensor placed at the centre of the coach. However, its nearest neighbour (6) does not present the same behaviour and presents the greatest RMS mean value, curbing conclusions about an expected smaller vibration at the vehicle's centre. Regarding day 3, there is no greater or lesser tendency for vibration depending on the position in the trainset. Sensor 7, for example, shows greater vibration in sections A (backwards) and B (forwards).

When comparing sections of the same day, it appears that the order of the sensors in terms of magnitude of vibration is approximately the same on a given day. This finding contributes to the conclusion that the sensor-to-sensor variation, i.e., higher or lower noise level from sensor to sensor for hardware and software issues, is relevant to the dispersion of results. Thus, conclusions about tendencies to greater or lesser

vibration depending on position are not possible for this data set.

Finally, similarity coefficients were calculated for the RMS vertical accelerations and summarized in Table 54 and Figures 45 to 47 (boxplots of Pearson correlation, consistency, and total agreement coefficients). In contrast to the differences found in the raw signals, it is not possible to conclude the influence of the sensor arrangement on the greater or lesser similarity of the RMS responses. The high correlations between sensors, even at positions with different vibration signatures (i.e., sensor 5 at the centre section of the coach and sensor 8 over the bogie on day 2 and under speed variation), evidence the prevalence of the sensor-to-sensor variation on the results at this vibration magnitude. The range of variation between sensors on days 2 and 3 is similar to the differences observed on days 1 and 4, whose behaviour is mainly conditioned by sensor-to-sensor variation. Moreover, the difference in relation to the raw signal behaviour evidences the smoothing effect of calculating a statistic on a given section (in this case, RMS within 200-m) sections, which increases correlations between responses apart from differences in signals.

Table 54 - Statistical summary of the correlation coefficients for the RMS frequency-weighted vertical accelerations, individual sensors, Italian tests

Day	Mean / standard deviation Pearson's r			Mean / standard deviation consistency coefficient			Mean / standard deviation total agreement coefficient		
	Const. speed, A	Const. speed, B	Speed var.	Const. speed, A	Const. speed, B	Speed var.	Const. speed, A	Const. speed, B	Speed var.
#1	0.74 / 0.09	0.66 / 0.12	0.66 / 0.08	0.71 / 0.10	0.62 / 0.13	0.65 / 0.09	0.45 / 0.22	0.29 / 0.21	0.31 / 0.21
#2	0.84 / 0.05	0.75 / 0.17	0.85 / 0.05	0.82 / 0.05	0.73 / 0.18	0.82 / 0.06	0.55 / 0.20	0.47 / 0.27	0.69 / 0.14
#3	0.66 / 0.12	0.86 / 0.05	0.72 / 0.10	0.66 / 0.12	0.85 / 0.06	0.72 / 0.10	0.35 / 0.22	0.47 / 0.26	0.59 / 0.13
#4	0.90 / 0.06	0.75 / 0.16	0.81 / 0.09	0.90 / 0.06	0.74 / 0.18	0.74 / 0.13	0.72 / 0.23	0.52 / 0.27	0.63 / 0.18

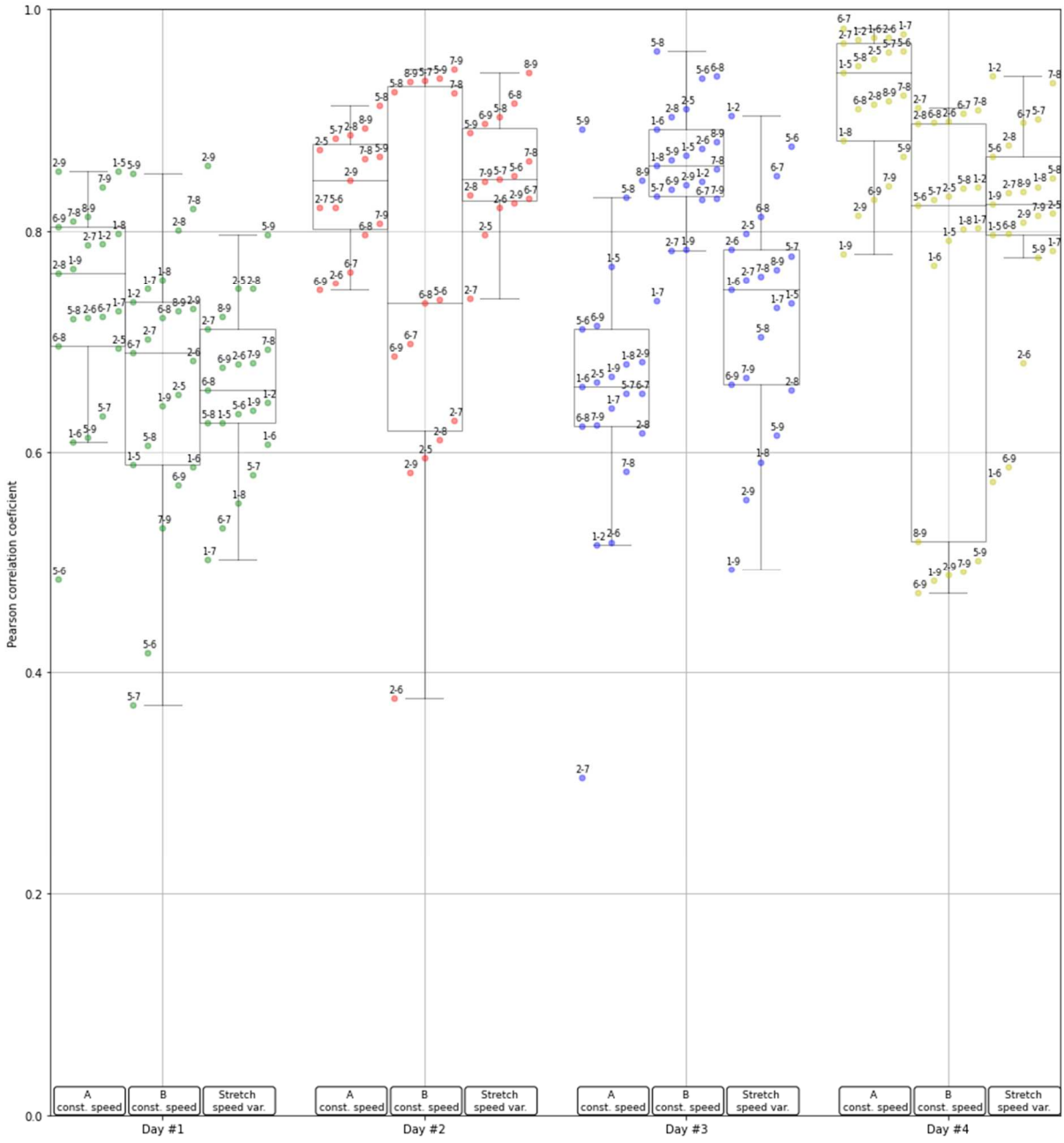

Figure 45 - Boxplot of the Pearson correlation coefficients for the RMS frequency-weighted vertical accelerations

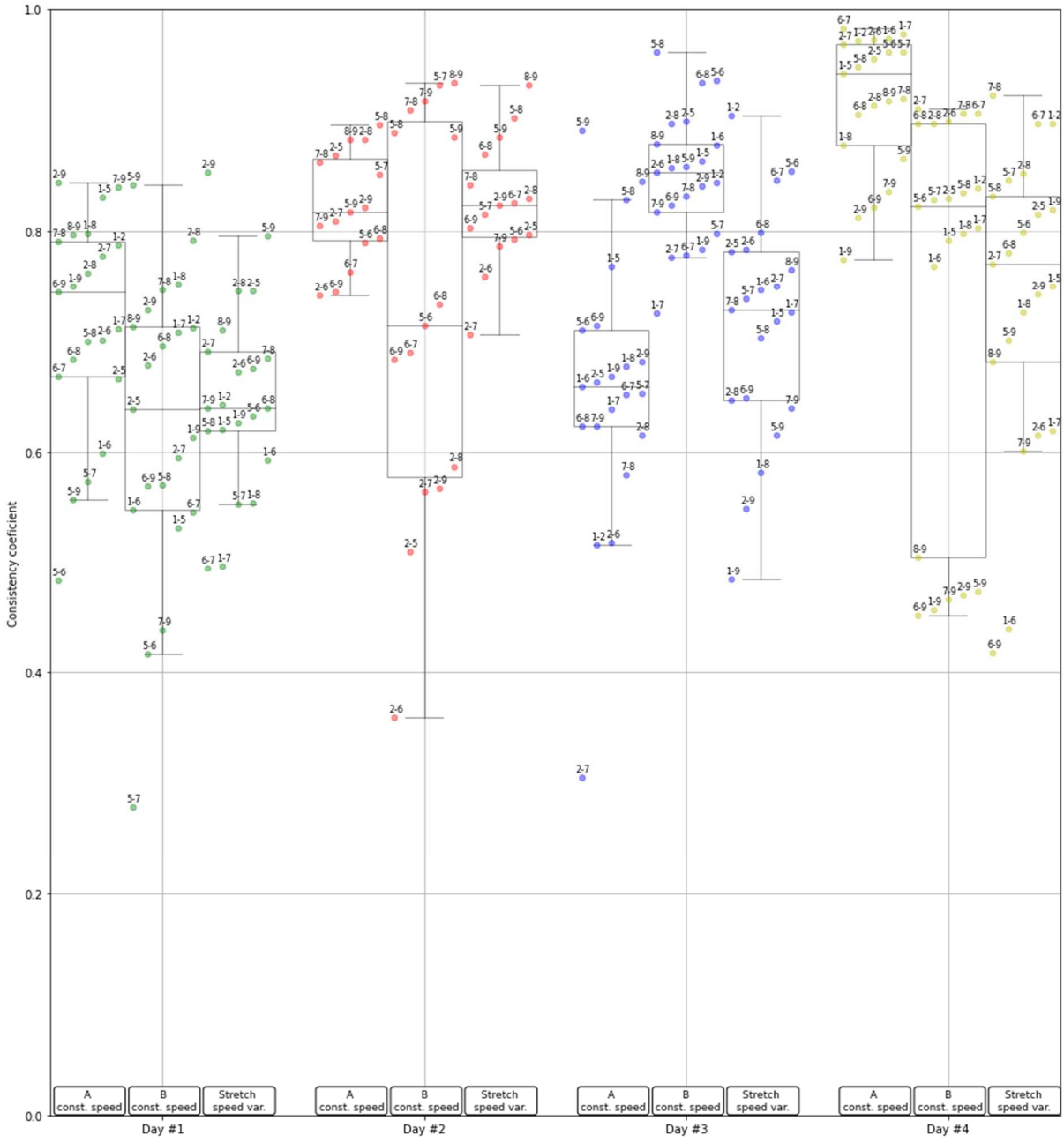

Figure 46 - Boxplot of the consistency coefficients for the RMS frequency-weighted vertical accelerations

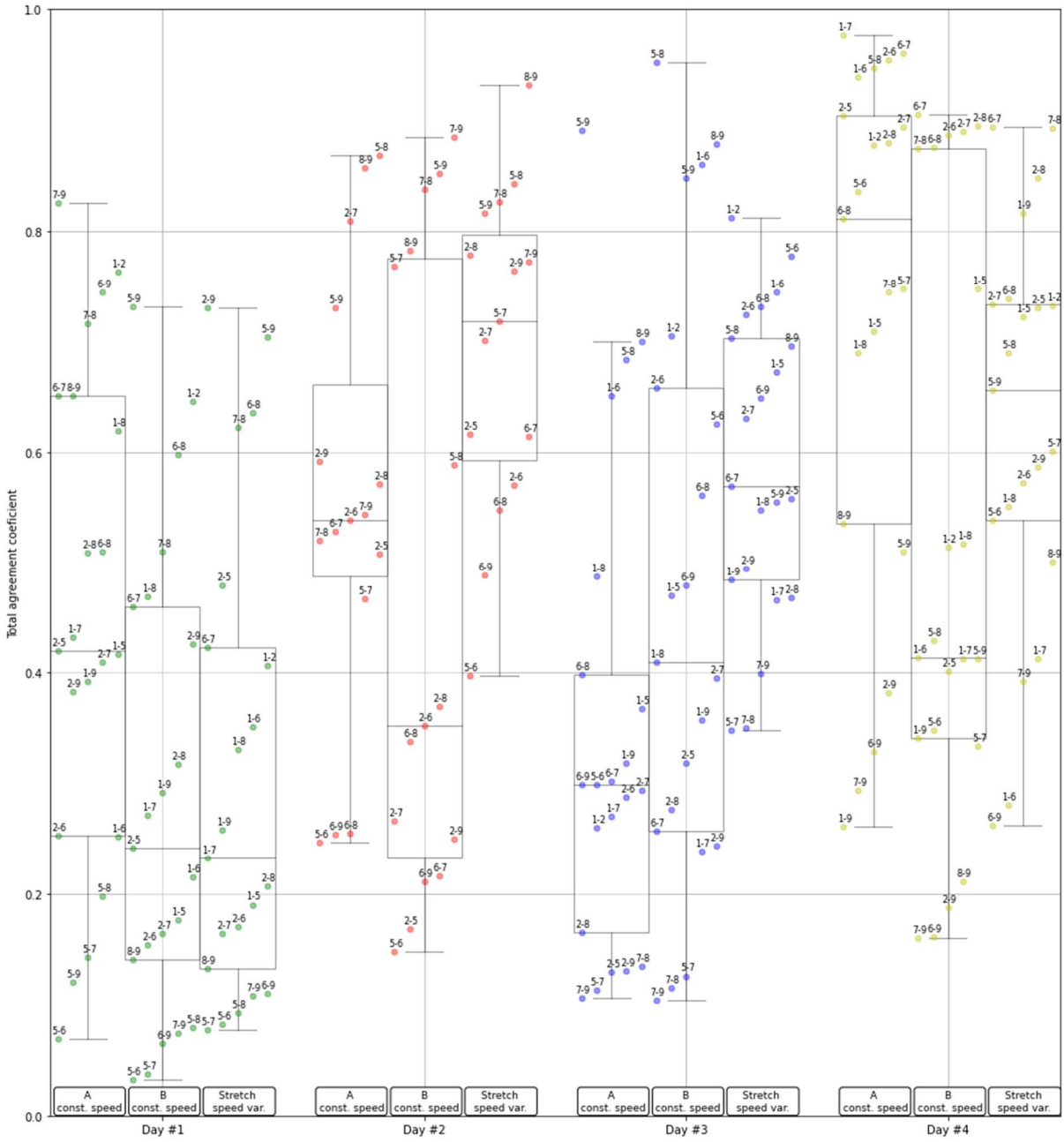

Figure 47 - Boxplot of the total agreement coefficients for the RMS frequency-weighted vertical accelerations

7.3.1.1.3 Correlation with track geometry parameters

Lastly, the correlation analysis with the track irregularities is carried out. This step aims to verify whether there is a higher correlation with the track parameters depending on the sensor position and to evaluate whether there is a degradation in mean signal and mean result performances when considering eventual variation in sensor response due to position apart speed variation. The results are presented in Tables 55 to 62 only for correlation coefficients above 0.3 for the mean signal or the mean result. For day 2, there is no consistent trend of higher correlation with track

parameters for sensors closer to the bogie pivot.

Table 55 - Correlation between sensors responses and track parameters, lateral acceleration, second test day, stretch A

	2	5	6	7	8	9	Mean signal	Mean result
Cross level	0.38	0.31	0.24	0.21	0.18	0.31	0.19	0.31
Longitudinal level, right, D1	0.33	0.31	0.24	0.21	0.2	0.32	0.19	0.30
Twist, 3 m	0.36	0.31	0.23	0.21	0.18	0.29	0.19	0.30
Longitudinal level, left, D1	0.34	0.29	0.23	0.17	0.17	0.31	0.19	0.30

Table 56 - Correlation between sensors responses and track parameters, lateral acceleration, second test day, stretch B

	2	5	6	7	8	9	Mean signal	Mean result
Alignment, right, D1	0.67	0.71	0.74	0.69	0.66	0.68	0.7	0.71
Alignment, left, D1	0.74	0.74	0.71	0.66	0.6	0.65	0.7	0.71
Cross level	0.55	0.63	0.65	0.6	0.57	0.59	0.63	0.62
Twist, 3 m	0.53	0.6	0.6	0.57	0.54	0.58	0.6	0.59
Alignment, left, D2	0.5	0.53	0.56	0.52	0.51	0.52	0.53	0.54
Longitudinal level, right, D1	0.5	0.52	0.5	0.49	0.46	0.49	0.52	0.51
Longitudinal level, left, D1	0.44	0.48	0.47	0.48	0.46	0.49	0.48	0.49
Alignment, left, D3	0.33	0.44	0.42	0.44	0.42	0.49	0.46	0.43
Alignment, right, D3	0.33	0.44	0.42	0.44	0.42	0.49	0.46	0.43
Alignment, right, D2	0.42	0.43	0.47	0.44	0.44	0.44	0.46	0.46
Longitudinal level, left, D2	0.44	0.44	0.46	0.42	0.43	0.46	0.44	0.46
Longitudinal level, left, D3	0.37	0.4	0.4	0.37	0.37	0.42	0.39	0.4
Longitudinal level, right, D3	0.36	0.39	0.39	0.36	0.36	0.4	0.38	0.39
Longitudinal level, right, D2	0.36	0.35	0.37	0.32	0.35	0.36	0.36	0.36

Table 57 - Correlation between sensors responses and track parameters, vertical acceleration, second test day, stretch A

	2	5	6	7	8	9	Mean signal	Mean result
Longitudinal level, right, D1	0.56	0.59	0.5	0.55	0.57	0.57	0.61	0.60
Twist, 3 m	0.56	0.57	0.46	0.56	0.56	0.53	0.58	0.59
Longitudinal level, left, D1	0.56	0.56	0.5	0.55	0.58	0.56	0.58	0.60
Cross level	0.54	0.55	0.44	0.55	0.55	0.52	0.57	0.57
Longitudinal level, right, D2	0.39	0.41	0.34	0.37	0.4	0.38	0.43	0.41
Longitudinal level, left, D2	0.42	0.4	0.36	0.39	0.44	0.4	0.42	0.44
Alignment, right, D1	0.32	0.33	0.25	0.29	0.32	0.32	0.33	0.33

Table 58 - Correlation between sensors responses and track parameters, vertical acceleration, second test day, stretch B

	2	5	6	7	8	9	Mean signal	Mean result
Alignment, left, D1	0.58	0.68	0.53	0.66	0.66	0.64	0.64	0.71
Longitudinal level, left, D1	0.43	0.62	0.45	0.63	0.62	0.62	0.63	0.63
Alignment, right, D1	0.48	0.68	0.41	0.67	0.65	0.69	0.62	0.67
Longitudinal level, right, D1	0.4	0.58	0.4	0.58	0.58	0.58	0.58	0.58
Cross level	0.47	0.61	0.42	0.58	0.6	0.59	0.56	0.61
Gauge	0.54	0.6	0.47	0.61	0.6	0.58	0.55	0.64
Twist, 3 m	0.47	0.58	0.43	0.57	0.58	0.57	0.54	0.6
Alignment, left, D2	0.36	0.49	0.22	0.48	0.44	0.52	0.44	0.47
Alignment, left, D3	0.34	0.41	0.3	0.38	0.39	0.44	0.37	0.43
Longitudinal level, left, D2	0.23	0.41	0.34	0.40	0.39	0.40	0.37	0.4
Alignment, right, D3	0.34	0.41	0.3	0.38	0.39	0.44	0.37	0.43
Alignment, right, D2	0.27	0.38	0.16	0.41	0.36	0.44	0.35	0.38
Longitudinal level, right, D3	0.13	0.44	0.32	0.35	0.35	0.37	0.33	0.36
Longitudinal level, right, D2	0.16	0.34	0.24	0.34	0.27	0.33	0.29	0.31

Table 59 - Correlation between sensors responses and track parameters, lateral acceleration, third test day, stretch A

	1	2	5	6	7	8	9	Mean signal	Mean result
Alignment, left, D2	0.41	0.43	0.51	0.39	0.43	0.42	0.35	0.37	0.45
Alignment, right, D2	0.39	0.43	0.47	0.38	0.39	0.4	0.33	0.36	0.43
Cross level	0.28	0.22	0.18	0.3	0.23	0.24	0.22	0.32	0.24
Longitudinal level, right, D1	0.36	0.3	0.32	0.31	0.3	0.3	0.29	0.31	0.32

Table 60 - Correlation between sensors responses and track parameters, lateral acceleration, third test day, stretch B

	1	2	5	6	7	8	9	Mean signal	Mean result
Longitudinal level, left, D1	0.44	0.47	0.47	0.46	0.36	0.43	0.31	0.45	0.45
Longitudinal level, right, D1	0.44	0.47	0.47	0.46	0.36	0.42	0.31	0.44	0.45
Twist, 3 m	0.34	0.33	0.48	0.38	0.3	0.31	0.34	0.4	0.38
Alignment, left, D2	0.38	0.32	0.43	0.36	0.29	0.30	0.42	0.39	0.37
Cross level	0.34	0.39	0.46	0.38	0.32	0.36	0.36	0.38	0.41
Alignment, right, D2	0.35	0.31	0.42	0.34	0.28	0.28	0.41	0.36	0.36
Alignment, right, D1	0.34	0.45	0.4	0.37	0.38	0.39	0.4	0.36	0.42

Table 61 - Correlation between sensors responses and track parameters, vertical acceleration, third test day, stretch A

	1	2	5	6	7	8	9	Mean signal	Mean result
Longitudinal level, right, D1	0.56	0.61	0.74	0.42	0.55	0.56	0.67	0.64	0.68
Longitudinal level, left, D1	0.56	0.65	0.75	0.46	0.50	0.56	0.70	0.63	0.70
Longitudinal level, left, D2	0.4	0.57	0.54	0.4	0.49	0.48	0.62	0.56	0.60
Longitudinal level, right, D2	0.36	0.56	0.5	0.37	0.45	0.41	0.57	0.50	0.55
Cross level	0.34	0.08	0.29	0.25	0.41	0.28	0.25	0.44	0.30

Table 62 - Correlation between sensors responses and track parameters, vertical acceleration, third test day, stretch B

	1	2	5	6	7	8	9	Mean signal	Mean result
Cross level	0.53	0.60	0.65	0.59	0.54	0.63	0.65	0.61	0.64
Longitudinal level, right, D1	0.57	0.58	0.60	0.55	0.49	0.57	0.55	0.59	0.59
Longitudinal level, left, D1	0.49	0.50	0.53	0.48	0.44	0.48	0.48	0.51	0.51
Twist, 3 m	0.37	0.46	0.54	0.45	0.43	0.49	0.54	0.49	0.51
Alignment, right, D1	0.51	0.54	0.5	0.47	0.45	0.48	0.53	0.48	0.52
Alignment, right, D2	0.35	0.49	0.45	0.4	0.54	0.41	0.37	0.38	0.46
Alignment, left, D2	0.35	0.47	0.43	0.37	0.53	0.39	0.34	0.36	0.44
Alignment, left, D1	0.37	0.39	0.39	0.34	0.38	0.34	0.33	0.30	0.38

Considering the performance of the single metrics calculated for the sensor group, the mean signal performs worse (coefficient equivalent to or below that for the mean result) than the arrangement presented in the validation section, a result expected due to the non-redundancy of the signals. Even in a constant speed section, the mean signal depends on fine alignment in time or space to avoid destructive interference. Furthermore, although the sensors have similar responses regarding RMS, the same is not true for the signal's shape. The mean result, however, proved to be more robust to context variations.

The correlation with track parameters was also calculated for stretches including speed variation on the Italian railway. In addition to the degradation of the relationship between vibration and track parameters, the results illustrated in Tables 63 to 68 enable the identification of the loss of performance of the mean signal, an expected result of the composition of signals different in shape and magnitude due to the influence of speed. In terms of mean response, even if composing results obtained at different speeds, there is reasonable performance concerning the track characterisation. This result is further evidence of the superior robustness of the mean result as an indicator of the sensor group in non-redundant arrangements.

Table 63 - Correlation between sensors responses and track parameters, lateral acceleration, second test day, stretch with speed variation

	2	5	6	7	8	9	Mean signal	Mean result
Longitudinal level, right, D1	0.44	0.49	0.35	0.33	0.37	0.38	0.35	0.43
Longitudinal level, left, D1	0.44	0.50	0.35	0.35	0.34	0.37	0.32	0.42
Cross level	0.37	0.40	0.22	0.24	0.28	0.27	0.25	0.32

Table 64 - Correlation between sensors responses and track parameters, vertical acceleration, second test day, stretch with speed variation

	2	5	6	7	8	9	Mean signal	Mean result
Longitudinal level, left, D1	0.42	0.60	0.40	0.49	0.49	0.46	0.44	0.51
Longitudinal level, right, D1	0.41	0.59	0.40	0.45	0.48	0.46	0.44	0.49
Cross level	0.28	0.44	0.24	0.34	0.31	0.29	0.28	0.33

Table 65 - Correlation between sensors responses and track parameters, lateral acceleration, third test day, stretch with speed variation

	1	2	5	6	7	8	9	Mean signal	Mean result
Longitudinal level, right, D3	0.55	0.52	0.45	0.42	0.39	0.39	0.39	0.49	0.53
Longitudinal level, left, D3	0.55	0.52	0.45	0.42	0.39	0.38	0.38	0.48	0.52
Longitudinal level, left, D2	0.53	0.50	0.38	0.31	0.27	0.24	0.22	0.41	0.42
Longitudinal level, right, D2	0.52	0.51	0.38	0.31	0.26	0.23	0.21	0.41	0.42
Longitudinal level, left, D1	0.48	0.50	0.35	0.30	0.26	0.22	0.21	0.39	0.40
Longitudinal level, right, D1	0.48	0.50	0.33	0.27	0.24	0.21	0.19	0.38	0.38
Cross level	0.45	0.48	0.33	0.27	0.20	0.16	0.15	0.34	0.35

Table 66 - Correlation between sensors responses and track parameters, vertical acceleration, third test day, stretch with speed variation

	1	2	5	6	7	8	9	Mean signal	Mean result
Longitudinal level, right, D3	0.43	0.42	0.42	0.41	0.36	0.35	0.37	0.43	0.45
Longitudinal level, left, D3	0.41	0.41	0.42	0.40	0.35	0.34	0.36	0.41	0.44
Longitudinal level, left, D1	0.35	0.33	0.28	0.20	0.12	0.18	0.13	0.23	0.31
Longitudinal level, right, D1	0.34	0.31	0.27	0.18	0.10	0.16	0.12	0.22	0.30

Table 67 - Correlation between sensors responses and track parameters, lateral acceleration, fourth test day, stretch with speed variation

	1	2	5	6	7	8	9	Mean signal	Mean result
Alignment, left, D1	0.61	0.62	0.60	0.61	0.62	0.63	0.44	0.55	0.61
Alignment, right, D1	0.58	0.59	0.58	0.59	0.60	0.62	0.43	0.53	0.59
Alignment, left, 10 m	0.57	0.59	0.56	0.58	0.58	0.59	0.43	0.51	0.58
Gauge (standard deviation)	0.58	0.58	0.57	0.59	0.59	0.58	0.29	0.57	0.55
Alignment, right, 10 m	0.53	0.54	0.53	0.54	0.55	0.57	0.42	0.47	0.55
Alignment, left, D2	0.47	0.48	0.48	0.48	0.49	0.51	0.16	0.49	0.45
Alignment, right, D2	0.46	0.47	0.46	0.47	0.47	0.50	0.14	0.47	0.43
Cross level	0.40	0.41	0.40	0.40	0.41	0.43	0.20	0.38	0.39

Table 68 - Correlation between sensors responses and track parameters, vertical acceleration, fourth test day, stretch with speed variation

	1	2	5	6	7	8	9	Mean signal	Mean result
Longitudinal level, left, 10 m	0.24	0.47	0.28	0.49	0.45	0.54	0.22	0.54	0.39
Longitudinal level, left, D1	0.21	0.45	0.23	0.47	0.43	0.53	0.18	0.56	0.36
Longitudinal level, total, D1	0.20	0.46	0.20	0.46	0.43	0.53	0.17	0.58	0.35
Longitudinal level, right, 10 m	0.21	0.42	0.19	0.42	0.40	0.48	0.17	0.49	0.33
Longitudinal level, right, D1	0.19	0.42	0.16	0.41	0.39	0.48	0.14	0.52	0.32

7.3.1.2 Tests on CPTM Line 7

For the tests on CPTM Line 7 aboard a TRV and an in-service train, it was not feasible to analyse constant speed stretches as they were short in length. Thus, the results of the comparisons between the sensors reflect the influence of variations in the speed. Thus, this section is dedicated to characterising speed-independent behaviours and reserves a more attentive analysis of the influence of speed for the following section.

For the test aboard the TRV, reference data does not have a timestamp, curbing its direct use in data georeferencing. Thus, the following approach is employed for both trips (TRV and in-service train):

- Firstly, the longitudinal acceleration profiles, whose main components are due to the vehicle accelerations and decelerations, are used to correct synchronisation errors between the sensors. The correction uses the time-lagged cross-correlation, where the lag (time error) is the one that provides the highest correlation between them.

- Map matching is performed to the reference map provided by the CPTM using

devices 1 and 13 (at the extremities). Due to the advantageous position for signal reception, these sensors presented higher availability of GPS data during the test trip. Thus, the track chainage (in km) associated with sensors 1 and 13 at each epoch is obtained, and the arithmetic mean between these values is the track chainage associated with the vehicle centre at each epoch.

- The track chainage associated with each sensor is calculated from the known fixed distance from each sensor to the vehicle centre.
- Linear interpolation was performed to reference intervals without GPS data (either for the inertial sensor samples within the 1-second interval between GPS samples or for the intervals of GPS data unavailability).

7.3.1.2.1 Test aboard the TRV

Regarding the test aboard the TRV, the main goal is to describe the influence of sensor position in relation to the bogie centre. To this purpose, RMS frequency-weighted vertical accelerations were calculated considering three sensor groups: i) front cabin; ii) close to the vehicle's centre; and iii) rear cabin. For each group, the RMS values for the mean signal were also calculated. The results are presented in Figures 48 and 49 for the outward trip as representative of the behaviour also observed on the return trip. The same y-scale was adopted in the graphs in order to allow comparisons between sensor groups and between outward and return trips. The 200-m sections are identified according to their sequence, with increasing numbers from the beginning to the end of the trip. When describing the tests on the CPTM line, **outward trip** stands from trips from *Luz* to *Francisco Morato,* while **return trip** stands for the trips between *Francisco Morato* and *Lapa.* Sensor 3[45] was excluded from the graph, and further calculations and analyses for presenting results with discrepant calculations.

[45] Between the tests performed in Italy (2020) and those performed in Brazil (2022), sensor 3 was reconditioned, recalibrated, and tested, presenting adequate behaviour during tests prior to the CPTM tests. However, the sensor again behaved discrepantly during the test described in this section.

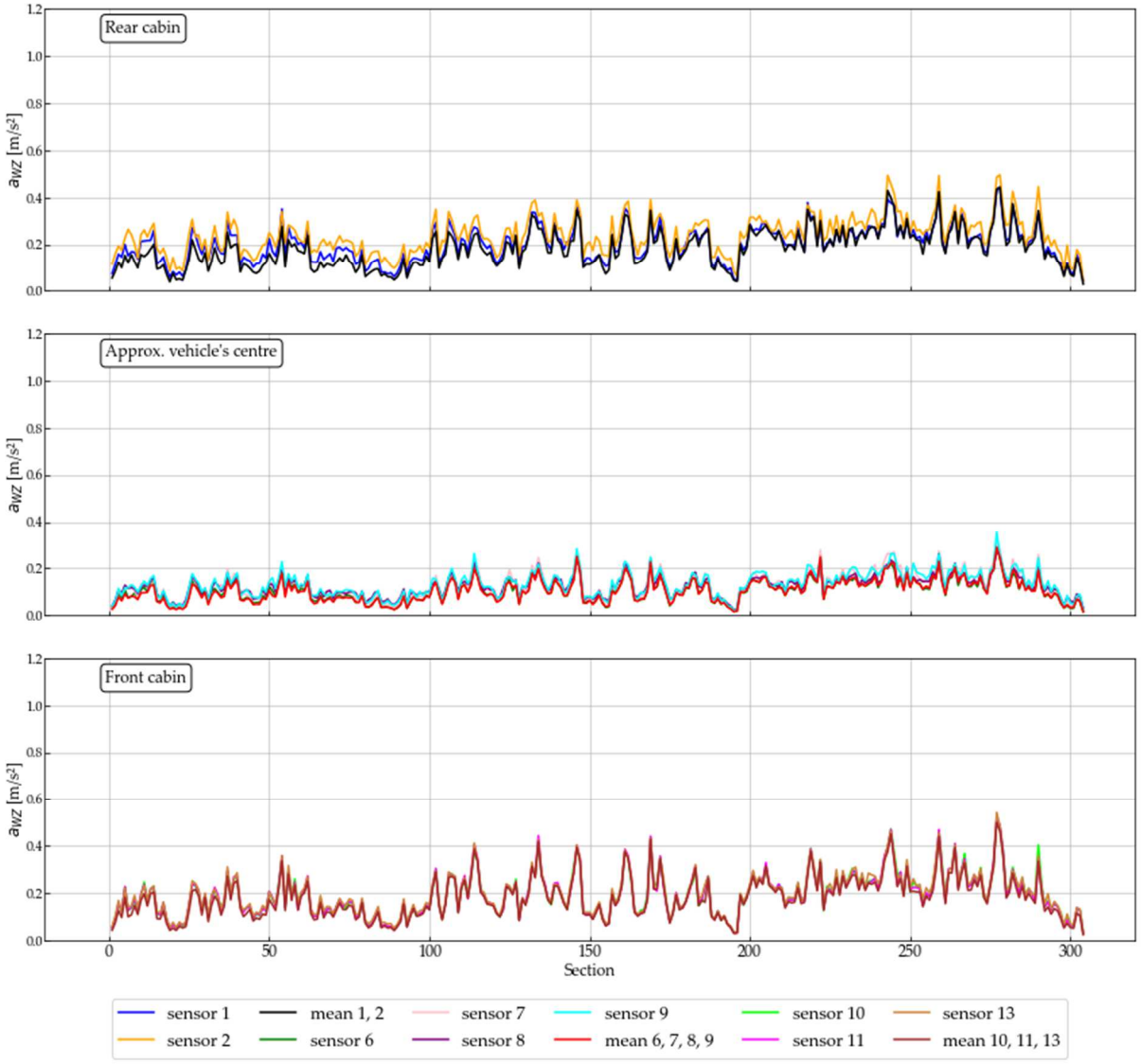

Figure 48 - RMS frequency-weighted lateral acceleration for the outward trip abroad the CPTM TRV

Based on the t-test results, the null hypothesis of equal means for the RMS values for vertical and lateral directions is rejected at 0.05 significance, and the differences found in the magnitude of the sensor responses are statistically significant. Regarding the graphic results, the expected higher vibration in the vertical direction is found, as well as the theoretical higher vibration at the extremities of the vehicle is identified. It is emphasized that even though speeds are lower in the Brazilian tests (mean speed of about 14 m/s), the levels of discomfort identified are considerably higher than those identified in the Italian tests. While the RMS frequency-weighted values for vertical acceleration ranged between 0.2 and 0.6 m/s² in the Italian tests for the same 200-m sections, the values for the Brazilian tests range between 0.2 to 1.2 m/s² due to the class difference between the tracks. This greater magnitude,

therefore, contributes to the clearer distinction of vibration patterns at the ends and at the centre of the vehicle.

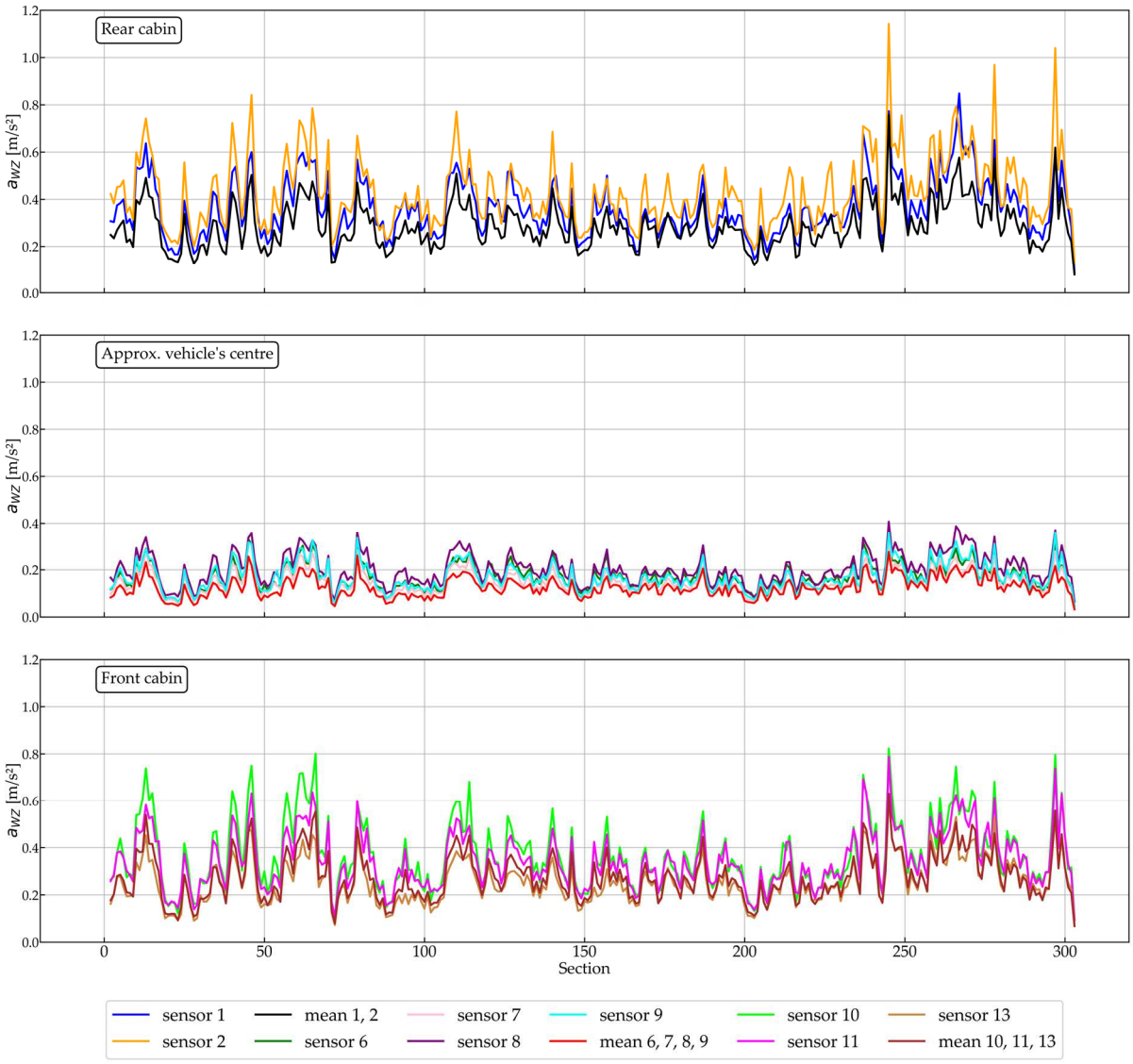

Figure 49 - RMS frequency-weighted vertical acceleration for the outward trip abroad the CPTM TRV

Tables 69 to 71 and 67 present the similarity coefficients between the sensors only for the outward trip as representative. Furthermore, the results are presented only for the vertical accelerations as representative of the behaviour verified for the lateral accelerations. The columns and rows identify the sensors, and those within brackets represent the mean signals for the listed sensors (redundant sensors).

Regarding the sensor group behaviour, the high similarity among the sensors in terms of the shape of the graph is verified by the strong correlation among the results

(average Pearson's coefficient of 0.91 for the sensor population). By way of comparison, it is worth remarking that an average coefficient of 0.82 (vertical acceleration, excluding defective sensors) was obtained for the configuration of the test day on the Italian high-speed network, whose sensor arrangement is the closest to the one adopted for the tests within the CPTM. Moreover, as already verified in the Italian tests, the result from the mean signal is usually lower than those from individual sensors and preserve approximately the same graphical shape, confirming the theoretical noise reduction without considerable loss of information.

Table 69 - Correlation coefficients between sensors for test aboard the CPTM TRV, RMS frequency-weighted vertical acceleration, outward trip

	1	**2**	**[1, 2]**	**6**	**7**	**8**	**9**	**[6, 7, 8, 9]**	**10**	**11**	**13**	**[10, 11, 13]**	**Mean signal**	**Mean result**
1	1	0.85	0.91	0.89	0.91	0.93	0.92	0.89	0.94	0.95	0.92	0.93	0.78	0.97
2	0.85	1	0.97	0.85	0.87	0.88	0.87	0.82	0.9	0.9	0.87	0.91	0.71	0.92
[1, 2]	0.91	0.97	1	0.9	0.91	0.91	0.91	0.88	0.92	0.93	0.92	0.93	0.76	0.96
6	0.89	0.85	0.9	1	0.99	0.94	0.96	0.98	0.89	0.91	0.95	0.92	0.86	0.92
7	0.91	0.87	0.91	0.99	1	0.95	0.97	0.98	0.92	0.94	0.96	0.94	0.85	0.94
8	0.93	0.88	0.91	0.94	0.95	1	0.97	0.95	0.94	0.95	0.95	0.94	0.8	0.96
9	0.92	0.87	0.91	0.96	0.97	0.97	1	0.97	0.94	0.95	0.97	0.95	0.82	0.95
[6, 7, 8, 9]	0.89	0.82	0.88	0.98	0.98	0.95	0.97	1	0.88	0.91	0.96	0.91	0.87	0.89
10	0.94	0.90	0.92	0.89	0.92	0.94	0.94	0.88	1	0.97	0.94	0.98	0.75	0.98
11	0.95	0.90	0.93	0.91	0.94	0.95	0.95	0.91	0.97	1	0.95	0.98	0.79	0.98
13	0.92	0.87	0.92	0.95	0.96	0.95	0.97	0.96	0.94	0.95	1	0.95	0.84	0.95
[10, 11, 13]	0.93	0.91	0.93	0.92	0.94	0.94	0.95	0.91	0.98	0.98	0.95	1	0.86	0.96
Mean signal	0.78	0.71	0.76	0.86	0.85	0.8	0.82	0.87	0.75	0.79	0.84	0.86	1	0.79
Mean result	0.97	0.92	0.96	0.92	0.94	0.96	0.95	0.89	0.98	0.98	0.95	0.96	0.79	1

Table 70 - Consistency coefficients between sensors for test aboard the CPTM TRV, RMS frequency-weighted vertical acceleration, outward trip

	1	2	[1, 2]	6	7	8	9	[6, 7, 8, 9]	10	11	13	[10, 11, 13]	Mean signal	Mean result
1	1	0.83	0.94	0.66	0.67	0.8	0.74	0.58	0.91	0.95	0.9	0.87	0.60	0.97
2	0.83	1	0.85	0.53	0.54	0.66	0.59	0.43	0.9	0.88	0.8	0.75	0.46	0.88
[1, 2]	0.94	0.85	1	0.63	0.64	0.78	0.70	0.55	0.89	0.93	0.87	0.86	0.60	0.96
6	0.66	0.53	0.63	1	0.99	0.92	0.96	0.95	0.55	0.66	0.79	0.85	0.86	0.72
7	0.67	0.54	0.64	0.99	1	0.92	0.97	0.94	0.56	0.68	0.79	0.86	0.85	0.73
8	0.8	0.66	0.78	0.92	0.92	1	0.96	0.87	0.69	0.81	0.89	0.92	0.79	0.86
9	0.74	0.59	0.7	0.96	0.97	0.96	1	0.92	0.63	0.75	0.85	0.9	0.82	0.8
[6, 7, 8, 9]	0.58	0.43	0.55	0.95	0.94	0.87	0.92	1	0.47	0.58	0.72	0.78	0.85	0.63
10	0.91	0.9	0.89	0.55	0.56	0.69	0.63	0.47	1	0.95	0.85	0.8	0.49	0.93
11	0.95	0.88	0.93	0.66	0.68	0.81	0.75	0.58	0.95	1	0.93	0.9	0.60	0.98
13	0.90	0.80	0.87	0.79	0.79	0.89	0.85	0.72	0.85	0.93	1	0.96	0.73	0.95
[10, 11, 13]	0.87	0.75	0.86	0.85	0.86	0.92	0.9	0.78	0.8	0.9	0.96	1	0.80	0.93
Mean signal	0.6	0.46	0.6	0.86	0.85	0.79	0.82	0.85	0.49	0.6	0.73	0.8	1	0.64
Mean result	0.97	0.88	0.96	0.72	0.73	0.86	0.8	0.63	0.93	0.98	0.95	0.93	0.64	1

Table 71 - Total agreement coefficients between sensors for test aboard the CPTM TRV, RMS frequency-weighted vertical acceleration, outward trip

	1	2	[1, 2]	6	7	8	9	[6, 7, 8, 9]	10	11	13	[10, 11, 13]	Mean signal	Mean result
1	1	0.57	0.81	0.17	0.17	0.33	0.22	0.13	0.89	0.94	0.63	0.70	0.13	0.96
2	0.57	1	0.44	0.09	0.09	0.16	0.11	0.07	0.74	0.63	0.3	0.34	0.07	0.55
[1, 2]	0.81	0.44	1	0.22	0.23	0.46	0.29	0.16	0.7	0.79	0.81	0.87	0.12	0.92
6	0.17	0.09	0.22	1	0.98	0.61	0.91	0.87	0.16	0.17	0.37	0.31	0.79	0.18
7	0.17	0.09	0.23	0.98	1	0.63	0.93	0.85	0.17	0.17	0.37	0.32	0.77	0.19
8	0.33	0.16	0.46	0.61	0.63	1	0.79	0.43	0.3	0.32	0.71	0.63	0.41	0.37
9	0.22	0.11	0.29	0.91	0.93	0.79	1	0.71	0.21	0.22	0.48	0.42	0.65	0.24
[6, 7, 8, 9]	0.13	0.07	0.16	0.87	0.85	0.43	0.71	1	0.12	0.13	0.27	0.22	0.83	0.12
10	0.89	0.74	0.7	0.16	0.17	0.3	0.21	0.12	1	0.94	0.56	0.63	0.13	0.88
11	0.94	0.63	0.79	0.17	0.17	0.32	0.22	0.13	0.94	1	0.62	0.7	0.13	0.96
13	0.63	0.3	0.81	0.37	0.37	0.71	0.48	0.27	0.56	0.62	1	0.94	0.28	0.7
[10, 11, 13]	0.7	0.34	0.87	0.31	0.32	0.63	0.42	0.22	0.63	0.7	0.94	1	0.4	0.49
Mean signal	0.13	0.07	0.12	0.79	0.77	0.41	0.65	0.83	0.13	0.13	0.28	0.4	1	0.14
Mean result	0.96	0.55	0.92	0.18	0.19	0.37	0.24	0.12	0.88	0.96	0.7	0.49	0.14	1

Concerning the influence of the sensor position, the result confirms the expected behaviour and a significant difference in vibration magnitude is observed, with greater vibration at the ends of the vehicle compared to the central position. The sensors positioned approximately at the central position presented a graphic result similar in shape to that presented in the extreme positions, as expressed by the correlation coefficients. Nevertheless, the magnitudes are notably lower at the central position, as can be inferred from the total agreement coefficients. Table 72 summarizes this finding and highlights the high concordance between extremities and only moderate concordance between a sensor positioned at the end of the vehicle and one positioned at the centre.

As a general conclusion of the TRV test, it is stated that the responses have the same shape and allow characterization by the identification of peaks (high correlation between all sensors) but have different levels depending on the position in the car (low agreement between centre and extremity). This distinction between centre and extremities is a result not obtained when analysing the tests on the Italian railway. Thus, it can be inferred that these low-cost sensors have sensitivity to describe this expected difference only in the context of greater vibrations as for the Brazilian tests.

Table 72 - Mean concordance coefficients, by sensor, between sensors for test aboard the CPTM TRV, RMS frequency-weighted vertical acceleration, outward and return trip

	Mean concordance coefficient *vs.* sensors at extremities	**Mean concordance coefficient *vs.* sensors at the centre**
1 (extremity)	0.79	0.24
2 (extremity)	0.64	0.14
6 (centre)	0.30	0.86
7 (centre)	0.26	0.83
8 (centre)	0.48	0.73
9 (centre)	0.34	0.89
10 (extremity)	0.81	0.23
11 (extremity)	0.81	0.25
13 (extremity)	0.55	0.51

Regarding the correlation with the track parameters (Tables 73 to 76), sensors at the ends and in the centre show a similar adherence to the track quality. The results are presented for correlation above 0.4 for the mean signal or for the mean result, with the values for ranges D0, D1, D2 and D3 extracted from the raw data provided by CPTM according to EN 13848-1 (COMITÉ EUROPÉEN DE NORMALISATION,

2019). In addition, given the influence of speed variations, a subgroup for speeds above 17 m/s were selected. This threshold is adopted due to its proximity to the maximum speed during the test and the fact that the speed profile varies significantly, curbing the identification of sufficiently long intervals of constant speed contrary to the Italian tests.

With the proposed selection by speed, a relatively homogeneous data set is obtained, which allows an analysis analogous to that performed for stretches at constant speed. This fact is evident in the higher correlation between vibrations and track parameters after this sectioning, Tables 75 and 76. In addition, the mean signal performs better in this context, reinforcing the conclusion that its performance loss is associated with speed variations, as verified in the Italian tests. The high correlation of vertical accelerations with the longitudinal level at short wavelengths corroborates the findings of the previous steps. From Table 76, the moderate correlation with rail wear (high-frequency vibration) is also highlighted, a probable result of the lower performance of the TRV's suspension system.

Table 73 - Correlation between sensors responses and track parameters for lateral accelerations, test aboard the CPTM TRV, outward trip

	1	**2**	**[1, 2]**	**6**	**7**	**8**	**9**	**[6, 7, 8, 9]**	**10**	**11**	**13**	**[10, 11, 13]**	**Mean signal**	**Mean result**
Alignment, right, D1	0.35	0.34	0.35	0.36	0.34	0.33	0.34	0.35	0.39	0.39	0.39	0.4	0.43	0.37
Long. level, right, D0	0.4	0.42	0.4	0.38	0.42	0.37	0.41	0.37	0.42	0.41	0.42	0.38	0.37	0.42

Table 74 - Correlation between sensors responses and track parameters for vertical accelerations, test aboard the CPTM TRV, outward trip

	1	**2**	**[1, 2]**	**6**	**7**	**8**	**9**	**[6, 7, 8, 9]**	**10**	**11**	**13**	**[10, 11, 13]**	**Mean signal**	**Mean result**
Long. level, left, 10 m	0.13	0.13	0.08	0.28	0.26	0.17	0.22	0.31	0.12	0.15	0.24	0.25	0.46	0.13
Long. level, right, 10 m	0.15	0.15	0.09	0.26	0.25	0.16	0.21	0.28	0.13	0.15	0.22	0.24	0.43	0.13
Long. level, left, D1	0.12	0.12	0.08	0.25	0.23	0.15	0.2	0.26	0.12	0.15	0.23	0.24	0.42	0.12
Long. level, right, D1	0.14	0.14	0.09	0.24	0.23	0.15	0.2	0.25	0.14	0.15	0.21	0.23	0.39	0.13
Long. level, left, D0	0.48	0.45	0.4	0.52	0.53	0.49	0.52	0.49	0.5	0.48	0.48	0.49	0.39	0.48
Alignment, right, D1	0.34	0.3	0.34	0.35	0.35	0.36	0.31	0.34	0.37	0.38	0.38	0.38	0.42	0.37

Table 75 - Correlation between sensors responses and track parameters for lateral accelerations and speed above 17 m/s, test aboard the CPTM TRV, outward trip

	1	2	[1, 2]	6	7	8	9	[6, 7, 8, 9]	10	11	13	[10, 11, 13]	Mean signal	Mean result
Long. level, right, 10 m	0.68	0.6	0.63	0.6	0.56	0.62	0.54	0.61	0.65	0.69	0.67	0.69	0.69	0.66
Long. level, left, 10 m	0.67	0.6	0.64	0.61	0.6	0.6	0.5	0.61	0.66	0.69	0.65	0.69	0.69	0.66
Long. level, right, D1	0.66	0.62	0.62	0.58	0.55	0.6	0.53	0.58	0.64	0.67	0.66	0.66	0.67	0.65
Long. level, left, D1	0.63	0.58	0.6	0.58	0.57	0.57	0.47	0.57	0.64	0.67	0.64	0.67	0.66	0.63
Long. level, left, 20 m	0.61	0.49	0.57	0.56	0.51	0.56	0.47	0.57	0.59	0.63	0.6	0.64	0.64	0.59
Alignment, left, D1	0.48	0.48	0.46	0.54	0.52	0.53	0.54	0.53	0.55	0.57	0.57	0.57	0.63	0.55
Long. level, right, 20 m	0.61	0.51	0.57	0.53	0.48	0.54	0.49	0.54	0.58	0.61	0.59	0.62	0.6	0.58
Long. level, left, D2	0.48	0.37	0.45	0.47	0.39	0.46	0.38	0.47	0.48	0.51	0.49	0.53	0.55	0.47
Long. level, left, D0	0.56	0.6	0.55	0.54	0.63	0.55	0.6	0.53	0.6	0.57	0.59	0.55	0.54	0.61
Long. level, right, D2	0.46	0.36	0.42	0.42	0.34	0.41	0.39	0.42	0.45	0.48	0.46	0.49	0.47	0.44
Alignment, left, D2	0.39	0.36	0.36	0.37	0.36	0.36	0.34	0.36	0.4	0.41	0.4	0.42	0.42	0.4
Alignment, right, D1	0.34	0.3	0.34	0.35	0.35	0.36	0.31	0.34	0.37	0.38	0.38	0.38	0.42	0.37

Table 76 - Correlation between sensors responses and track parameters for vertical accelerations and speed above 17 m/s, test aboard the CPTM TRV, outward trip

	1	2	[1, 2]	6	7	8	9	[6, 7, 8, 9]	10	11	13	[10, 11, 13]	Mean signal	Mean result
Long. level, left, 10 m	0.29	0.28	0.26	0.61	0.58	0.4	0.48	0.63	0.24	0.32	0.49	0.52	0.84	0.29
Long. level, right, 10 m	0.31	0.32	0.27	0.6	0.57	0.41	0.47	0.59	0.25	0.32	0.46	0.49	0.81	0.31
Long. level, left, D1	0.28	0.29	0.25	0.58	0.54	0.38	0.44	0.56	0.25	0.33	0.47	0.5	0.80	0.29
Long. level, right, D1	0.34	0.36	0.3	0.58	0.56	0.43	0.48	0.54	0.31	0.38	0.46	0.5	0.76	0.35
Long. level, left, 20 m	0.21	0.17	0.19	0.45	0.41	0.26	0.34	0.45	0.16	0.22	0.34	0.37	0.64	0.20
Long. level, right, 20 m	0.25	0.26	0.24	0.44	0.42	0.31	0.36	0.42	0.21	0.27	0.35	0.38	0.60	0.26
Long. level, left, D0	0.69	0.63	0.59	0.79	0.81	0.75	0.79	0.72	0.7	0.71	0.73	0.74	0.54	0.72
Long. level, right, D0	0.53	0.44	0.44	0.63	0.66	0.59	0.61	0.6	0.54	0.54	0.58	0.6	0.52	0.54
Long. level, left, D2	0.08	0.1	0.09	0.32	0.29	0.13	0.21	0.31	0.06	0.1	0.21	0.24	0.51	0.08
Long. level, right, D2	0.1	0.16	0.11	0.29	0.27	0.18	0.22	0.27	0.09	0.13	0.19	0.22	0.44	0.12
Alignment, left, D1	0.31	0.46	0.4	0.41	0.45	0.34	0.39	0.31	0.39	0.39	0.42	0.42	0.42	0.4
Rail head wear, left	0.51	0.51	0.49	0.56	0.55	0.51	0.57	0.48	0.49	0.55	0.57	0.52	0.42	0.54
Rail head wear, right	0.38	0.48	0.43	0.36	0.41	0.46	0.41	0.28	0.48	0.46	0.42	0.41	0.17	0.47

7.3.1.2.2 Test aboard an in-service train

Three consecutive trips made abroad an in-service train on line 7 with sensors

installed at different coaches and homologous positions (approximately the same distance to the bogie). The comparison, thus, reflects the influence of the differential position of the sensor populations under the speed variations of a regular trip on this line.

The results for vertical accelerations are presented in Figure 50 and Tables 77 to 79 only for the first outward trip as representative results of successive trips. Sensor 6 presented discrepant behaviour and was excluded from the results. The proper analysis of speed influence and the comparison between passages will be reserved for the following sections. There is statistical evidence, resulting from the t-test, that the RMS vertical acceleration results are different in mean at a significance level of 0.05, except for the pairs of sensors 1 and 8, 1 and 9, 3 and 7, and 8 and 9. Nonetheless, it is not possible to state that the variation from one level of vibration to another is due to the difference in position (i.e., if there is a tendency for greater vibration in the rear cars), with disagreements to be attributed to performance variations between sensors and between suspensions. Sensor 13, for example, presented significantly higher vibration than the others for both as the rear (outward trips) and as the front (return trips) sensor.

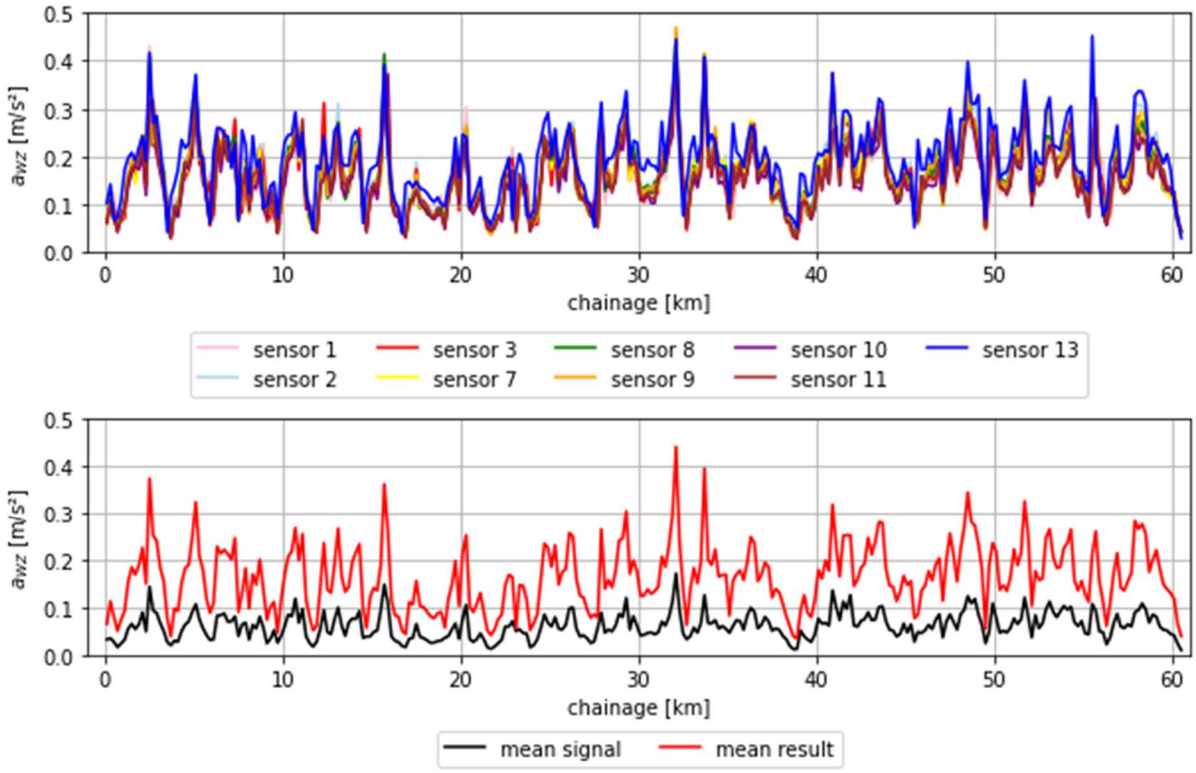

Figure 50 - RMS frequency-weighted vertical accelerations for the first outward trip aboard the CPTM TUE

Table 77 - Pearson's correlation coefficient between the RMS frequency-weighted vertical accelerations, first outward trip aboard the CPTM's TUE

	1	2	3	Mean [2,3]	7	8	9	Mean [8,9]	10	11	Mean [10,11]	13	Mean signal	Mean result
1	1	0.95	0.95	0.92	0.9	0.92	0.92	0.91	0.88	0.88	0.89	0.76	0.89	0.94
2	0.95	1	0.99	0.97	0.96	0.95	0.95	0.92	0.91	0.91	0.92	0.83	0.93	0.97
3	0.95	0.99	1	0.97	0.97	0.95	0.95	0.92	0.91	0.91	0.91	0.83	0.94	0.97
Mean [2,3]	0.92	0.97	0.97	1	0.94	0.91	0.9	0.9	0.87	0.87	0.88	0.80	0.93	0.94
7	0.9	0.96	0.97	0.94	1	0.97	0.97	0.95	0.93	0.93	0.92	0.91	0.95	0.99
8	0.92	0.95	0.95	0.91	0.97	1	0.99	0.97	0.95	0.95	0.94	0.88	0.94	0.99
9	0.92	0.95	0.95	0.9	0.97	0.99	1	0.97	0.95	0.96	0.95	0.88	0.93	0.99
Mean [8,9]	0.91	0.92	0.92	0.9	0.95	0.97	0.97	1	0.93	0.93	0.93	0.86	0.94	0.97
10	0.88	0.91	0.91	0.87	0.93	0.95	0.95	0.93	1	0.99	0.99	0.84	0.91	0.96
11	0.88	0.91	0.91	0.87	0.93	0.95	0.96	0.93	0.99	1	0.99	0.86	0.9	0.96
Mean [10,11]	0.89	0.92	0.91	0.88	0.92	0.94	0.95	0.93	0.99	0.99	1	0.85	0.92	0.96
13	0.76	0.83	0.83	0.80	0.91	0.88	0.88	0.86	0.84	0.86	0.85	1	0.88	0.9
Mean signal	0.89	0.93	0.94	0.93	0.95	0.94	0.93	0.94	0.91	0.9	0.92	0.88	1	0.96
Mean result	0.94	0.97	0.97	0.94	0.99	0.99	0.99	0.97	0.96	0.96	0.96	0.9	0.96	1

Table 78 - Consistency coefficient between the RMS frequency-weighted vertical accelerations, first return trip aboard the CPTM's TUE

	1	2	3	Mean [2,3]	7	8	9	Mean [8,9]	10	11	Mean [10,11]	13	Mean signal	Mean result
1	1	0.93	0.93	0.89	0.9	0.92	0.92	0.91	0.87	0.88	0.88	0.75	0.61	0.94
2	0.93	1	0.99	0.96	0.96	0.95	0.95	0.92	0.89	0.9	0.88	0.85	0.6	0.97
3	0.93	0.99	1	0.96	0.97	0.94	0.95	0.92	0.89	0.9	0.89	0.85	0.62	0.97
Mean [2,3]	0.89	0.96	0.96	1	0.94	0.9	0.9	0.9	0.85	0.85	0.85	0.82	0.66	0.94
7	0.9	0.96	0.97	0.94	1	0.97	0.97	0.95	0.92	0.93	0.91	0.91	0.62	0.98
8	0.92	0.95	0.94	0.9	0.97	1	0.99	0.96	0.93	0.94	0.93	0.88	0.62	0.98
9	0.92	0.95	0.95	0.9	0.97	0.99	1	0.97	0.94	0.96	0.94	0.88	0.61	0.99
Mean [8,9]	0.91	0.92	0.92	0.9	0.95	0.96	0.97	1	0.92	0.93	0.93	0.85	0.68	0.96
10	0.87	0.89	0.89	0.85	0.92	0.93	0.94	0.92	1	0.98	0.99	0.81	0.64	0.95
11	0.88	0.9	0.9	0.85	0.93	0.94	0.96	0.93	0.98	1	0.98	0.83	0.62	0.96
Mean [10,11]	0.88	0.88	0.89	0.85	0.91	0.93	0.94	0.93	0.99	0.98	1	0.82	0.67	0.95
13	0.75	0.85	0.85	0.82	0.91	0.88	0.88	0.85	0.81	0.83	0.82	1	0.56	0.9
Mean signal	0.61	0.6	0.62	0.66	0.62	0.62	0.61	0.68	0.64	0.62	0.67	0.56	1	0.65
Mean result	0.94	0.97	0.97	0.94	0.98	0.98	0.99	0.96	0.95	0.96	0.95	0.9	0.65	1

Table 79 - Total agreement coefficient between the RMS frequency-weighted vertical accelerations, first outward trip aboard the CPTM's TUE

	1	2	3	Mean [2,3]	7	8	9	Mean [8,9]	10	11	Mean [10,11]	13	Mean signal	Mean result
1	1	0.91	0.93	0.84	0.9	0.92	0.92	0.83	0.86	0.88	0.82	0.68	0.22	0.94
2	0.91	1	0.98	0.86	0.95	0.93	0.93	0.79	0.84	0.87	0.77	0.82	0.2	0.96
3	0.93	0.98	1	0.91	0.97	0.94	0.95	0.84	0.87	0.89	0.82	0.78	0.23	0.97
Mean [2,3]	0.84	0.86	0.91	1	0.89	0.86	0.86	0.9	0.84	0.83	0.85	0.63	0.3	0.87
7	0.9	0.95	0.97	0.89	1	0.97	0.97	0.87	0.9	0.92	0.85	0.83	0.23	0.98
8	0.92	0.93	0.94	0.86	0.97	1	0.99	0.89	0.92	0.94	0.87	0.8	0.24	0.98
9	0.92	0.93	0.95	0.86	0.97	0.99	1	0.9	0.93	0.96	0.88	0.8	0.24	0.98
Mean [8,9]	0.83	0.79	0.84	0.9	0.87	0.89	0.9	1	0.89	0.87	0.93	0.62	0.34	0.87
10	0.86	0.84	0.87	0.84	0.9	0.92	0.93	0.89	1	0.98	0.96	0.68	0.26	0.93
11	0.88	0.87	0.89	0.83	0.92	0.94	0.96	0.87	0.98	1	0.94	0.74	0.24	0.95
Mean [10,11]	0.82	0.77	0.82	0.85	0.85	0.87	0.88	0.93	0.96	0.94	1	0.61	0.31	0.87
13	0.68	0.82	0.78	0.63	0.83	0.8	0.8	0.62	0.68	0.74	0.61	1	0.15	0.83
Mean signal	0.22	0.2	0.23	0.3	0.23	0.24	0.24	0.34	0.26	0.24	0.31	0.15	1	0.23
Mean result	0.94	0.96	0.97	0.87	0.98	0.98	0.98	0.87	0.93	0.95	0.87	0.83	0.23	1

In order to verify the adherence of the vibration to the track quality, correlation with the track parameters was calculated (tables 80 and 81) under the same principles as in the previous section (TRV test). Considering the first outward trip, there was no correlation coefficient with track parameters greater than 0.4. Performing the speed sectioning (above 17 m/s), a higher correlation between vibrations and track parameters is obtained. There is a moderate correlation with longitudinal level for both lateral and vertical acceleration as a possible indirect relationship. Regarding the mean signal, its performance loss is evident by the lower correlation with the parameters compared to the mean result. Also not surprisingly, there was no correlation with rail wear as an effect of suspensions for a passenger train, in contrast to what was observed for the TRV.

Table 80 - Correlation between sensors responses and track parameters for lateral accelerations and speed above 17 m/s, test aboard the CPTM EMU, first outward trip

	1	2	3	[1,3]	7	8	9	[8,9]	10	11	[10,11]	13	Mean signal	Mean result
Long. level, left, 10 m	0.52	0.41	0.41	0.46	0.42	0.49	0.5	0.46	0.42	0.43	0.42	0.39	0.44	0.47
Long. level, right, D1	0.52	0.4	0.4	0.45	0.41	0.49	0.5	0.43	0.41	0.41	0.41	0.41	0.43	0.46
Long. level, right, 10 m	0.5	0.42	0.41	0.47	0.42	0.47	0.48	0.42	0.4	0.4	0.4	0.4	0.43	0.46
Long. level, left, D1	0.52	0.41	0.41	0.45	0.42	0.49	0.49	0.45	0.41	0.41	0.41	0.41	0.41	0.46
Alignment, left, D1	0.52	0.47	0.48	0.41	0.47	0.49	0.49	0.4	0.43	0.42	0.42	0.49	0.4	0.5
Long. level, left, 20 m	0.47	0.39	0.39	0.43	0.39	0.44	0.45	0.39	0.35	0.35	0.35	0.37	0.39	0.42

Table 81 - Correlation between sensors responses and track parameters for vertical accelerations and speed above 17 m/s, test aboard the CPTM EMU, first outward trip

	1	**2**	**3**	**[1,3]**	**7**	**8**	**9**	**[8,9]**	**10**	**11**	**[10,11]**	**13**	**Mean signal**	**Mean result**
Long. level, right, 20 m	0.41	0.45	0.42	0.43	0.42	0.44	0.45	0.39	0.47	0.48	0.47	0.36	0.41	0.45
Long. level, right, D2	0.43	0.45	0.42	0.4	0.43	0.46	0.47	0.43	0.44	0.45	0.45	0.38	0.41	0.46
Long. level, left, D2	0.4	0.39	0.37	0.37	0.38	0.42	0.43	0.38	0.42	0.44	0.44	0.33	0.4	0.42
Long. level, right, 10 m	0.41	0.42	0.4	0.38	0.38	0.41	0.42	0.33	0.49	0.49	0.48	0.32	0.39	0.44
Long. level, left, 20 m	0.36	0.39	0.36	0.37	0.36	0.39	0.4	0.34	0.46	0.46	0.46	0.32	0.39	0.41
Long. level, right, D1	0.42	0.4	0.39	0.36	0.37	0.4	0.41	0.33	0.47	0.48	0.47	0.33	0.38	0.42

7.3.2 Number of sensors and sensor weight

Since a collective approach assumes a performance gain with an increase in the number of redundant sensors N when calculating the mean signal from redundant sensors, this thesis assesses for the set validation stretch how the correlation with the reference data behaves depending on N. Therefore, the following procedure is carried out:

- Combination of the 7 sensors into subgroups of x sensors, with x ranging from 1 to 7.
- The mean signal is obtained for each subgroup, and the correlation with the reference sensor A is calculated.
- Finally, the mean correlation for groups with the same number of components is calculated.

In parallel to the variation of the number of sensors, the variation of the weight of each sensor according to the inverse of the variance is also tested, in a classical approach in signal processing. For brevity, the resulting coefficients are graphically presented in Figure 51.

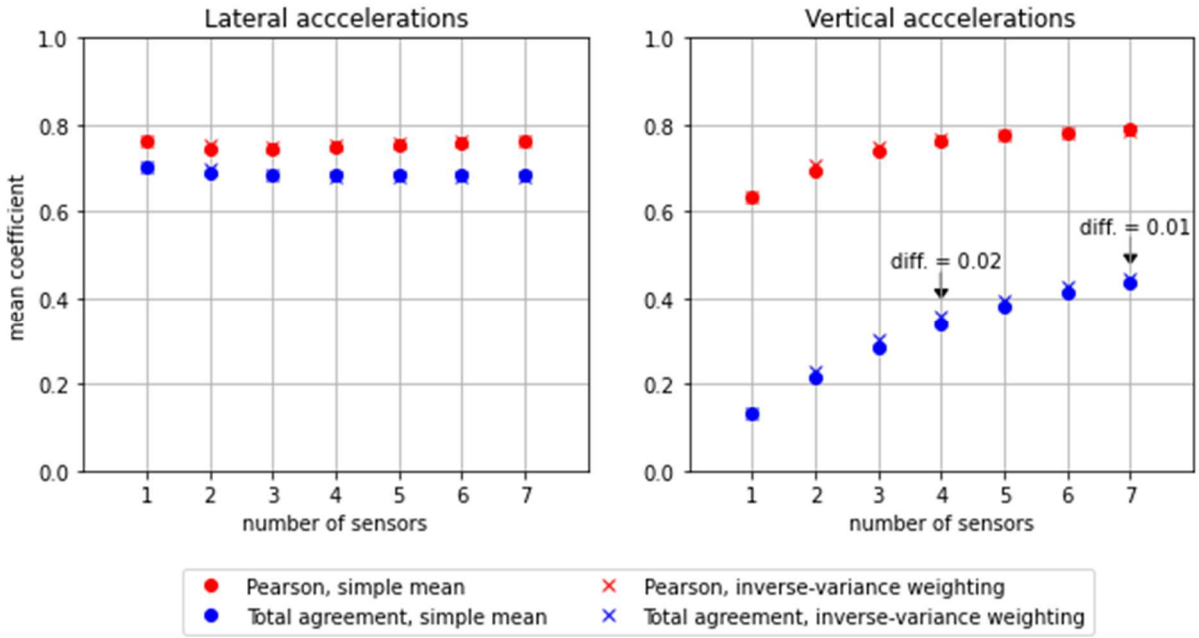

Figure 51 - Correlation and total agreement variation according to the number of sensors for lateral (left) and vertical (right), for validation stretch

Initially, a high gain in correlation and total agreement is verified for the vertical axis when increasing the number of sensors, confirming the positive contribution of noise reduction. Once again, no significant gain is observed in relation to the lateral axis, probably due to the result of lower magnitude and less adherence to lateral irregularities. As for the inverse-variance weighting, little or no contribution is identified. In this respect, it should be noted that a discrepant behaviour of the sensors may occur with a lower or higher variance in relation to the variance of the other sensors, as described in the previous chapter. Moreover, the variations of this parameter occur in very short stretches of instability for this sensor group.

7.3.3 Pitch and roll estimation and gravity compensation

This section compares the performance of two pitch and roll estimation algorithms: a) the proposed accelerometer-free algorithm; and b) the EKF attitude output of the RTIMULib using gyroscope and accelerometer for pitch and roll. Initially, the accuracy of the estimates is assessed in comparison with the reference data for the first seventy kilometres of the validation stretch. Figure 52 compares the two methods with a third calculation from numerical integration of the angular rate (with elevated

integration drift). It can be concluded that the acceleration-based algorithm yields an incorrect estimation for intervals with sustained radial acceleration (horizontal curves), with incidental similar magnitude. When speed is above balance speed, the residual lateral acceleration induces the algorithm to output an inclination in the opposite direction. As an additional example of inaccuracy when using acceleration for this task, Figure 53 compares the proposed and the RTIMULib methods for a section at a speed close to the equilibrium speed. Furthermore, the integration drift is apparent from the simple integration of angular speed in time.

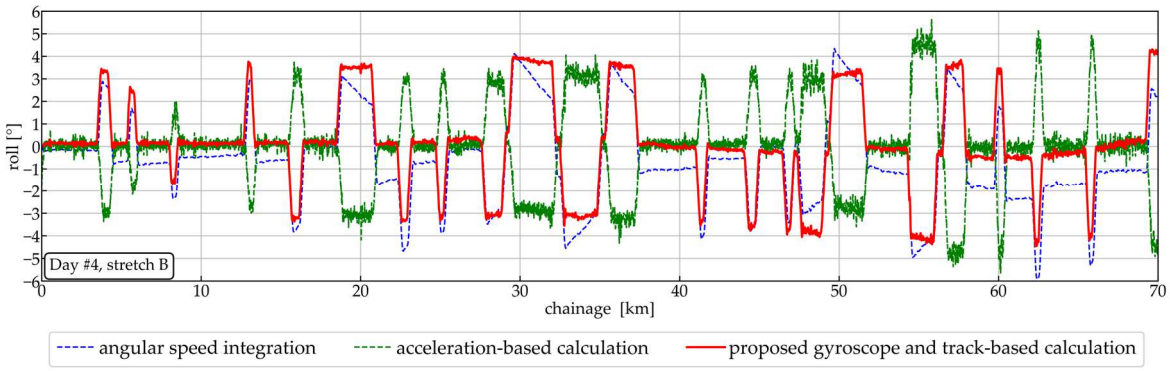

Figure 52 - Roll angle calculation results for the validation stretch

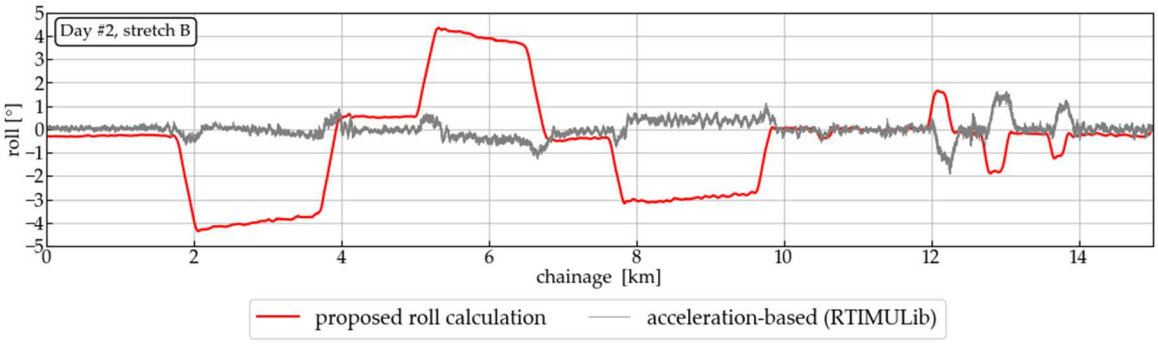

Figure 53 - Roll angle calculations for stretch B, day 2, Italian test week

For the validation stretch, the cant angle α calculated from surveyed superelevation is used as reference data and is related to vehicle roll angle θ through the suspension roll coefficient. As the measures are not the same, only correlation analysis will be carried out rather than absolute error or total agreement. The resulting correlation coefficient of 0.99 for the proposed algorithm reveals the coherence of the measured roll angles minus the factor due to the roll coefficient, as illustrated in Figure 54. For the RTIMULib estimate, a correlation coefficient of -0.55 was obtained. As an additional example of results coherence, absolute roll results for the stretch B on the first test day (Italian test week) were plotted in a Geographic

Information System (Figure 55) to illustrate the concomitance of roll angle and curves and evidence potentiality in curve identification.

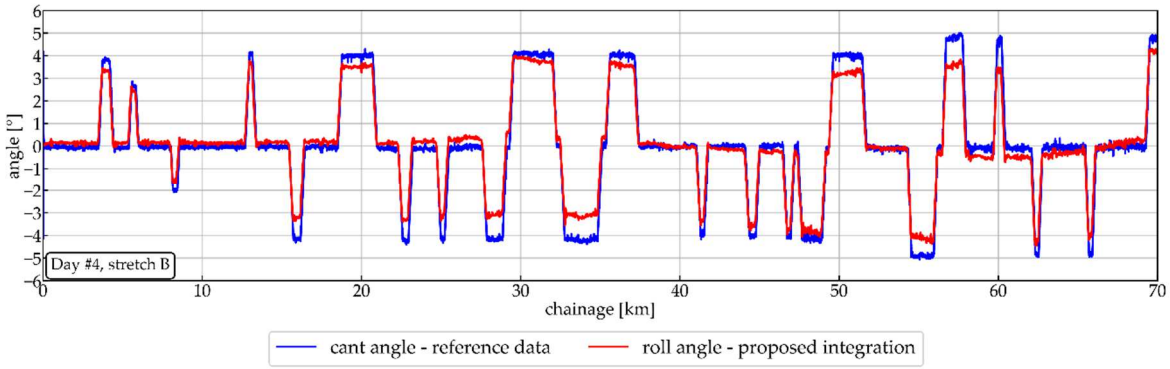

Figure 54 - Estimated roll angle *versus* reference cant angle

Figure 55 - Map of roll angle (absolute values) *versus* track geometry for the first day, stretch B

For pitch angle, the main issue on accelerometer-based result is the noisy result due to the impact of the longitudinal acceleration of the train, as demonstrated in Figure 56 for the validation stretch. For the sake of clarity, only the first 30 km of the stretch are depicted as representative of the overall behaviour. Regarding validation, slope data derived from DGPS- heights (reference position data) does not offer short-wavelength components. Moreover, it does not reflect the influence of the suspension on how the vehicle perceives track slope. However, this slope data enables coherence assessment of the estimated pitch angles, as presented in Figure 56. The coefficient of 0.88 confirms the coherence of the pitch angles calculated by the proposed algorithm, while the coefficient of 0.2 for the RTIMULib estimate highlights the noise impact. Besides validation, Figure 57 also presents the proposed integration without the correction due to pressure transients in tunnels (mapped in

Figure 58) to highlight their impact on pitch estimation and the importance of track-based corrections.

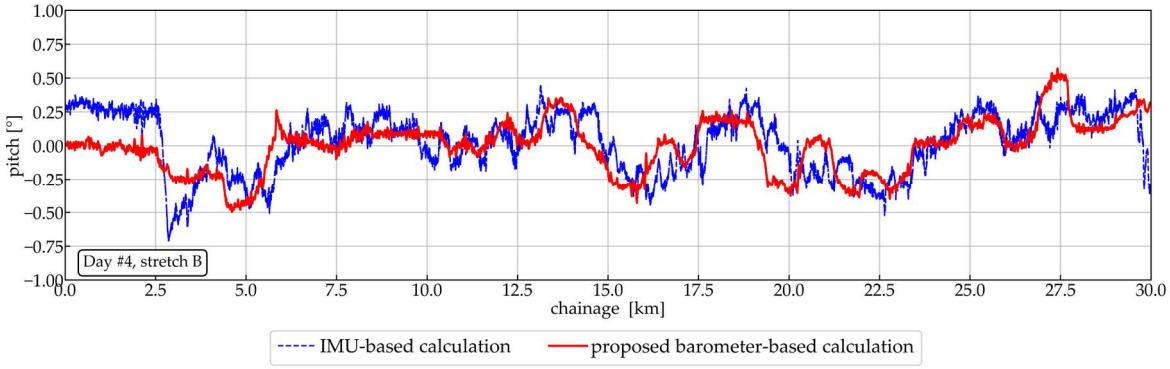

Figure 56 - Roll angle calculation result for the fourth day, stretch B

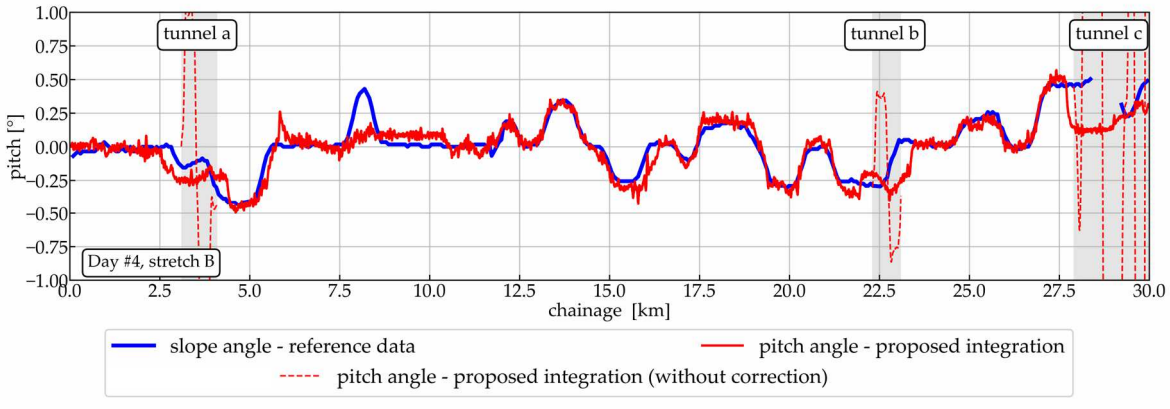

Figure 57 - Estimated pitch angle *versus* reference slope angle

Figure 58 - Satellite image of the tunnels of the fourth day, stretch B: tunnels a (left), b (centre), and c (right) according to the convention of Figure 16. Extracted from Google Maps (GOOGLE MAPS, 2021)

While the proposed algorithms may be more accurate, the actual use of low-cost sensors would benefit from strategies already implemented on smartphones and not

impacted by integration drift or pressure transients. Thus, in order to identify the influence of pitch and roll estimation inaccuracies on gravity compensation and, thus, on the quality of the comfort analysis, a comparison in terms of correlation and total agreement was carried out considering two situations:

- Pitch and roll estimated through EKF by the RTIMULib, identified in this section as a_{EKF} for brevity.
- Pitch and roll estimated through the proposed accelerometer-free algorithm, named a_{corr}.

Tables 82 and 83 show the maximum and the minimum values for the correlation and total agreement in two stages: before and after the frequency-weighting in accordance with ISO 2631. The correlation and total agreement coefficients before the frequency-weighting indicate little similarity between the signals as a natural result of the elevated deviations in roll estimates and gravity compensation. For the vertical acceleration, the high correlation (above 0.99) and total agreement (above 0.95) evidence the reduced influence of macrogeometry on this component. After applying the filters in accordance with ISO 2631 and before the RMS calculation, the correlation between the situations improves substantially for the lateral acceleration (Pearson's r above 0.95; total agreement above 0.94) and remains elevated (above 0.99 for both) for vertical one. This elevated agreement between the two situations agrees with the hypothesis that, at wavelengths shorter than those associated with the track macrogeometry, the information contained in the compensated signals is the same or very close regardless of the method used to estimate pitch and roll.

Table 82 - Comparison in terms of correlation and total agreement between lateral accelerations derived from both techniques, maximum and minimum values

Before frequency-weighting	
Pearson's r correlation coefficient	[0.18, 0.41]
Total agreement coefficient	[0.05, 0.11]

After frequency-weighting	
Pearson's r correlation coefficient	[0.95, 0.97]
Total agreement coefficient	[0.94, 0.97]

Table 83 - Comparison in terms of correlation and total agreement between vertical accelerations derived from both techniques, maximum and minimum values

Before frequency-weighting	
Pearson's r correlation coefficient	[0.99, 1]
Total agreement coefficient	[0.95, 0.99]

After frequency-weighting	
Pearson's r correlation coefficient	[0.99, 1]
Total agreement coefficient	[0.99, 1]

Regarding the agreement with the reference inertial values after the RMS calculation for 200-m sections (Tables 84 and 85), the performance in the two situations is also elevated. Regarding individual sensors, the performance is almost always slightly better when using the a_{corr}, probably influenced by the fact that the proposed algorithm already averages the angular accelerations and pressure readings. Thus, part of the effect of increased accuracy through noise reduction is already incorporated into the individual results, albeit at a reduced magnitude. The difference in terms of mean signals, thus, is virtually null.

Table 84 - Comparison between low-cost sensors and the reference accelerometer (A) considering 200-m RMS frequency-weighted accelerations

Lateral acceleration, Pearson's correlation								
	1	2	5	6	7	8	9	Mean signal
a_{EKF}	.81	.81	.79	.82	.80	.81	.49	.76
a_{corr}	.82	.82	.80	.83	.80	.82	.49	.77

Lateral acceleration, Pearson's correlation								
	1	2	5	6	7	8	9	Mean signal
a_{EKF}	.55	.73	.59	.74	.73	.72	.38	.79
a_{corr}	.55	.73	.60	.73	.73	.72	.38	.79

Table 85 - Comparison between low-cost sensors and the reference accelerometer (A) considering 200-m RMS frequency-weighted accelerations

Lateral acceleration, total agreement								
	1	2	5	6	7	8	9	Mean signal
a_{EKF}	.76	.77	.76	.77	.76	.76	.36	.72
a_{corr}	.77	.78	.79	.78	.76	.77	.35	.71

Lateral acceleration, total agreement								
	1	2	5	6	7	8	9	Mean signal
a_{EKF}	.07	.19	.06	.19	.20	.18	.04	.44
a_{corr}	.07	.20	.06	.19	.21	.18	.04	.44

Thus, considering the limitation in the proposed method when considering gyroscope drift during long intervals and the impact of pressure transients, the more appropriate solution for general cases is the EKF-based RTIMULib solution. At any rate, the use of barometric altimetry has proved worthy in eventual feature matching strategies to be studied in further work.

7.3.4 Position accuracy

As the tests in the Italian railway were performed aboard a train recording vehicle and most of the reference data was obtained concurrently and referenced in time, the more straightforward and accurate georeferencing is based on time matching. However, when proposing a system aboard passenger trains, this reference time will not be available, and the georeferencing is performed through simple map matching, i.e., the association of the GPS coordinates obtained at each sample to the reference track map.

In order to measure the impact of this less accurate georeferencing technique, both methods were applied for a selected stretch of the Italian tests. The entire track between Florence and Rome (about 255 km), inspected on the 4th day of the test week abroad RFI track recording vehicles, was selected owing to the challenging scenario for GPS reception with long tunnel stretches and mountainous relief. From the reference GPS data (inspection train), approximately 14% of the trip was reported

to have signal unavailability (tunnels or significant obstructions) and 15% Horizontal Dilution of Precision (HDOP) factor above 2[46].

It is important to emphasize that the generic georeferencing (i.e., without concomitant reference position data) inside tunnels is performed through linear interpolation considering the chainage at the beginning and the end (fixed points for interpolation). Hence, even small variations in speed result in considerable internal maximum error. In the present case, a maximum error due to interpolation of approximately one kilometre in a tunnel of just over 16 km was identified as a result of speed variation.

Table 86 presents the correlation between the RMS results obtained by applying the georeferencing technique 1 (use of reference position data, T1) and technique 2 (generic map matching, T2). For the mean signal, temporal alignment of the signals was performed (the sensors are redundant), and the resulting signal was georeferenced using the mean position solution among the sensors. The results consider all the Florence-Rome trip, with its speed variations. A substantial influence of the GPS imprecision on results is identified, especially when considering unavailability due to environmental conditions.

Table 86 - Correlation coefficients between the 200-m RMS frequency-weighted accelerations using the two different georeferencing techniques

Sensor	Technique #1 x Technique #2 (all the stretches)	Technique #1 x Technique #2 (non-tunnel stretches)	Technique #1 x Technique #2 (tunnel stretches)
1	0.80	0.94	0.57
2	0.82	0.93	0.62
5	0.88	0.95	0.72
6	0.86	0.93	0.69
7	0.77	0.93	0.51
8	0.85	0.93	0.68
9	0.82	0.95	0.62
Mean	0.91	0.96	0.71

Finally, the correlation with track parameters was also obtained for both techniques for constant speed stretch (subdivision of validation stretch of about 70 km). Table 87

[46] The Dilution of Precision factor is a measure of the instantaneous geometry of the visible satellites, a quality factor for satellite positioning. The factor is inversely proportional to the volume of the polyhedron formed by the receiver-satellite vectors. The larger this volume (and the lower the DOP factor), the better the satellite geometry for the positioning activity. For the Horizontal Dilution of Precision (HDOP), values below 2 are indicative of good geometry regarding horizontal position (HOFMANN-WELLENHOF; LICHTENEGGER; WASLE, 2008).

presents only the five most correlated track geometry features to illustrate the influence of the georeferencing technique. From this comparison, it is deduced that the influence on the results is of medium importance, with technique 2 always worse than the use of reference position data. Moreover, using an average position of the group of sensors merely slightly reduces the inaccuracy since the systematic errors dependent on the scenario for signal reception are not removed. At any rate, it should be noted that the smaller proportion of tunnels and obstructions for this stretch (HDOP greater than 2 for 11% of the time, signal unavailability 7% of the time) and the constant speed favours the generic map matching technique.

Table 87 - Correlation coefficients between track parameters and RMS frequency-weighted results using the two different georeferencing techniques

	Sensor 1		**Sensor 2**		**Sensor 5**		**Sensor 6**		**Sensor 7**		**Sensor 8**		**Sensor 9**		**Mean**	
	T1	T2	T1	T2	T1	T2	T1	T2	T1	T2	T1	T2	T1	T2	T1	T2
Long. level, left, D1	0.69	0.66	0.87	0.83	0.73	0.66	0.85	0.80	0.89	0.85	0.85	0.82	0.39	0.38	0.89	0.86
Long. level, right, D1	0.70	0.66	0.82	0.76	0.72	0.66	0.84	0.77	0.84	0.79	0.81	0.77	0.26	0.24	0.85	0.81
Long. level, left, 10 m	0.69	0.66	0.86	0.82	0.72	0.70	0.89	0.84	0.88	0.84	0.84	0.81	0.27	0.27	0.90	0.87
Long. level, right, 10 m	0.69	0.65	0.81	0.75	0.71	0.68	0.83	0.77	0.83	0.78	0.80	0.76	0.30	0.28	0.82	0.79
Long. level, total	0.69	0.65	0.77	0.76	0.67	0.67	0.79	0.78	0.78	0.78	0.80	0.78	0.24	0.23	0.81	0.80

7.3.5 Speed variation

From the approximate quadratic influence of speed on trains vibration measurements, as well as the intended indirect use of comfort results in track characterization, this section aims to characterize how the speed variations degrade both the relationship between sensors (when installed in different positions) and the relationship between measured comfort and track parameters. Thus, the following analyses will be considered:

- Characterisation of constant speed stretch by the definition of a speed variance threshold
- Description of the influence of speed variation on the relationship between sensors' responses when installed in different positions.

- Description of the influence of speed variation on the relationship between vibration levels and track parameters.

Initially, the characterization of the constant speed for indirect track monitoring purposes is performed. For this purpose, a 5-km moving window was defined and the following values were calculated within it: a) mean correlation between the RMS acceleration values and the longitudinal level (left, range D1, the parameter with the highest correlation); and b) standard deviation of the speed. The representative graphs are depicted in Figure 59. The strong negative correlation (-0.79) between the two parameters and the rapid decrease of r for a small increase of std reveals the high influence of speed variations on the speed of the road. From this graph, a limit standard deviation of about 1.5 m/s yield is suitable for the definition of stretches without significant degradation of the track-vibration relationship.

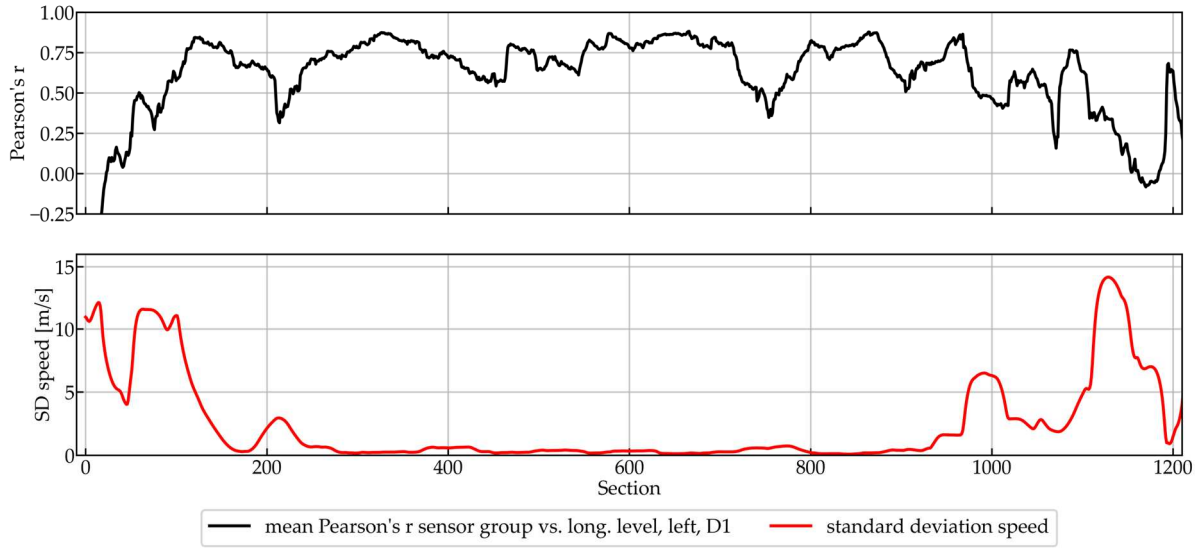

Figure 59 - Graphic description of the influence of speed variance in the correlation between vibrations and longitudinal level (left, D1)

From the established models, it is possible to describe the relationship between accelerations a and speed v as approximately quadratic for a given level of track irregularity C , the (i.e, $a \approx C \cdot v^2$, with expected deviations due to the nonlinear influence of suspensions). Thus, regarding the influence of speed variation on the relationship between sensors' responses when installed in different positions, the following ratios can be calculated: a) the RMS acceleration ratio between sensors i and j ($a_{RMS,i}/a_{RMS,j}$) at a given section, and b) the speed ratio between sensors i and j (v_i/v_j) at a given section. Considering C a constant property for each section, the

relationship between the ratios should be approximately quadratic and, thus, the relationship between $a_{RMS,i}/a_{RMS,j}$ and $(v_i/v_j)^2$ should be approximately linear (more apparent on a scatter plot). This procedure was adopted for two datasets:

- Florence-Rome stretch, day 4 of test week on the Italian railway network. The sensor i is the mean signal for the sensor group, while the sensor j is the reference sensor A. By selecting the mean and the reference signals, as well as getting the speed from reference data, the influence of the sensor inaccuracies is reduced. Moreover, a subset considering only non-constant speed stretches is selected to reduce the influence of sensors' variation.

- The first round trip aboard an in-service train on CPTM Line 7 for the entire sensor set. As the variation in speed between immediate sensors close is smaller, a subset is created only for differences between sensors 1 and 13. Between the extremes, greater variations in speed and vibration are expected, and the result tends to be less disturbed by the sensors' low quality and elevated variance.

Additionally, the datasets were sectioned to exclude low speeds, given the known loss of performance of inertial methods in describing track parameters in such conditions. The limit values of 8.5 m/s and 12 m/s were adopted for the Italian and Brazilian tests, respectively. The scatterplots for the variables $a_{RMS,i}/a_{RMS,j}$ and $(v_i/v_j)^2$ are presented in Figures 60 and 61. The total plots confirm that the most significant proportional variations in speed, which occur at low speeds, is not quadratically related to the acceleration ratios. Nevertheless, for the subgroup without low speeds, a moderate linear relationship between $a_{RMS,i}/a_{RMS,j}$ and $(v_i/v_j)^2$ can be identified, with expected deviation due to the nonlinearities in the suspension system and the variances in the sensor population. Thus, it can be concluded that the very low-cost sensors (considering both the acceleration gathered by the IMU and the speed estimates obtained from GPS receivers) allow a reasonable description of the vehicle dynamics, consistent with the behaviour expected from the models.

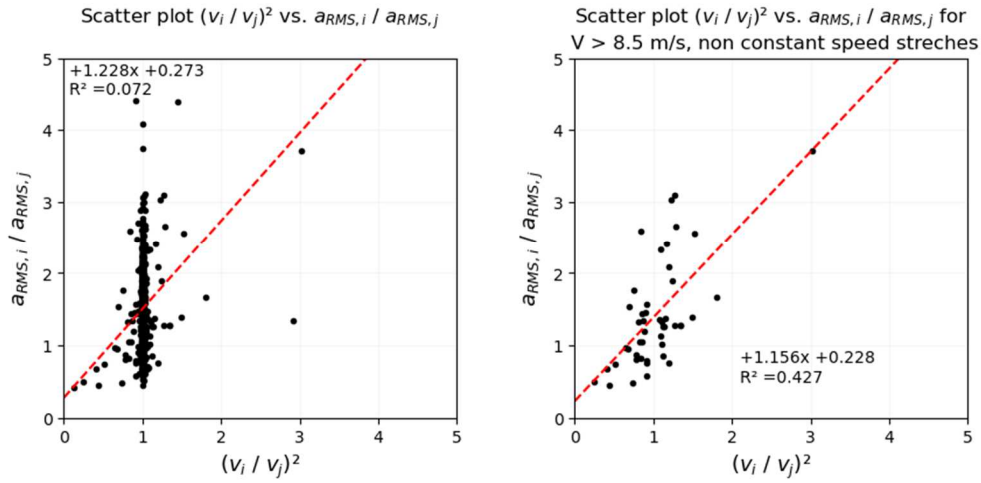

Figure 60 - Scatter plots of $(v_i/v_j)^2$ versus $a_{RMS,i}/a_{RMS,j}$ for all the dataset (left), and for data with speeds above 8.5 m/s in non-constant speeds stretches (right), Italian test.

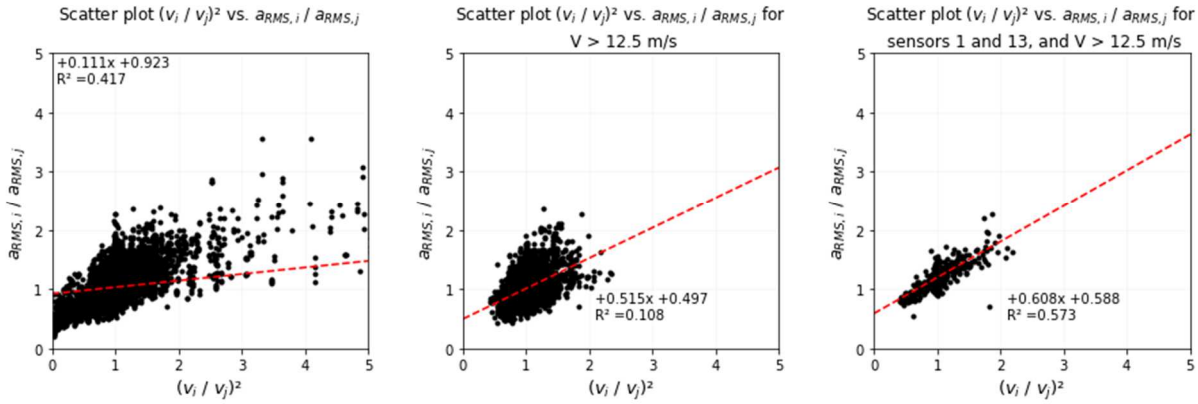

Figure 61 - Scatter plots of $(v_i/v_j)^2$ *versus* $a_{RMS,i}/a_{RMS,j}$ for all the dataset (left), data for speeds above 12.5 m/s (centre), and considering only sensors 1 and 13 with speeds above 12.5 m/5 (right), CPTM test.

Based on the ability of the sensors to reasonably describe the influence of speed on vibrations, this thesis assesses strategies for handling acceleration and speed data to extract information associated with track quality. The following approaches are proposed: a) weighting by the square of the speed (RMS/v²); and b) sectioning the data by speed intervals, allowing comparisons between more similar data. The results are presented in Table 88 in terms of correlation with longitudinal level, left, range D1. The comparisons between the coefficients demonstrate that the gain in the weighted approach exists but is of limited effect. It is also found that even evaluation in terms of speed intervals does not result in improved correlations and, in the case of the last interval (56 m/s < v < 70 m/s), even worsens the result as an effect of the imprecision in the speed estimation. Since there is a predominance of a long

constant speed stretch and higher speeds for this interval, the original data already presents high correlation. Even though the speed intervals are wide, some improvement over the zero scenario (first row of Table 88) would be expected, in which only very low speeds are excluded.

Table 88 - Correlation between RMS frequency-weighted acceleration values (original and weighted by the square of the speed) and longitudinal level (Left, D1) for day 2 of the Italian test week

		1	2	5	6	7	8	Mean signal
v > 8.5 m/s	RMS	0,08	0,29	0,11	0,23	0,16	0,29	0,37
	RMS/v²	0,30	0,39	0,34	0,38	0,27	0,38	0,38
8.5 m/s < v < 28 m/s	RMS	0,08	0,28	0,23	0,36	0,22	0,31	0,34
	RMS/v²	0,13	0,26	0,24	0,31	0,20	0,30	0,31
28 m/s < v < 42 m/s	RMS	0,02	0,31	0,08	0,26	0,08	0,24	0,41
	RMS/v²	0,13	0,51	0,25	0,45	0,18	0,41	0,60
42 m/s < v < 56 m/s	RMS	0,09	0,32	0,36	0,54	0,18	0,45	0,63
	RMS/v²	0,10	0,29	0,35	0,56	0,17	0,42	0,61
56 m/s < v < 70 m/s	RMS	0,62	0,83	0,64	0,84	0,75	0,79	0,87
	RMS/v²	0,57	0,82	0,62	0,80	0,67	0,78	0,84

7.4 REPEATABILITY ANALYSES

This section evaluates the ability of the proposed collective technique to yield reliable and consistent results on successive passages aboard the same (or very similar) vehicle and on the same line. Thus, the repeatability analysis will consider the following datasets:

- Two successive passages on a stretch of the Rome Metro Line C concerning three round trips between *Giardinetti* and *Pantano* stations.
- Three successive passages on CPTM Line 7, concerning three round trips between *Luz* and *Francisco Morato* stations.

7.4.1 Rome Metro Line C

In this section, **outward trip** stands for trips from *Torre Nova* to *Pantano*, while **return trip** stands for the trips between *Pantano* and *Giardinetti*. The outward trip starts from *Torre Nova* due to problems in the GPS position fix between *Giardinetti* and *Torrenova* during the first outward trip.

Firstly, in order to verify whether the measurement conditions were similar for the successive trips considering vehicle characteristics and speed profile. With regard to the vehicle, the tests were carried out in a metro line with a homogeneous vehicle fleet and possible marginal variations considering differences in maintenance and occupancy between trains.

Regarding speed, a comparison between the GPS speed profiles obtained during the different passages is conducted (Figure 62). Concerning this aspect, it is important to perform the total agreement analysis in the space domain since occasional operational differences (e.g., due to braking or long stop in a given station) distort the whole speed curve in the time domain even though the speed obtained for all other sections is consistent with the other passages. As a result, the total agreement coefficient obtained for outward trips is 0.95, and for return trips is 0.96.

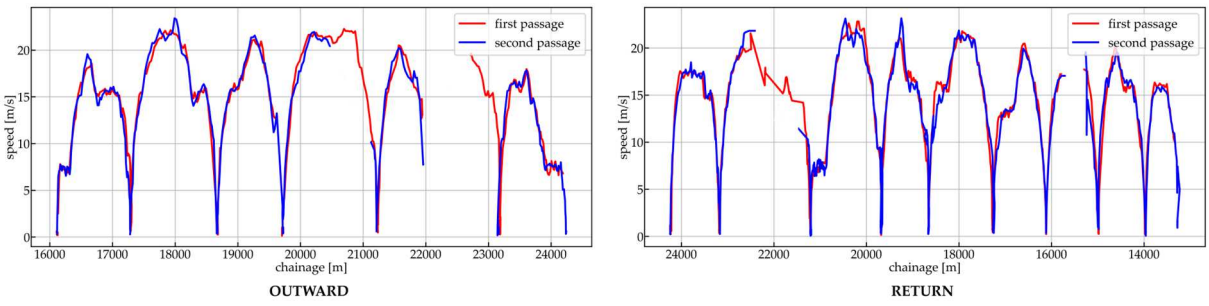

Figure 62 - Speed profiles for the test trips on the Metro Roma Line C

Before the repeatability analysis, a graphic presentation of the comparison of the results between sensors is conducted to order to characterize the group behaviour (Figures 63 and 64). Sensor 6 presented discrepant behaviour and was excluded from the mean signal calculation, while sensor 7 results are not adherent due to higher noise problem.

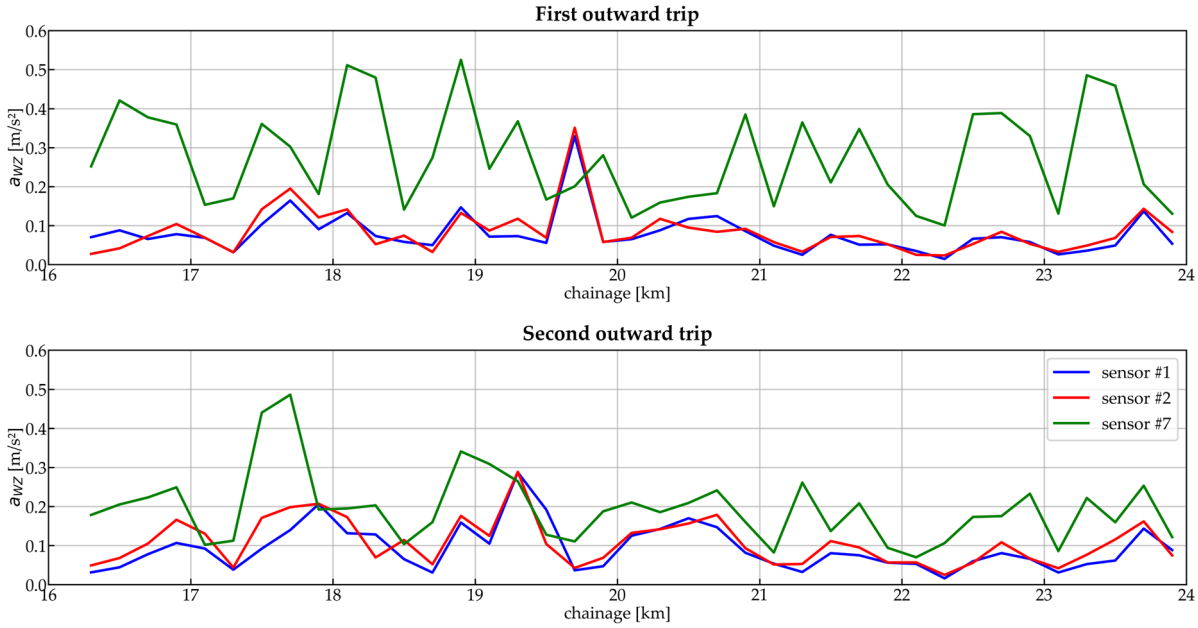

Figure 63 - RMS frequency-weighted vertical accelerations for the outward trips on Line C

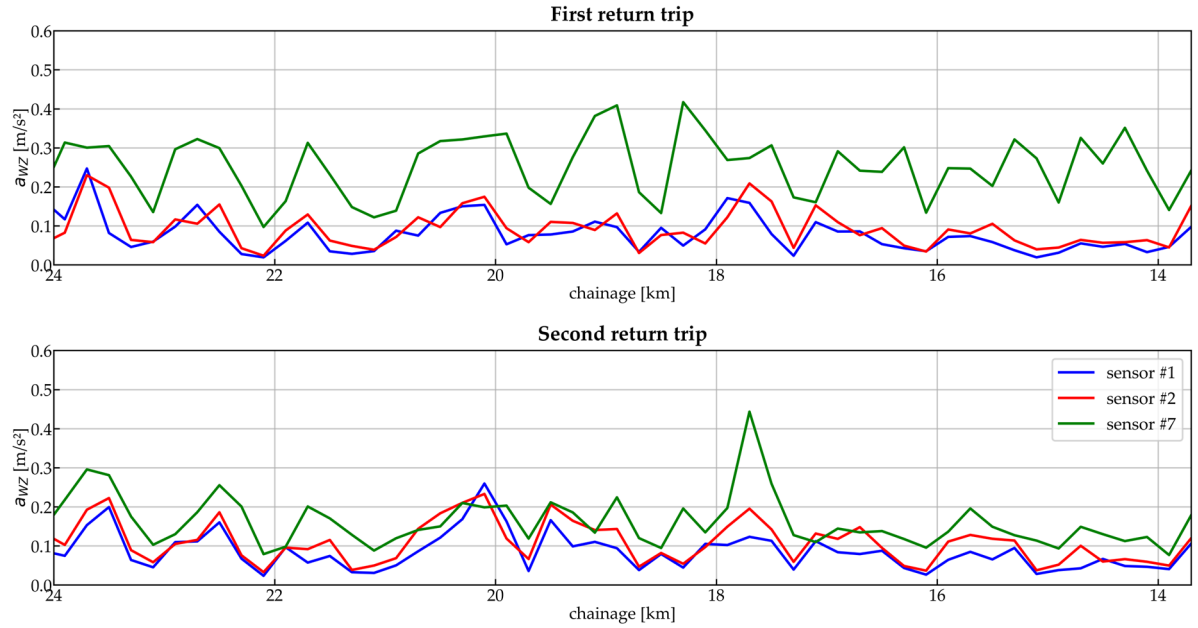

Figure 64 - RMS frequency-weighted vertical accelerations for the return trips on Line C

The comparison between the successive passages is performed in terms of total agreement (Table 89) and is depicted in Figure 65. Sensors 1 and 2 outperformed sensor 7 with moderate to high agreement between return passages, as was assumed from group behaviour in the previous graph. However, the coefficients regarding the outward trips indicate lower agreement, which may be explained by the

mismatch at the peak identified between kilometres 19 and 20, associated with GPS unavailability at the Borghesiana station. The remotion of the corresponding stretches resulted in remarkable changes in the coefficient for the outward passages, resulting in moderate to strong agreement, result resented in Table 90. The individual and collective (considering the mean signal for 1 and 2) results showed to be statistically consistent in successive passages, with weaknesses to be credited to the positioning system inaccuracy and eventual unavailability.

Table 89 - Total agreement coefficient between successive passages on Line C

		Outward trips					Return trips				
		First passage					First passage				
		1	2	Mean [1,2]	7		1	2	Mean [1,2]	7
Second passage	1	0.24	0.3	0.25	0.29	Second passage	1	0.61	0.7	0.67	0.54
	2	0.32	0.41	0.35	0.34		2	0.77	0.83	0.82	0.77
	Mean [1,2]	0.3	0.37	0.32	0.33		Mean [1,2]	0.77	0.82	0.82	0.71
	7	0.07	0.18	0.13	0.47		7	0.42	0.42	0.44	0.46

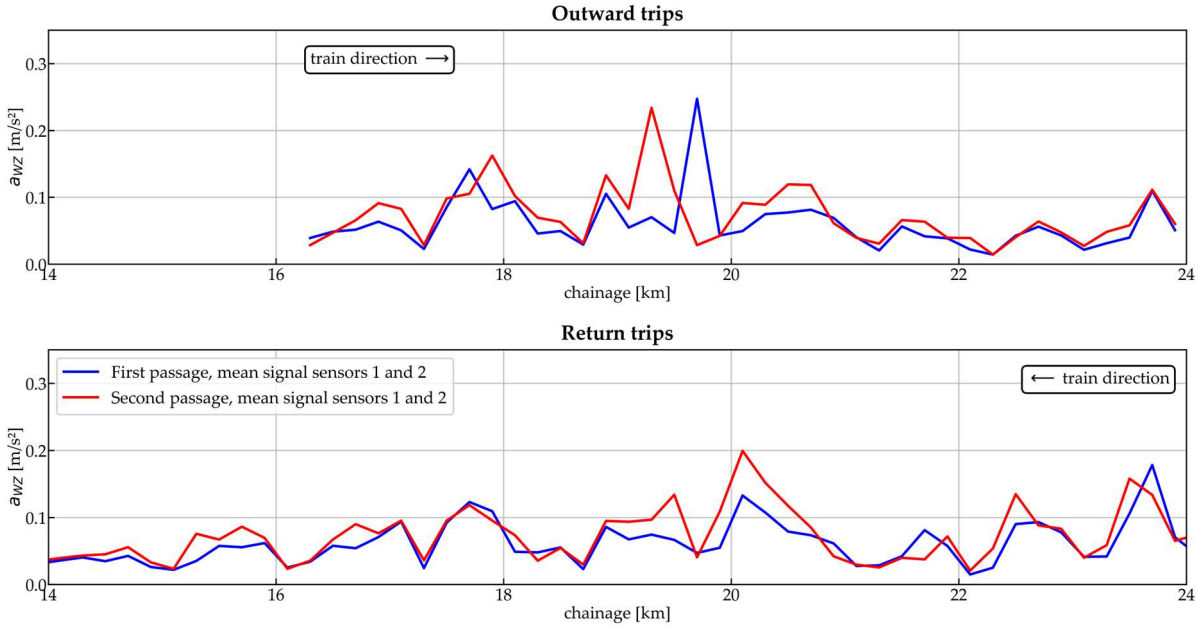

Figure 65 - Comparison between the successive passages on Line C

Table 90 - Total agreement coefficient after removing underground stretches from outward trips

		Outward trips					Return trips				
		First passage					First passage				
		1	2	Mean [1,2]	7		1	2	Mean [1,2]	7
Second passage	1	0.82	0.79	0.27	0.22	Second passage	1	0.61	0.7	0.67	0.54
	2	0.74	0.78	0.25	0.30		2	0.77	0.83	0.82	0.77
	Mean [1,2]	0.79	0.81	0.37	0.34		Mean [1,2]	0.77	0.82	0.82	0.71
	7	0.07	0.18	0.11	0.47		7	0.42	0.42	0.44	0.46

7.4.2 CPTM Line 7

For the repeatability analysis on CPTM Line 7, the calculations applied for Line C were replicated considering three successive passages. Firstly, the comparison between the speed profiles (Figure 66) developed during each test trip resulted in the total agreement coefficients presented in Table 91. The low correlation regarding the third return trip was expected since the train was not operating in passenger service on the last return trip to return directly to the Lapa yard.

Table 91 - Total agreement coefficient for the speed profiles of the successive passages, tests on CPTM Line 7

Outward trip				Return trip			
	1st	**2**nd	**3rd**		**1**st	**2**nd	**3rd**
1st	1	0.79	0.80	**1st**	1	0.62	0.24
2nd	0.79	1	0.79	**2nd**	0.62	1	0.34
3rd	0.80	0.79	1	**3rd**	0.24	0.34	1

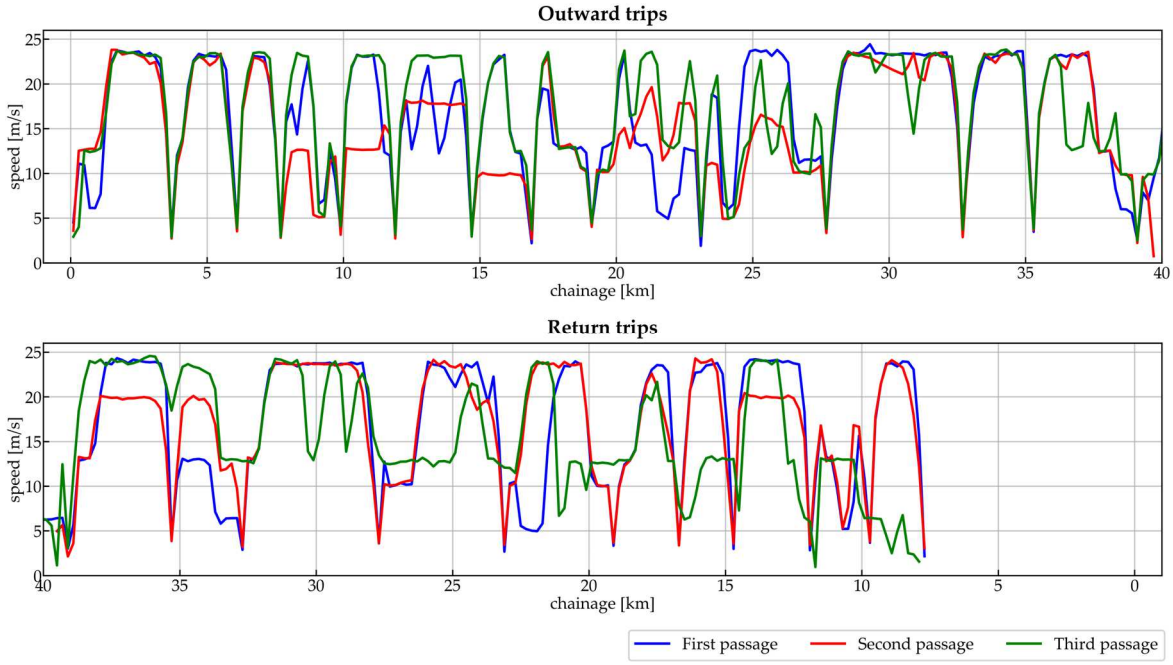

Figure 66 - Speed profiles of the successive passages, tests on CPTM Line 7

The RMS results are depicted in Figures 67 and 68, where the strong agreement between sensors in the same trip is identifiable and compatible with the coefficients presented in section 7.3.3. The comparison between successive passages is graphically presented in Figure 69, with apparent higher coherence between outward trips. For return trips, the stretch between Lapa and Luz stations is not considered since it was not part of the third return trip.

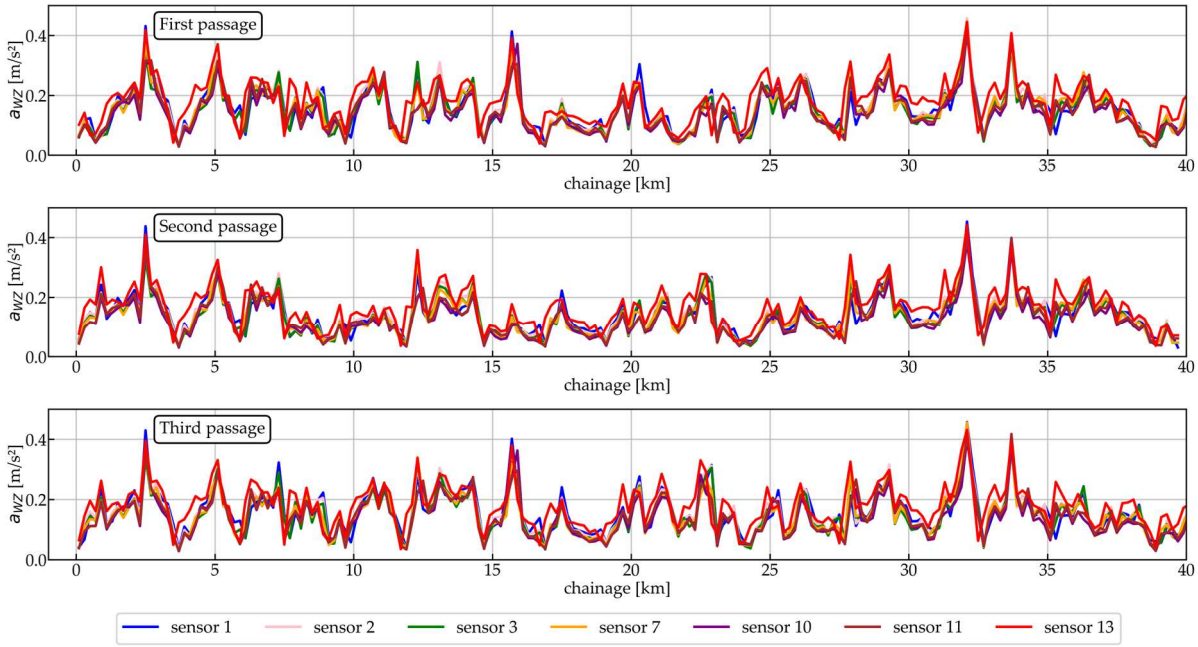

Figure 67 - RMS frequency-weighted vertical accelerations for the outward trips on CPTM Line 7

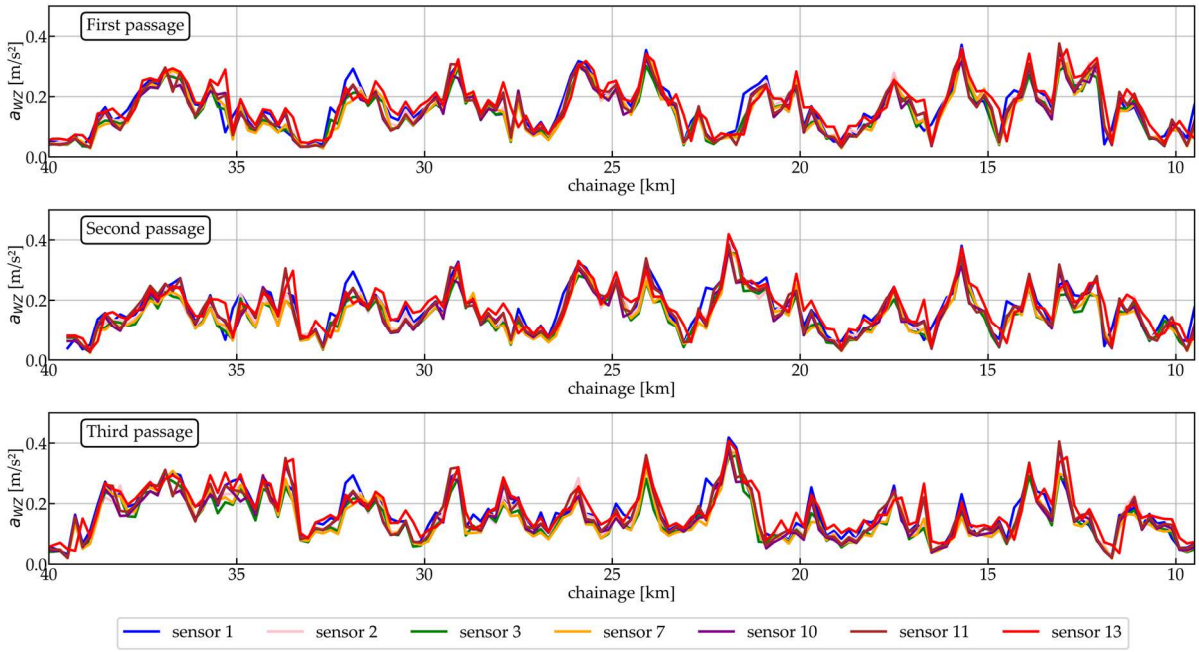

Figure 68 - RMS frequency-weighted vertical accelerations for the return trips on CPTM Line 7

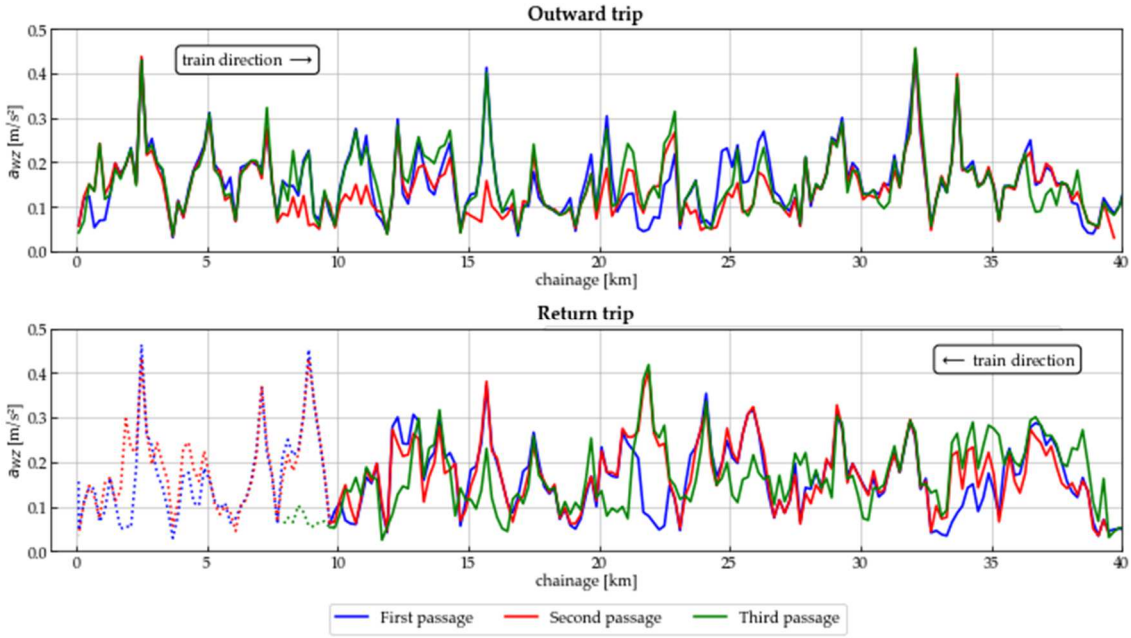

Figure 69 - Comparison between successive passages for the three round trips on CPTM Line 7

Moreover, the repeatability analysis is performed through the total agreement coefficients presented in Tables 93 to 98. By comparing the mean coefficients for successive trips and for sensors on the same trip (Table 92), it can be noted that the variations cannot be attributed exclusively to the sensors variations, but mainly to variations in the measurement conditions. The moderate to high coefficients for the outward trips reflect the potential consistency of the very low-cost sensor when the monitoring conditions are favourable, i.e., when the speed profiles agree. However, the substantial loss of coherence due to variations in speed (even minor ones, such as those between passages 1 and 2) in return trips demonstrates the fragility of the eventual use of the data to characterize the track quality when subjected to the speed profile of real trips and its possible operational changes. Thus, apart from operational variations, the consistency of the set of consumer-grade sensors in the train vibration monitoring is validated.

Table 92 - Mean total agreement coefficient for the sensor group, successive passages on CPTM Line 7

Outward trip				Return trip			
	1st	**2**nd	**3rd**		**1**st	**2**nd	**3rd**
1st	0.90	0.70	0.79	**1st**	0.94	0.74	0.25
2nd	0.70	0.91	0.77	**2nd**	0.74	0.93	0.46
3rd	0.79	0.77	0.90	**3rd**	0.25	0.46	0.92

Table 93 - Total agreement between the first outward trip and the second outward trip

		First passage													
		1	2	3	[2,3]	7	8	9	[8,9]	10	11	[10,11]	13	Mean signal	Mean result
Second passage	1	0.77	0.74	0.72	0.65	0.7	0.69	0.69	0.61	0.63	0.67	0.59	0.61	0.16	0.72
	2	0.76	0.78	0.75	0.68	0.75	0.73	0.73	0.62	0.66	0.7	0.6	0.68	0.16	0.76
	3	0.76	0.79	0.78	0.71	0.77	0.74	0.75	0.65	0.68	0.72	0.63	0.67	0.17	0.77
	[2,3]	0.68	0.71	0.74	0.74	0.72	0.7	0.7	0.7	0.68	0.67	0.68	0.52	0.23	0.71
	7	0.73	0.76	0.75	0.68	0.78	0.75	0.76	0.66	0.69	0.73	0.64	0.7	0.17	0.77
	8	0.73	0.73	0.72	0.65	0.74	0.74	0.75	0.65	0.68	0.72	0.63	0.67	0.17	0.75
	9	0.73	0.74	0.73	0.66	0.75	0.75	0.76	0.66	0.7	0.74	0.65	0.68	0.17	0.76
	[8,9]	0.68	0.66	0.69	0.68	0.7	0.71	0.72	0.71	0.7	0.7	0.69	0.54	0.21	0.7
	10	0.7	0.7	0.7	0.66	0.71	0.73	0.73	0.66	0.74	0.76	0.69	0.6	0.17	0.74
	11	0.7	0.72	0.71	0.65	0.72	0.73	0.74	0.64	0.73	0.77	0.67	0.64	0.16	0.75
	[10,11]	0.69	0.69	0.71	0.7	0.72	0.73	0.74	0.71	0.77	0.77	0.75	0.56	0.21	0.74
	13	0.51	0.55	0.52	0.44	0.58	0.55	0.56	0.45	0.48	0.54	0.43	0.72	0.1	0.58
	Mean signal	0.21	0.2	0.22	0.27	0.23	0.24	0.24	0.32	0.25	0.23	0.3	0.14	0.7	0.22
	Mean result	0.74	0.76	0.74	0.67	0.75	0.74	0.75	0.64	0.69	0.74	0.64	0.7	0.16	0.77

Table 94 - Total agreement between the first outward trip and the third outward trip

		First passage													
		1	2	3	[2,3]	7	8	9	[8,9]	10	11	[10,11]	13	Mean signal	Mean result
Third passage	1	0.86	0.83	0.83	0.75	0.82	0.83	0.83	0.8	0.76	0.77	0.72	0.65	0.2	0.84
	2	0.85	0.87	0.87	0.78	0.86	0.86	0.86	0.81	0.79	0.81	0.74	0.72	0.19	0.87
	3	0.83	0.85	0.87	0.8	0.87	0.85	0.85	0.83	0.79	0.81	0.76	0.69	0.21	0.86
	[2,3]	0.71	0.72	0.78	0.83	0.77	0.74	0.74	0.82	0.74	0.72	0.79	0.52	0.3	0.75
	7	0.78	0.81	0.83	0.75	0.86	0.85	0.85	0.82	0.79	0.81	0.76	0.73	0.2	0.85
	8	0.78	0.79	0.8	0.72	0.83	0.85	0.85	0.82	0.79	0.81	0.76	0.7	0.2	0.84
	9	0.78	0.79	0.81	0.71	0.83	0.84	0.85	0.82	0.79	0.81	0.76	0.7	0.2	0.84
	[8,9]	0.69	0.68	0.73	0.73	0.75	0.75	0.76	0.82	0.75	0.74	0.78	0.54	0.27	0.74
	10	0.72	0.75	0.77	0.72	0.8	0.8	0.81	0.81	0.84	0.84	0.83	0.61	0.22	0.81
	11	0.73	0.77	0.78	0.7	0.81	0.81	0.82	0.79	0.83	0.85	0.8	0.66	0.2	0.82
	[10,11]	0.68	0.7	0.74	0.73	0.77	0.76	0.77	0.81	0.82	0.8	0.84	0.55	0.26	0.76
	13	0.58	0.62	0.6	0.48	0.67	0.69	0.69	0.6	0.59	0.63	0.53	0.82	0.12	0.68
	Mean signal	0.19	0.19	0.21	0.26	0.22	0.22	0.22	0.28	0.23	0.22	0.28	0.14	0.82	0.21
	Mean result	0.8	0.82	0.83	0.74	0.85	0.86	0.86	0.82	0.81	0.83	0.77	0.73	0.2	0.86

Table 95 - Total agreement between the second outward trip and the third outward trip

		Second passage													
		1	2	3	[2,3]	7	8	9	[8,9]	10	11	[10,11]	13	Mean signal	Mean result
Third passage	1	0.82	0.79	0.83	0.78	0.81	0.78	0.8	0.79	0.76	0.77	0.76	0.61	0.23	0.81
	2	0.81	0.86	0.88	0.82	0.87	0.83	0.84	0.81	0.79	0.82	0.78	0.68	0.22	0.86
	3	0.78	0.81	0.86	0.83	0.85	0.8	0.81	0.82	0.79	0.81	0.8	0.63	0.25	0.83
	[2,3]	0.7	0.73	0.79	0.83	0.79	0.74	0.75	0.81	0.75	0.74	0.79	0.55	0.31	0.76
	7	0.74	0.79	0.83	0.79	0.86	0.8	0.82	0.82	0.77	0.8	0.78	0.67	0.25	0.82
	8	0.72	0.74	0.78	0.74	0.81	0.79	0.8	0.81	0.78	0.8	0.79	0.62	0.25	0.79
	9	0.71	0.73	0.78	0.73	0.81	0.78	0.8	0.81	0.77	0.8	0.79	0.62	0.25	0.79
	[8,9]	0.62	0.62	0.69	0.72	0.72	0.69	0.71	0.79	0.71	0.71	0.78	0.5	0.35	0.69
	10	0.66	0.69	0.74	0.74	0.76	0.73	0.75	0.78	0.81	0.81	0.84	0.55	0.28	0.75
	11	0.69	0.72	0.76	0.72	0.79	0.76	0.78	0.78	0.82	0.84	0.83	0.6	0.25	0.79
	[10,11]	0.61	0.61	0.68	0.71	0.7	0.67	0.69	0.75	0.75	0.75	0.82	0.48	0.33	0.68
	13	0.66	0.72	0.72	0.61	0.78	0.75	0.76	0.67	0.67	0.71	0.62	0.85	0.15	0.77
	Mean signal	0.16	0.16	0.18	0.21	0.19	0.18	0.18	0.23	0.19	0.18	0.23	0.12	0.84	0.17
	Mean result	0.76	0.79	0.83	0.79	0.85	0.81	0.83	0.82	0.81	0.83	0.81	0.67	0.24	0.84

Table 96 - Total agreement between the first return trip and the second return trip

		First passage													
		1	2	3	[2,3]	7	8	9	[8,9]	10	11	[10,11]	13	Mean signal	Mean result
Second passage	1	0.78	0.75	0.72	0.61	0.74	0.8	0.8	0.7	0.77	0.78	0.73	0.68	0.16	0.78
	2	0.72	0.77	0.74	0.64	0.76	0.8	0.79	0.74	0.77	0.77	0.74	0.71	0.17	0.78
	3	0.7	0.76	0.76	0.68	0.79	0.79	0.78	0.78	0.77	0.77	0.76	0.68	0.19	0.78
	[2,3]	0.62	0.7	0.73	0.73	0.75	0.71	0.7	0.82	0.71	0.69	0.74	0.59	0.25	0.71
	7	0.68	0.73	0.73	0.65	0.77	0.77	0.77	0.76	0.76	0.76	0.75	0.69	0.19	0.76
	8	0.72	0.74	0.72	0.61	0.75	0.8	0.8	0.73	0.78	0.78	0.74	0.71	0.17	0.78
	9	0.72	0.74	0.71	0.6	0.75	0.79	0.8	0.71	0.76	0.78	0.73	0.71	0.16	0.77
	[8,9]	0.68	0.73	0.75	0.71	0.78	0.77	0.76	0.81	0.77	0.75	0.79	0.65	0.22	0.76
	10	0.68	0.72	0.7	0.62	0.73	0.76	0.75	0.73	0.8	0.79	0.78	0.67	0.18	0.76
	11	0.69	0.72	0.69	0.6	0.72	0.76	0.77	0.71	0.79	0.8	0.76	0.68	0.17	0.76
	[10,11]	0.65	0.71	0.71	0.68	0.74	0.74	0.73	0.78	0.78	0.77	0.8	0.63	0.21	0.74
	13	0.61	0.64	0.6	0.49	0.65	0.71	0.71	0.61	0.67	0.68	0.62	0.74	0.13	0.69
	Mean signal	0.15	0.18	0.2	0.26	0.21	0.18	0.18	0.29	0.19	0.18	0.22	0.14	0.71	0.18
	Mean result	0.72	0.75	0.73	0.63	0.76	0.8	0.8	0.74	0.78	0.79	0.75	0.71	0.17	0.78

Table 97 - Total agreement between the first return trip and the third return trip

		First passage													
		1	2	3	[2,3]	7	8	9	[8,9]	10	11	[10,11]	13	Mean signal	Mean result
Third passage	1	0.22	0.26	0.24	0.2	0.26	0.26	0.28	0.25	0.23	0.26	0.22	0.21	0.05	0.25
	2	0.19	0.27	0.25	0.2	0.26	0.25	0.28	0.25	0.24	0.27	0.23	0.21	0.05	0.25
	3	0.19	0.27	0.26	0.22	0.27	0.26	0.28	0.26	0.24	0.27	0.24	0.21	0.06	0.26
	[2,3]	0.16	0.23	0.23	0.21	0.23	0.21	0.23	0.24	0.21	0.22	0.22	0.17	0.07	0.22
	7	0.2	0.27	0.26	0.22	0.28	0.26	0.28	0.26	0.25	0.27	0.24	0.23	0.06	0.26
	8	0.2	0.25	0.24	0.2	0.26	0.26	0.28	0.25	0.24	0.27	0.24	0.22	0.05	0.25
	9	0.22	0.27	0.26	0.21	0.28	0.28	0.31	0.27	0.26	0.29	0.25	0.24	0.06	0.27
	[8,9]	0.21	0.27	0.26	0.24	0.28	0.27	0.29	0.29	0.26	0.28	0.27	0.22	0.08	0.27
	10	0.2	0.26	0.25	0.21	0.26	0.26	0.28	0.26	0.29	0.31	0.28	0.22	0.06	0.27
	11	0.21	0.27	0.25	0.21	0.27	0.26	0.29	0.26	0.29	0.32	0.28	0.23	0.06	0.27
	[10,11]	0.21	0.27	0.26	0.24	0.28	0.27	0.28	0.29	0.3	0.31	0.31	0.22	0.08	0.28
	13	0.2	0.25	0.23	0.18	0.26	0.26	0.28	0.24	0.24	0.26	0.22	0.26	0.05	0.26
	Mean signal	0.05	0.08	0.08	0.1	0.08	0.07	0.07	0.09	0.08	0.07	0.09	0.05	0.23	0.07
	Mean result	0.21	0.27	0.26	0.21	0.27	0.27	0.29	0.26	0.26	0.29	0.25	0.23	0.06	0.27

Table 98 - Total agreement between the second return trip and the third return trip

		Second passage													
		1	2	3	[2,3]	7	8	9	[8,9]	10	11	[10,11]	13	Mean signal	Mean result
Third passage	1	0.47	0.47	0.44	0.39	0.44	0.46	0.47	0.43	0.42	0.45	0.4	0.42	0.1	0.46
	2	0.43	0.49	0.47	0.42	0.46	0.45	0.47	0.44	0.43	0.46	0.42	0.4	0.11	0.47
	3	0.42	0.48	0.48	0.45	0.46	0.44	0.45	0.45	0.42	0.44	0.42	0.38	0.13	0.46
	[2,3]	0.37	0.44	0.46	0.49	0.44	0.4	0.4	0.45	0.39	0.39	0.43	0.32	0.17	0.41
	7	0.4	0.47	0.47	0.43	0.46	0.44	0.45	0.45	0.42	0.43	0.42	0.39	0.13	0.45
	8	0.43	0.47	0.45	0.4	0.45	0.46	0.48	0.44	0.44	0.46	0.42	0.42	0.11	0.46
	9	0.45	0.48	0.46	0.4	0.47	0.48	0.5	0.46	0.44	0.48	0.43	0.44	0.11	0.48
	[8,9]	0.3	0.38	0.38	0.39	0.39	0.36	0.36	0.4	0.35	0.35	0.38	0.29	0.14	0.36
	10	0.46	0.51	0.49	0.44	0.49	0.49	0.5	0.48	0.52	0.53	0.5	0.44	0.13	0.51
	11	0.48	0.52	0.5	0.44	0.51	0.51	0.53	0.49	0.53	0.56	0.51	0.46	0.12	0.53
	[10,11]	0.47	0.52	0.52	0.5	0.52	0.51	0.51	0.53	0.54	0.54	0.55	0.44	0.16	0.52
	13	0.4	0.44	0.41	0.35	0.42	0.43	0.45	0.39	0.4	0.43	0.37	0.45	0.09	0.44
	Mean signal	0.11	0.13	0.15	0.19	0.14	0.12	0.12	0.15	0.13	0.12	0.15	0.09	0.51	0.12
	Mean result	0.45	0.5	0.48	0.43	0.48	0.48	0.49	0.46	0.46	0.49	0.45	0.43	0.11	0.49

8 CONCLUSION

Although this thesis has chosen to address a broad research topic with several possible approaches, from the hardware and software development of the sensor sets to the possibility of creating inertial indexes related to track quality, it may be stated that the objectives were met within the scope of the limitations of the consumer-grade sensors and the collective monitoring approaches. Specifically, this thesis investigated these sensors' individual and collective behaviour in a train vibration monitoring application for comfort assessment and, indirectly, track quality characterization.

This research hypothesised that the collective use of consumer-grade sensors would overcome the limitations of these very low-cost, low-quality instruments. Initially, the collective approach offers an inherent increase in reliability, arising from the possibility of discrepancy identification from group behaviour. Furthermore, the combination of similar sensors subjected to the same vibration enables the obtention of a mean signal with reduced noise compared to individual signals. Lastly, concerning the performance of the collective estimations, the theory identifies that combining one or more similar sensors improves accuracy only when individual sensors have a minimum adherence to the monitored phenomenon. Thus, one of the main contributions of this thesis is the confirmation of this minimum adherence regarding train vibration and, in specific situations, track quality. As an example of behaviour verified for other stretches, it is noteworthy that the remarkable increase in correlation between vibration and short wavelength irregularities (range D1) when combining the redundant signals in the validation section. For irregularities in the range D3, however, there was no increase in correlation when combining the sensors, indicating that they individually have less adherence to the features at the associated frequency, as observed for other test sections.

From these examinations, the thesis proposes a method to extract more accurate information from the sensor group and overcome its individual limitations. The possibility of testing in different scenarios, such as urban commuter trains and high-speed trains, also brought a multiplicity of constraints, problems, and solutions to the sensors’ performance and increased the representativeness of the results. In

addition, the possible collaborative system based on the passengers' smartphones conditioned the alternatives of materials and methods, in a way that this work provides relevant bases for future developments.

The proposed collective method can be described in terms of its two core aspects:

1. **Identification of the discrepant sensors**. Instead of generic methods based on, for example, the coefficient of variance, the method proposes identification based on the expected behaviour of acceleration signals on a typical train trip and in different sensor distributions. Specifically, Pearson's coefficient is recommended for the longitudinal and lateral acceleration signals, axes in which the correlation between sensors is less penalized by the distance between sensors. A threshold coefficient of 0.45 (median coefficient of a sensor with the others) was successfully adopted for the sensors and the dataset considered.

2. **Calculation of a combined result representative of the sensor collectivity**, namely the mean signal and the mean result. For the mean signal, the synchronization correction through time-lagged cross-correlation is mandatory to avoid destructive interference. Furthermore, the median signal only produces the theoretical noise reduction without loss of information when the sensors are redundant (i.e., subjected to the same vibration). Considering the high correlation between track parameters on left and right sides for a given section, the results allowed to identify as redundant the sensors that are approximately located on the same transversal section of the train. Another relevant attribute is the robustness to short-term temporary malfunctioning sensors (intervals of about seconds). For non-redundant sensors, the mean result remains the most appropriate solution when considering the possibility of loss of information when combining non-redundant signals.

Regarding the specific objectives, this thesis accomplished them according to the following description:

- **Development of a mini portable track monitoring device.** The sensor set for this application was defined as containing at least: a triaxial accelerometer, a triaxial gyroscope, a pressure module, a GNSS module, and

a single-board microcomputer (besides additional items such as the SD card and the power supply to ensure apparatus autonomy). The importance of the triaxial accelerometer is evident due to the objective of monitoring vehicle vibration. Moreover, the gyroscope and the magnetometer are needed for a complete attitude description. The pressure module, although not strictly necessary, was proved relevant in altitude estimation and eventual feature map algorithm to correct positioning errors. Finally, using a GNSS module with an external antenna was proven to be important due to the flexibility in using active antennas or antennas with longer cables in environments with relevant GNSS signal blockage.

- **Data fusion technique.** The time-lagged cross-correlation proved to be necessary for data alignment. Furthermore, the simple calculation of the mean signal after the removal of discrepant signals resulted in the theoretical noise reduction (of about $1/\sqrt{N}$) despite its simplicity and it is a valid data combining tool compared with the inverse-variance weighting or the windowed identification of discrepant signals. For the mean signal calculation, the sensors must be redundant to obtain noise reduction without loss of information. The mean feature (mean response after comfort index calculation), on the other hand, does not reduce the effect of noise but has proven to be robust to variations in sensor arrangement, and is still suitable as an average index of the sensor population in cases of non-redundant sensors.

- **Description of the influence of the sensor arrangement (number and distribution).** Regarding the number of sensors, the gain in accuracy was demonstrated when increasing the number of sensors, especially for the vertical signals. This attribute of the collective approach comes from the sufficient individual adherence of the consumer-grade sensors to the observed phenomena, namely vehicle vibration and, indirectly, track quality. Regarding the variation in sensor position, the results demonstrated that although the individual signals and results show a considerable correlation in stretches of constant speed, the fusion of sensors at different positions does not produce the gain observed for the redundancy scenario because of the differences in the signals. In extreme situations, when considering a complete

trip and its speed variations, the mean signal suffers considerable loss of information due to destructive interference. In these contexts, the mean results are more appropriate and robust to these differences in signal.

- **Influence of the sensor inaccuracies in position, time, and attitude**. The inaccuracies in time are properly solved through the time-lagged cross-correlation. For the attitude inaccuracies, the usual attitude algorithm (accelerometer-based) yields proper results for the wavelengths of interest, but the remark remains about the impossibility of using them directly in the actual pitch and roll description. Regarding georeferencing, it has been identified that this is one of the main weaknesses of the low-cost approach, and the challenge remains in GPS unavailability scenarios.

- **Monitorable track parameters.** Under the ideal condition of constant speed, as expected, the lateral accelerations are moderately correlated to alignment. In contrast, the vertical accelerations are strongly correlated to the longitudinal level and may be appropriately used as an indirect quality indicator, especially under the collective method. However, the consumer-grade sensor presented considerably lower sensitivity to irregularities in the range D3 and presented good performance limited to ranges D1 and D2. As the sensors are sensitive to macrogeometry variations (large displacements), the problem lies in the sensitivity to small displacements at long wavelengths. Under speed variations, there is a substantial decline in correlation between track parameters and vibration. As a product derived from the description of the influence of speed variations on acceleration variation, using an index derived from accelerations and compensating for the speeds did not perform well and highlighted that the variations in speed curb the use of accelerations as indirect quality indexes.

- **Development of a tool for ride comfort monitoring.** With the accomplished objectives, it was possible to define an initial set of instruments and techniques for comfort monitoring under the collective concept, dealing with limitations inherent to the very low-cost sensors and offering more accurate and robust results.

Future research developments should include using data gathered by smartphones

in real situations, i.e., with free orientation during a trip. It is considered that the logic of discrepant sensor identification applies to the identification of temporarily discrepant sensors due to user interaction with the device. In any case, describing the attitude in a free-riding scenario added to the train's accelerations would require alternative strategies.

Another critical aspect for further research is the use of alternative georeferencing strategies. The excellent results concerning the estimation of the track slope based on the barometric height, as well as the considerable correlation with track irregularities in favourable situations (at constant speed), reveal the possibility of using this information together with the reference map in a feature-matching algorithm, as partially explored in previous work.

Finally, the development of analyses of track characterization from low-cost, low-quality inertial sensors under the influence of suspensions and speed variations remains challenging. However, in a real collaborative scenario of profuse production of vibration data (as in the case of passengers' smartphones), indirect characterisation methods and better estimates could occur in the statistical learning framework.

9 BIBLIOGRAPHY

ABDELHAMID, S.; HASSANEIN, H. S.; TAKAHARA, G. Vehicle as a mobile sensor. **The 9th International Conference on Future Networks and Communications**, v. 34, p. 286–295, 2014.

ABUHAMDIA, T.; TAHERI, S.; MEDDAH, A.; DAVIS, D. Rail Defect Detection Using Data From Tri-Axial Accelerometers. In: **Proceedings of the 2014 Joint Rail Conference JRC2014**, May 2014.

AITKEN, A. C. On Least Squares and Linear Combination of Observations. In: **Proceedings of the Royal Society of Edinburgh**, Royal Society of Edinburgh, 1935.

ALESSANDRONI, G.; CARINI, A.; LATTANZI, E.; FRESCHI, V.; BOGLIOLO, A. A Study on the Influence of Speed on Road Roughness Sensing: The SmartRoadSense Case. **Sensors**, v. 17, n. 2, 2017.

ALFI, S.; DE ROSA, A.; BRUNI, S. Estimation of lateral track irregularities from on-board measurement: Effect of wheel-rail contact model. **IET Conference Publications**, v. 2016, n. CP701, p. 1–7, 2016.

AUER, F. Multi-function track recording cars. **RTR (Plasser & Theurer)**, n. 3+4, p. 32–36, 2013.

AZZOUG, A.; KAEWUNRUEN, S. Ridecomfort: A development of crowdsourcing smartphones in measuring train ride quality. **Frontiers in Built Environment**, v. 3, n. February, p. 1–12, 2017.

BALOUCHI, F.; BEVAN, A.; FORMSTON, R. Development of railway track condition monitoring from multi-train in-service vehicles. **Vehicle System Dynamics**, v. 59, n. 9, p. 1397–1417, 2021. Available at: <https://doi.org/10.1080/00423114.2020.1755045>.

BARBOSA, R. S. New method for railway track quality identification through the safety dynamic performance of instrumented railway vehicle. **Journal of the Brazilian Society of Mechanical Sciences and Engineering**, v. 38, n. 8, p. 2265–2275, 2016.

BARBOSA, R. S. **Segurança em Sistemas Metro-Ferroviários**. 2017. Associate professorship thesis, Polytechnic School of the University of São Paulo, 2017.

BERMAN, B. **Enhancing Automotive IMUs - IMU trends for autonomous vehicles**. Available at: <https://www.sae.org/news/2019/06/imu-trends-for-autonomous-vehicles>. Accessed: 30 Jun. 2021.

BHARDWAJ, B.; BRIDGELALL, R.; LU, P.; DHINGRA, N. Signal Feature Extraction and Combination to Enhance the Detection and Localization of Railroad Track Irregularities. **IEEE Sensors Journal**, v. 21, n. 5, p. 6555–6563, 2020.

BISSACOT, J. A. R. **Os trilhos percorridos até aqui- História e panorama atual da CPTM em seus 25 anos.** 24ª Semana de Tecnologia Ferroviária, 2018.

BLASCHKE, T.; HAY, G. J.; WENG, Q.; RESCH, B. Collective sensing: Integrating geospatial technologies to understand urban systems - An overview. **Remote**

Sensing, v. 3, n. 8, p. 1743–1776, 2011.

BLITZKOW, D. Sistema de Posicionamento por Satélites GPS. In: **Informações Espaciais II - Notas de aula**. São Paulo, Brazil. Almada, 2004. p. 9–39.

BOCCIOLONE, M.; CAPRIOLI, A.; CIGADA, A.; COLLINA, A. A measurement system for quick rail inspection and effective track maintenance strategy. **Mechanical Systems and Signal Processing**, v. 21, n. 3, p. 1242–1254, 2007.

BONGINI, E.; GRASSIE, S.; SAXON, M. "Noise Mapping" of a Railway Network: Validation and Use of a System Based on Measurement of Axlebox Vibration. In: AL., T. M. ET (Ed.). **Noise and Vibration Mitigation for Rail Trans. Sys.** Springer-Verlag Berlin Heidelberg, 2011. p. 1–8.

BOSCH. **BMP280 Digital Pressure Sensor - Bosch Sensortec Datasheet 1.14**, 2015. Available at: <https://cdn-shop.adafruit.com/datasheets/BST-BMP280-DS001-11.pdf>.

BRIDGELALL, R. Connected Vehicle Approach for Pavement Roughness Evaluation. **Journal of Infrastructure Systems**, v. 20, n. 1, p. 04013001, 2014. Available at: <http://ascelibrary.org/doi/10.1061/%2528ASCE%2529IS.1943-555X.0000167>.

BROOKS, M. **Correlation and Cross-Correlation - Fourier Series and Transforms**, 2015. . Available at: <http://www.ee.ic.ac.uk/hp/staff/dmb/courses/E1Fourier/00800_Correlation.pdf>.

BROWN, R. G.; HWANG, P. Y. C. **Introduction to random signals and applied kalman filtering**. Second Edition. New York: John Wiley & Sons, 2012.

CASTANEDO, F. A review of data fusion techniques. **The Scientific World Journal**, v. 2013, 2013.

CHEN, Q.; ZHOU, Y.; FANG, B.; ZHANG, Q.; NIU, X. Experimental Study on the Potential of Vehicle's Attitude Response to Railway Track Irregularity in Precise Train Localization. **IEEE Transactions on Intelligent Transportation Systems**, v. 23, n. 11, p. 20452–20463, 2022.

CHOI, S. Identifying Parametric Models Used to Estimate Track Irregularities of a High-Speed Railway. **Machines**, v. 11, n. 1, 2023.

CLARIVATE. Web of Science - Quik reference guide. v. 11, n. 0, p. 11–13, 2021.

COLE, C. Longitudinal Train Dynamics. In: IWNICKI, S. (Ed.). **Handbook of Railway Vehicle Dynamics**. London, UK: Taylor & Francis Group, 2006.

COMITÉ EUROPÉEN DE NORMALISATION. **EN 13803-2:2006 + A1:2009 Railway applications - Track - Track alignment design parameters - Track gauges 1435mm and wider Part 2: Switches and crossings and comparable alignment design situations with abrupt changes of curvature**. Brussels, Comité Européen de Normalisation, 2009a.

COMITÉ EUROPÉEN DE NORMALISATION. **EN 12299 - Railway Applications - Ride comfort for passengers - Measurement and evaluation.** Brussels, Comité Européen de Normalisation, 2009b.

COMITÉ EUROPÉEN DE NORMALISATION. **EN 13803-1:2010 - Railway applications - Track - Track alignment design parameters - Track gauges 1435 mm and wider - Part 1: Plain line.** Brussels, Comité Européen de Normalisation, 2010a.

COMITÉ EUROPÉEN DE NORMALISATION. **EN 15686:2010 - Railway applications - Testing for the acceptance of running characteristics of railway vehicles with cant deficiency compensation system and/or vehicles intended to operate with higher cant deficiency than stated in EN 14363:2005.** Brussels, Comité Européen de Normalisation, 2010b.

COMITÉ EUROPÉEN DE NORMALISATION. **EN 13848-6 - 2014 - Railway applications - Track - Track geometry quality - Part 6 - Characterisation of track geometry quality.** Brussels, Comité Européen de Normalisation, 2014.

COMITÉ EUROPÉEN DE NORMALISATION. **EN 13848-5:2017 - Railway applications - Track - Track geometry quality - Part 5: Geometric quality levels - Plain line.** Brussels, Comité Européen de Normalisation, 2017a.

COMITÉ EUROPÉEN DE NORMALISATION. **EN 15273-1:2017 + A1:2016 - Railway applications - Gauges - Part 1: General - Common rules for infrastructure and rolling stock**. Brussels, Comité Européen de Normalisation, 2017b.

COMITÉ EUROPÉEN DE NORMALISATION. **EN 13848-1 2019 - Railway applications - Track - Track geometry quality - Part 1: Characterization of track geometry.** Brussels, Comité Européen de Normalisation, 2019.

COMITÉ EUROPÉEN DE NORMALISATION. **EN 15302 2021 - Railway Applications - Wheel-rail contact geometry parameters - Definitions and methods for evaluation.** Brussels, Comité Européen de Normalisation, 2021.

COMITÉ EUROPÉEN DE NORMALISATION. **EN 14363:2016 + A2:2022 - Railway applications – Testing for the acceptance of running characteristics of railway vehicles – Testing of running behaviour**. Brussels, Comité Européen de Normalisation, 2022.

COMPANHIA PAULISTA DE TRENS METROPOLITANOS. **Concorrência Internacional 8085132011 - Serviços de projeto e fabricação de 65 trans, constituídos de 8 carros cada, totalizando 520 carros, para as linhas da Companhia Paulista de Trans Metropolitanos - CPTM**, São Paulo, Brazil, 2013.

COMPANHIA PAULISTA DE TRENS METROPOLITANOS. **Relatório da Audiência pública de 05/10/2016,, referente à "prestação de serviços de manutenção preventiva e corretiva de Trens Unidades Elétricos das Séries 2000, 2070 (2000 fase II), 2100, 3000, 7000, 7500, 8500, 9000 e 9500 da CPTM.** São Paulo, Brazil, 2016.

DAHLBERG, T. Track Issues. In: IWNICKI, S. (Ed.). **Handbook of Railway Vehicle Dynamics**. London, UK: Taylor & Francis Group, 2006.

DE CELIS, R.; CADARSO, L. Attitude Determination Algorithms through Accelerometers, GNSS Sensors, and Gravity Vector Estimator. **International Journal of Aerospace Engineering**, v. 2018, 2018.

DE OLIVEIRA, R. H. de. **Veículo-sensor: estado da arte e proposta de método orientativo para especificação do sistema de posicionamento veicular**. 2017. Master's thesis, Polytechnic School of the University of São Paulo, 2017.

DE OLIVEIRA, R. H. de; FILHO, F. G. V. de A.; PISSARDINI, R. de S.; LOPRENCIPE, G. MONITORAMENTO DO CONFORTO E DA QUALIDADE VIÁRIA BASEADO EM SENSORES DE BAIXO CUSTO: INVESTIGAÇÃO EXPLORATÓRIA

NO TRANSPORTE FERROVIÁRIO. **In: Anais do 36º Congresso de Pesquisa e Ensino em Transportes, Fortaleza, Ceará**. Fortaleza, Ceará: 2022.

DE OLIVEIRA, R. H.; LOPRENCIPE, G.; DE ALMEIDA FILHO, F. G. V.; PISSARDINI, R. D. S. Experimental investigation on the use of multiple very low-cost inertial-based devices for comfort assessment and rail track monitoring. **Measurement.** August, 2022.

DE ROSA, A.; KULKARNI, R.; QAZIZADEH, A.; BERG, M.; DI GIALLEONARDO, E.; FACCHINETTI, A.; BRUNI, S. Monitoring of lateral and cross level track geometry irregularities through onboard vehicle dynamics measurements using machine learning classification algorithms. **Proceedings of the Institution of Mechanical Engineers, Part F: Journal of Rail and Rapid Transit**, v. 235, n. 1, p. 107–120, 2021.

DEEKS, J. J.; ALTMAN, D. G.; BRADBURN, M. J. Systematic Reviews in Health Care. In: EGGER, M.; SMITH, G. D.; ALTMAN, D. G. (Ed.). **Systematic Reviews in Health Care: Meta-Analysis in Context**. 2001.

DELLAERT, F. **Sensor Fusion as Weighted Averaging**. Available at: <https://piazza.com/class_profile/get_resource/hpa4u5hmxk599/hs3g1ig289y5r6>.

DENNIS, E. P.; HONG, Q.; WALLACE, R.; TANSIL, W.; SMITH, M. Pavement Condition Monitoring with Crowdsourced Connected Vehicle Data. **Transportation Research Record: Journal of the Transportation Research Board**, v. 2460, n. 1, p. 31–38, 2014.

DICKEY, D. A. Stationarity Issues in Time Series Models. **SAS Global Forum**, p. 1–17, 2005.

DIGGLEN, F. Van. **A-GPS: Assisted GPS, GNSS, and SBAS**. London, UK: Artech House, 2009.

DO, N. T.; ABDULRAZAGH, P. H.; GÜL, M.; HENDRY, M. T.; ROGHANI, A.; TOMA, E. Evaluating passenger railway ride quality over long distances using smartphones. **2020 Joint Rail Conference, JRC 2020**, May, 2020.

DOW, A. **The Railway: British Track Since 1804**. Pen & Sword Books Limited, 2014.

DU, Y.; SUN, B.; LI, F.; MA, H.; ZHANG, W.; HUANG, W. Detection of rail corrugation based on fiber laser accelerometers. **Measurement Science and Technology**, v. 24, n. 9, p. 094014, 2013.

ENTEZAMI, M.; WESTON, P.; STEWART, E.; YEO, G.; WANG, L. SAADE, M.; ROBERTS, C.; LEWIS, R.; HAYWARD, M.; MORLEY, S. BAYRAM, S.; KONO, T. Lineside and On-board Monitoring Techniques for Infrastructure and Rolling Stock on High-Speed Lines. **International Journal of Railway Technology**, v. 5, n. 4, p. 49–77, 2016.

ESVELD, C. **Modern railway track**. Zaltbommel: MRT-Productions, 2001.

EUSTON, M.; COOTE, P.; MAHONY, R.; KIM, J.; HAMEL, T. A complementary filter for attitude estimation of a fixed-wing UAV. **2008 IEEE/RSJ International Conference on Intelligent Robots and Systems, IROS**, p. 340–345, 2008.

FINGER, M. **Rail infrastructure and rolling stock: investments, asset renewal and regulation** (M. Finge, N. Bert, D. Kupfer, Eds.). Florence, European University

Institute, 2014.

FIVASIM. **AndroSensor - App description**. Available at: <http://www.fivasim.com/androsensor.html>. Accessed: 22 jun. 2017.

FLINTSCH, G. W.; VALERI, S. M.; KATICHA, S. W.; IZEPPI, E. D. de L.; MEDINA-FLINTSCH, A. Probe Vehicles Used to Measure Road Ride Quality. **Transportation Research Record: Journal of the Transportation Research Board**, v. 2304, n. 1, p. 158–165, 2012.

FRAUNDORF, P. **Proper-velocity and f ≤ mα from the metric**. Physics & Astronomy/CNS, U. Missouri. St. Louis, USA, 2010.

GADE, K. **Introduction to Inertial Navigation - tutorial for Geodesy**. Hoenefoss, Norway, 2005.

GANTI, R. K.; YE, F.; LEI, H. Mobile crowdsensing: Current state and future challenges. **IEEE Communications Magazine**, v. 49, n. 11, p. 32–39, 2011.

GARG, V. K.; DUKKIPATI, R. V. **Dynamics of railway vehicle systems**. Academic Press, 1984.

GHOSE, A.; BISWAS, P.; BHAUMIK, C.; SHARMA, M.; PAL, A.; JHA, A. Road condition monitoring and alert application: Using in-vehicle smartphone as internet-connected sensor. **2012 IEEE International Conference on Pervasive Computing and Communications Workshops, PERCOM Workshops 2012**, n. March, p. 489–491, 2012.

GONZALO, A. P.; ENTEZAMI, M.; ROBERTS, C.; WESTON, P.; STEWART, E.; HAYWARD, M.; HSU, S. S. Railway track location estimation using onboard inertial sensors. **Vehicle System Dynamics**, v. 60, n. 10, p. 3631–3649, 2022. Available at: <https://doi.org/10.1080/00423114.2021.1968443>.

GOODALL, R. Active Suspension Technology and its Effect upon Vehicle-Track Interaction. In: **System Dynamics and Long-Term Behaviour of Railway Vehicles, Track and Subgrade**. Springer-Verlag, New York, 2003, p. 35–50.

GOOGLE. **Google Developers - Motion Sensors**. Available at: <https://developer.android.com/reference/android/motionsensors.htm>. Accessed: 20 jun. 2017.

GOOGLE MAPS. **Central Italy - Itinerary Map and Satellite Image**. Available at: <https://www.google.com.br/maps>. Accessed: 1 fev. 2021.

GRASSIE, S. L. Measurement of railhead longitudinal profiles: A comparison of different techniques. **Wear**, v. 191, n. 1–2, p. 245–251, 1996.

GREWAL, M. S.; ANDREWS, A. P. **Kalman Filtering - Theory and Practice with MATLAB**. Hoboken, New Jersey: Wiley-IEEE Press, 2008.

GROVES, P. D. **Principles of GNSS, Inertial, and Multisensor Integrated Navigation Systems**. London: Artech House, 2008.

GROVES, P. D. The Complexity Problem in Future Multisensor Navigation and Positioning Systems: A Modular Solution. **The Journal of Navigation**, v. 67, n. 02, p. 311–326, 2013.

GUERRERO-IBÁÑEZ, J.; ZEADALLY, S.; CONTRERAS-CASTILLO, J. Sensor technologies for intelligent transportation systems. **Sensors (Switzerland)**, v. 18, n.

4, p. 1–24, 2018.

GUERRIER, S. **Integration of Skew-Redundant MEMS-IMU with GPS for Improved Navigation Performance**. 2008. PhD Thesis, École Polytechnique Fédérale de Lausanne, 2008.

HAIGERMOSER, A.; LUBER, B.; RAUH, J.; GRÄFE, G. Road and track irregularities: Measurement, assessment and simulation. **Vehicle System Dynamics**, v. 53, n. 7, p. 878–957, 2015.

HALL, D. L.; LLINAS, J. Multisensor Data Fusion. In: LIGGINS, M.; HALL, D. L.; LLINAS, J. (Ed.). **Handbook of Multisensor Data Fusion: Theory and Practice**. 2nd ed. ed. Taylor & Francis Group, 2008.

HALL, D. L.; MCMULLEN, S. A. H. **Mathematical Techniques in Multisensor Data Fusion**. Norwood, MA: Artech House, 2004.

HAVLICEK, L. L.; PETERSON, N. L. Robustness of the Pearson Correlation against violations of assumptions. **Perceptual and Motor Skills**, v. 43, p. 1319–1334, 1976.

HEIRICH, O.; LEHNER, A.; ROBERTSON, P.; STRANG, T. Measurement and analysis of train motion and railway track characteristics with inertial sensors. **IEEE Conference on Intelligent Transportation Systems, Proceedings, ITSC**, p. 1995–2000, 2011.

HEIRICH, O.; STEINGASS, A.; LEHNER, A.; STRANG, T. Velocity and Location Information from Onboard Vibration Measurements of Rail Vehicles. **Proceedings of the 16th International Conference on Information Fusion**, p. 1835–1840, 2013.

HIGUCHI, T.; YAMAGUCHI, H.; HIGASHINO, T. Mobile devices as an infrastructure: A survey of opportunistic sensing technology. **Journal of Information Processing**, v. 23, n. 2, p. 94–104, 2015.

HOBEROCK, L. L. A survey of longitudinal acceleration comfort studies in ground transportation vehicles. **Journal of Dynamic Systems, Measurement and Control, Transactions of the ASME**, v. 99, n. 2, p. 76–84, 1977.

HOELZL, C.; DERTIMANIS, V.; LANDGRAF, M.; ANCU, L.; ZURKIRCHEN, M.; CHATZI, E. On-board monitoring for smart assessment of railway infrastructure: A systematic review. **In: The Rise of Smart Cities**. Elsevier, 2022.

HOFMANN-WELLENHOF, B.; K, L.; M., W.; LEGAT, K.; WIESER, M. **Navigation: principles of positioning and guidance**. Wien: Springer, 2013.

HOFMANN-WELLENHOF, B.; LICHTENEGGER, H.; WASLE, E. **GNSS – Global Navigation Satellite Systems - GPS, GLONASS, Galileo, and more**. Springer, New York, 2008.

HONG, K. C.; HUSSIN, F. A.; SAMAN, A. B. S. Automated train track misalignment detection system based on inertia measurement unit. **2014 IEEE Student Conference on Research and Development, SCOReD 2014**, p. 1–5, 2014.

HUMPHERYS, J.; REDD, P.; WEST, J. A fresh look at the kalman filter. **SIAM Review**, v. 54, n. 4, p. 801–823, 2012.

HUNDLEBY, J. D.; NUNNALLY, J. **Psychometric Theory**. 3rd Edition, McGraw-Hill, 1994.

HUNGRIA, L. H. **Segurança operacional de trens de carga**. São Paulo: All Print

Editora, 2017.

INGLE, V. K.; PROAKIS, J. G. **Digital Signal Processing using MATLAB**. Pacific Grove: Brooks-Cole, 2000.

INTERNATIONAL CIVIL AVIATION ORGANIZATION. **MANUAL OF THE ICAO STANDARD ATMOSPHERE**. 3rd Edition, 1993.

INTERNATIONAL CIVIL AVIATION ORGANIZATION. **Manual on Required Navigation Performance (RNP)**. ICAO Publications, 1999.

INTERNATIONAL ORGANIZATION FOR STANDARDIZATION. **ISO 2631-1 - Mechanical vibration and shock - Evaluation of human exposure to whole-body vibration - Part 1: General requirements.** Genève, CH, 1997.

INTERNATIONAL ORGANIZATION FOR STANDARDIZATION. **ISO 10056 - Mechanical vibration - Measurement and analysis of whole-body vibration to which passengers and crew are exposed in railway vehicles.** Genève, CH, 2003. .

INTERNATIONAL ORGANIZATION FOR STANDARDIZATION. **ISO 8041 - Human response to vibration - Measuring instrumentation.** Genève, CH, 2005. .

INTERNATIONAL ORGANIZATION FOR STANDARDIZATION; INTERNATIONAL ELECTROTECHNICAL COMISSION; INSTITUTE OF ELECTRICAL AND ELECTRONICS ENGINEERS. **ISO/IEC/ IEEE 24765 - Systems and software engineering — Vocabulary**. 2017.

INVENSENSE. **MPU-6000 and MPU-6050 Product Specification Revision 3.3.** Sunnyvale, CA. InvenSense Inc., 2012. Available at: <www.invensense.com>.

INVENSENSE. **MPU-9250 Product Specification Revision 1.1.** San Jose, CA. InvenSense Inc., 2019. .

IONTCHEV, E.; KENOV, R.; MILETIEV, R. Inertial measurement system for evaluation of the bogie-railway system dynamics. **Proceedings of the International Spring Seminar on Electronics Technology**, p. 345–348, 2013.

IRVINE, T. **Vibrationdata Tutorial Page**. Available at: <http://www.vibrationdata.com/tutorials.htm>. Accessed: 4 May 2021.

IWNICK, S. Manchester Benchmarks for Rail Vehicle Simulation Manchester Benchmarks for Rail Vehicle Simulation. **Vehicle System Dynamics**, 1998.

IWNICKI, S. **Handbook of Railway Vehicle Dynamics**. London, UK: Taylor & Francis Group, 2006.

JEKELI, C. **Geometric reference systems in geodesy**. Ohio State University, 2012.

JOHNSON, D. M. Gauging Issues. In: IWNICKI, S. (Ed.). **Handbook of Railway Vehicle Dynamics**. London, UK: Taylor & Francis Group, 2006.

JUSTA, J.; ŠMÍDL, V.; HAMÁČEK, A. Fast AHRS filter for accelerometer, magnetometer, and gyroscope combination with separated sensor corrections. **Sensors (Switzerland)**, v. 20, n. 14, p. 1–19, 2020.

KALMAN, R. E. A New Approach to Linear Filtering and Prediction Problems. **Journal of Basic Engineering**, v. 82, n. 1, p. 35, 1960.

KANG, B. B. Influence of train length on the lateral vibration of a high-speed train

equipped with articulated bogies. **Journal of Mechanical Science and Technology**, v. 28, n. 9, p. 3517–3527, 2014.

KIM, Y. G.; CHOI, S.; KIM, S. W.; KIM, Y. M.; PARK, T. W. An experimental study on the ride comfort of the Korean high-speed train. **Experimental Techniques**, v. 33, n. 6, p. 30–37, 2009.

KOHN, A. F. Autocorrelation and Cross-Correlation Methods. In: AKAY, M. (Ed.). **Wiley Encyclopedia of Biomedical Engineering**. Hoboken: John Wiley & Sons Inc., 2006.

KRAFT, S.; CAUSSE, J.; COUDERT, F. Vehicle response-based track geometry assessment using multi-body simulation. **Vehicle System Dynamics**, v. 56, n. 2, p. 190–220, 2018.

LEDERMAN, G.; CHEN, S.; GARRETT, J. H.; KOVACEVIC, J.; NOH, H. Y.; BIELAK, J. Track monitoring from the dynamic response of a passing train: A sparse approach. **MECHANICAL SYSTEMS AND SIGNAL PROCESSING**, v. 90, p. 141–153, jun. 2017a.

LEDERMAN, G.; CHEN, S.; GARRETT, J. H.; KOVAČEVIĆ, J.; NOH, H. Y.; BIELAK, J. A data fusion approach for track monitoring from multiple in-service trains. **Mechanical Systems and Signal Processing**, v. 95, p. 363–379, 2017b.

LEE, J. K.; PARK, E. J.; ROBINOVITCH, S. N. Estimation of attitude and external acceleration using inertial sensor measurement during various dynamic conditions. **IEEE Transactions on Instrumentation and Measurement**, v. 61, n. 8, p. 2262–2273, 2012.

LEE, J. S.; CHOI, S.; KIM, S. S.; KIM, Y. G.; KIM, S. W.; PARK, C. Track condition monitoring by in-service trains: a comparison between axle-box and bogie accelerometers. **In: 5th IET Conference on Railway Condition Monitoring and Non-Destructive Testing (RCM 2011)**, 2011.

LEE, J. S.; CHOI, S.; KIM, S. S.; PARK, C.; KIM, Y. G. A mixed filtering approach for track condition monitoring using accelerometers on the axle box and bogie. **IEEE Transactions on Instrumentation and Measurement**, v. 61, n. 3, p. 749–758, 2012.

LEE, U.; ZHOU, B.; GERLA, M.; MAGISTRETTI, E.; BELLAVISTA, P.; CORRADI, A. Mobeyes: Smart mobs for urban monitoring with a vehicular sensor network. **IEEE Wireless Communications**, v. 13, n. 5, p. 52–57, 2006.

LI, B.; HARVEY, B.; GALLAGHER, T. Using barometers to determine the height for indoor positioning. **2013 International Conference on Indoor Positioning and Indoor Navigation, IPIN 2013**, n. October, 2013.

LI, C.; LUO, S.; COLE, C.; SPIRYAGIN, M. An overview: modern techniques for railway vehicle on-board health monitoring systems. **Vehicle System Dynamics**, v. 55, n. 7, p. 1045–1070, 2017. Available at: <https://doi.org/10.1080/00423114.2017.1296963>.

LI, Z.; MOLODOVA, M.; NUNEZ, A.; DOLLEVOET, R. Improvements in Axle Box Acceleration Measurements for the Detection of Light Squats in Railway Infrastructure. **IEEE Transactions on Industrial Electronics**, v. 62, n. 7, p. 4385–4397, 2015.

LIN, L. I. A Concordance Correlation Coefficient to Evaluate Reproducibility Author (

s): Lawrence I-Kuei Lin Published by : International Biometric Society Stable URL : http://www.jstor.org/stable/2532051 REFERENCES Linked references are available on JSTOR for thi. **Biomatrics**, v. 45, n. 1, p. 255–268, 1989.

LIU, R. K.; XU, P.; SUN, Z. Z.; ZOU, C.; SUN, Q. X. Establishment of track quality index standard recommendations for beijing metro. **Discrete Dynamics in Nature and Society**, v. 2015, 2015.

MANJU, Y. **DYNAMIC BEHAVIOUR OF HIGH SPEED TRAIN: PERFORMANCES AND COMPARISION BETWEEN ETR1000, ETR500, ICE3 and TGV**. 2019. University of Rome, 2019.

MANOLAKIS, D. G.; INGLE, V. K.; KOGON, S. M. **Statistical and Adaptive Signal Processing: Spectral Estimation, Signal Modeling, Adaptive Filtering, and Array Processing**. Norwood, MA: Artech House, 2005.

MATISA. **Véhicules d'auscultation sur la voie du succès - L'optimisation de la gestion des réseaux**. MATISA Matériel Industriel S.A., 2017.

MCGRAW, K. O.; WONG, S. P. Forming Inferences about Some Intraclass Correlation Coefficients. **Psychological Methods**, v. 1, n. 1, p. 30–46, 1996.

MERMEC. **Track Measurement - Ride Quality**. Available at: <http://www.mermecgroup.com/inspect/track-measurement/1019/ride-quality.php>. Accessed: 20 jul. 2020.

MERTINS, A. **Signal analysis: wavelets, filter banks, time-frequency transforms and applications**. London, UK: John Wiley & Sons Inc., 1999.

MICHEL, T.; GENEVÈS, P.; FOURATI, H.; LAYAÏDA, N. Attitude estimation for indoor navigation and augmented reality with smartphones. **Pervasive and Mobile Computing**, v. 46, p. 96–121, 2018.

MONGIÒ, O. **Diagnóstico Integrado - Instrumento de melhoramento e desenvolvimento do transporte ferroviário.** Brasília, Brazil. Perotti Internacional Tecnologias Ferroviárias Ltda., 2014.

MORETTI, M. Sul Diamante, il treno diagnostico che ora interessa ai giapponesi. **Il Sole 24 Ore**, 2017. Available at: <https://www.ilsole24ore.com/art/sul-diamante-treno-diagnostico-che-ora-interessa-giapponesi-AEz27cHC>.

MORI, H.; TSUNASHIMA, H.; KOJIMA, T.; MATSUMOTO, A.; MIZUMA, T. Condition Monitoring of Railway Track Using In-service Vehicle. **Journal of Mechanical Systems for Transportation and Logistics**, v. 3, n. 1, p. 154–165, 2010.

MURPHY, C. Choosing the Most Suitable MEMS Accelerometer for Your Application — Part 1. **Analog Devices**, n. October, p. 1–6, 2017.

MUTTER, H.; SIMMONDS, K.; ARNOLD, G. .; CARTER, B. .; IRANI, F.; ELKINS, J.; SWEARINGEN, B.; DICRHE, R. **Metropolitan Atlanta Rapid Transit Authority - Transit vehicle engineering tests**. 1981.

NAGANUMA, Y.; TANAKA, M.; ICHIKAWA, K. **High-Speed Track Inspection Car in New Dr . Yellow**Central Japan Railway Company, 2000.

NAHIN, P. J.; POKOSKI, J. L. NCTR Plus Sensor Fusion Equals IFFN or Can Two Plus Two Equal Five? **IEEE Transactions on Aerospace and Electronic Systems**, v. AES-16, n. 3, p. 320–337, 1980.

NATIONAL GEODETIC SURVEY. **Datums and Reference Frames**. Available at: <https://geodesy.noaa.gov/datums/index.shtml>. Accessed: 8 Jul. 2021.

NATIONAL INSTITUTE OF STANDARDS AND TECHNOLOGY. **NIST/SEMATECH e-Handbook of Statistical Methods**. 2022.

NETIRAIL-INFRA. **Deliverable D4.6 Low cost smartphone based track and ride quality monitoring technology**. NETIRAIL-INFRA, 2017.

NETIRAIL-INFRA. **Deliverable D4.11 - Validated monitoring equipment produced by testing of instrumentation in the real environment**. NETIRAIL-INFRA, 2018.

NETWORK RAIL. **Train Infrastructure Interface Specification (TIIS) - IEP-TEHC-REQ-36**. Issue 03 ed. London, UK: Network Rail, 2007.

NICKERSON, C. A. E. A Note On "A Concordance Correlation Coefficient to Evaluate Reproducibility". **Biometrics**, v. 53, n. 4, p. 1503–1507, 1997.

NIELSEN, J.; BERGGREN, E. G.; LÖLGEN, T.; MÜLLER, R.; STALLAERT, B.; PESQUEUX, L. Overview of Methods for Measurement of Track Irregularities for Ground-Borne Vibration - Deliverable D2.5. **Chalmers University of Technology, Trafikverkt, DB, SBB, D2S International, Alstom**, p. 1–49, 2013.

OBRIEN, E. J.; QUIRKE, P.; BOWE, C.; CANTERO, D. Determination of railway track longitudinal profile using measured inertial response of an in-service railway vehicle. **Structural Health Monitoring**, v. 17, n. 6, p. 1425–1440, 2018.

ODASHIMA, M.; AZAMI, S.; NAGANUMA, Y.; MORI, H.; TSUNASHIMA, H. Track geometry estimation of a conventional railway from car-body acceleration measurement. **Mechanical Engineering Journal**, v. 4, n. 1, p. 16- 00498-16–00498, 2017.

OFFENBACHER, S.; NEUHOLD, J.; VEIT, P.; LANDGRAF, M. Analyzing major track quality indices and introducing a universally applicable TQI. **Applied Sciences (Switzerland)**, v. 10, n. 23, p. 1–17, 2020.

OPENSTREETMAP. **Planet dump retrieved from https://planet.osm.org**. Available at: <https://www.openstreetmap.org>. Accessed: 1 May 2023.

PAIXÃO, A.; FORTUNATO, E.; CALÇADA, R. Smartphone's Sensing Capabilities for On-Board Railway Track Monitoring: Structural Performance and Geometrical Degradation Assessment. **Advances in Civil Engineering**, v. 2019, 2019.

PASSARO, V. M. N.; CUCCOVILLO, A.; VAIANI, L.; DE CARLO, M.; CAMPANELLA, C. E. Gyroscope technology and applications: A review in the industrial perspective. **Sensors (Switzerland)**, v. 17, n. 10, 2017.

PENNY, W. D. **Signal Processing Course Notes**. 2000. Available at: <http://www.fil.ion.ucl.ac.uk/~wpenny/course/array.pdf>.

PETIT, G.; LUZUM, B. **IERS Conventions - IERS Technical Note 36**. 2010.

PITA, A. L. **Infraestructuras Ferroviarias**. Barcelona: Edicions de la Universitat Politècnica de Catalunya, 2006.

POLACH, O.; BERG, M.; IWNICKI, S. Simulation. In: IWNICKI, S. (Ed.). **Handbook of Railway Vehicle Dynamics**. London, UK: Taylor & Francis Group, 2006. p. 359–422.

PRUD'HOMME, A. André Mauzin (21), 1901-1995. **La Jaune et la Rouge - Les**

nouvelles de l'École polytechnique et de l'AX, 1997.

QUIRKE, P.; CANTERO, D.; OBRIEN, E. J.; BOWE, C. Drive-by detection of railway track stiffness variation using in-service vehicles. **Proceedings of the Institution of Mechanical Engineers, Part F: Journal of Rail and Rapid Transit**, v. 231, n. 4, p. 498–514, 2017.

RAILSYSTEM. **Suspension Systems for Rolling Stocks**. Available at: <https://railsystem.net/suspension-systems-for-rolling-stocks/>.

RASPBERRY PI FOUNDATION. **Raspberry Pi Zero W - Technical Specifications**. Available at: <https://www.raspberrypi.org/products/raspberry-pi-zero-w/>. Accessed: 17 Aug. 2020.

REAL, J. I.; MONTALBÁN, L.; REAL, T.; PUIG, V. Development of a system to obtain vertical track geometry measuring axle-box accelerations from inservice trains. **Journal of Vibroengineering**, v. 14, n. 2, p. 813–826, 2012.

REAL, J.; SALVADOR, P.; MONTALBÁN, L.; BUENO, M. Determination of rail vertical profile through inertial methods. **Proceedings of the Institution of Mechanical Engineers, Part F: Journal of Rail and Rapid Transit**, v. 225, n. 1, p. 14–23, 2010.

REAL, T.; MONTRÓS, J.; MONTALBÁN, L.; ZAMORANO, C.; REAL, J. I. Design and validation of a railway inspection system to detect lateral track geometry defects based on axle-box accelerations registered from in-service trains. **Journal of Vibroengineering**, v. 16, n. 1, p. 210–224, 2014.

RETE FERROVIARIA ITALIANA. **Specifiche Requisiti Dinamica di Marcia**. Roma, IT: Rete Ferroviaria Italiana, 2018a.

RETE FERROVIARIA ITALIANA. **Specifica dei Requisiti Funzionali - Sisteme di acquisizione della dinamica di marcia - RFI DPR-SRD.ING SR AD 02 I 07 A**. Roma, IT: Rete Ferroviaria Italiana, 2018b.

RICHARDS TECH. **RTIMULib2 - a versatile C++ and Python 9-dof, 10-dof and 11-dof IMU library**. Available at: <https://github.com/RTIMULib/RTIMULib2>. Accessed: 22 Sep. 2021.

ROBERTS, A.; TAYEBI, A. On the attitude estimation of accelerating rigid-bodies using GPS and IMU measurements. **Proceedings of the IEEE Conference on Decision and Control**, n. May 2014, p. 8088–8093, 2011.

ROCHAT, F. **Simplified tilt**. 2007. Kungliga Tekniska Högskolan, 2007.

RODRÍGUEZ, A.; SAÑUDO, R.; MIRANDA, M.; GÓMEZ, A.; BENAVENTE, J. Smartphones and tablets applications in railways, ride comfort and track quality. Transition zones analysis. **Measurement: Journal of the International Measurement Confederation**, v. 182, 2021.

ROGERS, R. M. **Applied Mathematics in Integrated Navigation Systems**. Blacksburg, Virginia: American Institute of Aeronautics and Astronautics, Inc., 2003.

SABATINI, A. M. Quaternion-based extended Kalman filter for determining orientation by inertial and magnetic sensing. **IEEE Transactions on Biomedical Engineering**, v. 53, n. 7, p. 1346–1356, 2006.

SAFRAN COLIBRYS. **Sensors for Inertial Navigation Systems**. Available at: <https://www.colibrys.com/mems-application/sensor-for-inertial-navigation-systems/>.

Accessed: 19 Mar. 2021.

SALVADOR, P.; NARANJO, V.; INSA, R.; TEIXEIRA, P. Axlebox accelerations: Their acquisition and time-frequency characterisation for railway track monitoring purposes. **Measurement: Journal of the International Measurement Confederation**, v. 82, n. 518, p. 301–312, 2016.

SAMSUNG. **What is the best Samsung S Series phone?** Available at: <https://www.samsung.com/uk/mobile-phone-buying-guide/best-samsung-s-series-phone/>. Accessed: 1 Feb. 2023.

SELIG, E. T.; WATERS, J. M. **Track Geotechnology and Substructure Management**. London, UK: Thomas Telford Publications, 1995.

SENODIA. **Magnetometer ST480M Final Specifications.** SENODIA Technologies Co., Ltd., 2014.

SERAJ, F.; MERATNIA, N.; HAVINGA, P. J. M. RoVi: Continuous transport infrastructure monitoring framework for preventive maintenance. **2017 IEEE International Conference on Pervasive Computing and Communications, PerCom 2017**, p. 217–226, 2017.

SHKEL, A. M. Precision navigation and timing enabled by microtechnology: Are we there yet? **Proceedings of the Institute of Navigation Pacific Positioning, Navigation and Timing Meeting, Pacific PNT**, v. 2013- April, p. 1049–1053, 2013.

SMITH, S. W. **The Scientist and Engineer's Guide to Digital Signal Processing**. Second ed. California Technical Publishing, 1999.

ST MICROELECTRONICS. **LSM6DS3 - iNEMO inertial module: always-on 3D accelerometer and 3D gyroscope Datasheet.** ST Microelectronics, 2017.

STARK, B. Failue Modes and Mechanisms. In: STARK, B. (Ed.). **MEMS Reliability Assurance Guidelines For Space Applications**. Pasadena, California: Jet Propulsion Laboratory, 1999.

STOW, J.; ANDERSSON, E. Field testing and instrumentation of railway vehicles. In: IWNICKI, S. (Ed.). **Handbook of Railway Vehicle Dynamics**. London, UK: Taylor & Francis Group, 2006.

SUH, Y. S.; PARK, S. K.; KANG, H. J.; RO, Y. S. Attitude estimation adaptively compensating external acceleration. **JSME International Journal, Series C: Mechanical Systems, Machine Elements and Manufacturing**, v. 49, n. 1, p. 172–179, 2006.

TALGO. **Technological Advantages - Talgo's Tilting System**. Available at: <http://web.talgoamerica.com/overview>. Accessed: 7 Feb. 2022.

TANIFUJI, K. A vertical vibration analysis of coupled bogie cars in a train for evaluation of riding comfort. **Vehicle System Dynamics**, v. 17, 1, p. 481–492, 1988.

TERRASSE, R. La « Section Mauzin ». **Revue d'histoire des chemins de fer**, v. 39, 2008.

THOMPSON, D.; JONES, C. Noise and Vibration from Railway Vehicles. In: IWNICKI, S. (Ed.). **Handbook of Railway Vehicle Dynamics**. London, UK: Taylor & Francis Group, 2006.

TITTERTON, D. H.; WESTON, J. L. **Strapdown Inertial Navigation Technology**

2nd Edition. London. 2004.

TSUNASHIMA, H.; HIROSE, R. Condition monitoring of railway track from car-body vibration using time–frequency analysis. **Vehicle System Dynamics**, v. 60, n. 4, p. 1170–1187, 2022. Available at: <https://doi.org/10.1080/00423114.2020.1850808>.

U-BLOX. **NEO-6 u-blox 6 GPS Modules Datasheet.** U-blox Holding AG, , 2011. . Available at: <https://www.u-blox.com/sites/default/files/products/documents/NEO-6_DataSheet_(GPS.G6-HW-09005).pdf>.

UNITED NATIONS. **Satellite navigation and location systems: background paper 4 (Resolution A/CONF.184/BP/4)Third United Nations Conference on the Exploration and Peaceful Uses of Outer Space**. Vienna: United Nations, 1998. .

VANNI, L. **Materiale di trazione elettrico**. Albino, Italy, 2011.

VECTORNAV. **Inertial sensors - general aspects**. Available at: <https://www.vectornav.com/resources/inertial-navigation-primer/theory-of-operation/theory-inertial>. Accessed: 25 abr. 2021.

VECTORNAV. **IMU Specifications**. Available at: <https://www.vectornav.com/resources/imu-specifications>. Accessed: 25 abr. 2021.

VINKÓ, Á.; BOCZ, P. Experimental investigation on condition monitoring opportunities of tramway tracks. **Periodica Polytechnica Civil Engineering**, v. 62, n. 1, p. 180–190, 2018.

VINKÓ, Á.; SIMONEK, T.; ÁGH, C.; CSIKÓS, A.; FIGURA, B. Feasibility of Onboard Smartphones for Railway Track Geometry Estimation: Sensing Capabilities and Characterization. **Periodica Polytechnica Civil Engineering**, v. 67, n. 1, p. 200–210, 2023.

WANG, P.; CUI, D.; AN, B.; CHEN, R.; XU, J. Observation and Simulation of Axle Box Acceleration in the Presence of Rail Weld in High-Speed Railway. **Applied Sciences**, v. 7, n. 12, p. 1259, 2017.

WEI, Z.; BOOGAARD, A.; NUNEZ, A.; LI, Z.; DOLLEVOET, R. An integrated approach for characterizing the dynamic behavior of the wheel-rail interaction at crossings. **IEEE Transactions on Instrumentation and Measurement**, v. 67, n. 10, p. 2332–2344, 2018.

WESTON, P. F.; LING, C. S.; ROBERTS, C.; GOODMAN, C. J.; LI, P.; GOODALL, R. M. Monitoring vertical track irregularity from in-service railway vehicles. **Proceedings of the Institution of Mechanical Engineers, Part F: Journal of Rail and Rapid Transit**, v. 221, n. 1, p. 75–88, 2007a.

WESTON, P. F.; LING, C. S.; ROBERTS, C.; GOODMAN, C. J.; LI, P.; GOODALL, R. M.; ROBERTS, C.; LI, P.; GOODALL, R. M. Monitoring lateral track irregularity from in-service railway vehicles. **Proceedings of the Institution of Mechanical Engineers, Part F: Journal of Rail and Rapid Transit**, v. 221, n. 1, p. 89–100, 2007b.

WESTON, P.; ROBERTS, C.; YEO, G.; STEWART, E. Perspectives on railway track geometry condition monitoring from in-service railway vehicles. **Vehicle System Dynamics**, v. 53, n. 7, p. 1063–1091, 2015. Available at: <https://doi.org/10.1080/00423114.2015.1034730>.

WICKENS, A. H. A History of Railway Vehicle Dynamics. In: IWNICKI, S. (Ed.).

Handbook of Railway Vehicle Dynamics. London, UK: Taylor & Francis Group, 2006.

WIDODO, R. B.; WADA, C. Attitude Estimation Using Kalman Filtering: External Acceleration Compensation Considerations. **Journal of Sensors**, v. 2016, 2016.

WOLAK, M. E.; FAIRBAIRN, D. J.; PAULSEN, Y. R. Guidelines for estimating repeatability. **Methods in Ecology and Evolution**, v. 3, n. 1, p. 129–137, 2012.

XING, L.; HANG, Y.; XIONG, Z.; LIU, J.; WAN, Z. Accurate attitude estimation using ARS under conditions of vehicle movement based on disturbance acceleration adaptive estimation and correction. **Sensors (Switzerland)**, v. 16, n. 10, 2016.

YAMAHA CORPRATION. **YAS532B Magnetic Field Sensor Type 3R Datasheet.** Yamaha Corporation, 2011.

ZEITSCHRIFT, A.; LINK, P.; DIENST, E.; ETH, E. L'inspection automatique des voies de chemins de fer. **Bulletin Technque de la Suisse Romande**, v. 8, 1941.

ZHAO, H.; GUO, L. L.; ZENG, X. Y. Evaluation of bus vibration comfort based on passenger crowdsourcing mode. **Mathematical Problems in Engineering**, v. 2016, 2016.

ZHU, X. Q.; LAW, S. S.; HUANG, L. Identification of Railway Ballasted Track Systems from Dynamic Responses of In-Service Trains. **Journal of Aerospace Engineering**, v. 31, n. 5, p. 04018060, 2018.

ZOCCALI, P.; LOPRENCIPE, G.; LUPASCU, R. C. Acceleration measurements inside vehicles: Passengers' comfort mapping on railways. **Measurement: Journal of the International Measurement Confederation**, v. 129, n. September 2017, p. 489–498, 2018. Available at: <https://doi.org/10.1016/j.measurement.2018.07.079>.

ZUCCHI, E. **La qualità del binario nelle linee AV/AC : studio dei dati rilevati dai treni diagnostici di RFI e analisi degli interventi manutentivi in previsione dell'aumento di velocità a 360 km/h**. Graduation thesis, Università di Bologna, 2013.